Geochemical impacts on radium mobility in the Midwestern Cambrian-Ordovician aquifer system

By

Madeleine Mathews

A dissertation submitted in partial fulfillment of

the requirements for the degree of

Doctor of Philosophy

(Environmental Chemistry and Technology)

at the

UNIVERSITY OF WISCONSIN-MADISON

2021

Date of final oral examination: 04/13/2021

The dissertation is approved by the following members of the Final Oral Committee:
Matthew Ginder-Vogel, Associate Professor, Environmental Chemistry & Technology
Madeline Gotkowitz, Research Division Chief, Montana Bureau of Mines and Geology
Christy Remucal, Associate Professor, Environmental Chemistry & Technology
James Hurley, Professor, Environmental Chemistry & Technology
Greg Harrington, Professor, Civil and Environmental Engineering
Sean Scott, Assistant Scientist, Wisconsin State Laboratory of Hygiene

Abstract

Geochemical impacts on radium mobility in the Midwestern Cambrian-Ordovician aquifer system

by

Madeleine Mathews

Doctor of Philosophy – Environmental Chemistry and Technology Program

University of Wisconsin – Madison

Associate Professor Matthew Ginder-Vogel

The Midwestern Cambrian-Ordovician aquifer system (MCOAS) covers a large portion of the Midwestern United States and is a major source for public and domestic water supply. Radium (Ra) is a contaminant frequently exceeding the EPA maximum contaminant level of 185 mBq/L (5 pCi/L) for combined ^{226}Ra and ^{228}Ra in the MCOAS. While elevated Ra is associated with low dissolved oxygen, old water, and elevated total dissolved solids in groundwater at the aquifer scale, it is difficult to predict elevated Ra occurrence at individual wells. This dissertation uses field and laboratory methods to examine the geochemical influences on Ra mobility within the MCOAS, to gain insight into the influence of local hydrogeology on Ra partitioning to the groundwater. Multiple factors impact Ra sources and mobility in the MCOAS at the local scale; at discrete intervals within the aquifer system, elevated total dissolved solids are related to elevated Ra in an unconfined aquifer, while low dissolved oxygen is related to elevated Ra in a confined aquifer. Local geochemical conditions control Ra sorption to rock, as determined by whole-rock parent-daughter isotope ratios and sequential extractions on representative MCOAS

bedrock samples. Potential hydrologic flow from Ra-rich stratigraphy to stratigraphy with lower sorptive capacity may result in increased Ra mobility within the MCOAS. The coupling of field and laboratory work compared the contribution of Ra from aquifer solids across specific stratigraphy. Isotopic evidence ($^{226}Ra/^{238}U$) demonstrates radionuclide mobility, where geochemical influences (e.g., ORP, alkalinity) likely influence U partitioning within the system. Additionally, Ra concentrations during a short-term pumping test are shown to be consistent with trends on 1-year timeframe, although the analytical method for Ra is important to verify trend precision. The larger implications of this project are that the presence of parent nuclides, as well as local geochemical and hydrologic conditions are important to consider in terms of predicting where elevated Ra will occur in groundwater samples. This approach provides new insight into how water-rock interactions within specific stratigraphy contribute Ra to the aqueous system within the MCOAS.

Table of Contents

List of Figures

List of Tables

Acknowledgements

Thank you to the many, many folks whose support was essential to finishing this dissertation. I could not have reached this point without the encouragement and cheer you all provided, whether in the form of research discussions, supportive feedback, fun adventures, or listening to my numerous talks and musings (and grumbles) throughout graduate school.

To my adviser, Matt Ginder-Vogel. Thank you for your endless support as I grew from a why-in-the-world-would-I-get-a-PhD Masters student, to my current excitement about academic research and teaching. It took me a while to realize that when Matt asks, "How's it going?", he is interested in his students' lives beyond just research. Thank you for pushing me to work hard and think critically about research, while prioritizing the more important aspects in life (i.e., the people). Also, thank you for supporting me in seeking out so many teaching opportunities; I have loved participating in both research and teaching in graduate school.

To Madeline Gotkowitz, thank you for taking endless time to teach me how to think critically about subsurface systems. I have happy memories of going field sampling with you in the sunshine in my very first semester in graduate school, and realizing that this environmental field could be pretty great if 'working' means also being outside. I have also learned a lot from you about asking questions and analyzing data. As I edit the final parts of my dissertation, I often think about questions you might ask about the data and interpretation.

To Sean Scott, thank you for the great discussions (and enthusiasm!) about isotopic work. I have learned so much from you about laboratory work, whether in terms of sample purification, running the 'machine', or hearing about the latest in the isotopic world. I consider you a great mentor and good friend, a rare and wonderful combination. I'd also like to thank Veronica Scott,

for many laughs, walks, and her support of Sean's and my many radium discussions. A chance meeting at a random conference has turned into such a great friendship.

I would also like to thank the other members of my committee, Christy Remucal, Jim Hurley, and Greg Harrington. I appreciate your time and energy in providing helpful feedback and questions throughout my time in graduate school. Thank you for helping me keep the research in perspective.

I appreciated the opportunity to work with Randy Hunt at the USGS Upper Midwest Water Science Center. Randy, thank you for reaching out to start this work examining how water quality informs water quantity, in terms of radium contamination. I have learned a lot from you on how to think about water quality at a larger scale, as well as the finer intricacies of running model calibration.

Thank you to the many organizations who collaborated with me to make this work possible. To the Wisconsin State Laboratory of Hygiene Trace Metal Lab, thank you for sharing your bench space with me, and answering many questions. To the Wisconsin Geological and Natural History Survey, particularly Pete Chase and Carsyn Ames, thank you for help with field work, access to rock core, and for the great geology stories. To the University Consortium, a collaboration with Hydrite and the University of Guelph, thank you for the enthusiasm to support a new research venture with your amazing monitoring well set-up, and your assistance with fieldwork.

Thank you also to the folks who have kept or currently keep WSEL running – namely Chris Worley and James Lazarcik. I think it would be practically impossible to number the times I have ran to your office with questions about lab work, instrumentation, the building, and so much more. Thank you both for your encouragement for everyone in WSEL, continual

maintenance to ensure that WSEL research can move forward, and enthusiasm in taking instruments or machines apart (so that they can be 'improved').

Throughout graduate school, I have been fortunate to participate in several teaching opportunities and programs at UW-Madison. Thank you to the Delta Program and the WISCIENCE Scientific Teaching Fellows for the hands-on instruction for learning how to apply scientific teaching methods. To Cara Theisen, thank you for your support and encouragement during teaching, and also your constructive feedback to continue improving. To Devin Wixon, thank you for encouraging me to continue working on my teaching skills throughout graduate school.

To my labmates, officemates and colleagues, thank you for the many years (!) of laughter, silliness, research feedback, and endless conversations about science. Interacting with all of you has definitely made me a better scientist, but also a scientist who wants to keep growing and learning. In particular, thank you to Lily Schacht, Amy Plechacek, Gabrielle Campagnola, and Marie Dematatis for the field and lab assistance. Lily, also thanks for the silliness, cooking exploits, and paper edits.

To my family, thank you for the support and love throughout my life, but particularly during graduate school. I consider myself quite fortunate to be related to each one of you. Looking forward to more days of outdoor adventures and good meals.

To my partner, Jered, thank you for your support as I wrap up the PhD whirlwind. I appreciate your kindness, thoughtfulness, and silliness (and patience). To many more adventures!

Chapter 1

Introduction

1.1 Motivation

In this dissertation, we examine the impact of geochemical factors on the mobilization of the contaminant radium (Ra) in the Midwestern Cambrian Ordovician aquifer system (MCOAS). Groundwater is an important source of drinking water for more than 2 billion people.[1-3] However, anthropogenic and naturally occurring contaminants threaten the safety of drinking groundwater.[4-12] The quality of water from a source dictates the quantity of water available for drinking.[13,14] Subpar water conditions can force a community to adopt expensive treatment or find an alternative water source.[2,4,5,15,16] Elevated Ra frequently occurs in groundwater sourced from the MCOAS, impacting drinking water quality.[15,17-19] There is a need to examine the geochemical and hydrologic interactions between Ra and aquifer solids at the local scale under aquifer-relevant conditions, in order to better use geochemical indicators to predict the release of Ra from minerals to groundwater.[17,20] This dissertation couples field and laboratory techniques to examine the geochemical influences on Ra occurrence at discrete intervals in the MCOAS.

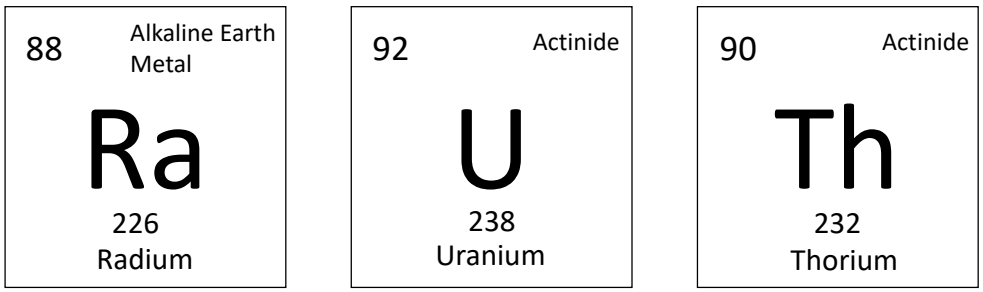

Figure 1.1 Elemental information about radium, uranium, and thorium.

1.2 Contaminants in groundwater

Groundwater is a major source of drinking water globally, but is threatened by anthropogenic and naturally occurring contamination, threatening its use as a potable water source. In 2011, almost 50% of drinking water globally was sourced from groundwater systems.[21] In the United States, groundwater is also widely used for clean drinking water; in the Midwestern US, 631 million gallons were withdrawn per day for combined public supply and domestic use in 2014.[8,22] However, human-induced contamination such as infiltration of fertilizers, human waste, industrial output, and more can degrade groundwater quality.[4] Additionally, naturally occurring contaminants, including arsenic, uranium, and radium, may partition from associations with aquifer solids due to hydrologic or geochemical changes.[4,6] It can be difficult to determine sources of naturally occurring contaminants, due to complex geologic interactions, but necessary in order to maintain groundwater as a sustainable, clean drinking water source.

1.3 General radium background

1.3.1 Elemental radium

The alpha decay of parent nuclides uranium (U) and thorium (Th) produces the naturally occurring contaminant Ra (Figure 1.1). Four isotopes of Ra exist naturally (^{223}Ra, ^{224}Ra, ^{226}Ra, and ^{228}Ra), each deriving from the ^{238}U, ^{235}U, or ^{232}Th isotope decay chains, with each decay chain ultimately producing a stable isotope of lead. However, the environmental abundance of each Ra isotope varies, depending both on the quantity of parent nuclide present and the length of the Ra half-life. For example, ^{223}Ra is rarely measured in environmental systems as parent ^{235}U makes up < 1% of naturally occurring U; additionally, ^{223}Ra has a short half-life (11 days)

and quickly decays to ^{219}Rn. The other Ra isotopes are observed at higher environmental levels due to greater concentrations of parent nuclides ^{238}U and ^{232}Th; however, half-life also impacts the prevalence of these Ra isotopes, with ^{224}Ra (3.6 days) found at lower levels than ^{226}Ra (1600 years) and ^{228}Ra (5.75 years) in natural systems (Figure 1.2). Once emitted to the aquifer system via alpha decay, like all other alkaline earth metals Ra is observed in the Ra(II) oxidation state and does not undergo redox chemistry. In particular, Ra has similar geochemical behavior to barium (Ba) due to similar ionic radii.[20,23]

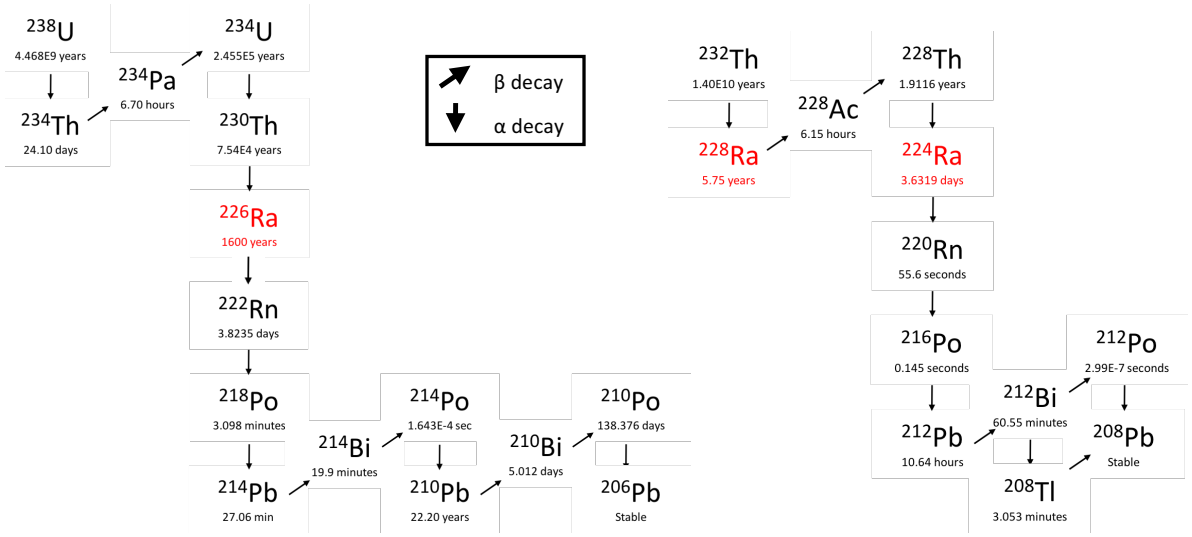

Figure 1.2 Decay chains for ^{238}U and ^{232}Th, with radium isotopes (^{226}Ra, ^{228}Ra, ^{224}Ra) highlighted in red.

1.3.2 Radium health concerns

Ingestion of Ra results in health issues, such as cancer. Once in the body, Ra accumulates in bone tissue and continues to undergo radioactive decay; this damages cell tissue, potentially causing cancer or other disease from long-term exposure.[24-28] The United States Environmental Protection Agency (US EPA) has set a limit for radioactivity in drinking water with the

Radionuclides Rule in 2000, in order to reduce the risk of cancer due to consuming radionuclides in drinking water.[29] The maximum contaminant level (MCL) for gross alpha radioactivity is 555 mBq/L (15 pCi/L). For Ra, the MCL is 185 mBq/L (5 pCi/L) for the combined activity of the two major isotopes, ^{226}Ra and ^{228}Ra. Compliance with this rule is important to maintain public health; a New Jersey study observed 100% increase in bone cancer occurrence at study sites with gross alpha or combined Ra levels exceeding the MCL, in comparison to sites with levels below the MCL.[30] Additionally, although ^{226}Ra may occur at greater levels, ingestion exposure risk is typically greater for ^{228}Ra due to its increased radioactivity.[17,31]

1.4 Radium as a contaminant

Elevated Ra occurs in aquifer systems across the world, impacting drinking water quality for many. Globally, aquifers vary in dissolved Ra levels; some sites associated with oil and gas fields are of interest for research examining elevated Ra.[18,32-41] While Ra quantity varies across aquifer systems, many studies have determined that examining geochemical trends influencing the mobilization of Ra can provide information on the quality of the drinking water source. For example, the Ra isotope ratio (^{226}Ra/^{228}Ra) can be used to study groundwater flow path and determine a distinct isotope composition dependent on origin and age; comparison of parent and daughter isotopes (^{238}U/^{226}Ra) can also help designate main groundwater contributions and mixing or separation between aquifers.[42,43] Additionally, many studies examine the sorption capacity of the aquifer stratigraphy, in order to better understand mechanism of Ra release to groundwater.[44,45]

In the US, approximately 130 million people rely on groundwater as a drinking water source.[7] The Midwestern Cambrian-Ordovician aquifer system (MCOAS) has the most frequent

occurrence of elevated Ra in groundwater samples in the US.[18,46] Many studies examine geochemical influences on Ra mobilization to the aqueous system within the MCOAS. Elevated total dissolved solids (TDS), anoxic conditions, low pH, and older water are all associated with elevated dissolved Ra in the MCOAS.[17,18,47-49] Additionally, elevated Ra is frequently found in groundwater pumped from below the regional confining unit covering a large portion of the MCOAS, the Maquoketa shale.[17,50] A spatial and temporal investigation of Ra levels in the MCOAS in Wisconsin found that on average, combined levels of ^{226}Ra and ^{228}Ra increased regionally from 2000 to 2018.[19] Along flow lines in the MCOAS, desorption, mineral dissolution, parent nuclide location control Ra presence in groundwater.[51-53] Studies examining Ra in the MCOAS also use isotopic analyses to examine the release of Ra from aquifer solids.[54,55]

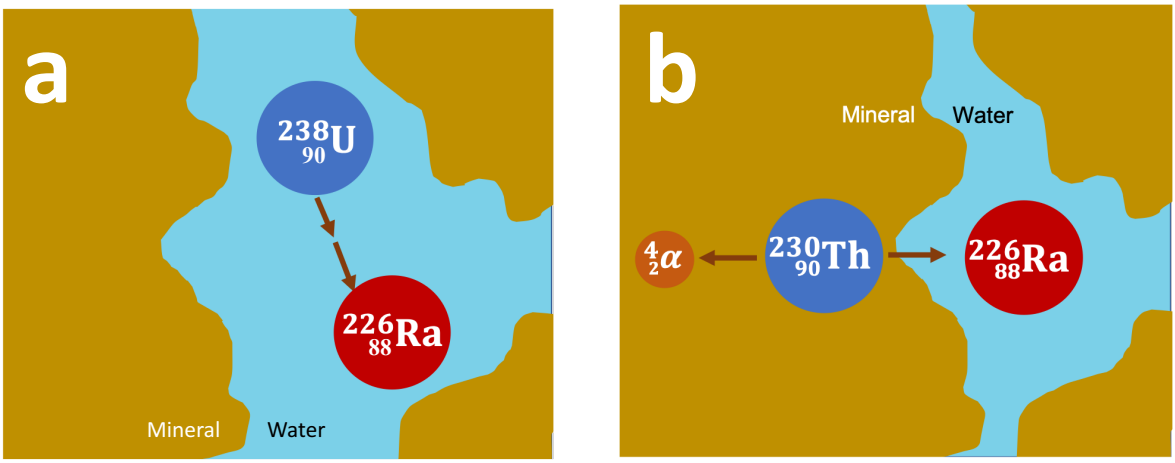

Figure 1.3 Conceptual figures depicting radioactive decay of uranium (a) and thorium (b) decay chains releasing ^{226}Ra isotopes within aquifer systems.

1.5 Sources of radium to aquifer systems

1.5.1 Radioactive decay and alpha recoil

Radioactive decay both contributes and removes Ra in aquifer systems. The alpha decay of parent nuclides (^{230}Th and ^{232}Th) forms the two main Ra isotopes, ^{226}Ra and ^{228}Ra, emitting an alpha particle and a daughter nucleus in opposite directions in a process known as alpha recoil.

Alpha recoil ejects the Ra nucleus forcibly away from the location of the parent nuclide in a random direction, a distance of 0.02 ± 0.05 mm.[20,47] Alpha recoil is a high energy process, with the potential to eject Ra into the aqueous system even from within the mineral lattice.[56,57] Additionally, the activities of parent and daughter nuclides can be compared to determine whether secular equilibrium is occurring; this equilibrium occurs when the rate of nuclide generation is the same as the rate of decay, and parent and daughter activities equilibrate. Typically in environmental systems, deviation from equilibrium suggests that physical or geochemical factors are removing the daughter nuclide from the site of parent decay.[58,59] The interactions of the parent nuclide with the aquifer system, such as concentration and mineral associations, are important to consider for examining Ra sources. Radioactive decay also removes Ra from the system; however, isotopes with longer half-lives (e.g., ^{226}Ra) will remain in the aquifer system for longer periods of time. Longer residence time increases the probability that geochemical factors induce Ra partitioning from aquifer solids.[60]

1.5.2 Radium parent nuclide aquifer associations

The presence of U and Th isotopes in aquifer systems provides information on potential mechanisms of Ra release to the aquifer system. Under secular equilibrium conditions, Ra activity is equivalent to U and Th activities; if other geochemical factors mobilize Ra from the site of decay, then secular equilibrium will not be observed locally.[59] The control of Th and U nuclides on the release of Ra to an aquifer system can be determined using the ^{228}Ra/^{226}Ra ratio in aquifer solids and groundwater.[54] As most whole-rock systems operate under equilibrium conditions, comparing the ^{228}Ra/^{226}Ra ratio to the ^{232}Th/^{238}U ratio provides information on Ra interactions with the aqueous and solid systems.

Radioactive decay and redox potential influence interactions between U and the aquifer system, impacting the location of ^{226}Ra production (Figure 1.3a). Uranium isotopic ratios ($^{234}U/^{238}U$) in groundwater are related to the alpha recoil process and the rate of geochemical removal.[61] The parent isotope (^{238}U) emits ^{234}U via alpha decay, damaging the mineral lattice in the process and making it easier for geochemical factors to release ^{234}U to the aqueous system. Overall, U is fairly soluble in groundwater, especially under oxic conditions; in particular, the U(VI) redox state is most mobile and easily forms complexes with calcium (Ca) and carbonate (CO_3^{2-}).[62-65] Sorption, to material such as Fe- and Mn-oxide minerals as well as natural organic matter, retards the mobility of U in aquifer systems.[65-68] Additionally, a correlation between U and elevated nitrate (NO_3^-) levels in groundwater is observed, likely due to the dissolution of U(IV) minerals by oxidative processes occurring with elevated NO_3^-.[69] However, independent of parent isotope location, naturally occurring U decay chains decay to produce Ra isotopes in aquifer systems. This continual decay produces an accumulation of ^{226}Ra when water resides in an aquifer for an extended period of time.[52]

In comparison to U, Th is strongly sorptive; consequently, mineral interactions figure more prominently in Ra production from Th isotopes (Figure 1.3b). Thorium, present in one oxidation state (i.e., IV), is considered immobile in aquifer systems in natural conditions.[62] The lower solubility results in higher Th retention within aquifer solids than U.[61,67] The interactions of Th with the aquifer are due to geochemistry or physical processes (e.g., sedimentation) rather than dissolution and aqueous mobilization.[28,70] Geochemical changes to mineral surface coatings may impact the mobility of Th within aquifer systems.[67] Therefore, Th decay from aquifer solids plays a major role in releasing Ra daughter isotopes, as Th isotopes present in the aqueous system are more limited.[28,70]

1.6 Geochemical controls on Ra in aquifer systems

1.6.1 Radium sorption mechanism

After the production of Ra via parent nuclide decay, interactions between Ra and aquifer minerals are important controls on Ra groundwater mobility (e.g., sorption). Radium associates easily with many mineral surfaces, retarding groundwater transport.[44,60] While sorption is a reversible process, the first-order rate constants for Ra adsorption ($1.0 \times 10^{-4} – 3.5 \times 10^{-1}$ s^{-1}) in comparison to the desorption rate constants ($9.3 \times 10^{-7} – 2.0 \times 10^{-4}$ s^{-1}) demonstrate the stronger tendency of Ra to sorb then desorb.[60,71,72]

1.6.2 Radium association with aquifer minerals

The minerals present within an aquifer influence the sorption capacity present within the groundwater system, impacting Ra partitioning to the aqueous phase. For example, shale, bitumen slate, and phosphate rocks are observed to have the highest ^{226}Ra concentrations in the Earth's crust.[20] For shale and bitumen slate, this is likely due to Ra associations with clay-rich organic material, while phosphate minerals are known to have high U concentrations.[20] Additionally, Ra is quickly and easily adsorbed to Fe- and Mn-(hydr)oxide minerals.[20,47,73-77] Clay materials, in particular bentonite and illite, largely remove Ra from solution due to sorption, although collapse of interlayers in layered clays can prevent further ion exchange.[78-81]

1.6.3. Geochemical influences on Ra mineral association

Aquifer geochemical conditions control Ra partitioning from aquifer solids to the aqueous system. Cation site competition, dissolution of solids containing Ra, redox state, lower pH, more stable inorganic complexes (e.g., chloride complexes), and dissolution of organic complexes can all contribute to increased dissolved Ra, depending on aquifer geochemical

conditions.[20] Increased dissolved cations fill sorption sites, leaving fewer open for other ions. Ion exchange, especially between alkaline earth metals like Ra, is very common.[20] Consequently, elevated Ra levels are associated with increased groundwater mineralization or high salt content (Figure 1.4a).[18,82,83] Increased Ra sorption tends to be observed as pH increases, as the point zero charge (PZC) of mineral surfaces impacts Ra sorption.[20] Generally, when pH is less than the PZC, anions are more easily sorbed; when pH is greater than the PZC, dissolved cations like Ra compete for sorption sites.[20]

While aquifer redox chemistry will not impact Ra redox state, it may affect mineral presence, and therefore sorption site availability (Figure 1.4b). Reducing conditions will cause Fe- and Mn- (hydr)oxide minerals to be unstable and to form in little quantity; additionally, the presence of dissolved Fe(II) and Mn(II) increases sorption site competition.[20,47,73-77] A reversible process, Ra sorption to Fe-(hydr)oxide minerals frequently changes, depending on aquifer pH conditions, mostly occurring above pH 8.[20] Manganese oxides strongly sorb Ra; however, these minerals are also affected as redox conditions influence the occurrence of aqueous Mn(II) in comparison to precipitates containing Mn(III) and Mn(IV).[20,84]

1.6.4 Radium co-precipitation

While Ra is typically present at ultra trace levels (< 185 mBq/L) in aquifer systems, and therefore unlikely to precipitate as a pure mineral, Ra will co-precipitates with other cations.[18,85] Ra strongly complexes with sulfate (SO_4^{2-}); under aqueous conditions with 70 mg/L SO_4^{2-}, half of the available Ra would exist as $RaSO_4$.[20] Depending on aquifer conditions, Ra co-precipitates with barite ($BaSO_4$).[86,87] Reducing conditions decrease the amount of SO_4^{2-} ions available for precipitation, increasing the amount of dissolved Ra in the system.[20] The ratio between Ra

isotopes and $BaSO_4$ can be used to examine mineral saturation in an aquifer system, demonstrating control of $BaSO_4$ precipitation on Ra mobility.[51]

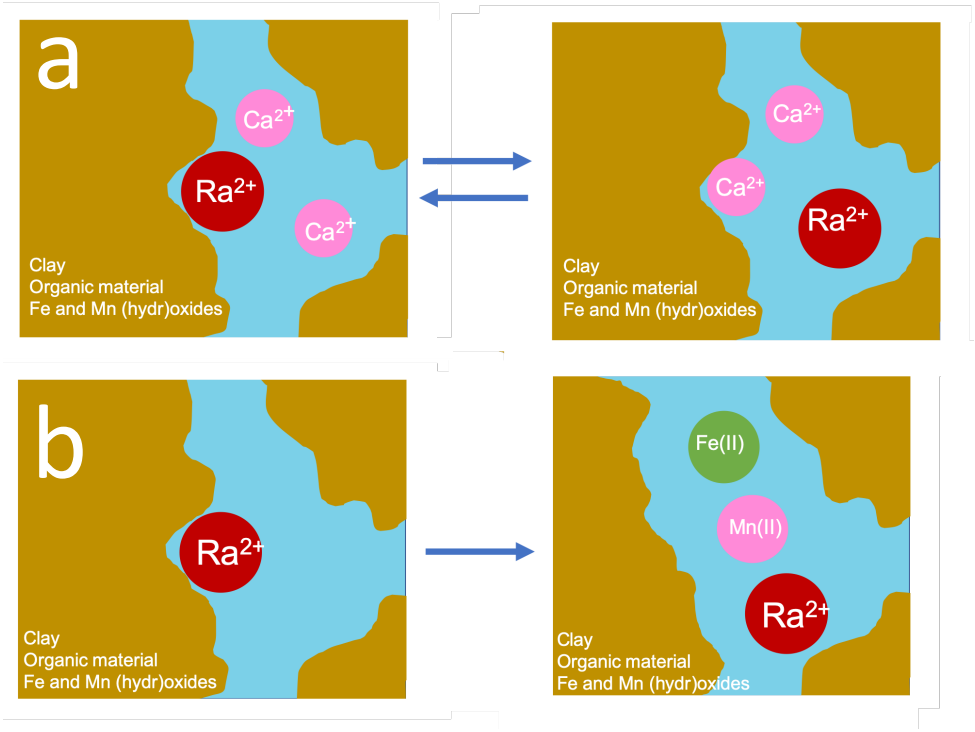

Figure 1.4 Conceptual model depicting geochemical factors influencing Ra partitioning from aquifer solids to the aqueous system. Figure 4a represents the impact of elevated cations present in an aquifer system on sorption site availability. Figure 4b describes dissolution of Fe- and Mn-(hydr)oxide minerals due to changing redox conditions, and subsequent loss of sorption sites.

1.7 Research Objectives

Other studies have examined geochemical influences on Ra interactions with aquifer systems extensively, providing information about Ra mobilization to the aqueous system. However, the impact of geochemical influences on Ra mineral associations has not been examined at the local aquifer scale. While much research has focused on experimental Ra-mineral associations or broad geochemical trends associated with elevated dissolved Ra, none has examined the influence of geochemically and hydrologically heterogeneous aquifer conditions on Ra release at the local scale. Better understanding of Ra partitioning at the local

scale will provide information for situations of elevated within large and/or geologically heterogeneous groundwater systems. This dissertation aims to fill in research gaps by 1) examining geochemical trends associated with dissolved Ra at discrete intervals in the MCOAS, 2) the geochemical association of Ra with aquifer solids compared across different lithologies, and 3) the impact of local geochemistry on releasing Ra from aquifer solids at depth within the MCOAS.

In Chapter 2, we examine the geochemical influences on Ra sources to groundwater at discrete intervals in the MCOAS. As many past studies examine geochemical factors associated with elevated Ra using water samples collected over long sections of the aquifer system, here we address the gap in knowledge aimed at examining Ra associated with specific stratigraphy in the MCOAS. We accomplish this by quantifying the relationship between aquifer solids and aqueous geochemistry in terms of Ra levels in groundwater. Additionally, we examine geologic sources of parent isotopes to compare to elevated Ra levels. By sampling at monitoring wells screened across discrete intervals in the MCOAS in the Madison, WI area, we examine geochemical influences on the groundwater quality at specific stratigraphic horizons within the system. We quantify the elemental composition of aquifer solids, examining the location of parent isotopes U and Th. We found elevated Ra associated with anoxic conditions, or elevated total dissolved solids, depending on stratigraphy. Parent nuclides U and Th associate with shaley intervals, but are also present at depth in the sandstone aquifers. Identification of geochemical and hydrogeological controls on Ra in groundwater associated with specific stratigraphic horizons provides information for long-term management of groundwater resources that limits uptake of water elevated in Ra.

In Chapter 3, we examine the geochemical associations between Ra and aquifer minerals, at discrete intervals in the MCOAS. Due to its highly sorptive nature, mineral associations quickly remove Ra from the aqueous system of the MCOAS, but geochemical changes can also influence release from the aquifer solids. Here, we ran a sequential extraction examining water-soluble metals (artificial groundwater), acido-soluble metals (1 M acetic acid), the reducible fraction (0.04 M hydroxylamine hydrochloride in 25% acetic acid), and a complete HF digestion. Activities of both U-238 and Ra-226 were examined for all fractions. Due to ultra trace Ra concentrations produced by the laboratory experiment, MC-ICPMS methods were used to purify and analyze samples for Ra. Secular equilibrium was determined between ^{238}U and ^{226}Ra across all examined stratigraphic units, typical of similar whole-rock systems. While the majority of Ra was associated with the HF digested fraction, the Ra association with minerals differend between the stratigraphic horizons. Local geochemical conditions strongly determine the release of Ra from the aquifer solids. Changes in subsurface geochemical conditions likely impact Ra mobility differently across different lithologies, and potentially influencing Ra mobility between geologic units.

In Chapter 4, we examine the impact of local geochemistry on Ra mobilization in MCOAS stratigraphy. Secular equilibrium between parent and daughter isotopes suggests that Ra remains close to the site of parent decay; therefore, geochemical factors may have major influence on the release of Ra associated with minerals to the groundwater system. In Dane Co., WI, we examine variation in Ra production from specific stratigraphic units related to U and Th occurrence, using geochemical and isotopic evidence. We obtained groundwater samples at discrete intervals in the MCOAS, then ran an extraction and digestion experiment on aquifer solids associated with the same site depths. Ra is close to equilibrium with parent isotopes of

uranium (U), although potential Ra mobilization varies by stratigraphic unit. These results indicate that general geochemical trends such as oxidative-reduction potential (ORP) and total dissolved solids (TDS) are weakly correlated to Ra levels, depending on the sorption capacity of minerals present and the site of parent decay. Correlation between aqueous $^{87}Sr/^{86}Sr$ and ^{226}Ra indicates that aqueous interactions with specific minerals containing more radiogenic $^{87}Sr/^{86}Sr$ are more likely to release Ra to groundwater. In summary, many of the broad geochemical indicators used to predict elevated Ra occurrence need to be considered alongside local geologic and hydrologic controls.

In Chapter 5, we use isotopic tools to examine the impact of water withdrawal from long-stemmed municipal wells on Ra occurrence in the MCOAS. While geochemistry controls Ra partitioning within local stratigraphy, municipal wells are constructed to open to long portions of the aquifer system, and often multiple stratigraphic units, mixing geochemical conditions across the borehole. Here, we use a short-term pumping test to investigate the impact of water withdrawal from municipal wells on aqueous Ra within the MCOAS. We also employ isotopic indicators (i.e., $^{87}Sr/^{86}Sr$ and $^{234}U/^{238}U$) of interactions between groundwater and aquifer solids to examine the impact of geochemical mixing more closely on Ra release within well boreholes. Initial geochemical turbulence was observed during the first hour of the pumping test, after which conditions stabilized to Ra levels observed in grab samples collected during typical well pumping conditions. Differences in precision between Ra analytical methods, namely decay counting and mass spectrometry, demonstrate that the ultra trace levels of Ra analyzed at the MCL require use of appropriately precise analytical methods. Finally, water-rock interactions are observed via isotopic indicators at broad geologic scales; in particular, a trend between $^{234}U/^{238}U$ and combined Ra introduces a potential isotopic tool that can contribute to predictions of elevated

Ra during well construction. Overall, the results demonstrate that development of isotopic tools can help predict Ra occurrence in the MCOAS, including more precise analytical methods and associations with isotopic indicators like [$^{234}U/^{238}U$].

1.8 References

1. Alley, W. M.; Healy, R. W.; LaBaugh, J. W.; Reilly, T. E., Flow and storage in groundwater systems. *science* **2002,** *296*, (5575), 1985-1990.
2. Famiglietti, J. S., The global groundwater crisis. *Nature Climate Change* **2014,** *4*, (11), 945-948.
3. WWAP (United Nations World Water Assessment Programme) *The United Nations World Water Development Report 2015: Water for a Sustainable World*; UNESCO: Paris, 2015.
4. Burri, N.; Weatherl, R.; Moeck, C.; Schirmer, M., A review of threats to groundwater quality in the anthropocene. *Science of The Total Environment* **2019,** *684*.
5. Konikow, L. F.; Kendy, E., Groundwater depletion: A global problem. *Hydrogeology Journal* **2005,** *13*, (1), 317-320.
6. Grützmacher, G.; Kumar, P. J. S.; Rustler, M.; Hannappel, S.; Sauer, U., Geogenic groundwater contamination—definition, occurrence and relevance for drinking water production. *Zbl Geol Paläont Teil I* **2013,** *1*, 69-75.
7. DeSimone, L. A.; McMahon, P. B.; Rosen, M. R. *The quality of our Nation's waters - Water quality in Principal Aquifers of the United States, 1991-2010*; U.S. Geological Survey: 2014; p 151.
8. Arnold, T. L.; Bexfield, L. M.; Musgrove, M.; Lindsey, B. D.; Stackelberg, P. E.; Barlow, J. R. B.; Desimone, L. A.; Kulongoski, J. T.; Kingsbury, J. A.; Ayotte, J. D.; Fleming, B. J.; Belitz, K., Groundwater-quality data from the National Water-Quality Assessment Project, January through December 2014 and select quality-control data from May 2012 through December 2014. *U.S. Geological Survey Report 1063* **2017**, 96.
9. Ayotte, J. D.; Szabo, Z.; Focazio, M. J.; Eberts, S. M., Effects of human-induced alteration of groundwater flow on concentrations of naturally-occurring trace elements at water-supply wells. *Applied Geochemistry* **2011,** *26*, (5), 747-762.
10. Friedly, J. C.; Davis, J. A.; Kent, D. B., Modeling hexavalent chromium reduction in groundwater in field-scale transport and laboratory batch experiments. *Water resources research* **1995,** *31*, (11), 2783-2794.
11. Izbicki, J. A.; Wright, M. T.; Seymour, W. A.; McCleskey, R. B.; Fram, M. S.; Belitz, K.; Esser, B. K., Cr(VI) occurrence and geochemistry in water from public-supply wells in California. *Applied Geochemistry* **2015,** *63*, 203-217.
12. Zapecza, O. S.; Szabo, Z., Natural Radioactivity in Ground Water - A Review. *National Water Summary 1986 - Ground-Water Quality: HYDROLOGIC CONDITIONS AND EVENTS* **1986**, 50-57.
13. Liu, J.; Liu, Q.; Yang, H., Assessing water scarcity by simultaneously considering environmental flow requirements, water quantity, and water quality. *Ecological Indicators* **2016,** *60*, 434-441.
14. van Vliet, M. T. H.; Flörke, M.; Wada, Y., Quality matters for water scarcity. *Nature Geoscience* **2017,** *10*, (11), 800-802.
15. Great Lakes-St. Lawrence River Basin Water Resources Council, Final Decision. In 2016.
16. Hahn, N. A., Radium in Wisconsin groundwater and removal methods for community water systems. **1984**.

17. Stackelberg, P. E.; Szabo, Z.; Jurgens, B. C., Radium mobility and the age of groundwater in public-drinking-water supplies from the Cambrian-Ordovician aquifer system, north-central USA. *Applied Geochemistry* **2018,** *89*, 34-48.
18. Szabo, Z.; dePaul, V. T.; Fischer, J. M.; Kraemer, T. F.; Jacobsen, E., Occurrence and geochemistry of radium in water from principal drinking-water aquifer systems of the United States. *Applied Geochemistry* **2012,** *27*, (3), 729-752.
19. Dematatis, M.; Plechacek, A.; Mathews, M.; Wright, D. B.; Udenby, F.; Gotkowitz, M. B.; Ginder-Vogel, M., Spatial and temporal variability of radium in the Wisconsin Cambrian-Ordovician aquifer system. *AWWA Water Science* **2020**.
20. International Atomic Energy Agency, The environmental behaviour of radium: revised edition. *Technical Reports Series No. 476* **2014**, (476), 44-51.
21. The United Nations world water development report 4: managing water under uncertainty and risk, executive summary. In 2012.
22. Dieter, C. A.; Maupin, M. A.; Caldwell, R. R.; Harris, M. A.; Ivahnenko, T. I.; Lovelace, J. K.; Barber, N. L.; Linsey, K. S., Estimated use of water in the United States in 2015. *U.S. Geological Survey Information Circular 1441* **2018**, 76.
23. Langmuir, D.; Riese, A. C., The thermodynamic properties of radium. *Geochimica et Cosmochimica Acta* **1985,** *49*, (7), 1593-1601.
24. Cohn, P.; Skinner, R.; Burger, S.; Falgiano, J.; Klotz, J., Radium in Drinking Water and the Incidence of Osteosarcoma: A Report to the New Jersey Department of Environmental Protection. **2003**.
25. Evans, R. D., Radium poisoning: a review of present knowledge. *American Journal of Public Health and the Nations Health* **1933,** *23*, (10), 1017-1023.
26. Canu, I. G.; Laurent, O.; Pires, N.; Laurier, D.; Dublineau, I., Health effects of naturally radioactive water ingestion: the need for enhanced studies. *Environmental health perspectives* **2011,** *119*, (12), 1676-80.
27. Mays, C. W.; Rowland, R. E.; Stehney, A. F., Cancer risk from the lifetime intake of Ra and U isotopes. *Health physics* **1985,** *48*, (5), 635-47.
28. Aieta, E. M.; Singley, J. E.; Trussell, A. R.; Thorbjarnarson, K. W.; McGuire, M. J., Radionuclides in Drinking Water: An Overview. *Journal (American Water Works Association)* **1987,** *79*, (4), 144-152.
29. US EPA *Radionuclides rule: a quick reference guide*; 2001.
30. Szabo, Z.; dePaul, V. T. *Radium-226 and radium-228 in shallow ground water, southern New Jersey*; 1998.
31. World Health Organization *Guidlines for drinking-water quality: fourth edition incorporating the first addendum.*; Geneva, 2017.
32. Okoro, E. E.; Okolie, A. G.; Sanni, S. E.; Joel, E. S.; Agboola, O.; Omeje, M., Assessment of naturally occurring radiation in lithofacies of oil field in Niger Delta region and its possible health implications. *Journal of Environmental Management* **2020,** *264*, 110498.
33. Omeje, M.; Wagiran, H.; Joel, E. S.; Olusegun, O. A.; Kayode, O. T., Radiological Risks Of Radium-226 On Groundwater Based-Drinking In Kubwa And Gosa Area Of Abuja, North Central Nigeria. *Sci. Int.(Lahore)* **2016,** *28*, (2), 1859-1863.
34. Asikainen, M.; Kahlos, H., Anomalously high concentrations of uranium, radium and radon in water from drilled wells in the Helsinki region. *Geochimica et Cosmochimica Acta* **1979,** *43*, (10), 1681-1686.

35. Tomita, J.; Satake, H.; Fukuyama, T.; Sasaki, K.; Sakaguchi, A.; Yamamoto, M., Radium geochemistry in Na–Cl type groundwater in Niigata Prefecture, Japan. *Journal of Environmental Radioactivity* **2010,** *101*, (3), 201-210.
36. Lauer, N. E.; Warner, N. R.; Vengosh, A., Sources of Radium Accumulation in Stream Sediments near Disposal Sites in Pennsylvania: Implications for Disposal of Conventional Oil and Gas Wastewater. *Environmental Science & Technology* **2018,** *52*, (3), 955-962.
37. Roba, C. A.; Niţă, D.; Cosma, C.; Codrea, V.; Olah, Ş., Correlations between radium and radon occurrence and hydrogeochemical features for various geothermal aquifers in Northwestern Romania. *Geothermics* **2012,** *42*, 32-46.
38. Lagacé, F.; Foucher, D.; Surette, C.; Clarisse, O., Radium geochemical monitoring in well waters at regional and local scales: an environmental impact indicator-based approach. *Chemosphere* **2018,** *205*, 627-634.
39. Felmlee, J. K.; Cadigan, R. A. *Radium and uranium concentrations and associated hydrogeochemistry in ground water in southwestern Pueblo County, Colorado*; 79-974; 1979.
40. Dickson, B. L.; Giblin, A. M.; Snelling, A. A., The source of radium in anomalous accumulations near sandstone escarpments, Australia. *Applied Geochemistry* **1987,** *2*, (4), 385-398.
41. Almeida, R. M. R.; Lauria, D. C.; …, A. C. F. J. o. E.; undefined, Groundwater radon, radium and uranium concentrations in Regiao dos Lagos, Rio de Janeiro State, Brazil. *Elsevier*.
42. Kiro, Y.; Weinstein, Y.; Starinsky, A.; Yechieli, Y., Application of radon and radium isotopes to groundwater flow dynamics: An example from the Dead Sea. *Chemical Geology* **2015,** *411*, 155-171.
43. Copia, L.; Plastino, W.; Nisi, S.; Ciarletti, M.; Povinec, P. P., 226Ra and uranium isotopic ratios characterization into the Gran Sasso aquifer, Italy. *Journal of Radioanalytical and Nuclear Chemistry* **2017,** *311*, (1), 385-393.
44. Copenhaver, S. A.; Krishnaswami, S.; Turekian, K. K.; Epler, N.; Cochran, J. K., Retardation of 238U and 232Th decay chain radionuclides in Long Island and Connecticut aquifers. *Geochimica et Cosmochimica Acta* **1993,** *57*, (3), 597-603.
45. Senior, L. A.; Vogel, K. L., *Radium and radon in ground water in the Chickies quartzite, southeastern Pennsylvania*. 1995.
46. Szabo, Z.; Fischer, J. M.; Hancock, T. C. *USGS Fact Sheet 2010-3113: Principal aquifers can contribute radium to sources of drinking water under certain geochemical conditions*; 2012; pp 6-6.
47. Sturchio, N. C.; Banner, J. L.; Binz, C. M.; Heraty, L. B.; Musgrove, M., Radium geochemistry of ground waters in Paleozoic carbonate aquifers, midcontinent, USA. *Applied Geochemistry* **2001,** *16*, (1), 109-122.
48. Gilkeson, R. H.; Cartwright, K.; Cowart, J. B.; Holtzman, R. B. *Hydrogeologic and Geochemical Studies of Selected Natural Radioisotopes and Barium in Groundwater in Illinois*; Washington, DC, 1983; pp 93-93.
49. Gilkeson, R. H.; Specht, S. A.; Cartwright, K.; Griffin, R. A.; Larson, T. E., Geologic studies to identify the source for high levels of radium and barium in Illinois ground-water supplies: a preliminary report. **1978**.
50. Luczaj, J.; Masarik, K., Groundwater Quantity and Quality Issues in a Water-Rich Region: Examples from Wisconsin, USA. *Resources* **2015,** *4*, (2), 323-357.

51. Grundl, T.; Cape, M., Geochemical factors controlling radium activity in a sandstone aquifer. *Ground Water* **2006,** *44*, (4), 518-527.
52. Weaver, T. R.; Bahr, J. M., Geochemical evolution in the Cambrian-Ordovician sandstone aquifer, eastern Wisconsin: 2. Correlation between flow paths and ground-water chemistry. *Ground Water* **1991,** *29*, (4), 510-515.
53. Weaver, T. R.; Bahr, J., Geochemical evolution in the Cambrian-Ordovician sandstone aquifer, eastern Wisconsin: 1. Major ion and radionuclide distribution. *Ground Water* **1991,** *29*, (3), 350-356.
54. Vinson, D. S.; Lundy, J. R.; Dwyer, G. S.; Vengosh, A., Implications of carbonate-like geochemical signatures in a sandstone aquifer: Radium and strontium isotopes in the Cambrian Jordan aquifer (Minnesota, USA). *Chemical Geology* **2012,** *334*, 280-294.
55. Gilkeson, R. H. *Isotopic studies of the natural sources of radium in groundwater in Illinois*; 1984; pp 50-50.
56. Sun, H.; Semkow, T. M., Mobilization of thorium, radium and radon radionuclides in ground water by successive alpha-recoils. *Journal of Hydrology* **1998,** *205*, (1), 126-136.
57. Fleischer, R. L., Alpha-recoil damage: Relation to isotopic disequilibrium and leaching of radionuclides. *Geochimica et Cosmochimica Acta* **1988,** *52*, (6), 1459-1466.
58. Tricca, A.; Porcelli, D.; Wasserburg, G. J., Factors controlling the groundwater transport of U, Th, Ra, and Rn. *Journal of Earth System Science* **2000,** *109*, (1), 95-108.
59. IUPAC, *Compendium of Chemical Terminology*. Blackwell Scientific Publications: Oxford, 1997.
60. Krishnaswami, S.; Graustein, W. C.; Turekian, K. K.; Dowd, J. F., Radium, thorium and radioactive lead isotopes in groundwaters: Application to the in situ determination of adsorption-desorption rate constants and retardation factors. *Water Resources Research* **1982,** *18*, (6), 1663-1675.
61. Tricca, A.; Wasserburg, G. J.; Porcelli, D.; Baskaran, M., The transport of U-and Th-series nuclides in a sandy unconfined aquifer. *Geochimica et Cosmochimica Acta* **2001,** *65*, (8), 1187-1210.
62. Cowart, J. B., Uranium isotopes and 226Ra content in the deep groundwaters of the Tri-State region, U.S.A. *Journal of Hydrology* **1981,** *54*, (1), 185-193.
63. Lively, R. S.; Jameson, R.; Alexander Jr, E. C.; Morey, G. B., Information Circular 36. Radium in the Mt. Simon-Hinckley Aquifer, East-Central and Southeastern Minnesota. **1992**.
64. Craft, E. S.; Abu-Qare, A. W.; Flaherty, M. M.; Garofolo, M. C.; Rincavage, H. L.; Abou-Donia, M. B., Depleted and Natural Uranium: Chemistry and Toxicological Effects. *Journal of Toxicology and Environmental Health, Part B* **2004,** *7*, (4), 297-317.
65. Ginder-Vogel, M.; Fendorf, S., Chapter 11 Biogeochemical Uranium Redox Transformations: Potential Oxidants of Uraninite. In *Developments in Earth and Environmental Sciences*, Barnett, M. O.; Kent, D. B., Eds. Elsevier: 2007; Vol. 7, pp 293-319.
66. Wang, Z.; Lee, S.-W.; Catalano, J. G.; Lezama-Pacheco, J. S.; Bargar, J. R.; Tebo, B. M.; Giammar, D. E., Adsorption of Uranium(VI) to Manganese Oxides: X-ray Absorption Spectroscopy and Surface Complexation Modeling. *Environmental Science & Technology* **2013,** *47*, (2), 850-858.
67. Reynolds, B. C.; Wasserburg, G. J.; Baskaran, M., The transport of U- and Th-series nuclides in sandy confined aquifers. *Geochimica et Cosmochimica Acta* **2003,** *67*, (11), 1955-1972.

68. Giammar, D., Geochemistry of uranium at mineral-water interfaces: rates of sorption-desorption and dissolution-precipitation reactions. **2001**.
69. Nolan, J. P., Mobilization of naturally occurring uranium in sediment into groundwater. *ETD collection for University of Nebraska - Lincoln* **2016**.
70. Cotton, S., *Lanthanide and Actinide Chemistry*. John Wiley & Sons, Ltd: Uppingham School, 2006.
71. Swarzenski, P. W.; Baskaran, M.; Rosenbauer, R. J.; Edwards, B. D.; Land, M., A combined radio-and stable-isotopic study of a California coastal aquifer system. *Water* **2013,** *5*, (2), 480-504.
72. Martin, P.; Akber, R. A., Radium isotopes as indicators of adsorption–desorption interactions and barite formation in groundwater. *Journal of Environmental Radioactivity* **1999,** *46*, (3), 271-286.
73. Beneš, P.; Strejc, P., Interaction of radium with freshwater sediments and their mineral components. *Journal of Radioanalytical and Nuclear Chemistry Articles* **1986,** *99*, (2), 407-422.
74. Ames, L. L.; McGarrah, J. E.; Walker, B. A.; Salter, P. F., Uranium and radium sorption on amorphous ferric oxyhydroxide. *Chemical Geology* **1983,** *40*, (1), 135-148.
75. Ames, L. L.; McGarrah, J. E.; Walker, B. A., Sorption of trace constituents from aqueous solutions onto secondary minerals. II. Radium. *Clays and clay minerals* **1983,** *31*, (5), 335-342.
76. Chen, M. A.; Kocar, B. D., Radium Sorption to Iron (Hydr)oxides, Pyrite, and Montmorillonite: Implications for Mobility. *Environmental Science & Technology* **2018,** *52*, (7), 4023-4030.
77. Bassot, S.; Mallet, C.; Stammose, D., Experimental Study and Modeling of the Radium Sorption onto Goethite. *MRS Proceedings* **2000,** *663*, 1081.
78. Tachi, Y.; Shibutani, T.; Sato, H.; Yui, M., Experimental and modeling studies on sorption and diffusion of radium in bentonite. *Journal of Contaminant Hydrology* **2001,** *47*, (2), 171-186.
79. Missana, T.; Colàs, E.; Grandia, F.; Olmeda, J.; Mingarro, M.; García-Gutiérrez, M.; Munier, I.; Robinet, J.-C.; Grivé, M., Sorption of radium onto early cretaceous clays (Gault and Plicatules Fm). Implications for a repository of low-level, long-lived radioactive waste. *Applied Geochemistry* **2017,** *86*, 36-48.
80. Komarneni, S.; Kozai, N.; Paulus, W. J., Environment: Superselective clay for radium uptake. *Nature* **2001,** *410*, (6830), 771-771.
81. Alhajji, E.; Al-Masri, M. S.; Khalily, H.; Naoum, B. E.; Khalil, H. S.; Nashawati, A., A Study on Sorption of 226Ra on Different Clay Matrices. *Bulletin of Environmental Contamination and Toxicology* **2016,** *97*, (2), 255-260.
82. Tamamura, S.; Takada, T.; Tomita, J.; Nagao, S.; Fukushi, K.; Yamamoto, M., Salinity dependence of 226Ra adsorption on montmorillonite and kaolinite. *Journal of Radioanalytical and Nuclear Chemistry* **2014,** *299*, (1), 569-575.
83. Nathwani, J. S.; Phillips, C. R., Adsorption of 226Ra by soils in the presence of Ca2+ ions. Specific adsorption (II). *Chemosphere* **1979,** *8*, (5), 293-299.
84. McMahon, P. B.; Chapelle, F. H., Redox processes and water quality of selected principal aquifer systems. *Ground Water* **2008,** *46*, (2), 259-271.
85. Curti, E., Coprecipitation of radionuclides with calcite: estimation of partition coefficients based on a review of laboratory investigations and geochemical data. *Applied Geochemistry* **1999,** *14*, (4), 433-445.

86. Zhang, T.; Gregory, K.; Hammack, R. W.; Vidic, R. D., Co-precipitation of radium with barium and strontium sulfate and its impact on the fate of radium during treatment of produced water from unconventional gas extraction. *Environmental Science and Technology* **2014,** *48*, (8).
87. Zhu, C., Coprecipitation in the barite isostructural family: 1. binary mixing properties. *Geochimica et Cosmochimica Acta* **2004,** *68*, (16), 3327-3337.

Chapter 2

Effect of geochemical conditions on radium mobility in discrete intervals within the Midwestern Cambrian-Ordovician aquifer system

2.1 Abstract

Radium (Ra) commonly occurs in groundwater obtained from the Midwestern Cambrian-Ordovician aquifer system (MCOAS) at activities approaching and exceeding the United States Environmental Protection Agency's Maximum Contaminant Level (MCL) of 5 pCi/L for combined ^{226}Ra and ^{228}Ra. The occurrence of Ra(II) in groundwater is dependent on a number of factors, including the prevalence of parent radionuclides within hydrogeological strata, as well as aquifer geochemical conditions. Interbedded aquifer and aquitard sequences within the MCOAS are stratified with respect to Ra(II) activity and geochemical conditions, and thus the formations that serve as Ra(II) sources to groundwater remain poorly constrained. This study analyzes aqueous samples collected from short-screened wells at various depths within the MCOAS near Madison, WI, USA, to determine geochemical parameters including dissolved oxygen; pH; major and minor ions; and metals, including ^{226}Ra, ^{228}Ra, and parent isotopes ^{238}U and ^{232}Th. Additionally, the elemental composition of aquifer solids is determined as a function of depth. Within solid phases, ^{238}U and ^{232}Th occur in both fine-grained facies and as coatings on sandstone minerals. Most groundwater samples contain dissolved combined Ra(II) lower than 2.5 pCi/L; however, one well completed in the unconfined and one well completed in the confined portion of the groundwater system exceed 3.5 pCi/L. In the confined system, anoxic

Reproduced with permission from *Applied Geochemistry*. Mathews, M.; Gotkowitz, M. B.; Ginder-Vogel, M. 2018, 97, 238-246. Mathews and Gotkowitz completed field work; Mathews completed all data analyses; Mathews, Gotkowitz, and Ginder-Vogel wrote the manuscript.

conditions are associated with elevated Ra(II) concentrations, while in the upper, oxic aquifer, elevated total dissolved solids are positively related to Ra(II). These results demonstrate that multiple factors impact Ra(II) sources and mobility in the regionally unconfined portion of the MCOAS.

2.2 Introduction

Radium (Ra) is a naturally occurring, radioactive contaminant, present in many groundwater systems. Ingestion of Ra is a human health concern, as it accumulates in bone tissue, where it continues to undergo radioactive decay.[1-7] Long-term exposure may damage cell tissue and is related to various types of bone disease. The United States Environmental Protection Agency (EPA) regulates Ra in drinking water at a maximum contaminant level (MCL) for Ra in drinking water of 5 pCi/L for the combined total of isotopes ^{226}Ra and ^{228}Ra.[8]

One source of radium to groundwater is the radioactive decay of parent elements uranium (U) and thorium (Th) (Figure A-1).[9-15] These parent isotopes are common to fine-grained sedimentary deposits, such as shale and siltstone, and/or transition metal (e.g., Fe and Mn) (hydr)oxide coatings on mineral grains.[11,16,17] Elevated concentrations of U and Th have also been observed in Precambrian crystalline bedrock.[18] Saline brines are also a possible source of dissolved U and Ra(II) to groundwater systems. During Pleistocene glaciation, increased pore pressure in the Lake Michigan basin, resulting from the overlying Laurentide ice sheet, may have driven saline groundwater West, providing a potential source of elevated Ra(II) concentrations in the Eastern portion of the MCOAS.[19-21]

Once in groundwater, Ra(II) mobility is largely controlled by sorption to transition metal (e.g., Fe and Mn) (hydr)oxide minerals and/or co-precipitation with barite ($BaSO_4$). These

processes are affected by local aquifer geochemical conditions.[14,16,22] For example, in the MCOAS, elevated dissolved Ra(II) is generally correlated with low pH, low dissolved oxygen (DO), and high total dissolved solids (TDS).[10,17,23-29] Reducing conditions are often associated with elevated dissolved Ra(II), because these conditions do not favor the presence of transition metal (hydr)oxides.[12,13,15,23,25,30-32] Elevated ionic strength is also associated with elevated dissolved Ra(II), due to sorption-site competition.[13,33] Within sulfate-rich, oxic aquifer systems, such as a regionally unconfined portion of the MCOAS in Southeast Wisconsin, co-precipitation with BaSO4 may limit dissolved Ra(II).[13,17]

Elevated dissolved Ra(II) is common to the MCOAS, and is commonly associated with anoxic conditions and elevated ionic strength.[13,25] Similar trends are observed throughout Wisconsin.[17,25,34] However, these studies rely on water samples collected from municipal wells open to hundreds of meters of aquifer, resulting in water produced from multiple hydrostratigraphic units.[13,17,20,22,25,29] This makes it difficult to attribute the geologic source of Ra to specific strata within the groundwater system.

This study investigates sources of dissolved Ra(II) within discrete hydrostratigraphic units in the MCOAS near Madison, Wisconsin, where the upper and lower sandstone aquifers are separated by a locally-confining shale aquitard.[20,35] Possible sources of Ra to groundwater include Ra-bearing aquifer solids, such as oxide rinds on silicate minerals; shales or other fine-grained, interbedded strata enriched in parent isotopes; and deep brines.[17,19,29,36-38] Here, water samples collected from a network of twenty-one short-screened monitoring wells, at depths ranging from 12 to 139 m, are analyzed to determine ^{226}Ra, ^{228}Ra, ^{238}U, ^{232}Th, ionic composition, pH, specific conductance, and DO (Figure 2.1). The elemental composition of aquifer solids is also determined. These data provide insight into the geologic sources of Ra and the geochemical

conditions that promote the mobility of Ra(II) within discrete hydrostratigraphic intervals.

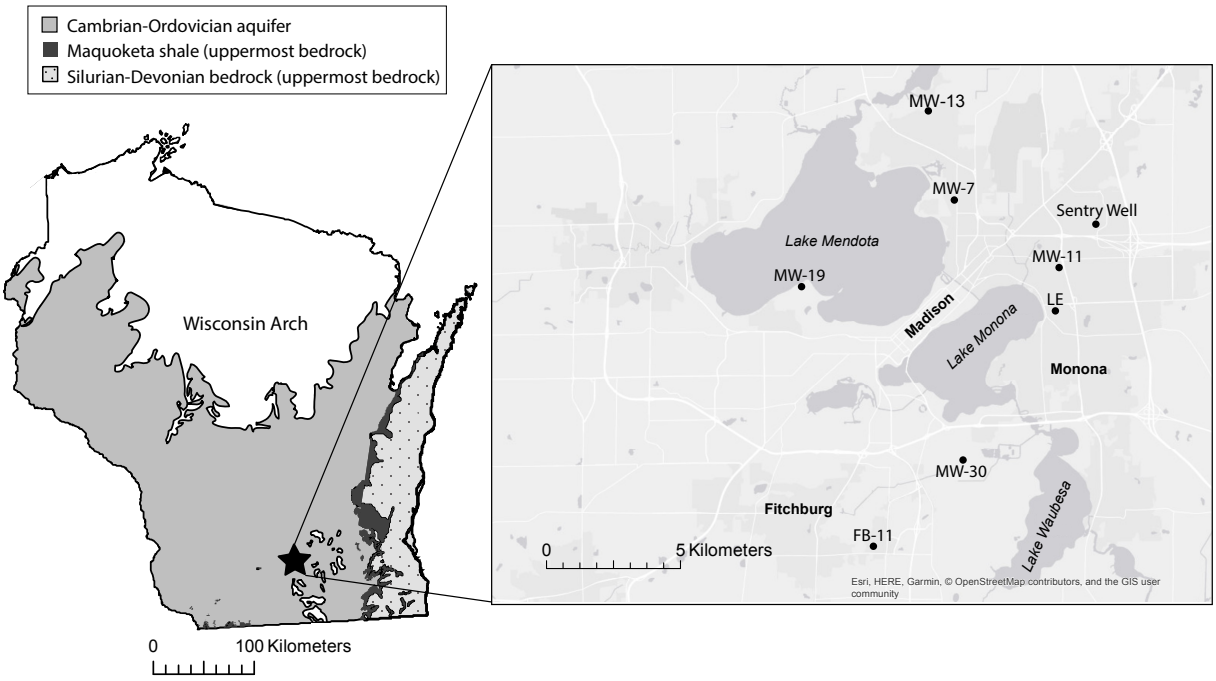

Figure 2.1 Extent of the Cambrian-Ordovician aquifer in Wisconsin. The Maquoketa shale underlies the Silurian-Devonian bedrock to the east, but forms the uppermost bedrock over a narrow area west of the Silurian. The inset map shows distribution of study sites; each site hosts multiple wells at various depths.

2.3 Materials and Methods

2.3.1 Regional hydrogeology

As discussed in Young and Siegel (1992), the MCOAS extends across much of the Midwestern United States, including parts of Minnesota, Wisconsin, Iowa, Missouri, and Illinois. It consists of a complexly layered sequence of sedimentary aquifers, with interbedded confining units, overlain by unconsolidated glacial drift. Crystalline Precambrian rock forms the base of the system and is overlain by marine-deposited Paleozoic sandstones, dolostones, and shales. These formations range from the Late Cambrian to Late Devonian age, with stratigraphic

units increasing in thickness away from the arches and toward basins. In Wisconsin, these layered sedimentary sequences slope from the Wisconsin Arch toward the Michigan basin in the East, the Illinois basin in the South, and toward Iowa and Minnesota to the West. The Maquoketa Shale confines much of the MCOAS in Eastern Wisconsin, but it is absent in Central and Western Wisconsin (Figure 2.1).[35]

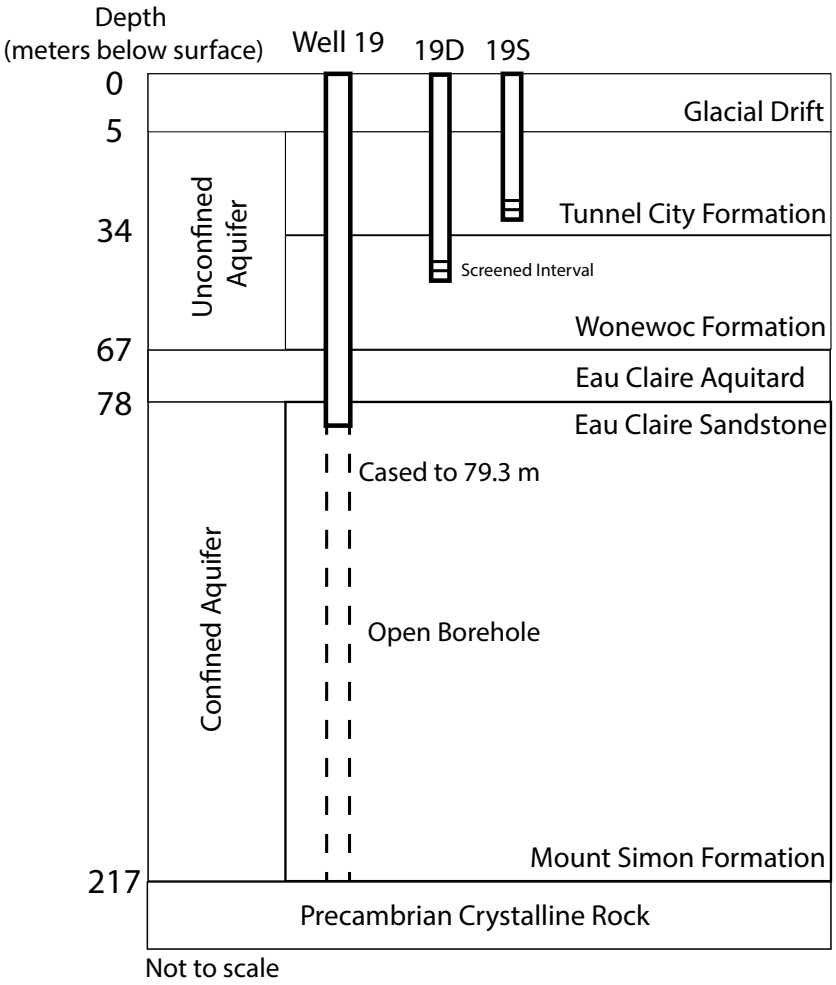

Figure 2.2 Representative hydrostratigraphy and well construction at the municipal well field site. Municipal wells such as Well 19 are open boreholes below the casing, while monitoring wells like MW-19D and MW-19S are screened across short intervals within hydrostratigraphic units. Figure not to scale.

Table 2.1 Sample field measurements and radium activity results from various sampling seasons. The Minimum Detectable Activity at a 95 % confidence interval is represented by MDA 95. Ports sampled from the Sentry Well are represented as SW. *Not applicable **Samples were not collected for analysis.

Sample ID	Sampling Date	Screen Midpoint (meters below surface)	Screen Length (meters)	Hydrostratigraphic Unit	pH	Temperature (°C)	Specific conductance (µS/cm)	DO (mg/L)	Radium-228 (pCi/L)	Radium-226 (pCi/L)	Combined Radium (pCi/L)
MW-PL1	10/27/16	*	*	Control	*	*	*	*	0.7 ± 0.4	0.5 ± 0.3	1.1 ± 0.5
MW-PL2	5/31/17	*	*	Control	*	*	*	*	< MDA 95	< MDA 95	< MDA 95
MW-7S	10/24/16	12	5	Tunnel City	7.1	12.2	3030	**	0.7 ± 0.4	0.4 ± 0.2	1.1 ± 0.4
MW-7S	5/30/17	12	5	Tunnel City	6.8	13.4	2390	9.1	< MDA 95	0.5 ± 0.3	0.9 ± 0.7
MW-11S	10/21/16	13	3	Tunnel City	7.0	11.2	2240	**	1.4 ± 0.5	0.7 ± 0.3	2.1 ± 0.6
MW-11S	5/25/17	13	3	Tunnel City	6.9	12.4	2300	7.3	< MDA 95	0.5 ± 0.3	< MDA 95
MW-19S	10/14/16	16	5	Tunnel City	7.3	12.2	1390	**	< MDA 95	0.3 ± 0.2	0.6 ± 0.4
MW-19S	12/11/17	16	5	Tunnel City	6.3	12.8	1250	8.8	**	**	**
MW-30S	10/14/16	19	5	Tunnel City	7.3	10.6	920	**	< MDA 95	0.2 ± 0.1	< MDA 95
MW-30S	12/11/17	19	5	Tunnel City	6.8	11.3	800	8.5	**	**	**
MW-13S	10/24/16	16	3	Tunnel City	7.2	11.3	1630	**	1.0 ± 0.4	0.10 ± 0.07	1.1 ± 0.4
MW-13S	12/11/17	16	3	Tunnel City	6.3	11.9	1030	9.9	**	**	**
SW – port 1	10/17/16	27	1.5	Tunnel City	7.3	13.0	1400	**	< MDA 95	0.5 ± 0.2	0.7 ± 0.5
SW – port 1	5/25/17	27	1.5	Tunnel City	7.0	11.3	1770	7.8	**	**	**
FB-11S	10/14/16	31	1.5	Tunnel City	7.5	10.0	830	**	0.4 ± 0.4	0.2 ± 0.1	0.6 ± 0.4
FB-11S	5/22/17	31	1.5	Tunnel City	7.2	11.1	1010	9.5	< MDA 95	< MDA 95	< MDA 95
MW-13D	10/24/16	34	1.5	Tunnel City	7.2	11.2	870	**	< MDA 95	0.4 ± 0.2	0.5 ± 0.4
MW-13D	12/11/17	34	1.5	Tunnel City	6.3	11.5	810	9.1	**	**	**
MW-30D	10/14/16	41	1.5	Tunnel City	7.4	10.5	850	**	< MDA 95	0.2 ± 0.1	1.23 ± 0.52
MW-30D	5/25/17	41	1.5	Tunnel City	6.9	11.2	1040	8.9	0.8 ± 0.5	0.4 ± 0.3	0.5 ± 0.5
FB-11D	10/14/16	52	1.5	Tunnel City	7.5	10.4	570	**	0.7 ± 0.5	0.4 ± 0.2	1.1 ± 0.5
FB-11D	12/11/17	52	1.5	Tunnel City	7.1	10.7	510	10.6	**	**	**

MW-11D	10/21/16	23.5	1.5	Wonewoc	7.1	11.4	1290	**	1.7 ± 0.6	0.6 ± 0.3	2.3 ± 0.7
MW-11D	5/22/17	23.5	1.5	Wonewoc	7.1	12.2	1460	5.8	< MDA 95	< MDA 95	< MDA 95
MW-7D	10/24/16	29	3	Wonewoc	7.1	11.8	2650	**	1.3 ± 0.5	0.8 ± 0.3	2.1 ± 0.6
MW-7D	5/30/17	29	3	Wonewoc	6.6	13.0	2810	10.4	1.1 ± 0.6	1.0 ± 0.4	2.1 ± 0.7
MW-19D	10/14/16	42	1.5	Wonewoc	7.2	11.7	2410	**	3.6 ± 0.6	1.6 ± 0.3	5.2 ± 0.6
MW-19D	5/22/17	42	1.5	Wonewoc	7.0	12.3	2110	10.6	3.4 ± 0.6	1.8 ± 0.4	5.2 ± 0.8
MW-19D	12/11/17	42	1.5	Wonewoc	6.3	12.0	1520	10.1	**	**	**
SW – port 2	10/17/16	63	1.5	Wonewoc	7.3	12.6	590	**	0.5 ± 0.4	0.09 ± 0.08	0.6 ± 0.5
SW – port 2	5/25/17	63	1.5	Wonewoc	7.2	11.3	710	8.2	**	**	**
MW-7VD	10/24/16	64	3	Wonewoc	7.3	11.0	820	**	1.2 ± 0.5	0.6 ± 0.3	1.8 ± 0.6
MW-7VD	5/30/17	64	3	Wonewoc	6.9	12.1	980	2.1	< MDA 95	0.3 ± 0.2	< MDA 95
LE-D	10/21/16	71	1.5	Wonewoc	7.3	10.9	620	**	< MDA 95	MDA 95	< MDA 95
LE-D	5/30/17	71	1.5	Wonewoc	6.7	11.9	760	2.8	< MDA 95	0.3 ± 0.2	< MDA 95
SW – port 3	5/12/16	81.5	1.5	Eau Claire aquitard	7.3	13.5	590	**	< MDA 95	< MDA 95	< MDA 95
SW – port 3	5/25/17	81.5	1.5	Eau Claire aquitard	7.2	11.4	720	6.3	**	**	**
SW – MS-132	10/17/16	91	1.5	Mount Simon	7.4	12.3	640	**	< MDA 95	0.4 ± 0.2	0.8 ± 0.6
SW – MS-132	5/25/17	91	1.5	Mount Simon	7.3	12	760	5.5	< MDA 95	0.3 ± 0.2	< MDA 95
LE-VD	10/21/16	81	1.5	Mount Simon	7.2	10.8	700	**	1.0 ± 0.4	0.8 ± 0.2	1.8 ± 0.5
LE-VD	5/30/17	81	1.5	Mount Simon	6.6	11.9	860	0.1	0.8 ± 0.5	0.4 ± 0.2	1.2 ± 0.5
SW – port 5	10/17/16	124	6	Mount Simon	7.4	12.0	570	**	1.1 ± 0.4	1.0 ± 0.3	2.1 ± 0.5
SW – port 5	5/25/17	124	6	Mount Simon	7.4	11.6	770	0.2	1.0 ± 0.5	0.9 ± 0.3	1.9 ± 0.6
SW – port 6	10/21/16	139	6	Mount Simon	7.7	12.0	630	**	2.0 ± 0.5	1.8 ± 0.4	3.8 ± 0.6
SW – port 6	5/25/17	139	6	Mount Simon	7.2	12.8	760	0.0	2.1 ± 0.5	2.5 ± 0.5	4.6 ± 0.7

2.3.2 Local hydrogeology and sampling sites

This study examines Ra(II) concentration and groundwater geochemistry in the MCOAS near Madison, Wisconsin, which is about 250 m thick in this region.[39] Relatively impermeable Precambrian crystalline rock forms the base of the Cambrian groundwater system and is overlain by the coarse- to medium-grained sandstone of the Mount Simon Formation. The Eau Claire Formation, which overlies the Mount Simon, consists of an upper sandstone facies underlain by interbedded siltstone and shale layers. These fine-grained deposits make up the locally extensive Eau Claire aquitard, which varies from 0 to 15 m in thickness across the greater Madison region. The aquitard restricts the exchange of water between the overlying formations and the underlying Mount Simon sandstone (Figure 2.1). The dolomitic Eau Claire sandstone forms the base of the upper bedrock aquifer and is overlain by the quartz sandstone of the Wonewoc Formation and the glauconitic sandstone of the Tunnel City Formation. In upland areas, the water table lies within the upper-most bedrock formations. In low-lying areas near the lakes and streams, the water table is relatively shallow and lies within saturated fine-grained till and lacustrine sediment that overlie bedrock. Land use in the study area is principally urban; however, agricultural areas surround the area. Extensive pumping for regional water supplies has reversed pre-development conditions, resulting in downward hydraulic gradients from the upper, unconfined aquifer to the deep, confined aquifer, over much of the study area.[39]

A network of twenty-one monitoring wells, with screen lengths ranging from 1.5 to 6.0 m, were sampled during this study. The wells are distributed across eight field sites in the greater Madison area, with six of these sites associated with nearby municipal wells (Figure 2.1). Each of the field sites hosts two monitoring wells at various depths, with the exception of MW-7, which has three monitoring wells, and the Sentry Well (Table 2.1, Figure 2.2). The Sentry Well contains a FLUTe™ multi-level

sampling device that consists of six sampling ports at a variety of depths, isolated from each other with hydraulic seals. The well network was installed for an unrelated study; construction details are described in Gotkowitz et al. (2016).[40] The monitoring wells target specific hydrostratigraphic units and are completed in the Tunnel City Formation (n = 10), the Wonewoc Formation (n = 6), the Eau Claire aquitard (n = 1), and the Mount Simon Formation (n = 4). For the purposes of this study, wells completed above the aquitard are referred to as unconfined. Wells screened within or below the aquitard are described as confined. Dedicated gas displacement pumps were used to purge and collect samples from the ports of the Sentry Well. A submersible electric pump was used to sample all other wells.

2.3.3 Groundwater characterization

During the Fall of 2016, all twenty-one monitoring wells in the study were sampled. A subset of thirteen wells were sampled a second time, in the spring of 2017. These wells were selected to include wells above and below the aquitard. Prior to sample collection, monitoring wells were purged of approximately 10 well volumes, using a stainless-steel submersible pump. Sentry well (SW) ports were purged a minimum of five times over a two-day period, prior to sample collection.

During both sampling campaigns, pH, temperature, and specific conductance were measured in the field following purging. DO was also measured in a flow-through cell during the second round of sampling. Samples for Ra(II) analysis were not filtered, in order to remain consistent with compliance sampling methods required of municipal water supply systems, and preserved with concentrated nitric acid to pH $\leq$ 2. Samples for aqueous metals analysis were field-filtered (0.45 μm) and acid preserved (pH $\leq$ 2), while samples for inorganic ion were

filtered. Both types of samples were stored at 4 °C until further analysis. Analysis for uranium (^{238}U) and thorium (^{232}Th) was conducted on samples collected during the second round of sampling.

^{226}Ra and ^{228}Ra analyses were conducted by Eurofins Eaton Analytical, Inc., in a manner consistent with the Georgia Tech method.[41] Radium values at or below the instrumental detection level were designated as Minimum Detectable Activity (MDA) or < MDA and have a value of 0 pCi/L on figures; the MDA is the concentration that can be measured with ± 100% certainty at the 95% confidence level. Analysis of ^{238}U and ^{232}Th was conducted, using a ThermoScientific ELEMENT2 High Resolution inductively coupled plasma mass spectrometer (Table A–1). A Dionex ICS-2100 ion chromatography system was used to determine the concentration of nitrate (NO_3^-), sulfate (SO_4^{2-}), and chloride (Cl^-) in water samples (Table A–1). A PerkinElmer Optima 4300 DV inductively-coupled plasma optical emission spectrometer was used to quantify dissolved barium (Ba^{2+}), calcium (Ca^{2+}), iron (Fe^{2+}), magnesium (Mg^{2+}), manganese (Mn^{2+}), and sodium (Na^+) in aqueous samples (Table A–1). Tritium (^3H) concentrations were compiled from previous studies conducted at these wells by the Wisconsin Geological and Natural History Survey (WGNHS) (Table A–2).[42]

A quality control sample was collected during each sampling round to evaluate the potential contribution of Ra(II) from field equipment. Control samples were collected by flushing the submersible pump and tubing with 40 L of ultrapure water, followed by collection of 4 L of ultrapure water for analysis. Sample MW-PL1 was collected through the entire length of the tubing in 2016, while MW-PL2 was collected through a short length (5 m) of tubing.

2.3.4 Solid-phase characterization

Aquifer solids were selected from well cuttings archived at the WGNHS. Cuttings collected during the construction of municipal well 19 in 1969 were available at 1.5 m intervals from the surficial glacial drift to the Precambrian crystalline bedrock at 219 m below ground surface (Figure 2.2). Cuttings were prepared by placing in a medical grade polyethylene sample container, with a piece of 4.0 μm polypropylene thin film secured across the vial top by a rubber band. Elemental composition was determined using a Thermo Fisher Niton XL3t GOLDD+ hand-held X-ray fluorescence (XRF) analyzer. The vial was turned to allow cuttings to rest on the film across the XRF stage.[43,44]

XRF analysis was conducted in "Test All Geo" mode, using the 8 mm aperture opening and a 50 kV beam, following established procedures.[44] A 105-s total filter duration time (main filter 30 s, light filter 30 s, low filter 30 s, and high filter 15 s) was applied to each sample. XRF analysis was monitored using standards from the United States Geological Survey (USGS) for shale, carbonate, and quartz sandstone. Minimum detection limits for Ra parent isotopes were 1.24 mg/L for thorium and 2 mg/L for uranium.[45] Geologic and geophysical logs available from the WGNHS were compared with the XRF results to identify the depth and thickness of hydrostratigraphic intervals.

Table 2.2 Redox category designation.[25,46]

Redox Process	DO (mg/L)	Mn(II) (mg/L)	Number of Wells
Oxic	≥ 0.5	< 0.05	18
Suboxic	< 0.5	< 0.05	1
Anoxic	≤ 0.5	≥ 0.05	2

2.4 Results

The pH of the samples ranged from 6.3 to 7.7, while the specific conductance values

ranged from 510 to 3030 µS/cm (Table 2.1). Tritium, an indicator of groundwater age, ranged from < 0.8 to 11 ± 2 TU in the unconfined aquifer and from < 0.8 to 5.3 ± 0.6 TU in the confined system (Figure A-2, Table A–2).

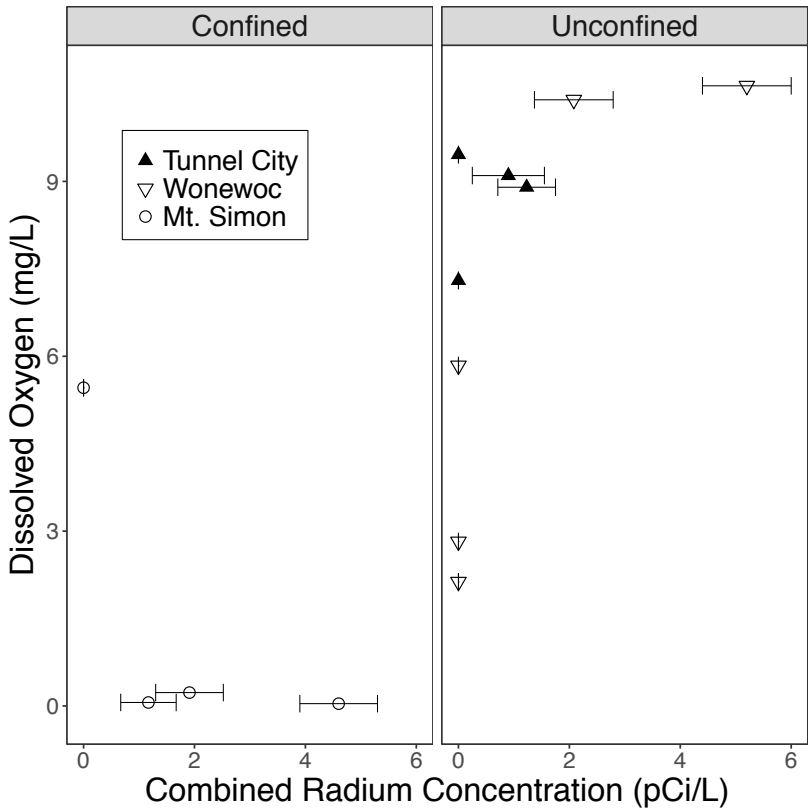

Figure 2.3 The relationship between combined radium concentration ($^{226}Ra + ^{228}Ra$) and DO from spring 2017 sampling, distinguished by hydrostratigraphic unit and aquifer designation. Error estimates are shown for combined Ra(II) concentrations above minimum detectable activity at the 95 % confidence level (MDA 95); values at or below MDA 95 are represented as 0 pCi/L.

Overall, concentrations of parent isotopes ^{238}U and ^{232}Th were low in groundwater. Aqueous ^{238}U concentrations ranged from 0.0004 ± 0.00001 to 5.3 ± 0.1 µg/L, while ^{232}Th ranged from non-detectable to 0.005 ± 0.002 µg/L (Figure 2.4). The sample with the highest ^{238}U concentration, 5.3 ± 0.1 µg/L, was collected from the Mount Simon, just below the Eau Claire. The DO concentration in groundwater varied between the upper aquifer and the underlying

confined aquifer (Table 2.2). Based upon these measurements, 18 wells were oxic (DO ≥ 0.5 mg/L, Mn(II) < 0.05 mg/L), 1 well suboxic (DO < 0.5 mg/L, Mn(II) < 0.05 mg/L), and 2 wells anoxic (DO < 0.5 mg/L, Mn(II) ≥ 0.05 mg/L). In the confined aquifer, DO ranged from 0.04 to 5.46 mg/L, and Ra(II) ranged from < MDA 95 to 4.6 pCi/L. In the unconfined aquifer, DO concentrations ranged from 2.13 to 10.64 mg/L, and Ra(II) ranged from < MDA 95 to 5.2 pCi/L. Ra generally increased with increasing DO (Figure 2.3).

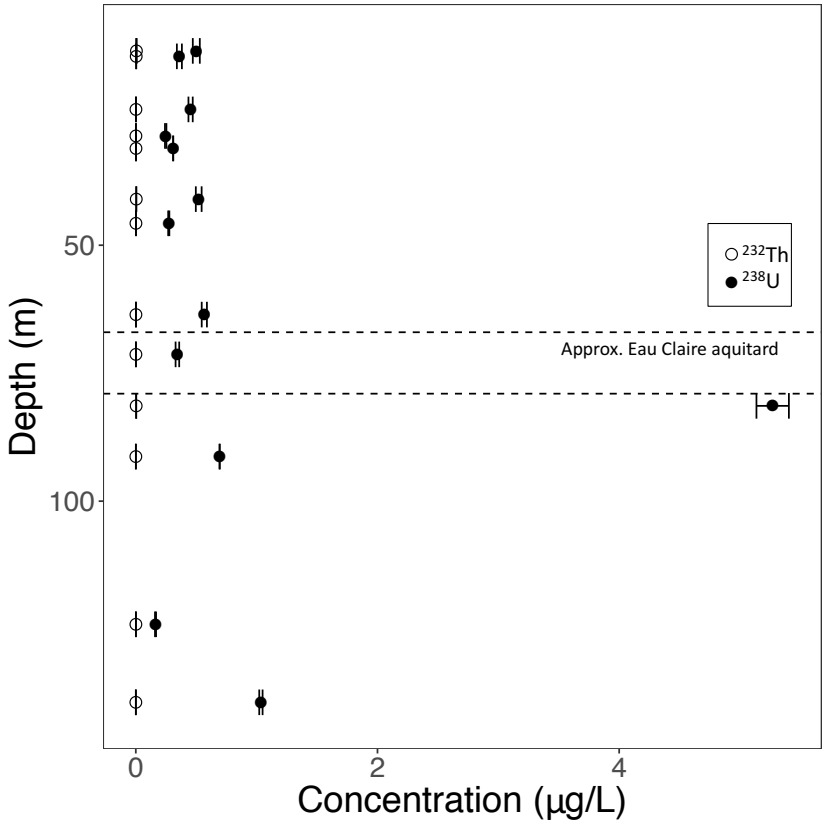

Figure 2.4 Aqueous concentrations of Ra parent isotopes, ^{238}U and ^{232}Th, as a function of depth below ground surface.

In this study, combined Ra(II) concentrations less than 1.1 ± 0.5 pCi/L were considered below the limit of quantification, due to the presence of combined Ra(II) at this concentration in control sample MW-PL1. The combined Ra(II) concentration in most groundwater samples

ranged from non-detectable to 2.2 pCi/L, with two wells, MW-19D and SW – port 6, exceeding this range (Figure 2.4). Wells with Ra(II) exceeding detection levels in Spring 2017 were at concentrations within the error bounds reported from the Fall 2016 samples, and other samples exhibited little variation. Both samples collected from well MW-19D, screened in the Wonewoc sandstone, contained 5.2 pCi/L Ra (II); all other samples completed in the unconfined aquifer had Ra(II) concentrations less than the MCL. Dissolved Ra(II) in well SW – port 3, the only well associated with the Eau Claire aquitard, was below the MDA. Among samples from the Mount Simon sandstone, the highest combined Ra(II) concentration, 4.6 ± 0.7 pCi/L, was collected from the deepest well, SW–port 6, at 139 m at depth.

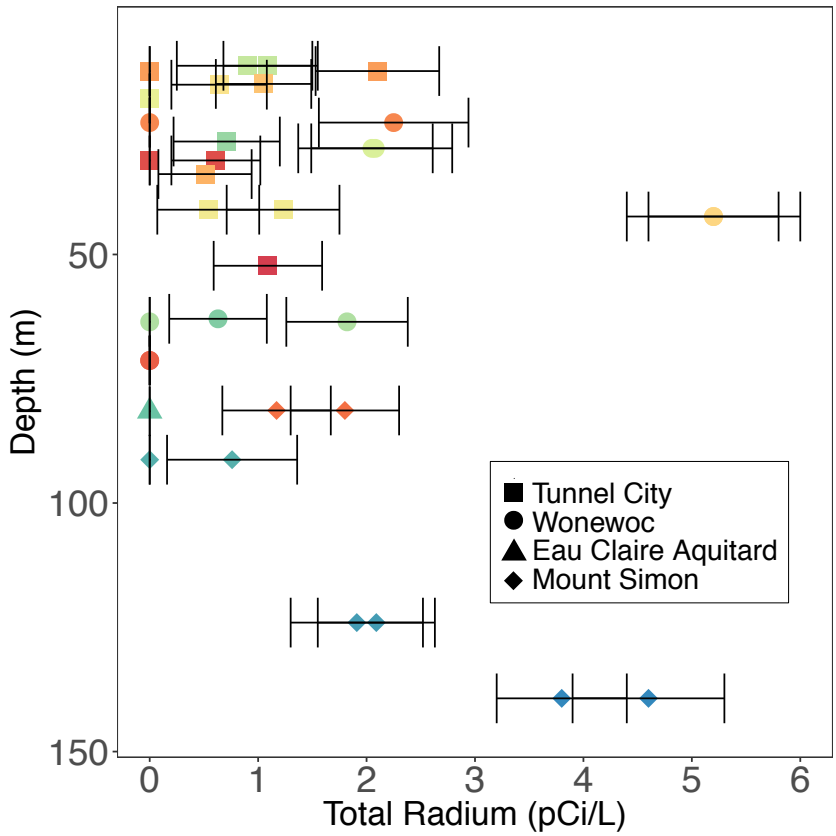

Figure 2.5 Combined radium concentration ($^{226}Ra+^{228}Ra$) by well depth from both sampling periods. Results from wells sampled twice to examine replicability are shown with the same color. Dissolved Ra(II) values at or below minimum detectable activity at the 95 % confidence interval (MDA 95) are plotted at 0 pCi/L.

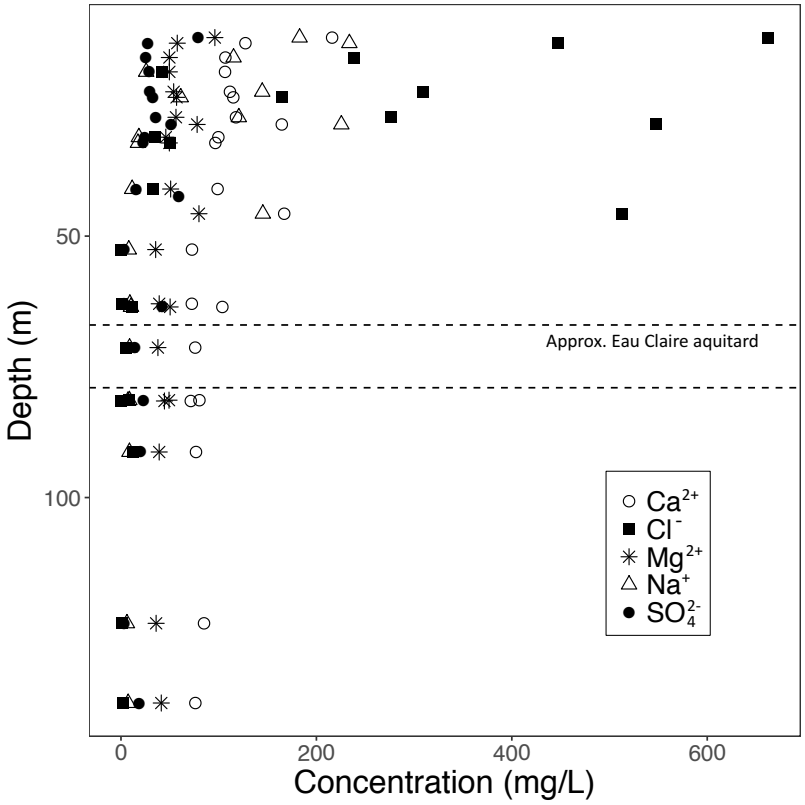

Figure 2.6 Concentration of major ions versus depth from surface, from monitoring wells in Madison, WI from 2016 samples.

Specific conductance, used here as an indicator of total dissolved solids, varied widely in groundwater, from 510 to 3030 µS/cm. The highest concentrations of Ca^{2+} (max. 220 mg/L at 12-m depth), Cl^- (max. 660 mg/L at 12-m depth), Mg^{2+} (max. 120 mg/L at 29-m depth), Na^+ (max. 240 mg/L at 29-m depth), and SO_4^{2-} (max. 79 mg/L at 12-m depth) were observed in wells completed in the unconfined aquifer. Major ion concentrations decreased with depth, as did specific conductance, which ranged from 570 to 860 µS/cm in wells completed in the confined system (Figures 2.6 and 2.7).

In general, there was a weak correlation between Ra(II) concentration and specific conductance in the Wonewoc sandstone ($r^2 = 0.54$) and the Tunnel City stratigraphic unit ($r^2 =$

0.25; Figure 2.7). Estimated Ba^{2+} activities, calculated according to the method described in Brezonik and Arnold (2011), did not vary significantly (p-value = 0.34) as a function of aquifer formation (Table A–1).[47] The calculated barite saturation index (SI) did not exceed a value of 1 for any of the samples collected in this study (Calculation A-4, Figure A-3). While Ba^{2+} concentration increased as sulfate concentration increased within the Wonewoc, this trend was not observed in groundwater from the Tunnel City unit (Figure A-3).

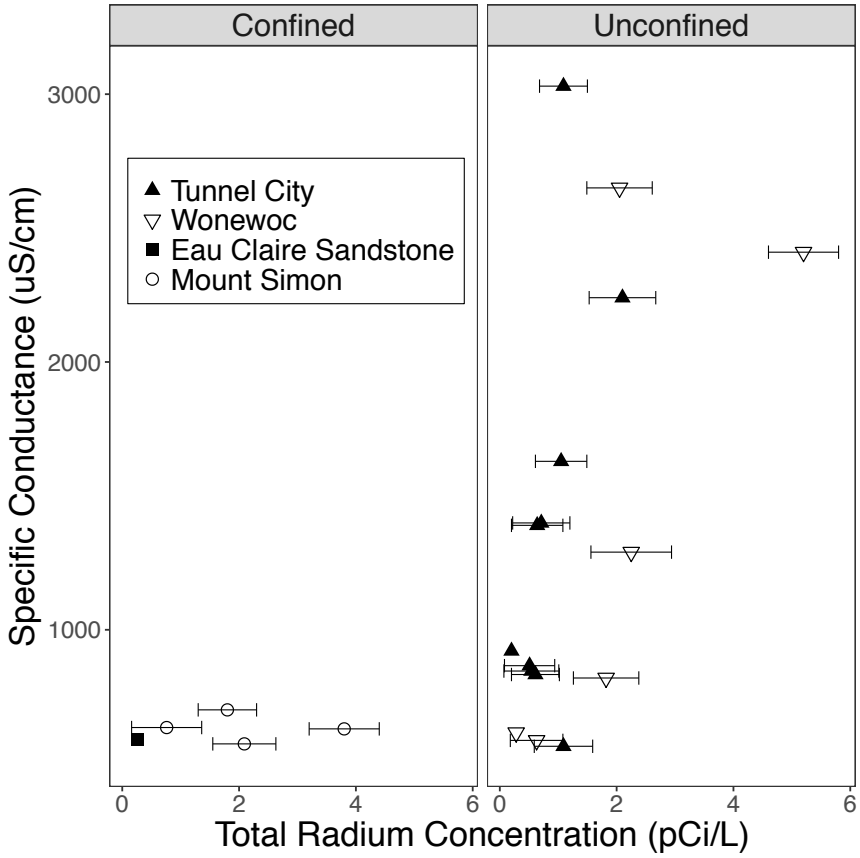

Figure 2.7 The relationship between combined radium (^{226}Ra + ^{228}Ra) and specific conductance from fall 2016 sampling, distinguished by hydrostratigraphic units and aquifer designation. Ra(II) concentrations at or below the minimum detectable activity at the 95 % confidence interval (MDA 95) are represented as 0 pCi/L.

Figure 2.8 Solid-phase elemental composition from X-ray fluorescence analysis of municipal well 19. Concentration scales differ for each element grouping. Elemental weight abundance is either presented as parts per million (ppm) or weight percent (%), defining 1 % = 10,000 ppm.

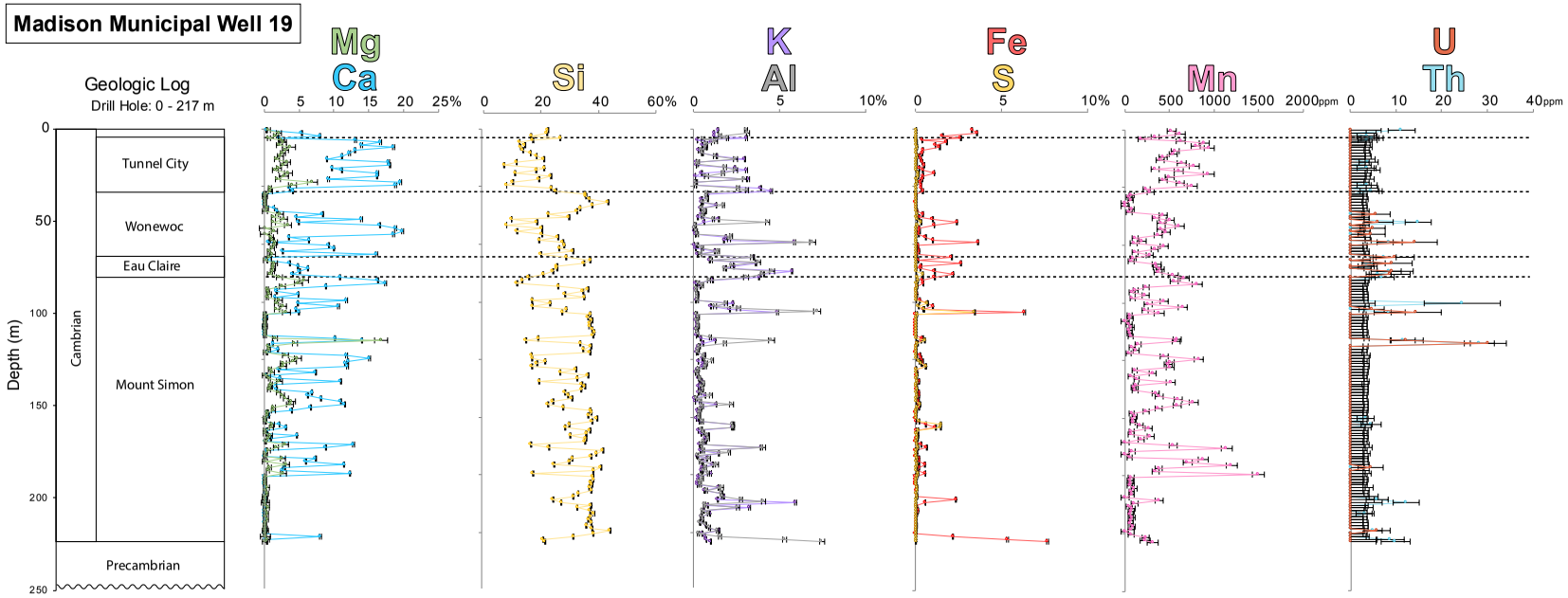

XRF analyses of aquifer solids from municipal Well 19 demonstrated the heterogeneity of elemental composition within discrete stratigraphic horizons (Figure 2.8). Primary elements at the study site included Si (median 30, ranging 8–45% by weight), Ca (median 4, ranging 0–20% by weight), and Mg (median 1, ranging 0–17% by weight). Samples with elevated K and Al indicated clay mineralogy (e.g., 67–78 m below the surface) and corresponded to the depth of the Eau Claire aquitard at well 19. Elevated Fe concentrations appear in the Wonewoc Formation (median 0.2, ranging 0–3.7% by weight), the Eau Claire Formation (median 1.1, ranging 0.2–2.7% by weight), and the Mount Simon Formation (median 0.1, ranging 0–6.3% by weight). Manganese concentrations in aquifer solids were more consistent, with a median of 0.02% by weight over the groundwater system, ranging 0–0.15% by weight. Solid-phase concentrations of U (median 8, ranging 0–10 mg/ kg) and Th (median 5, ranging 0–8 mg/kg) were notable in the Eau Claire aquitard (Figure 2.8). Elevated concentrations of U and Th were also observed at several depths in both the Wonewoc (U median 0, ranging 0–14 mg/kg; Th median 0, ranging 0–15 mg/kg) and Mount Simon sandstones (U median 0, ranging 0–30 mg/kg; Th median 0, ranging 0–28 mg/kg; Figure 2.8).

2.5 Discussion

This study focuses on determining dissolved Ra(II) concentrations in discrete hydrostratigraphic intervals, within a locally-confined region of the MCOAS, in order to build upon studies that rely on data from wells with long open intervals.[13,17,20,22,25,29] In this study, a majority of monitored depths have dissolved Ra(II) concentrations below background levels, but differences in geochemical conditions appear to result in locally elevated Ra(II).

Low DO, low pH, and/or high specific conductance in groundwater systems are often

correlated with Ra(II) concentrations above the MCL, both in general and within the MCOAS.[10,13,17,23-29] Groundwater in the study area is relatively neutral in pH (e.g., 6.3 to 7.7), and Ra(II) mobilization due to acidic conditions is unlikely (Table 2.1). The two wells with elevated dissolved Ra(II) are dissimilar (Figure 2.5, Table 2.1). MW-19D, completed in the unconfined aquifer, is oxic with elevated specific conductance; SW – port 6 is completed in the confined aquifer, and is anoxic with low dissolved solids. This suggests that multiple factors contribute to elevated Ra(II) in this setting.

Radium parent radionuclides (^{238}U and ^{232}Th) are found in association with fine-grained sedimentary layers, including shale aquitards, or oxide coatings on mineral grains.[17,20,36,37,48] Aqueous and solid-phase parent radionuclide concentrations are relatively low throughout most of the stratigraphic section in the study area (Figures 2.5 and 2.8). The solid-phase composition varies with depth; higher concentrations of U and Th occur in the Eau Claire aquitard, and the Wonewoc and Mount Simon Formations contain elevated U and Th (Figure 2.8). Since U and Th are present in the unconfined and confined aquifers and in the Eau Claire aquitard, production of Ra(II) via radioactive decay from U and Th can occur in any of these hydrostratigraphic units. However, shale layers, although enriched in parent nuclides, tend to have relatively low dissolved Ra(II), due to their high sorption capacity.[10,13,16] This is consistent with the less than detectable level of combined dissolved Ra(II) from SW – port 3, completed within the Eau Claire aquitard (Figure 2.5).

The 3H content of water is a general indicator of groundwater age. Eight wells produced water with low tritium (< 0.8 TU), suggesting that these wells produce old (pre-1950) water (Table A–2). Thirteen wells produced water with tritium > 4 TU, indicating more recent recharge, since 1950.[25] The two wells with dissolved Ra(II) above 3 pCi/L differ with respect to

tritium. Tritium at MW-19D, 10 ± 2 TU, indicates recently recharged groundwater, whereas tritium levels are below detection in SW – port 6.

Radium partitioning to Fe and/or Mn (hydr)oxides can decrease aqueous Ra(II) concentrations.[12-14] However, anoxic conditions contribute to Ra(II) mobility and an increase in concentrations, due to the absence or dissolution of these minerals.[11,13] In groundwater samples from the confined system, elevated Ra(II) is associated with low DO (Figure 2.3). In several samples obtained from the unconfined system, the DO content ranges from 2.1 to 7.3 mg/L, while Ra(II) remains undetectable. However, in five samples from the unconfined system with DO ≥ 8.9 mg/L, dissolved Ra(II) ranges from non-detectable to 5.2 pCi/L (Figure 2.3). Due to the oxic nature of the unconfined aquifer, the occurrence of elevated dissolved Ra(II) in the unconfined aquifer is not likely due to the absence of Fe and Mn (hydr)oxides.[13] Additionally, there is no evidence of elevated ^{238}U or ^{232}Th in the unconfined aquifer (Table A–1). This suggests that elevated dissolved Ra(II) in the unconfined aquifer is likely due to other geochemical conditions, discussed below.

Elevated dissolved Ra(II) is commonly correlated with elevated ionic strength.[26,32,49,50] In this study, concentrations of Ca^{2+}, Cl^{-}, Mg^{2+}, Na^{+}, and SO_4^{2-} are elevated in groundwater in the Tunnel City and Wonewoc hydrostratigraphic units (Figure 2.6). Increased specific conductance is also observed with elevated combined Ra(II) concentration in the unconfined aquifer (Figure 2.7). Despite the large range in TDS, water in all wells remains undersaturated with respect to $BaSO_4$ (Figure A-3). This indicates that $BaSO_4$ formation is likely not an important factor in controlling Ra(II) concentration in this setting.[13,17,25]

Geochemistry in the well pair, MW-19S and MW-19D, differ from each other. These wells, installed within 10 m of each other, are completed in the unconfined aquifer at depths of

16 and 42 m, respectively. Water from the deeper well, MW-19D, contains 5.2 pCi/L combined Ra (II), the highest concentration amongst the study wells, while Ra(II) is below the detection limit at MW-19S (Table 2.1). Consistent with greater Ra(II) mobility associated with elevated ionic strength, MW-19D had higher Cl^-, and TDS, than MW-19S. This, in addition to higher tritium at MW-19D, suggests good connectivity from the water table to MW-19D.[42,51] Elevated TDS and relatively young groundwater age at the deeper of the paired wells suggest the presence of a preferential flow pathway, such as a fracture, connecting MW-19D to the surface. Such fractures in the Tunnel City and Wonewoc Formations are well documented in the study area.[39,51] These results indicate that groundwater quality in the upper aquifer is affected by chloride-rich urban storm water impacted by sanitary sewers and/or road salt. Although the direct contribution of dissolved Ra(II) from infiltration of storm water cannot be ruled out, the elevated TDS correlated with greater dissolved Ra(II) in the unconfined aquifer supports increased Ra mobility due to sorption site competition. In contrast, absence of redox-sensitive transition metal (hydr)oxides likely contributes to mobility of dissolved Ra(II) in the confined aquifer.

2.6 Conclusions

This study utilizes short-screened monitoring wells to characterize variability in the distribution of Ra(II) and identify potential Ra sources and sinks within specific hydrostratigraphic strata within the MCOAS Overall, ^{238}U and ^{232}Th concentrations were relatively low in both the aqueous and solid-phase samples analyzed as part of this study. Background concentrations of dissolved Ra(II) in this region of the MCOAS ranged from non-detectable to 2.4 pCi/L; however, elevated Ra(II) was observed at discrete depths in both the upper, unconfined surface aquifer and the underlying confined aquifer. Anoxic conditions in the

confined system likely result in the absence of Fe and Mn (hydr)oxides, resulting in limited Ra(II) sorption sites.[14,16,22] In wells in the unconfined aquifer that reflect the impact of surface processes (e.g., elevated specific conductance), elevated dissolved Ra(II) is attributed to sorption site competition.

Multiple mechanisms, including absence or dissolution of Fe and Mn (hydr)oxide coatings and elevated dissolved ion content, result in elevated Ra(II) within these discrete aquifer intervals. This study expands knowledge of the contribution of dissolved Ra(II) from distinct hydrostratigraphic units within the MCOAS. While low levels of Ra are observed throughout the system, local changes in hydrostratigraphic geochemistry can result in elevated Ra(II) in the groundwater.

2.7 Acknowledgements

This study was funded by the University of Wisconsin Water Resources Institute. We thank the Madison Water Utility for their assistance and cooperation with this work. Uranium and thorium trace metal analyses were performed by the Wisconsin State Laboratory of Hygiene. Pete Chase, WGNHS, assisted with sample collection. We also thank Elizabeth Tomaszewki, Lily Schacht, and three anonymous reviewers for comments and recommendations that greatly improved this manuscript.

2.8 References

1. Canu, I. G.; Laurent, O.; Pires, N.; Laurier, D.; Dublineau, I., Health effects of naturally radioactive water ingestion: the need for enhanced studies. *Environmental health perspectives* **2011,** *119*, (12), 1676-80.
2. Evans, R. D., Radium poisoning: a review of present knowledge. *American Journal of Public Health and the Nations Health* **1933,** *23*, (10), 1017-1023.
3. Guse, C. E.; Marbella, A. M.; George, V.; Layde, P. M., Radium in Wisconsin drinking water: an analysis of osteosarcoma risk. *Archives of Environmental Health: An International Journal* **2002,** *57*, (4), 294-303.
4. Agency, I. A. E. *The Environmental Behaviour of Radium*; 310; 1990; p 612.
5. Mays, C. W.; Rowland, R. E.; Stehney, A. F., Cancer risk from the lifetime intake of Ra and U isotopes. *Health physics* **1985,** *48*, (5), 635-47.
6. Moss, M. E.; Kanarek, M. S.; Anderson, H. A.; Hanrahan, L. P.; Remington, P. L., Osteosarcoma, seasonality, and environmental factors in Wisconsin, 1979–1989. *Archives of Environmental Health: An International Journal* **1995,** *50*, (3), 235-241.
7. Rowland, R. E.; Stehney, A. F.; Lucas, H. F., Dose-response relationships for female radium dial workers. *Radiation Research* **1978,** *76*, (2), 368-368.
8. U.S, E. P. A. *Technical fact sheet: final rule for (non-radon) radionuclides in drinking water*; 2000; pp 5-5.
9. Copenhaver, S. A.; Krishnaswami, S.; Turekian, K. K.; Epler, N.; Cochran, J. K., Retardation of 238U and 232Th decay chain radionuclides in Long Island and Connecticut aquifers. *Geochimica et Cosmochimica Acta* **1993,** *57*, (3), 597-603.
10. Gilkeson, R. H. *Isotopic studies of the natural sources of radium in groundwater in Illinois*; 1984; pp 50-50.
11. International Atomic Energy Agency, The environmental behaviour of radium: revised edition. *Technical Reports Series No. 476* **2014**, (476), 44-51.
12. Reynolds, B. C.; Wasserburg, G. J.; Baskaran, M., The transport of U- and Th-series nuclides in sandy confined aquifers. *Geochimica et Cosmochimica Acta* **2003,** *67*, (11), 1955-1972.
13. Szabo, Z.; dePaul, V. T.; Fischer, J. M.; Kraemer, T. F.; Jacobsen, E., Occurrence and geochemistry of radium in water from principal drinking-water aquifer systems of the United States. *Applied Geochemistry* **2012,** *27*, (3), 729-752.
14. Tricca, A.; Porcelli, D.; Wasserburg, G. J., Factors controlling the groundwater transport of U, Th, Ra, and Rn. *Journal of Earth System Science* **2000,** *109*, (1), 95-108.
15. Tricca, A.; Wasserburg, G. J.; Porcelli, D.; Baskaran, M., The transport of U-and Th-series nuclides in a sandy unconfined aquifer. *Geochimica et Cosmochimica Acta* **2001,** *65*, (8), 1187-1210.
16. Gilkeson, R. H.; Specht, S. A.; Cartwright, K.; Griffin, R. A.; Larson, T. E., Geologic studies to identify the source for high levels of radium and barium in Illinois ground-water supplies: a preliminary report. **1978**.
17. Grundl, T.; Cape, M., Geochemical factors controlling radium activity in a sandstone aquifer. *Ground Water* **2006,** *44*, (4), 518-527.
18. Mursky, G.; Anderson, J. W.; Cook, T. R.; Meddaugh, W. S., Uranium and thorium in selected Precambrian rock units in Wisconsin. *Geoscience Wisconsin* **1989,** *13*.

19. Siegel, D. I., Sulfur isotope evidence for regional recharge of saline water during continental glaciation, north-central United States. *Geology* **1990,** *18*, (11), 1054-1054.
20. Weaver, T. R.; Bahr, J., Geochemical evolution in the Cambrian-Ordovician sandstone aquifer, eastern Wisconsin: 1. Major ion and radionuclide distribution. *Ground Water* **1991,** *29*, (3), 350-356.
21. Winter, B. L.; Johnson, C. M.; Simo, J. A.; Valley, J. W., Paleozoic fluid history of the Michigan Basin: evidence from dolomite geochemistry in the middle Ordovician St. Peter Sandstone. *Journal of Sedimentary Research* **1996,** *65*, (2).
22. Vinson, D. S.; Lundy, J. R.; Dwyer, G. S.; Vengosh, A., Implications of carbonate-like geochemical signatures in a sandstone aquifer: Radium and strontium isotopes in the Cambrian Jordan aquifer (Minnesota, USA). *Chemical Geology* **2012,** *334*, 280-294.
23. Ayotte, J. D.; Szabo, Z.; Focazio, M. J.; Eberts, S. M., Effects of human-induced alteration of groundwater flow on concentrations of naturally-occurring trace elements at water-supply wells. *Applied Geochemistry* **2011,** *26*, (5), 747-762.
24. Krishnaswami, S.; Bhushan, R.; Baskaran, M., Radium isotopes and 222Rn in shallow brines, Kharaghoda (India). *Chemical Geology: Isotope Geoscience section* **1991,** *87*, (2), 125-136.
25. Stackelberg, P. E.; Szabo, Z.; Jurgens, B. C., Radium mobility and the age of groundwater in public-drinking-water supplies from the Cambrian-Ordovician aquifer system, north-central USA. *Applied Geochemistry* **2018,** *89*, 34-48.
26. Tomita, J.; Satake, H.; Fukuyama, T.; Sasaki, K.; Sakaguchi, A.; Yamamoto, M., Radium geochemistry in Na–Cl type groundwater in Niigata Prefecture, Japan. *Journal of Environmental Radioactivity* **2010,** *101*, (3), 201-210.
27. Interior, U. S. D. o. t.; Survey, U. S. G., Prinicipal aquifers can contribute radium to sources of drinking water under certain geochemical conditions. *Fact Sheet 2010–3113* **2012**.
28. Vinson, D. S.; Tagma, T.; Bouchaou, L.; Dwyer, G. S.; Warner, N. R.; Vengosh, A., Occurrence and mobilization of radium in fresh to saline coastal groundwater inferred from geochemical and isotopic tracers (Sr, S, O, H, Ra, Rn). *Applied Geochemistry* **2013,** *38*, 161-175.
29. Vinson, D. S.; Vengosh, A.; Hirschfeld, D.; Dwyer, G. S., Relationships between radium and radon occurrence and hydrochemistry in fresh groundwater from fractured crystalline rocks, North Carolina (USA). *Chemical Geology* **2009,** *260*, (3-4), 159-171.
30. Burghardt, D.; Kassahun, A., Development of a reactive zone technology for simultaneous in situ immobilisation of radium and uranium. *Environmental Geology* **2005,** *49*, (2), 314-320.
31. Gonneea, M. E.; Morris, P. J.; Dulaiova, H.; Charette, M. A., New perspectives on radium behavior within a subterranean estuary. *Marine Chemistry* **2008,** *109*, (3-4), 250-267.
32. Nathwani, J. S.; Phillips, C. R., Adsorption of 226Ra by soils in the presence of Ca2+ ions. Specific adsorption (II). *Chemosphere* **1979,** *8*, (5), 293-299.
33. Wilson, J. T., Water-quality assessment of the Cambrian-Ordovician aquifer system in the Northern Midwest, United States. *U.S. Geological Survey Scientific Investigations Report 2011-5229* **2012**, 154.
34. Vinson, D. S.; Lundy, J. R.; Dwyer, G. S.; Vengosh, A., Radium isotope response to aquifer storage and recovery in a sandstone aquifer. *Applied Geochemistry* **2018**.
35. Young, H. L.; Siegel, D. I., Hydrogeology of the Cambrian-Ordovician Aquifer System in the Northern Midwest, United States. *U.S. Geological Survey Professional Paper 1405-B 99.* **1992**.

36. Gilkeson, R. H.; Cartwright, K.; Cowart, J. B.; Holtzman, R. B. *Hydrogeologic and Geochemical Studies of Selected Natural Radioisotopes and Barium in Groundwater in Illinois*; Washington, DC, 1983; pp 93-93.
37. Sturchio, N. C.; Banner, J. L.; Binz, C. M.; Heraty, L. B.; Musgrove, M., Radium geochemistry of ground waters in Paleozoic carbonate aquifers, midcontinent, USA. *Applied Geochemistry* **2001,** *16*, (1), 109-122.
38. Weaver, T. R.; Bahr, J. M., Geochemical evolution in the Cambrian-Ordovician sandstone aquifer, eastern Wisconsin: 2. Correlation between flow paths and ground-water chemistry. *Ground Water* **1991,** *29*, (4), 510-515.
39. Parsen, M. J.; Bradbury, K. R.; Hunt, R. J.; Feinstein, D. T., *The 2016 groundwater flow model for Dane County, Wisconsin*. 2016; p 56-56.
40. Gotkowitz, M. B.; Bradbury, K. R.; Borchardt, M. A.; Zhu, J.; Spencer, S. K., Effects of climate and sewer condition on virus transport to groundwater. *Environmental Science & Technology* **2016,** *50*, (16), 8497-8504.
41. Georgia Institute of, T., The determination of radium-226 and radium-228 in drinking water by gamma-ray spectrometry using HPGE or Ge(Li) detectors, revision 1.2. **2004**.
42. Gotkowitz, M. B. Evaluating remedies for pathogen contamination of urban groundwater. 2015.
43. Rowe, H.; Hughes, N.; Geology, K. R. C.; Undefined, The quantification and application of handheld energy-dispersive X-ray fluorescence (ED-XRF) in mudrock chemostratigraphy and geochemistry. *Elsevier* **2012**.
44. Zambito, J. J.; McLaughlin, P. I.; Haas, L. D.; Stewart, E. K.; Bremmer, S. E.; Hurth, M. J., Sampling methodologies and data analysis techniques for geologic materials using portable X-ray fluorescence (pXRF) elemental analysis. **2016**.
45. Haas, L.; Zambito, J.; Hart, D. *Portable X-Ray Fluorescence (pXRF) Measurements of Uranium and Thorium in Madison, Wisconsin, Water Utility Wells 4 and 27*; Madison, 2017; pp 10-10.
46. McMahon, P. B.; Chapelle, F. H., Redox processes and water quality of selected principal aquifer systems. *Ground Water* **2008,** *46*, (2), 259-271.
47. Brezonik, P. L.; Arnold, W. A., *Water chemistry : an introduction to the chemistry of natural and engineered aquatic systems*. 2011; p 782-782.
48. Senior, L. A.; Vogel, K. L., *Radium and radon in ground water in the Chickies quartzite, southeastern Pennsylvania*. 1995.
49. Oden, J. H.; Szabo, Z. *Arsenic and radionuclide occurrence and relation to geochemistry in groundwater of the Gulf Coast Aquifer System in Houston, Texas, 2007–11*; 2016.
50. Sajih, M.; Bryan, N. D.; Livens, F. R.; Vaughan, D. J.; Descostes, M.; Phrommavanh, V.; Nos, J.; Morris, K., Adsorption of radium and barium on goethite and ferrihydrite: A kinetic and surface complexation modelling study. *Geochimica et Cosmochimica Acta* **2014,** *146*, 150-163.
51. Gellasch, C. A.; Bradbury, K. R.; Hart, D. J.; Bahr, J. M., Characterization of fracture connectivity in a siliciclastic bedrock aquifer near a public supply well (Wisconsin, USA). *Hydrogeology Journal* **2013,** *21*, (2), 383-399.

Chapter 3

Association of radionuclide isotopes with aquifer solids in the Midwestern Cambrian-Ordovician aquifer system

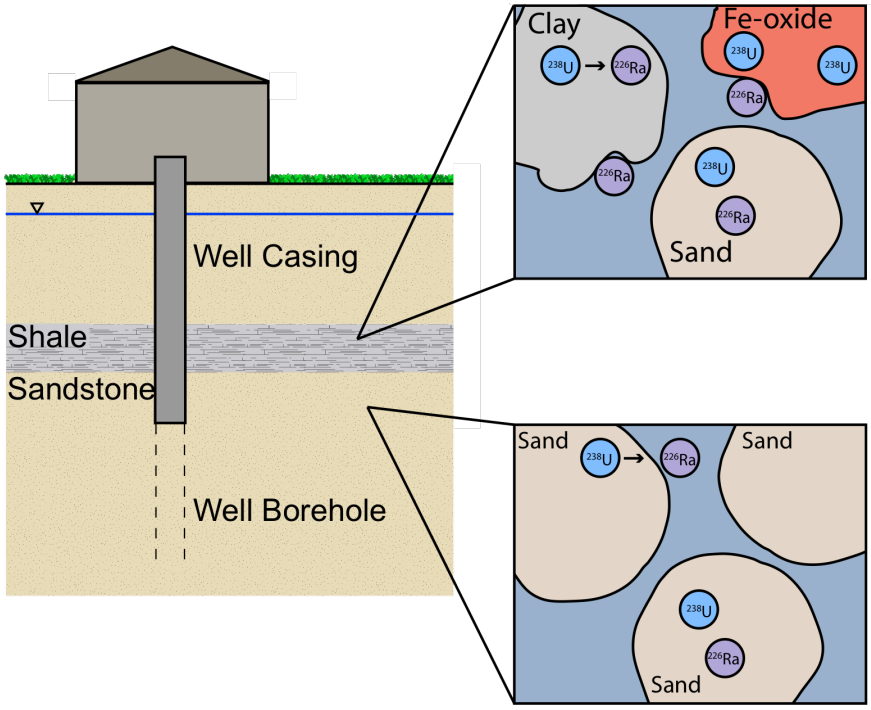

3.1 Abstract

Groundwater, an important source of drinking water globally, is susceptible to contamination by naturally occurring metals and radionuclides. Regional trends in groundwater quality are useful to predict contaminant occurrence but are difficult to translate to local scales due to complex contaminant-solid phase associations. Here, we use multi-collector inductively coupled plasma mass spectrometry techniques to quantify ultra-trace radium (Ra) levels in the aqueous phase of sequential extractions of aquifer solids. Results demonstrate that local-scale geochemistry drives Ra partitioning to groundwater in the U.S. Midwestern Cambrian-

Reproduced with permission from *ACS Earth and Space Chemistry*. Mathews, M.; Scott, S. R.; Gotkowitz, M. B.; Ginder-Vogel, M. 2021. Mathews completed all laboratory experiments and data analyses; Mathews, Scott, Gotkowitz, and Ginder-Vogel wrote the manuscript.

Ordovician aquifer system. Whole-rock, parent and daughter isotope activity ratios indicate that Ra remains close to the site of ^{238}U decay in some stratigraphic units where the $^{238}U/^{226}Ra$ ratio is similar to the equilibrium value; however, other stratigraphic units display isotope ratios indicative of Ra leaching. Additionally, Ra varies in prevalence across examined stratigraphy, in both whole-rock and extraction fraction values; average whole-rock ^{226}Ra activity is 70 ± 10 mBq/cm^3 in the Maquoketa shale in comparison to 6 ± 1 mBq/cm^3 average whole-rock ^{226}Ra in the St Peter sandstone. This suggests that Ra mobilization depends on both the reactive solid-phases present in the stratigraphy and on the influence of local geochemical conditions on solid-phase-contaminant interactions. Variation in conditions, such as redox or competitive ion exchange, will impact Ra partitioning to groundwater differently across stratigraphy, depending on solid-phase associations.

3.2 Introduction

Groundwater is a major source of drinking water worldwide, with an estimated 2.5 billion people relying solely on groundwater for daily water needs.[1] Contaminant presence impacts the quantity of groundwater available for drinking, as degraded water quality dictates overall water availability.[2,3] Regulatory and research efforts often focus on prevention and/or remediation of anthropogenic contaminants in groundwater; however, naturally occurring contaminants (e.g., Ra, As) are already present within many aquifer systems and can be mobilized by changes in geochemical conditions.[4-11] In extreme cases, water quality may be degraded by naturally occurring constituents, increasing water stress within a community and thus requiring expensive water treatment or alternate water sources.[12,13] Local-scale spatial variability (e.g., within a municipality) in well water quality, combined with annual and decadal temporal variation, also complicate management of municipal well fields.[14] A better understanding of processes

controlling naturally occurring contaminant speciation and partitioning within aquifer systems may contribute to maintaining groundwater as a potable water resource.[15,16]

Determining the processes controlling the distribution of naturally occurring contaminants within a heterogeneous aquifer is challenging, in part because complex flow paths within regional aquifer systems, and local flow paths impacted by groundwater pumping, affect subsequent contaminant partitioning into the groundwater. *In situ* contaminant-solid mineral associations are also difficult to ascertain, as many studies examine water samples from municipal wells, which are screened over long intervals across heterogeneous groundwater systems. Naturally occurring contaminants in aquifers and aquitards are often associated with reactive solid-phase surfaces and when released degrade water quality.[17,18] For some radiogenic contaminants, alpha decay can eject daughter nuclides from the mineral lattice into the aqueous phase (e.g., ^{226}Ra from the ^{238}U decay chain).[19] Geochemical factors, including changes in redox conditions and/or total dissolved solids (TDS), influence contaminant partitioning to aquifer solids through processes including precipitation/dissolution and sorption/desorption.[4,7,20-27] Competition for sorption sites at high ionic strength results in a decrease in surface sorption capacity for specific, naturally occurring contaminants, resulting in contaminant partitioning into the aqueous phase.[17,28-31] Additionally, the dissolution and/or absence of iron (Fe) and manganese (Mn) oxides due to anoxic aquifer conditions can cause elevated levels of associated contaminants.[4,7,19,21,23,32]

Radium (Ra) is one example of a naturally occurring contaminant that degrades groundwater quality upon partitioning to the aqueous phase. Radium is a naturally occurring radionuclide found at elevated levels in regionally important groundwater systems, including the Midwestern Cambrian-Ordovician (MCOAS) and the North Atlantic Coastal Plain aquifer systems.[4,7] Since long-term ingestion of water containing elevated Ra can result in osteosarcoma

and other bone disease, the US Environmental Protection Agency regulates Ra in drinking water with a maximum contaminant level (MCL) of 185 mBq/L (5 pCi/L) for the combination of the two major isotopes, ^{226}Ra and ^{228}Ra. Guidelines from the World Health Organization recommend an individual dose criterion of 0.1 mSv for total radionuclides in drinking water consumption for one year, where mSv is a unit of radiation dose measuring the health impact of ionizing radiation on the human body.[16,33-37]

Geochemical interactions between Ra and aquifer solids in groundwater systems affect Ra partitioning to the aqueous system.[38] In the laboratory, Ra sorption to solid-phases such as clay and transition metal oxides (e.g., Fe, Mn) has been verified.[39-43] At the laboratory scale, contaminant-solid interactions can be examined via sequential extraction of rock core obtained from aquifer systems to determine contaminant distribution between various solid-phases. Due to the low concentrations of concern, counting methods used to analyze Ra often require large sample volumes (often > 500 mL) and/or generate relatively high analytical detection limits, which limits applicability in situations where sample volume is limited.[44-47] Analytical techniques such as multi-collector inductively coupled plasma mass spectrometry (MC-ICPMS) can measure isotopes of contaminants at ultra-trace levels in the small sample volumes produced by laboratory experiments.[48-50]

Analysis of leachate from sequential extractions produces information about the association of ^{226}Ra and ^{238}U with aquifer solids, and about the mobility of daughter isotopes from the site of parent decay.[51,52] Here, we use MC-ICPMS to quantify ^{226}Ra associated with various fractions of aquifer solids from sequential extraction experiments examining multiple stratigraphic units from the MCOAS. The sensitivity of the MC-ICPMS technology provides quantitative results to examine partitioning from ultra-trace Ra levels in MCOAS solids. This

work enables examination of Ra availability across different types of bedrock, in order to better understand the influence of geochemical factors on local-scale Ra release to groundwater.

3.3 Materials and Methods

3.3.1 Midwestern Cambrian-Ordovician aquifer system

The MCOAS underlies a large portion of the Midwestern United States, including parts of Minnesota, Iowa, Missouri, Illinois, Indiana, and Wisconsin. More than 630 million gallons per day of groundwater is withdrawn for public and domestic water supply.[53] The Cambrian and Ordovician sedimentary bedrock is largely composed of permeable marine sandstones and carbonate rock; the clastic rocks are typically cemented by calcite ($CaCO_3$) and dolomite ($(Ca,Mg)CO_3$). In some locations, these permeable and prolific aquifers are separated by locally or regionally confining shale aquitards. Crystalline Precambrian basement rock underlies this groundwater system. A large portion of the Cambrian and Ordovician formations are regionally confined by the Maquoketa shale, particularly in eastern Wisconsin, and throughout the formation's extent in Iowa, Illinois, Indiana, and Missouri. Groundwater below the Maquoketa shale is typically anoxic, with an estimated groundwater age ranging from 6,000 to 40,000 years before present.[54,55] Elevated Ra commonly occurs in groundwater obtained from this confined system.[32] Broad geochemical trends associated with elevated Ra include low dissolved oxygen and elevated TDS.[4,7,23,52,56] Sampling at discrete intervals within the MCOAS suggests similar geochemical trends related to elevated Ra in the groundwater.[38]

3.3.2 Sample selection and preparation

This study examined a core collected in 1961 from a regionally confined portion of the MCOAS in Sheboygan County, Wisconsin. Subsamples examined include the lower Maquoketa

shale, the Galena dolostone, the St Peter sandstone, and sandstone of the Tunnel City Group (Figure 3.1). At this location, the subsample of the Maquoketa shale was taken from the Scales Member, which consists primarily of gray dolomitic shale with 0.1% total organic carbon and some fine disseminated iron sulfides. It is underlain by the Galena Formation, a massive dolostone with occasional vugs and chert nodules. The fine- to medium-grained, clean quartz sandstone of the St Peter Formation is poorly cemented where sampled. The 132 m thickness of Tunnel City Group has heterogeneous lithology, consisting primarily of sandstone and glauconitic sandstone, with minor amounts of quartzite and interbedded dolomite; a glauconitic sandstone interval was sampled for this experiment (Figure 3.1).

Subsamples of each stratigraphic unit were selected from the core and prepared for the experiment. Although the ~150 mm diameter core was stored under atmospheric conditions, visual inspection for Fe oxidation rinds revealed the extent of oxidation was limited to < 3 mm on the core's outer edge. To obtain samples representative of the regionally confined aquifer system, we cut into the middle of each core length and removed the oxidized edges. After preparation, samples were kept in an anoxic environment where each was pulverized, then finely ground by agate mortar and pestle. Samples were then sieved through a 1-mm mesh into 500-mL centrifuge tubes. Each depth was subsampled in triplicate to account for heterogeneity within individual samples.

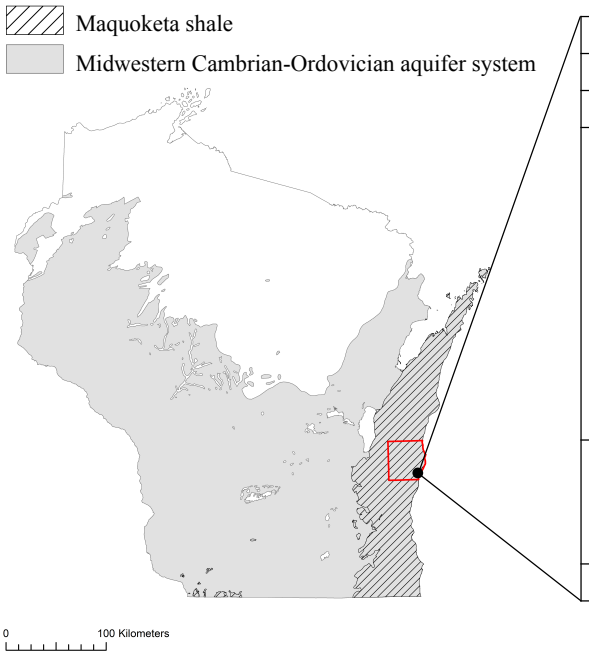

Geologic time	Stratigraphic unit (depth below surface)*
Pleistocene	Glacial drift (0 - 40 m)
Silurian	Niagara dolostone (40 - 226 m)
Ordovician	**Maquoketa shale** (226 - 296 m) Subsampled depth: 294 m
	Galena dolostone (296 - 332 m) Subsampled depth: 307 m
	Decorah dolostone (332 - 340 m)
	Platteville dolostone (340 - 360 m)
	St Peter sandstone (360 - 417 m) Subsampled depth: 379 m
Cambrian	**Tunnel City sandstone** (417 - 549 m) Subsampled depth: 423 m
	Mt. Simon sandstone (549 - 570 m)
Precambrian	Crystalline bedrock

*Table not to scale

Figure 3.1 Midwestern Cambrian-Ordovician aquifer system extent in Wisconsin (grey), and the portion confined by the Maquoketa shale (diagonal lines). The inset shows the location of the borehole in Sheboygan Co., and the representative stratigraphy at the drill site. Stratigraphy in bold are the units examined in this study, with specified subsampled depth.

3.3.3 Sequential extraction

Sequential extractions were conducted at room temperature in an anoxic chamber (Table 3.1). The first extraction targeted water-soluble metals, using synthetic groundwater comprised of a saturated solution of trace metal grade calcium carbonate ($CaCO_3$) in ultrapure water, purged with nitrogen gas until anoxic, then the solution was brought to ~pH 8 with trace metal grade hydrochloric acid (HCl). A rock to extractant mass ratio of 1:10 was initially utilized: 200 mL of each extracting reagent was added to 20 g of the prepared bedrock sample. The solution was then shaken for less than a minute, and then sat for 16 hours. Each sample was then centrifuged at 4000 rpm for 30 minutes and supernatant filtered with a 0.45-µm PTFE membrane filter. The filtrate was then preserved with trace metal grade nitric acid (HNO_3) to pH < 2. The second extraction used 1 M trace metal grade acetic acid added to the solid from the previous step and

targeted sorbed metals and metals associated with carbonate minerals; however, it is possible that some Fe and Mn (hydr) oxides may dissolve in this step.[57] This suspension was also shaken, then sat for 16 hours before centrifuging and filtering, as previously described. The third extracting reagent was 0.04 M hydroxylamine hydrochloride in 25% v/v acetic acid and targeted remaining Mn oxide and some Fe oxides with hydroxylamine hydrochloride as the reducing agent.[57-62] After addition of 200 mL of the extracting reagent to the remaining solid, samples were shaken and then sat for 16 hours at room temperature, after which each was centrifuged and filtered as in previous steps.[63-65] Note that barite is not a targeted mineral in these extractions, since the low dissolved sulfate content of the system indicates that it is undersaturated. X-ray diffraction analysis of aquifer solids subsamples from before and after the extraction was conducted to further examine changes in crystalline mineral phases (Figures B-2 – B-9).

Table 3.1 Sequential extraction and digestion methods. RT = room temperature.

Fraction	Targeted Associations	Reagent	Temperature, Time
Water-soluble	Water-soluble ions	Calcium carbonate (saturated)	RT, 16 hours
Acido-soluble	Sorbed metals, carbonate minerals[64]	1 M acetic acid	RT, 16 hours
Reducible	Mn and Fe oxides	0.04 M hydroxylamine hydrochloride in 25% v/v acetic acid	RT, 16 hours
HF digested	Residual metals; mineral lattice	Conc. HF, HNO_3, HCl	100-110 °C, 24 hours

3.3.4 Rock digestion

The remaining solids were dried and then completely digested at the conclusion of the sequential extraction. Each sample was baked at 50 °C until dry. Next, 0.5 g dry weight of each was placed into a clean Teflon bottle, to which 2 mL concentrated trace metal grade HNO_3 and 1

mL concentrated trace metal grade hydrochloric acid (HCl) were added, then heated at ~100 °C in a block heater overnight. After initial heating, 1 mL concentrated trace metal grade hydrofluoric acid (HF) and 3 mL of ultrapure water were added to all samples; all samples were then heated at 100-110 °C for an additional 24 hours.[64] Containers were cooled to room temperature, then 1 mL HCl and 1 mL ultrapure water were added to the digestion liquid; samples were heated uncapped from 105 to 85 °C. An addition of 4 mL concentrated HNO_3 was added to each sample, and heated uncapped from 105 to 95 °C; this step was repeated until few or no solids were observed in the samples. Hydrofluoric acid was added to any samples with visible silicate minerals and samples were heated; then the series of evaporations was repeated. Finally, the samples were diluted with 50 mL ultrapure water, and 50 mL saturated boric acid solution.[64,66]

3.3.5 General chemical analysis

Alkalinity and pH were determined for the water-soluble samples. A PerkinElmer Optima 4300 DV inductively coupled plasma optical emission spectrometer was used to analyze for bulk metals (e.g., Ca, Mg, Na, Mn, Fe, Ba, Sr) in all samples. Isotopic analysis for Ra parent isotopes ^{238}U and ^{232}Th was conducted using a ThermoScientific ELEMENT2 high resolution inductively coupled plasma mass spectrometer at the Wisconsin State Laboratory of Hygiene Trace Elements Clean Laboratory.

3.3.6 Preparation for Ra isotopic analysis

Each aqueous sample from the sequential extractions was purified through a series of columns prior to Ra isotopic analysis.[67] Column volume (CV) is contingent on sample volume, specified for each column purification step below. The resins were stored in dilute acid; to fill a column, the resin was shaken to suspend, and the slurry was added to the column to the

appropriate volume via pipette. Initially, each sample was evaporated to dryness, dissolved in one CV of conc. HNO_3 and taken to dryness again, then the dried sample was dissolved in one CV of conc. HNO_3 and one CV of ultrapure water (e.g., ~7 M HNO_3) and heated at ~110 °C under reflux.

The first column isolated the cations from the rest of the sample. Here, typical CVs were 2 mL of AG1-X8 (100 - 200 mesh) anion exchange resin. The addition of the sample load (e.g., sample dissolved in 2 CV ~7 HNO_3) and subsequent 1.5 CV of ~7M HNO_3 washes containing Ra were collected and taken to dryness. One CV conc. HCl was added, then taken to dryness prior to purification on the second column.

The second column separated the Ra + barium (Ba) fraction from the majority of the matrix elements from the isolated cation fraction from the first column; here, typical CVs were 2 mL of AG50W-X8 (200 – 400 mesh) cation exchange resin. Each dried sample collected from the first column was dissolved in one CV of 1 M HCl for loading onto the column, and heated at ~110 °C under reflux. Five progressively stronger washes of HCl were passed through the column, until the Ra fraction was collected in 4.5 CV of 6 M HCl, followed by 2 CV of 8 M HCl; the Ra fraction was determined via elution chemistry. The Ra + Ba fraction was taken to dryness, and one CV of conc. HNO_3 was added; then the sample was taken to dryness again for the third column.

The third and fourth columns removed Ba remaining in the sample after the second column purification. To separate the Ra and Ba, a 0.5 mL Eichrom SrSpec resin settled over 0.2 mL of Eichrom Prefilter inert resin beads was used. The sample was dissolved in 0.5 CV of 3 M HNO_3 for loading onto the column. Once loaded, one CV of 3 M HNO_3 was passed through, then the Ra fraction was eluted with five CV of 3 M HNO_3 and collected. The collected samples were

then evaporated. The column was then cleaned with 2 alternating washes of ultrapure water and 3 M HNO_3, then the SrSpec column procedure was repeated for complete Ba removal.

The final column removed ^{228}Th produced via decay during the sample purification process. It was similar to the first column, but with one CV equal to 1 mL of AG1-X8 resin. After the fifth column, the samples were evaporated; then 100 µL of 16M HNO_3 was added and heated at 145 °C to decompose organic residue from the resin. After evaporation, 25 µL of 16M HNO_3 was added, and samples were briefly (< 5 min) heated at 130 °C; 0.5 mL ultrapure water was then added to each sample in preparation for isotopic composition measurements.

3.3.7 Radium isotopic analyses

Mean beam intensities of ^{226}Ra were measured using the Neptune Plus MC-ICPMS at the Wisconsin State Laboratory of Hygiene. Isotope ratios were measured using a single SEM/RPQ detector in dynamic mode. Total yields were determined using a calibration curve created from dilutions of the NIST4967A ^{226}Ra solution standard. Ra standard yields and isotope ratios were used to calculate the activities of ^{226}Ra in the samples; these were converted to number of atoms, from which Ra activities were calculated. The detector was calibrated before each analytical session using a dilute tuning solution containing ^{238}U. A rock standard (USGS SBC-1) was digested in the same manner as the other HF digested rocks and run through the purification columns and analyzed on the MC-ICPMS. Final ^{226}Ra activities were corrected using a factor of 0.59 based on an average of yields determined from the NIST4967A and SBC-1 standards processed by column purification alongside samples. Uncertainty in ^{226}Ra activities is calculated from the standard deviation of the measured beam intensity.

3.4 Results

3.4.1 Whole-rock ^{226}Ra and ^{238}U

Although not the primary objective of this work, the whole-rock $^{238}U/^{226}Ra$ ratio is an essential measurement to understanding how the total amount of Ra varies across different stratigraphic units (Table 3.2). Note that here we define activity (A) as the radioactive decay of a nuclide:

$$A = N * \lambda \tag{3.1}$$

where N is the number of atoms, and λ is the radioactive decay constant; the number of atoms per g rock is first converted to dpm then to mBq per cm^3 aquifer, using bulk rock properties for porosity and dry bulk density (Table S1). The activity ratio is defined as the ratio of whole-rock daughter and parent nuclide activities (e.g., ^{226}Ra and ^{238}U); whole-rock activities are the sum of the radionuclide from each experimental fraction. The Maquoketa shale has the highest content of radionuclides; whole-rock ^{238}U activities average 99 ± 5 mBq/cm^3 from three samples, with average whole-rock ^{226}Ra activity of 70 ± 10 mBq/cm^3, where the uncertainty represents standard deviation (results from individual samples provided in Table 2). The St Peter sandstone samples have the lowest amount measured, with 9.3 ± 0.9 mBq/cm^3 average whole-rock ^{238}U activities, and 6 ± 1 mBq/cm^3 average whole-rock ^{226}Ra activities. Whole-rock radionuclide content in the Galena dolostone and Tunnel City are between that of the Maquoketa shale and St Peter sandstone. Radionuclide levels in the Galena dolostone are closer to the Maquoketa shale than the St Peter sandstone, with average whole-rock ^{238}U activity of 71 ± 4 mBq/cm^3, and whole-rock ^{226}Ra activity of 59 ± 3 mBq/cm^3. The Tunnel City sandstone is similar to the St Peter sandstone, with 19 ± 1 mBq/cm^3 average whole-rock ^{238}U activity and 19 ± 4 mBq/cm^3 average

whole-rock ^{226}Ra activity. Overall, stratigraphy with greater whole-rock ^{238}U activity also contains greater whole-rock ^{226}Ra activity.

Table 3.2 Measured whole-rock radionuclide activities per sample, as a sum of all fractions. Uncertainty represents instrumental error. Units are mBq/cm^3 aquifer unless otherwise specified. SRM = Standard reference material

Stratigraphic Unit	Depth (m)	^{238}U	^{226}Ra
Maquoketa shale – 1	294	94 ± 1	88 ± 1
Maquoketa shale – 2	294	98 ± 1	75 ± 4
Maquoketa shale – 3	294	104 ± 1	59 ± 2
Galena dolostone – 1	307	74.6 ± 0.7	58.98 ± 0.09
Galena dolostone – 2	307	66.7 ± 0.5	61 ± 1
Galena dolostone – 3	307	72.8 ± 0.8	56 ± 1
St Peter sandstone – 1	379	10.2 ± 0.2	5 ± 1
St Peter sandstone – 2	379	8.5 ± 0.2	7.7 ± 0.3
St Peter sandstone – 3	379	9.2 ± 0.2	6.5 ± 0.3
Tunnel City sandstone – 1	423	18.6 ± 0.2	15 ± 1
Tunnel City sandstone – 2	423	18.0 ± 0.1	22 ± 1
Tunnel City sandstone – 3	423	20.4 ± 0.3	18.6 ± 0.4
SBC-1	SRM	64.8 ± 0.7 mBq/g rock	65 ± 1 mBq/g rock

The whole-rock ^{238}U/^{226}Ra activity ratio for each stratigraphic unit is compared to an equilibrium value determined from the ^{238}U/^{226}Ra ratio for the standard reference material (SRM) SBC-1, a value of 0.94. Student's t-test was conducted on each sample group to compare differences between the whole-rock ^{238}U/^{226}Ra ratio and the equilibrium value.[68] The ^{238}U/^{226}Ra ratio increases as either ^{238}U is added or ^{226}Ra is removed from the system; therefore, the Student's t-test was also conducted for the value 1.88, which is twice the equilibrium value. Samples from the Galena dolostone have an average whole-rock ^{238}U/^{226}Ra activity ratio of 1.2 ± 0.1, where uncertainty represents the standard deviation (Figure 3.2). The whole-rock ^{238}U/^{226}Ra ratio for samples in the Maquoketa shale and St Peter sandstone varies (averaging 1.4 ± 0.4 and 1.5 ± 0.5, respectively). The Tunnel City sandstone samples have an average whole-rock ^{238}U/^{226}Ra ratio of 0.84 ± 0.04. There is no significant difference between the whole-rock ^{238}U/^{226}Ra ratio for each sample group, and the equilibrium value of 0.94 ($p > 0.05$ for all groups). The whole-rock

$^{238}U/^{226}Ra$ ratios for the Maquoketa shale and St Peter sandstone are also not significantly different than twice the equilibrium value 1.88 ($p > 0.05$), while the whole-rock $^{238}U/^{226}Ra$ ratios for the Tunnel City and Galena are significantly different than 1.88 ($p < 0.05$).

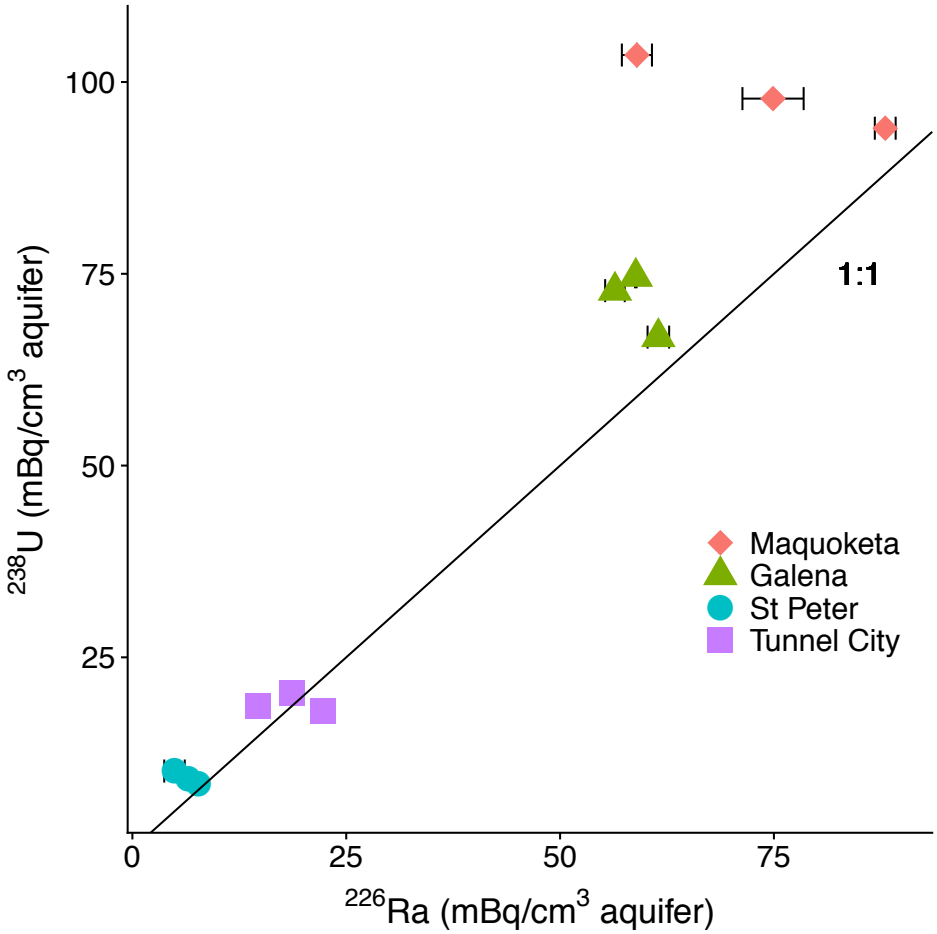

Figure 3.2 Total ^{238}U and ^{226}Ra activities per volume of aquifer sampled in each bedrock unit. The black line represents a 1:1 activity ratio. Error bars represent instrumental uncertainty.

3.4.2 Activity of ^{226}Ra in targeted extractions

The amount of ^{226}Ra in the final, HF digested fraction is similar for all stratigraphic units; however, the amount of ^{226}Ra in the less recalcitrant fractions (e.g., water-soluble, acido-soluble, reducible fractions) varies by stratigraphic unit (Figure 3.3a and b). For all samples, the majority of ^{226}Ra is in the HF digested fraction: 99% for Galena dolostone (58 ± 2 mBq/cm^3), 98% for

Maquoketa shale (70 ± 10 mBq/ cm^3), 92% for St Peter sandstone (6 ± 1 mBq/ cm^3), and 94% for Tunnel City sandstone (17 ± 4 mBq/ cm^3). In the Maquoketa shale, the ^{226}Ra removed prior to HF digestion distributes between the water-soluble (0.2%), acido-soluble (63%) and reducible (37%) fractions (0.004 ± 0.001 mBq/ cm^3, 1.01 ± 0.08 mBq/ cm^3, 0.6 ± 0.1 mBq/ cm^3, respectively). For the non-HF digested fraction, the Galena dolostone and St Peter sandstone are more similar in terms of ^{226}Ra content in the reducible fraction at 60% and 59%, respectively (Table S2). However, for the non-HF digested portion, ^{226}Ra in the Galena dolostone is largely found in the acido-soluble fraction (63%), compared to the St Peter sandstone where most of the ^{226}Ra is found in the reducible fraction (77%,). Most of the non-HF digested ^{226}Ra in the Tunnel City sandstone unit is in the reducible fraction (94%, or 1.1 ± 0.3 mBq/ cm^3), with the water-soluble and acido-soluble fractions containing much less (0.4% and 6%, or 0.0047 ± 0.0005 mBq/ cm^3 and 0.06 ± 0.03 mBq/ cm^3, respectively). Although > 85% of ^{238}U is associated with the HF digested fraction, ^{238}U distribution across fractions also varies by stratigraphic unit (Figure C-1).

3.4.3 Geochemistry of water-soluble fraction

The leachate from the water-soluble fraction follows a similar chemistry for the examined stratigraphic units, although trace metal concentrations vary (Figure 3.4, Table C-3). Dissolved magnesium (Mg^{2+}) in the water-soluble fraction leachate varies in concentration across the Maquoketa shale, Galena dolostone, St Peter sandstone, and Tunnel City sandstone (22 ± 2 μg/cm^3, 9.5 ± 0.7 μg/cm^3, 0.4 ± 0.1 μg/cm^3, and 4 ± 1 μg/cm^3 respectively). Dissolved potassium (K^+) is similar, with the greatest concentration in the Maquoketa shale (13 ± 1 μg/cm^3), similar concentrations for the Galena dolostone and Tunnel City sandstone (2.9 ± 0.2 μg/cm^3, 2.5 ± 0.5 μg/cm^3), and a much smaller concentration in the St Peter sandstone (0.5 ± 0.1 μg/cm^3). Dissolved iron (Fe(II)) ranges from 0.007 ± 0.004 μg/cm^3 to 0.027 ± 0.004 μg/cm^3. More variability is

observed in dissolved manganese (Mn(II)) concentrations, ranging from 0.24 ± 0.06 μg/cm^3 in the Tunnel City sandstone to 0.0031 ± 0.0003 μg/cm^3 in the St Peter Sandstone.

3.5 Discussion

3.5.1 Sources of ^{226}Ra to groundwater

Possible sources of Ra to groundwater include ejection from alpha recoil, as well as desorption from or dissolution of Ra bearing solid-phases; geochemical factors influencing these processes vary greatly in their relative time scales (Figure 3.5). While Ra is present across the stratigraphic units examined in this study, the large majority is retained within the aquifer solids. This suggests the low aqueous Ra activities typically observed in MCOAS groundwater result from immobilization within, or association with, aquifer solid-phases, rather than absence of Ra from the system (Figure 3.3a). As the overall aquifer system is close to secular equilibrium, alpha recoil by parent isotopes does not appear to partition ^{226}Ra into the aqueous system at elevated levels, although some indication of ^{226}Ra leaching may be indicated by disequilibrium observed in some stratigraphic units. Some possible explanations for equilibrium observed in the overall aquifer system are that ^{226}Ra may eject out of the mineral lattice to associate with aquifer solids or eject into solution but rapidly repartition to the solid-phase surface. The location of the parent isotope within the mineral lattice is also important, as it is estimated that ^{226}Ra is only ejected a distance of 0.02 ± 0.05 mm by alpha recoil, which suggests that it could remain within the original solid depending on grain size (Figure 3.5).[19,69] The solids digested in the HF fraction are not easily modified or dissolved under typical aquifer conditions, so geochemical changes in the aquifer system will not impact release of ^{226}Ra from this portion of the aquifer material. Therefore, ^{226}Ra present in groundwater is likely due to the impact of local geochemical conditions on ^{226}Ra found in the water-soluble, acido-soluble, and reducible fractions.

While sequential extractions provide information about the association of ^{226}Ra with portions of the aquifer solids, it is challenging to examine Ra in groundwater at the field or experimental scale, due to ultra-trace analyte concentrations present amidst complex geochemical and hydrologic interactions. MC-ICPMS is beneficial for analyzing aqueous Ra at environmentally relevant concentrations and volumes.[48-50] For aqueous analysis, the large sample volume and wide range of detection limits makes many EPA-approved methods (e.g., gamma spectrometry, ICP-MS, liquid scintillation counting) difficult to use for smaller-scale experiments.[44-47] Many of these methods use decay counting methods to analyze for aqueous ^{226}Ra and require at least a sample size of 1 L with detection limits for these methods ranging from 0.37 – 37 mBq/L (0.01 – 1.0 pCi/L).[70]

3.5.2 Potential ^{226}Ra leaching

The stratigraphic units examined in this study formed during the Ordovician and Cambrian geologic eras, more than 443 million years ago; therefore, secular equilibrium is expected in the whole-rock samples.[19,21,71-74] Comparison of parent and daughter nuclide activities (e.g., mBq/cm^3 ^{238}U and mBq/cm^3 ^{226}Ra) provides information about potential ^{226}Ra leaching from the site of parent decay in the aquifer system (Figure 3.2). Secular equilibrium, where parent and daughter nuclides reach equivalent activities, occurs in parent-daughter systems that have not been impacted by transport (e.g., removal of the daughter isotope) for a time period that is significantly longer than the daughter isotope half-life. As the half-life of the parent isotope ^{238}U (4.5×10^9 years) is much longer than the half-life of its daughter isotope, ^{226}Ra (1.6×10^3 years), after ~2 million years and in the absence of transport processes, ^{238}U and ^{226}Ra isotope activities should be equivalent.[75]

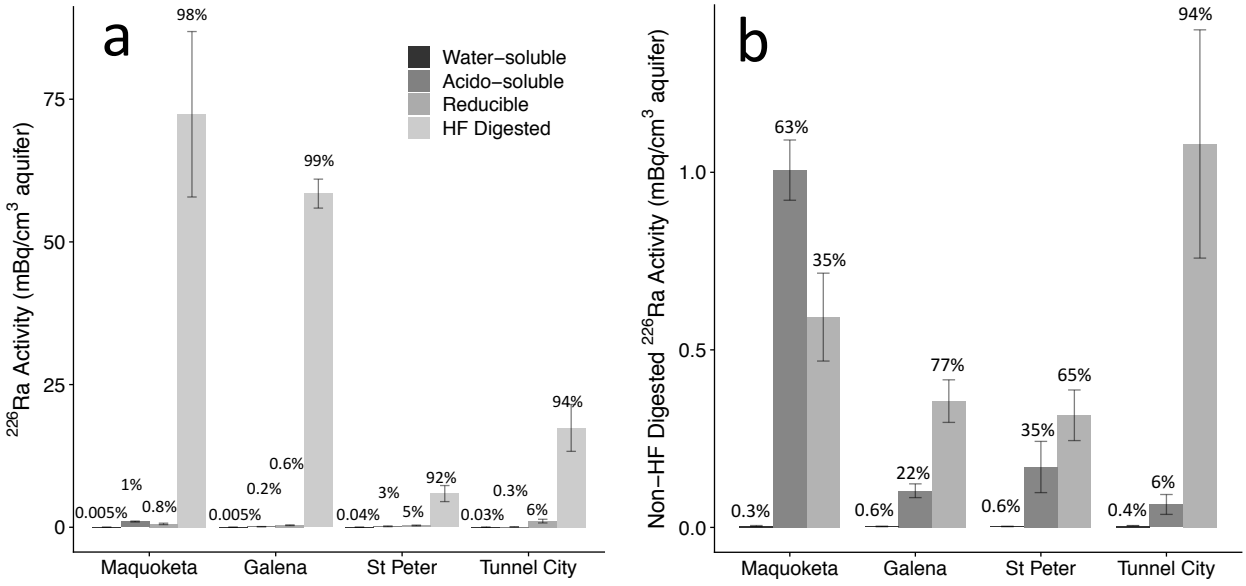

Figure 3.3 Average ^{226}Ra per aquifer volume, separated into sequential extraction and digestion fractions for each stratigraphic unit. (a) shows distribution across all fractions including the digestion. Percentage values indicate the proportion of the specified fraction in comparison to the total ^{226}Ra for the stratigraphic unit. (b) shows the distribution within each stratigraphic unit for the non-HF digested fractions. Percentage values indicate the proportion of the specified fraction in comparison to the total non-HF digested ^{226}Ra for the stratigraphic unit. In both, error bars represent sample variability. Note different y-axis ranges.

^{226}Ra leaching potential varies by stratigraphic unit, where some units are more likely to support ^{226}Ra transport.[20,24,25,27,76] As there is not a significant difference between the whole-rock ^{238}U/^{226}Ra equilibrium value of 0.94 and the average ratios determined for the four stratigraphic units examined in this study ($p > 0.05$ for all sample groups), the overall aquifer system is close to secular equilibrium (Figure 3.2). However, for the Maquoketa shale and the St Peter sandstone sample groups, the whole-rock ^{238}U/^{226}Ra ratios are not significantly different than twice the equilibrium value (i.e., 1.88), which suggests disequilibrium and therefore potential Ra leaching. The observed disequilibrium in these units is likely due to Ra removal mechanisms that promote the partitioning of ^{226}Ra to the aqueous system, such as damage of the mineral lattice due to alpha recoil, or changes in available sorption sites.

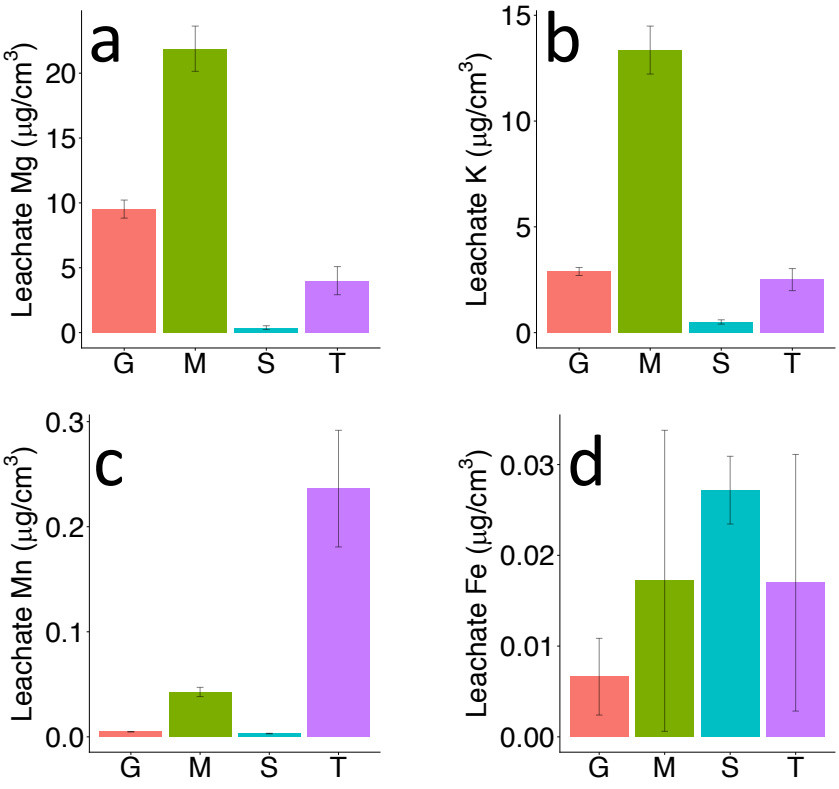

Figure 3.4 Geochemical indicators determined in the water-soluble fraction for each stratigraphic unit. Note different y-axis ranges. Uncertainty represents standard deviation of individual samples. G = Galena dolostone, M = Maquoketa shale, S = St Peter sandstone, T = Tunnel City sandstone

3.5.3 Association of ^{226}Ra with aquifer solids

In all stratigraphic units, most ^{226}Ra and ^{238}U is in the HF digested fraction (> 90% for ^{226}Ra, > 85% for ^{238}U); indicating that the majority of these radionuclides are encased within the solid (Figures 3.3, B-1),[77] and will not readily partition to the aqueous system due to geochemical changes (Figure 3.3a). The absolute quantity of ^{226}Ra varies across stratigraphic units; ranging from an average of 70 ± 10 mBq/cm^3 aquifer in the Maquoketa shale, to an average of 6 ± 1 mBq/cm^3 aquifer in the St Peter sandstone (Table 3.2). Elevated Ra concentrations in shale layers are frequently observed; this may be in part due to the enriched presence of clay minerals and/or increased parent isotope levels.[19,78-81] It is important to consider potential hydrologic interactions

between stratigraphic units with elevated Ra (e.g., Maquoketa shale) and units containing lower amounts of Ra (e.g., St Peter sandstone), as introduced changes in water chemistry (e.g., elevated TDS, anoxic conditions) due to intra-stratigraphy flow patterns may influence conditions promoting Ra leaching.

Table 3.3 Mass balance for total exchangeable ^{226}Ra associated with each stratigraphic unit. Partition coefficient is estimated at the maximum contaminant level (185 mBq/L ^{226}Ra). ^{226}Ra in water is in relation to total exchangeable ^{226}Ra. Uncertainty represents standard deviation of individual samples.

Stratigraphic Unit	Est. porosity	Total exchangeable ^{226}Ra (mBq/cm^3)	Total exchangeable ^{226}Ra (mBq/L)	Partition coefficient	^{226}Ra in water (%)
Maquoketa shale	0.08	1.6 ± 0.2	2.0e4 ± 2e3	0.009 ± 0.001	0.9 ± 0.1
Galena dolostone	0.05	0.46 ± 0.04	9.4e3 ± 8e2	0.020 ± 0.002	2.0 ± 0.2
St Peter sandstone	0.12	0.5 ± 0.1	4e3 ± 1e3	0.045 ± 0.009	4.5 ± 0.9
Tunnel City sandstone	0.17	1.1 ± 0.3	7e3 ± 2e3	0.03 ± 0.01	3 ± 1

3.5.4 Geochemical influences on ^{226}Ra leaching

Geochemical processes like dissolution, desorption, or ion exchange within the aquifer system can result in the release of Ra associated with the non-HF digested fractions (e.g., the water-soluble, acido-soluble, and reducible fractions). Some solid-phases associated with the various fractions suggest that the dissolution of key minerals release ^{226}Ra, including Mn- and Fe-(hydr)oxides associated with the reducible fraction.[59] The large proportion of ^{226}Ra present in the Tunnel City sandstone reducible fraction ^{226}Ra (94 %) indicates that Mn- and Fe-(hydr)oxide are likely an important control on ^{226}Ra partitioning in this unit. Additionally, a large portion of the ^{226}Ra (63 %) is released in the acido-soluble fraction in the Maquoketa shale. This suggests that Ra may be present as easily desorbed surface complexes or with carbonate minerals, since

these are the phases targeted by this extraction.[61] The Galena dolostone and St Peter sandstone have similar volume-normalized quantities of ^{226}Ra in the acido-soluble fraction (0.10 ± 0.2 mBq/L and 0.17 ± 0.07 mBq/L, respectively) and the reducible fraction, (0.36 ± 0.06 mBq/L and 0.32 ± 0.07 mBq/L, respectively). The slightly larger acido-soluble fraction in the St Peter may contribute to the increased leachability of ^{226}Ra observed in the greater $^{238}U/^{226}Ra$ ratio for the St Peter samples, suggesting a greater amount of weakly sorbed Ra in the St Peter sandstone than in the Galena dolostone.

Evaluation of leachate chemistry from the water-soluble fraction of the sequential extractions provides further information about the critical factors controlling Ra partitioning from solid to aqueous phase (e.g., redox state). The St Peter sandstone has the smallest amounts of Mg^{2+}, Mn(II) and K^{+}, but the largest amounts of Fe(II) in comparison to the other stratigraphic units. The cycling of trace metals like Fe(II) through geochemical factors like precipitation and redox changes may control Ra partitioning in the St Peter sandstone (Figure 3.4). Similarly, the Tunnel City sandstone has larger amounts of Fe(II) and Mn(II); this supports sequential extraction data in that transition metal oxides are likely major controls for Ra partitioning in this unit. Additionally, the presence of cations like Mg^{2+} and K^{+} in water leachate, such as in the Maquoketa shale or Galena dolostone, suggests that sorption site competition between these cations and Ra is likely occurring in these units. Notably, the Maquoketa shale water leachate has a similar amount of Fe(II) as the Tunnel City sandstone water leachate. If transition metal oxides are present in the Maquoketa shale, Mg^{2+} and K^{+} likely take up some of the sorption sites present in those minerals in this unit.

Geochemical conditions such as elevated TDS and reducing conditions impact available sorption sites within aquifer solids; these conditions have been observed to increase dissolved Ra

activity in the MCOAS.[4,7,19,20,23,38] The variation in ^{226}Ra-solid association in the non-HF digested fractions across stratigraphic units implies that geochemical conditions (e.g., redox conditions, TDS level, pH) within each formation have different effects on ^{226}Ra partitioning into the aqueous system, particularly impacting sorption (Figure 3b). While sorption is a reversible process, first-order rate constants for Ra adsorption, $1.0 \times 10^{-4} - 3.5 \times 10^{-1}$ s^{-1}, are much larger than for desorption, $9.3 \times 10^{-7} - 2.0 \times 10^{-4}$ s^{-1} (Figure 3.5).[76,82] Both of these rate constants are also orders of magnitude smaller than the half-life of ^{226}Ra (5.05×10^{10} s); ^{226}Ra will experience sorption and desorption many times before undergoing radioactive decay. However, this depends on geochemical conditions which might enhance either sorption or desorption. Phases affected by reducing redox conditions may dissolve and/or be absent depending on redox conditions, causing fewer sorption sites to be present.[40-43] Elevated TDS in groundwater results in increased sorption site competition, and fewer available sites for Ra sorption.[28,29] For example, the impact of high TDS in the Maquoketa shale is more likely to result in elevated Ra in the groundwater in comparison to high TDS in the St Peter sandstone, due to higher levels of ^{226}Ra and greater association of ^{226}Ra with the water-soluble and acido-soluble fractions in the Maquoketa shale (Figure 3.3b). Additionally, ^{226}Ra is emitted via alpha recoil 0.02 ± 0.05 mm from the site of parent decay.[69] Not only will geochemical reactions like sorption impact ^{226}Ra presence in groundwater, but the proximity of parent nuclides to Ra sorption sites is also important to consider. This suggests that the impact of specific geochemical conditions varies in importance across stratigraphy.

Comparison of the exchangeable ^{226}Ra in the examined stratigraphic units with the maximum contaminant level (MCL) of 185 mBq/L for total aqueous ^{226}Ra and ^{228}Ra activities further develops how hydrologic and geochemical conditions will influence ^{226}Ra mobilization

across different bedrock units. Specifically, we calculated a mass balance designed to examine what percentage of ^{226}Ra would be in the water in comparison to the exchangeable ^{226}Ra associated with the aquifer solids for each stratigraphic unit (Table 3.3). ^{226}Ra activities were converted from mBq/cm^3 to mBq/L, with the addition of 185 mBq/L of aqueous ^{226}Ra to compare the MCL to the overall exchangeable ^{226}Ra content, via Equation 3.2:

$$^{226}Ra_{ex,aq} = MCL + \frac{\left(^{226}Ra_{ex}\right) * \left(\frac{1e6\ cm^3}{m^3}\right)}{n * 1000\frac{L}{m^3}} \tag{3.2}$$

Where $^{226}Ra_{ex,aq}$ is the total exchangeable ^{226}Ra estimated for an aqueous system, in mBq/L; MCL is the Ra maximum contaminant level at 185 mBq/L of ^{226}Ra; $^{226}Ra_{ex}$ is the total exchangeable ^{226}Ra, in mBq/cm^3; and *n* is porosity. The partition coefficient, D, is calculated by Equation 3.3:

$$D = \frac{MCL}{^{226}Ra_{ex,aq}} \tag{3.3}$$

These calculations determine variation between each stratigraphic unit and the percent ^{226}Ra estimated to be in the aqueous fraction at the MCL. The St Peter sandstone has the greatest amount of ^{226}Ra estimated to be in the aqueous system, while the Maquoketa shale has the least amount (5 ± 1 % and 0.9 ± 0.1 %, respectively). Stratigraphic units like the Maquoketa shale likely have greater sorption capacity, resulting in a smaller D value and less ^{226}Ra in the aqueous phase in comparison to overall solid-phase associations. Sandstone units like the St Peter have a larger percentage of ^{226}Ra in the aqueous phase in relation to the total ^{226}Ra; this suggests that if Ra is present within the St Peter sandstone, it is more likely that it will be in the aqueous phase than in the Maquoketa shale. The range of partition coefficients among these four stratigraphic units further confirms that the geochemical associations available within a stratigraphic unit are

major controls for ^{226}Ra mobilization, and that this control varies across different types of bedrock.

Our study demonstrates an innovative approach, combining sequential extraction experiments on aquifer solids with sensitive analytical techniques (e.g., MC-ICPMS) to examine contaminant interactions in groundwater. For radioactive contaminants, examining isotopic processes such as secular equilibrium can reveal further information about transport within an aquifer system. Secular equilibrium between ^{226}Ra and ^{238}U in the examined stratigraphic units suggests that ^{226}Ra leaching depends on available solid-phase associations, and varies with different stratigraphic units (Figure 3.2). While geochemical associations between Ra and solid-phases are therefore important controls on contaminant mobility, this association varies across stratigraphy as demonstrated by the assorted distribution of Ra across non-HF digested fractions (Figure 3.3b). Local-scale geochemical variation within stratigraphic units can result in Ra partitioning from the aquifer solids to the aqueous system, through processes such as desorption and mineral dissolution or absence.

Some limitations of this study include use of geochemical leachate rather than groundwater samples, and assumptions about reactive solid-phase associations assumed based on the sequential extractions. While extraction experiments provide valuable information as to analyte-rock interactions, they are limited via experimental controls in comparison to the complex interactions occurring in aquifer systems. It is recognized that the identification of direct Ra-mineral associations is more specific to examining Ra interactions with particular minerals present within bedrock. Nonetheless, the quantification of Ra-solid interaction via sequential extractions targets the fractions of aquifer materials expected to have the largest impact on Ra partitioning to the aqueous phase in this portion of the MCOAS.

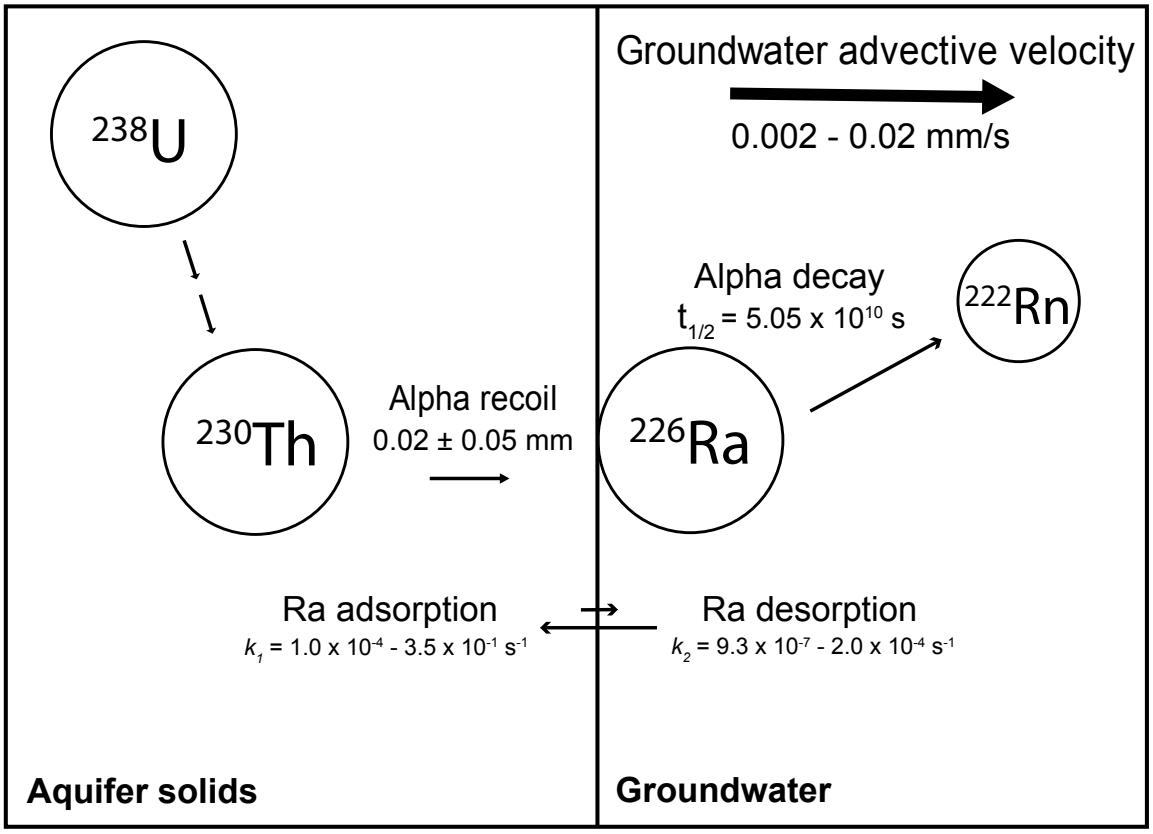

Figure 3.5 Conceptual diagram depicting the time scales of geochemical processes influencing Ra associations with aquifer solids in the MCOAS. Estimates of alpha recoil distance,[76] ^{226}Ra decay constant,[82] average groundwater transport,[83] and first-order rate constants for Ra adsorption-desorption in natural fresh to brackish groundwater[83] are included.

3.6 Environmental Implications

Local geochemistry controls the partitioning of Ra and other contaminants to the aqueous system. Some bedrock formations have elevated levels of contaminants that partition more easily to groundwater (e.g., Ra in the Maquoketa shale); changing geochemical conditions at an individual well can influence the partitioning of contaminants at that site. Physical well features may also affect the quality of water pumped across bedrock formation, such as casing depth, total well depth, and relative transmissivity of sedimentary layers. Additionally, changes in well pumping rates can change hydraulic gradients, and as a result can alter groundwater flow paths and impact metal mobility by introducing new geochemical conditions.[83] Examples of this include

drawing groundwater containing elevated dissolved solids to a different part of the aquifer system, or inducing flow of oxygenated, recently recharged water across Ra-enriched shale aquitards. Such changes may affect solid-phase presence, releasing sorbed contaminants into the aqueous system.[83]

Understanding the impact of local geochemistry and changes in groundwater flow systems on Ra partitioning can inform well construction and ultimately reduce the uptake of naturally occurring contaminant by wells. While geochemical trends that affect contaminant partitioning are apparent at the regional scale (e.g., Ra in the MCOAS), prediction of local-scale contaminant concentrations is complicated by the influence of local geochemistry, lithologic heterogeneity, and by wells open to multiple stratigraphic units. Use of sensitive methods that identify ultra-trace level Ra concentrations demonstrates that local geochemistry is a major control on Ra release to the aqueous system. These data will support development of geochemical and hydrologic models to assess the influence of groundwater withdrawal on the partitioning of contaminants to groundwater in systems such as the MCOAS, where interbedded shale, sandstone and carbonates affect contaminant mobility within heavily used aquifer systems.

3.7 Acknowledgements

We thank the Wisconsin State Laboratory of Hygiene for support and training in multi-collector inductively coupled plasma mass spectrometry techniques, and specifically Joel Overdier for uranium analysis. Samples in this report are curated at the Wisconsin Geological and Natural History Survey's (WGNHS) core repository. We thank WGNHS, particularly Esther Stewart and Pat McLaughlin, for providing access to samples from core 60000086, descriptions, and lab facilities. Laboratory assistance provided by Gabrielle Campagnola, Amy Plechacek, James Lazarcik, and Lily Schacht was greatly appreciated. Thanks to Lily Schacht and Amy

Plechacek for providing excellent insight into the writing of the manuscript. Funding for this project is provided by the Wisconsin Groundwater Research and Monitoring Program as well as the Wisconsin Department of Natural Resources. MM is supported by funding from the Grainger Wisconsin Distinguished Graduate Fellowship.

3.8 References

1. WWAP (United Nations World Water Assessment Programme) *The United Nations World Water Development Report 2015: Water for a Sustainable World*; UNESCO: Paris, 2015.
2. Liu, J.; Liu, Q.; Yang, H., Assessing water scarcity by simultaneously considering environmental flow requirements, water quantity, and water quality. *Ecological Indicators* **2016,** *60*, 434-441.
3. Zeng, Z.; Liu, J.; Savenije, H. H. G., A simple approach to assess water scarcity integrating water quantity and quality. *Ecological Indicators* **2013,** *34*, 441-449.
4. Stackelberg, P. E.; Szabo, Z.; Jurgens, B. C., Radium mobility and the age of groundwater in public-drinking-water supplies from the Cambrian-Ordovician aquifer system, north-central USA. *Applied Geochemistry* **2018,** *89*, 34-48.
5. Grützmacher, G.; Kumar, P. J. S.; Rustler, M.; Hannappel, S.; Sauer, U., Geogenic groundwater contamination—definition, occurrence and relevance for drinking water production. *Zbl Geol Paläont Teil I* **2013,** *1*, 69-75.
6. Fendorf, S.; Wielinga, B. W.; Hansel, C. M., Chromium Transformations in Natural Environments: The Role of Biological and Abiological Processes in Chromium(VI) Reduction. *International Geology Review* **2000,** *42*, (8), 691-701.
7. Szabo, Z.; dePaul, V. T.; Fischer, J. M.; Kraemer, T. F.; Jacobsen, E., Occurrence and geochemistry of radium in water from principal drinking-water aquifer systems of the United States. *Applied Geochemistry* **2012,** *27*, (3), 729-752.
8. Polizzotto, M. L.; Harvey, C. F.; Li, G.; Badruzzman, B.; Ali, A.; Newville, M.; Sutton, S.; Fendorf, S., Solid-phases and desorption processes of arsenic within Bangladesh sediments. *Chemical Geology* **2006,** *228*, (1), 97-111.
9. Polizzotto, M. L.; Harvey, C. F.; Sutton, S. R.; Fendorf, S., Processes conducive to the release and transport of arsenic into aquifers of Bangladesh. *Proceedings of the National Academy of Sciences of the United States of America* **2005,** *102*, (52), 18819.
10. Oden, J. H.; Szabo, Z. *Arsenic and radionuclide occurrence and relation to geochemistry in groundwater of the Gulf Coast Aquifer System in Houston, Texas, 2007–11*; 2016.
11. Berg, M.; Trang, P. T. K.; Stengel, C.; Buschmann, J.; Viet, P. H.; Van Dan, N.; Giger, W.; Stüben, D., Hydrological and sedimentary controls leading to arsenic contamination of groundwater in the Hanoi area, Vietnam: The impact of iron-arsenic ratios, peat, river bank deposits, and excessive groundwater abstraction. *Chemical Geology* **2008,** *249*, (1), 91-112.
12. Stuyfzand, P. J.; Raat, K. J., Benefits and hurdles of using brackish groundwater as a drinking water source in the Netherlands. *Hydrogeology journal* **2010,** *18*, (1), 117-130.
13. Great Lakes-St. Lawrence River Basin Water Resources Council, Final Decision. In 2016.
14. Dematatis, M.; Plechacek, A.; Mathews, M.; Wright, D. B.; Udenby, F.; Gotkowitz, M. B.; Ginder-Vogel, M., Spatial and temporal variability of radium in the Wisconsin Cambrian-Ordovician aquifer system. *AWWA Water Science* **2020**.
15. Muehe, E.; Kappler, A., Arsenic mobility and toxicity in South and Southeast Asia–a review on biogeochemistry, health and socio-economic effects, remediation and risk predictions. *Environmental Chemistry* **2014,** *11*, 483-495.
16. Aieta, E. M.; Singley, J. E.; Trussell, A. R.; Thorbjarnarson, K. W.; McGuire, M. J., Radionuclides in Drinking Water: An Overview. *Journal (American Water Works Association)* **1987,** *79*, (4), 144-152.

17. Vinson, D. S.; Tagma, T.; Bouchaou, L.; Dwyer, G. S.; Warner, N. R.; Vengosh, A., Occurrence and mobilization of radium in fresh to saline coastal groundwater inferred from geochemical and isotopic tracers (Sr, S, O, H, Ra, Rn). *Applied Geochemistry* **2013,** *38*, 161-175.
18. Izbicki, J. A.; Wright, M. T.; Seymour, W. A.; McCleskey, R. B.; Fram, M. S.; Belitz, K.; Esser, B. K., Cr(VI) occurrence and geochemistry in water from public-supply wells in California. *Applied Geochemistry* **2015,** *63*, 203-217.
19. International Atomic Energy Agency, The environmental behaviour of radium: revised edition. *Technical Reports Series No. 476* **2014**, (476), 44-51.
20. Tricca, A.; Porcelli, D.; Wasserburg, G. J., Factors controlling the groundwater transport of U, Th, Ra, and Rn. *Journal of Earth System Science* **2000,** *109*, (1), 95-108.
21. Vinson, D. S.; Lundy, J. R.; Dwyer, G. S.; Vengosh, A., Implications of carbonate-like geochemical signatures in a sandstone aquifer: Radium and strontium isotopes in the Cambrian Jordan aquifer (Minnesota, USA). *Chemical Geology* **2012,** *334*, 280-294.
22. Gilkeson, R. H.; Specht, S. A.; Cartwright, K.; Griffin, R. A.; Larson, T. E., Geologic studies to identify the source for high levels of radium and barium in Illinois ground-water supplies: a preliminary report. **1978**.
23. Grundl, T.; Cape, M., Geochemical factors controlling radium activity in a sandstone aquifer. *Ground Water* **2006,** *44*, (4), 518-527.
24. Reynolds, B. C.; Wasserburg, G. J.; Baskaran, M., The transport of U- and Th-series nuclides in sandy confined aquifers. *Geochimica et Cosmochimica Acta* **2003,** *67*, (11), 1955-1972.
25. Tricca, A.; Wasserburg, G. J.; Porcelli, D.; Baskaran, M., The transport of U-and Th-series nuclides in a sandy unconfined aquifer. *Geochimica et Cosmochimica Acta* **2001,** *65*, (8), 1187-1210.
26. Felmlee, J. K.; Cadigan, R. A. *Radium and uranium concentrations and associated hydrogeochemistry in ground water in southwestern Pueblo County, Colorado*; 79-974; 1979.
27. Vinson, D. S.; Vengosh, A.; Hirschfeld, D.; Dwyer, G. S., Relationships between radium and radon occurrence and hydrochemistry in fresh groundwater from fractured crystalline rocks, North Carolina (USA). *Chemical Geology* **2009,** *260*, (3-4), 159-171.
28. Nathwani, J. S.; Phillips, C. R., Adsorption of 226Ra by soils in the presence of Ca2+ ions. Specific adsorption (II). *Chemosphere* **1979,** *8*, (5), 293-299.
29. Tamamura, S.; Takada, T.; Tomita, J.; Nagao, S.; Fukushi, K.; Yamamoto, M., Salinity dependence of 226Ra adsorption on montmorillonite and kaolinite. *Journal of Radioanalytical and Nuclear Chemistry* **2014,** *299*, (1), 569-575.
30. Tomita, J.; Satake, H.; Fukuyama, T.; Sasaki, K.; Sakaguchi, A.; Yamamoto, M., Radium geochemistry in Na–Cl type groundwater in Niigata Prefecture, Japan. *Journal of Environmental Radioactivity* **2010,** *101*, (3), 201-210.
31. Krishnaswami, S.; Bhushan, R.; Baskaran, M., Radium isotopes and 222Rn in shallow brines, Kharaghoda (India). *Chemical Geology: Isotope Geoscience section* **1991,** *87*, (2), 125-136.
32. Luczaj, J.; Masarik, K., Groundwater Quantity and Quality Issues in a Water-Rich Region: Examples from Wisconsin, USA. *Resources* **2015,** *4*, (2), 323-357.
33. Evans, R. D., Radium poisoning: a review of present knowledge. *American Journal of Public Health and the Nations Health* **1933,** *23*, (10), 1017-1023.

34. Guse, C. E.; Marbella, A. M.; George, V.; Layde, P. M., Radium in Wisconsin drinking water: an analysis of osteosarcoma risk. *Archives of Environmental Health: An International Journal* **2002,** *57*, (4), 294-303.
35. Cohn, P.; Skinner, R.; Burger, S.; Falgiano, J.; Klotz, J., Radium in Drinking Water and the Incidence of Osteosarcoma: A Report to the New Jersey Department of Environmental Protection. **2003**.
36. Canu, I. G.; Laurent, O.; Pires, N.; Laurier, D.; Dublineau, I., Health effects of naturally radioactive water ingestion: the need for enhanced studies. *Environmental health perspectives* **2011,** *119*, (12), 1676-80.
37. World Health Organization *Guidlines for drinking-water quality: fourth edition incorporating the first addendum.*; Geneva, 2017.
38. Mathews, M.; Gotkowitz, M.; Ginder-Vogel, M., Effect of geochemical conditions on radium mobility in discrete intervals within the Midwestern Cambrian-Ordovician aquifer system. *Applied Geochemistry* **2018,** *97*, 238-246.
39. Alhajji, E.; Al-Masri, M. S.; Khalily, H.; Naoum, B. E.; Khalil, H. S.; Nashawati, A., A Study on Sorption of 226Ra on Different Clay Matrices. *Bulletin of Environmental Contamination and Toxicology* **2016,** *97*, (2), 255-260.
40. Ames, L. L.; McGarrah, J. E.; Walker, B. A.; Salter, P. F., Uranium and radium sorption on amorphous ferric oxyhydroxide. *Chemical Geology* **1983,** *40*, (1), 135-148.
41. Bassot, S.; Mallet, C.; Stammose, D., Experimental Study and Modeling of the Radium Sorption onto Goethite. *MRS Proceedings* **2000,** *663*, 1081.
42. Chen, M. A.; Kocar, B. D., Radium Sorption to Iron (Hydr)oxides, Pyrite, and Montmorillonite: Implications for Mobility. *Environmental Science & Technology* **2018,** *52*, (7), 4023-4030.
43. Sajih, M.; Bryan, N. D.; Livens, F. R.; Vaughan, D. J.; Descostes, M.; Phrommavanh, V.; Nos, J.; Morris, K., Adsorption of radium and barium on goethite and ferrihydrite: A kinetic and surface complexation modelling study. *Geochimica et Cosmochimica Acta* **2014,** *146*, 150-163.
44. Charette, M. A.; Dulaiova, H.; Gonneea, M. E.; Henderson, P. B.; Moore, W. S.; Scholten, J. C.; Pham, M. K., GEOTRACES radium isotopes interlaboratory comparison experiment. *Limnology and Oceanography: Methods* **2012,** *10*, (6), 451-463.
45. Nathwani, J. S.; Phillips, C. R., Rates of leaching of radium from contaminated soils: An experimental investigation of radium bearing soils from Port Hope, Ontario. *Water, Air, and Soil Pollution* **1978,** *9*, (4), 453-465.
46. van Es, E. M.; Russell, B. C.; Ivanov, P.; Read, D., Development of a method for rapid analysis of Ra-226 in groundwater and discharge water samples by ICP-QQQ-MS. *Applied Radiation and Isotopes* **2017,** *126*, 31-34.
47. Jia, G.; Jia, J., Determination of radium isotopes in environmental samples by gamma spectrometry, liquid scintillation counting and alpha spectrometry: a review of analytical methodology. *Journal of Environmental Radioactivity* **2012,** *106*, 98-119.
48. Geibert, W.; Rodellas, V.; Annett, A.; van Beek, P.; Garcia-Orellana, J.; Hsieh, Y.-T.; Masque, P., 226Ra determination via the rate of 222Rn ingrowth with the Radium Delayed Coincidence Counter (RaDeCC). *Limnology and Oceanography: Methods* **2013,** *11*, (11), 594-603.
49. Copia, L.; Nisi, S.; Plastino, W.; Ciarletti, M.; Povinec, P. P., Low-level 226Ra determination in groundwater by SF-ICP-MS: optimization of separation and pre-concentration methods. *Journal of Analytical Science and Technology* **2015,** *6*, (1), 22.

50. Sharabi, G.; Lazar, B.; Kolodny, Y.; Teplyakov, N.; Halicz, L., High precision determination of 228Ra and 228Ra/226Ra isotope ratio in natural waters by MC-ICPMS. *International Journal of Mass Spectrometry* **2010,** *294*, (2), 112-115.
51. Fleischer, R. L., Alpha-recoil damage: Relation to isotopic disequilibrium and leaching of radionuclides. *Geochimica et Cosmochimica Acta* **1988,** *52*, (6), 1459-1466.
52. Weaver, T. R.; Bahr, J., Geochemical evolution in the Cambrian-Ordovician sandstone aquifer, eastern Wisconsin: 1. Major ion and radionuclide distribution. *Ground Water* **1991,** *29*, (3), 350-356.
53. Stackelberg, P. E. *Groundwater quality in the Cambrian-Ordovician aquifer system, midwestern United States*; 2017-3056; Reston, VA, 2017; p 4.
54. Young, H. L.; Siegel, D. I., Hydrogeology of the Cambrian-Ordovician Aquifer System in the Northern Midwest, United States. *U.S. Geological Survey Professional Paper 1405-B 99.* **1992**.
55. Young, H. L., *Summary of ground-water hydrology of the Cambrian-Ordovician aquifer system in the northern Midwest, United States*. US Department of the Interior, US Geological Survey: 1992; Vol. 1405.
56. Weaver, T. R.; Bahr, J. M., Geochemical evolution in the Cambrian-Ordovician sandstone aquifer, eastern Wisconsin: 2. Correlation between flow paths and ground-water chemistry. *Ground Water* **1991,** *29*, (4), 510-515.
57. Kaakinen, J.; Kuokkanen, T.; Kujala, K.; Välimäki, I.; Jokinen, H., The Use of a Five-stage Sequential Leaching Procedure for Risk Assessment of Heavy Metals in Waste Rock Utilized in Railway Ballast. *Soil and Sediment Contamination: An International Journal* **2012,** *21*, (3), 322-334.
58. Fujikawa, Y.; Fukui, M., Variations in adsorption mechanisms of radioactive cobalt and cesium in rocks. *Journal of Contaminant Hydrology* **1991,** *8*, (2), 177-195.
59. Chao, T. T., Selective Dissolution of Manganese Oxides from Soils and Sediments with Acidified Hydroxylamine Hydrochloride. *Soil Science Society of America Journal* **1972,** *36*, (5), 764-768.
60. Robinson, G. D., Sequential chemical extractions and metal partitioning in hydrous Mn-Fe-oxide coatings: Reagent choice and substrate composition affect results. *Chemical Geology* **1984,** *47*, (1), 97-112.
61. Leermakers, M.; Mbachou, B. E.; Husson, A.; Lagneau, V.; Descostes, M., An alternative sequential extraction scheme for the determination of trace elements in ferrihydrite rich sediments. *Talanta* **2019,** *199*, 80-88.
62. Suresh, P. O.; Dosseto, A.; Handley, H. K.; Hesse, P. P., Assessment of a sequential phase extraction procedure for uranium-series isotope analysis of soils and sediments. *Applied Radiation and Isotopes* **2014,** *83*, 47-55.
63. Wang, X.; Xu, S.; Zhang, B.; Zhao, S., Deep-penetrating geochemistry for sandstone-type uranium deposits in the Turpan–Hami basin, north-western China. *Applied Geochemistry* **2011,** *26*, (12), 2238-2246.
64. Sawhney, B. L.; Stilwell, D. E., Dissolution and elemental analysis of minerals, soils, and environmental samples. In *Quantitative methods in soil mineralogy*, Amonette, J. E.; Zelazny, L. W., Eds. SSSA: Madison, WI, 1994; pp 49-82.
65. Mester, Z.; Sturgeon, R., *Sample Preparation for Trace Element Analysis*. Elsevier: 2003; Vol. XLI, p 1286.

66. Muratli, J. M.; McManus, J.; Mix, A.; Chase, Z., Dissolution of fluoride complexes following microwave-assisted hydrofluoric acid digestion of marine sediments. *Talanta* **2012,** *89*, 195-200.
67. Sims, K. W. W.; Hart, S. R.; Reagan, M. K.; Blusztajn, J.; Staudigel, H.; Sohn, R. A.; Layne, G. D.; Ball, L. A.; Andrews, J., 238U-230Th-226Ra-210Pb-210Po, 232Th-228Ra, and 235U-231Pa constraints on the ages and petrogenesis of Vailulu'u and Malumalu Lavas, Samoa. *Geochemistry, Geophysics, Geosystems* **2008,** *9*, (4).
68. de Winter, J., Using the Student's t-test with extremely small sample sizes. *Practical Assessment, Research & Evaluation* **2013,** *18*.
69. Sturchio, N. C.; Banner, J. L.; Binz, C. M.; Heraty, L. B.; Musgrove, M., Radium geochemistry of ground waters in Paleozoic carbonate aquifers, midcontinent, USA. *Applied Geochemistry* **2001,** *16*, (1), 109-122.
70. Office of Environmental Policy and Assistance - Air, W. a. R. D. E.-. *Compendium of EPA-approved analytical methods for measuring radionuclides in drinking water*; US Department of Energy: 1998.
71. Ostrom, M. E., Paleozoic Stratigraphic Nomenclature for Wisconsin. *Wisconsin Geological and Natural History Survey Information Circular 8* **1967**.
72. Stern, T. W.; Stieff, L. R., Part 13. Radium-Uranium equilibrium and radium-uranium ages of some secondary minerals. *US Geological Survey Professional Paper* **1959**, (320), 151.
73. Pietruszka, A. J.; Carlson, R. W.; Hauri, E. H., Precise and accurate measurement of 226Ra–230Th–238U disequilibria in volcanic rocks using plasma ionization multicollector mass spectrometry. *Chemical Geology* **2002,** *188*, (3-4), 171-191.
74. Michel, J., Redistibution of uranium and thorium series isotopes during isovolumetric weathering of granite. *Geochimica et Cosmochimica Acta* **1984,** *48*, 1249-1255.
75. IUPAC, *Compendium of Chemical Terminology*. Blackwell Scientific Publications: Oxford, 1997.
76. Krishnaswami, S.; Graustein, W. C.; Turekian, K. K.; Dowd, J. F., Radium, thorium and radioactive lead isotopes in groundwaters: Application to the in situ determination of adsorption-desorption rate constants and retardation factors. *Water Resources Research* **1982,** *18*, (6), 1663-1675.
77. Webster, I. T.; Hancock, G. J.; Murray, A. S., Modelling the effect of salinity on radium desorption from sediments. *Geochimica et Cosmochimica Acta* **1995,** *59*, (12), 2469-2476.
78. Iyengar, M. A. R., The natural distribution of radium. *The environmental behaviour of radium* **1990,** *1*, 59-128.
79. Warner, N. R.; Christie, C. A.; Jackson, R. B.; Vengosh, A., Impacts of shale gas wastewater disposal on water quality in western Pennsylvania. *Environmental science & technology* **2013,** *47*, (20), 11849-11857.
80. Haluszczak, L. O.; Rose, A. W.; Kump, L. R., Geochemical evaluation of flowback brine from Marcellus gas wells in Pennsylvania, USA. *Applied Geochemistry* **2013,** *28*, 55-61.
81. Rowan, E. L.; Engle, M. A.; Kirby, C. S.; Kraemer, T. F., Radium content of oil-and gas-field produced waters in the Northern Appalachian Basin (USA): Summary and discussion of data. *US Geological Survey Scientific Investigations Report* **2011,** *5135*, (2011), 31.
82. Swarzenski, P. W.; Baskaran, M.; Rosenbauer, R. J.; Edwards, B. D.; Land, M., A combined radio-and stable-isotopic study of a California coastal aquifer system. *Water* **2013,** *5*, (2), 480-504.

83. Ayotte, J. D.; Szabo, Z.; Focazio, M. J.; Eberts, S. M., Effects of human-induced alteration of groundwater flow on concentrations of naturally-occurring trace elements at water-supply wells. *Applied Geochemistry* **2011,** *26*, (5), 747-762.

Chapter 4

Isotopic analysis of radium association with aquifer solids at discrete intervals in the Midwestern Cambrian-Ordovician aquifer system

4.1 Abstract

Radium (Ra) is a naturally occurring contaminant that frequently occurs at elevated levels in the Midwestern Cambrian-Ordovician aquifer system (MCOAS). Geochemical indicators (e.g., dissolved oxygen or total dissolved solids) are useful tools for broadly characterizing elevated contaminant levels, but do not consistently correlate to elevated Ra within specific stratigraphic horizons. We present a coupled geochemical and isotopic study of groundwater and aquifer solids for major and trace elements, Ra, and uranium (U) at discrete intervals in the MCOAS. Through groundwater as well as extracted and digested solid samples, we find that Ra is close to equilibrium with parent isotopes of uranium (U); however, the potential for Ra mobilization varies by stratigraphic unit. Overall, the examined geochemical characteristics (e.g., ORP, TDS) do not fully describe Ra interactions within the system, suggesting alternative factors, like solid-phase associations, may be more important in the system. Minerals elevated in ^{87}Sr, such as feldspars and clays, may be more likely to also release ^{226}Ra to the aqueous system. Overall, the release of U and Ra due to water-rock interactions varies with discrete stratigraphy, depending on aqueous geochemistry and available mineral associations. Sources and sinks of Ra at depth within the MCOAS vary across stratigraphy, and are difficult to predict based on water samples taken from broad ranges of the aquifer system. Aqueous geochemistry (e.g., ORP, TDS) within aquifer

stratigraphy must be considered alongside both parent nuclide and Ra solid-phase associations in the aquifer system in order to fully describe Ra-solids interactions.

4.2 Introduction

The quality of a drinking water source dictates in part the quantity of potable water available, and is dependent on the infiltration and mobilization of contaminants.[1,2] Groundwater serves as a source of drinking water for more than 2 billion people globally, with potential threats to water quality coming from both above and below the surface.[3,4] Anthropogenic contaminants are introduced by humans to groundwater, while geogenic contaminants are naturally occurring and may mobilize to the aqueous system via subsurface geochemistry and hydrology.[5,6] Geogenic contaminants frequently occur at ultra trace levels in groundwater (e.g., radium); however, these concentrations are often still of concern to human health in drinking water.[7,8] Aqueous geochemistry influences water-rock interactions, like sorption site availability and/or mineral presence, can further impact the mobilization of contaminants into the aqueous system and increase contaminant levels.

Ingesting radium (Ra), a naturally occurring contaminant, can result in elevated risk for osteosarcoma and bone disease.[9-11] In aquifer systems, Ra is generated from the decay chains of uranium (^{238}U, ^{235}U) and thorium (^{232}Th) via alpha decay. In some cases, high recoil energy ejects Ra from the mineral lattice to the aqueous system. The US EPA has set a maximum contaminant level (MCL) of 185 mBq/L (5 pCi/L) for combined Ra (^{226}Ra + ^{228}Ra) in drinking water.[7] In the US, frequent occurrences of combined Ra above the MCL occur in the Midwestern Cambrian-Ordovician aquifer system (MCOAS).[12] Examination of combined Ra from nearly two decades of municipal well compliance data suggests increasing levels over time in the MCOAS in Wisconsin.[13]

It is necessary to increase understanding of geochemical controls (e.g., sorption, mineral dissolution) on the release of geogenic contaminants from the aquifer solids to the aqueous system in order to maintain aquifer systems for sustainable and clean drinking water.[5,14] Geochemical influences such as redox state and total dissolved solids (TDS) release naturally occurring contaminants (e.g., As, Cr, Ra, U) via water-rock interactions in subsurface environments. While changes in aquifer redox chemistry directly impact the mobility of a few geogenic contaminants (e.g., As, Cr, U), partitioning of all contaminants from aquifer solids is influenced by the presence or absence of redox-sensitive minerals.[15-23] Additionally, elevated TDS in groundwater can cause ion competition for sorption sites, leaving fewer available sites and more ions in the aqueous system.[12,23,24]

After Ra production via parent nuclide decay, geochemical factors influence Ra partitioning between groundwater and aquifer solids. Elevated Ra in groundwater is associated with anoxic conditions, elevated TDS, and/or older water.[12,24,25] Minerals like iron (Fe(III)) or manganese (Mn(III/IV)) (hydr)oxide minerals are more likely to dissolve or be absent from anoxic aquifer systems, reducing the number of overall sorption sites present.[26-30] Elevated TDS and older, more mineralized water have increased dissolved ions in the water available to compete for sorption sites, leaving fewer sites available for Ra(II) ions.[31-33] Ra is more likely to co-precipitate in concert with other minerals (e.g., barite) than form Ra minerals due to ultra trace Ra levels in aquifer systems.[34,35] Geochemical controls (e.g., anoxic conditions, elevated TDS) are associated with elevated Ra in groundwater withdrawn from deep municipal wells across the MCOAS, as well as with groundwater sampled from discrete hydrostratigraphic intervals.[12,24,25,36-38] Further investigation into the mobilization of Ra at discrete intervals due to

geochemical influences on radionuclide-solids interactions is necessary to better predict elevated Ra in the MCOAS.

Here, we examine the influence of geochemical conditions (e.g., alkalinity, ORP, TDS) on U and Ra partitioning from aquifer solids at discrete intervals within the MCOAS. Groundwater samples from a multi-level monitoring well completed in the MCOAS near the Village of Cottage Grove, Wisconsin were analyzed for ^{238}U, total dissolved solids (TDS), pH, ORP, and ionic composition (Figure 4.1). Additionally, rock samples from each interval were extracted and digested to examine Ra associations with aquifer solids. Sensitive analysis by multi-collector inductively coupled plasma mass spectrometry (MC-ICPMS) was used to examine ultra trace concentrations of ^{226}Ra in aqueous and rock samples, as well as $^{234}U/^{238}U$ and $^{87}Sr/^{86}Sr$. Overall, this study expands knowledge of U and Ra partitioning within stratigraphy in the MCOAS, investigating aqueous geochemistry and solid-phase associations via isotopic tools (e.g., $^{226}Ra/^{238}U$, $^{87}Sr/^{86}Sr$) to examine the contribution of Ra from discrete intervals within the aquifer system.

4.3 Methods

4.3.1 Study site

The MCOAS is composed of Paleozoic sandstone and dolostone aquifers with scattered siltstone and shale, overlying relatively impermeable Precambrian crystalline basement rock. At the study site, the coarse- to medium-grained sandstone of the Mt Simon formation forms the deepest aquifer (Figure 4.1). Fine-grained and silty sandstone of the Eau Claire formation overlies the Mt Simon and acts as a local confining unit at the study site. Sandstone of the Wonewoc Formation overlies the Eau Claire and forms a prolific regional aquifer. The glauconitic sandstone of the Tunnel City Group overlies the Wonewoc; while the Tunnel City produces less water than

the Wonewoc, it is another important local water source. The St Lawrence formation, a silty dolostone or dolomitic siltstone with trace glauconite and relatively low hydraulic conductivity, lies above the Tunnel City Group. The Readstown member, formed of interbedded sandstone, clay and dolostone fragments, overlies the St Lawrence formation. The Tonti member, a fine- to medium-grained sandstone, is the uppermost stratigraphic unit at this location.[39]

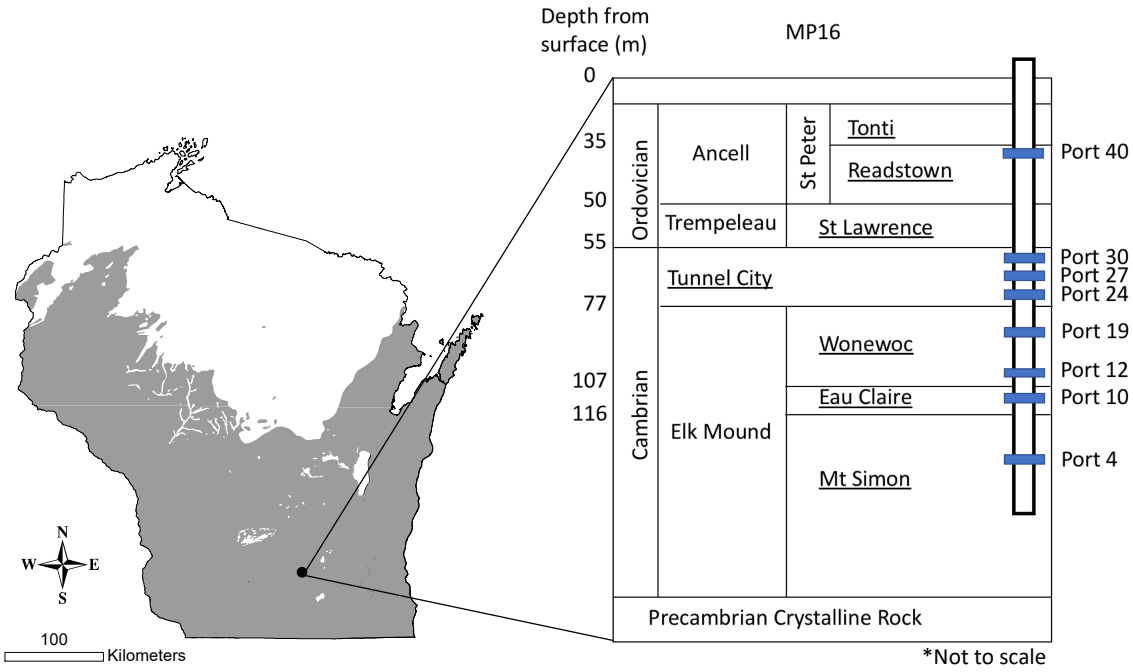

Figure 4.1 The extent of the Midwestern Cambrian-Ordovician aquifer system in Wisconsin, in grey. The inset shows the location of the multi-level monitoring well and representative stratigraphy for the study site. Blue rectangles demonstrate approximate location of port openings.

The multi-level well, MP16, used in this study is located near the Village of Cottage Grove, Wisconsin. Drilled in 2007, MP16 was selected for this study because it is outside of the influence of a nearby contaminant plume. MP16 is a Westbay MP® multi-level well with packer seals separating 46 discrete port intervals within the groundwater system; heads are monitored at each depth, or 'port', and a groundwater sample can be collected from each port. Drilling of MP16 included collection. A log of the core described lithology and other geologic traits at 5 cm scale.

For this study, 8 of the 46 ports were selected based on spectral gamma logs indicating solid-phase U and Th at depth. Further details about well construction and geophysical characterization at depth in the study site are available in Meyer et al., 2008 and Meyer et al., 2016.[40,41]

4.3.2 Groundwater sampling procedure

Groundwater samples were collected from eight ports at MP16 (Figure 4.1). Prior to sample collection, air was evacuated from four sample containers (1 L combined volume) using a peristaltic pump. The sample containers were attached to a sampler probe and lowered down the borehole on a wireline which was controlled by a data acquisition box at the surface. The sampler probe was landed at the approximate depth of the port of interest, and positioned at the port opening, using hydraulic head to verify location. The sampling valve was opened, and groundwater flowed within the packer interval into the sampling containers. Field parameters such as oxidation-reduction potential (ORP), pH, temperature, and TDS were measured using a Myron Ultra Meter II at the surface (Table 4.1). Samples for aqueous metals analysis were filtered (0.45 μm) and acid preserved with trace metal grade nitric acid (HNO_3) to pH < 2, while samples for general inorganic analysis were only filtered. All samples were stored at 4 °C prior to analysis. A sampling blank was collected by running ultrapure water through the sampling equipment. Measured ORP was used to estimate redox potential (pe) values, by adding the E_{ref} for Ag/AgCl reference electrodes (199 mV) to the field ORP reading.[42,43]

4.3.3 Aquifer solids extraction experiment

An extraction experiment was conducted on eight sections of core, corresponding to depth discrete intervals associated with the sampled MP16 ports (Table 4.1). The experiment was conducted at room temperature, under oxic conditions for five of the depths (Ports 19, 24, 27, 30, 40), and in anoxic conditions for three depths (Ports 4, 10, 12) as determined by aquifer redox

potential. Each subsample was pulverized to a fine powder via a shatterbox. Two of the depths were subsampled in triplicate (R-35 and MS-132), to account for possible sample heterogeneity. All extraction chemicals were trace metal grade. Acido-soluble (carbonates) and easily reduced phases (e.g., Fe- and Mn-(hydr)oxides) were dissolved by adding 400 mL of 0.04 M hydroxylamine hydrochloride in 25% trace metal grade acetic acid to 40 g of each rock sample, at a 1:10 rock to extractant ratio. After the addition of the extractant, the solution was shaken for a few seconds several times a day as equilibrium was reached. Metal concentrations (e.g., Ca, Fe) were monitored over time until there was < 10% change. Once equilibrium was reached, samples were centrifuged at 4000 rpm for 30 minutes; the decanted solution was filtered (0.45 μm) and stored at 4 °C until analysis.

4.3.4 Aquifer solids digestion

After extraction, subsamples of the aquifer solids were baked at 50 °C until dry, then digested. Digestion chemicals were trace metal grade unless otherwise stated. To 0.1 g of each sample, 1 mL ultrapure water, 3.5 mL concentrated HNO_3, 1.5 mL concentrated hydrochloric acid (HCl), and 1 mL concentrated hydrofluoric acid (HF) was added, in that order. Each sample was then sealed in a microwave vial with a screw cap and cover, and placed into the shields on a MAXI 44 Rotor, then set inside the cavity of a Milestone ETHOS Easy Microwave Digestion System. The digestion method ramped up to 100 °C for fifteen minutes, held at 100 °C for 10 minutes, then increased up to 185 °C over forty minutes, holding there for 35 minutes; this was followed by a ventilation and cooling period of 30 minutes. After HF-digestion, samples were dried on a hot plate at ~130 °C, then 10 mL 3 M Optima grade HCl was added and the solution was diluted to ~50 g total. For quality assurance, three digestion blanks were distributed

throughout the samples; USGS standard reference materials AGV-2, BCR-2, and TML were also digested (Table D-2 for $^{87}Sr/^{86}Sr$ literature values).[44-47]

4.3.5 General chemical analysis

Chemical analysis was conducted on groundwater, extraction, and HF-digested solution samples for relevant inorganic ions and metals. Alkalinity and inorganic ions were determined in groundwater samples within 48 hours of sampling. Alkalinity was analyzed using a Mettler Toledo G20 autotitrator while inorganic anions were analyzed by a Dionex ICS-2100 ion chromatography system to determine the concentrations of sulfate (SO_4^{2-}), and chloride (Cl^-). For the water and extraction fractions, an Agilent 5110 inductively-coupled plasma optical emission spectrometer was used for bulk metal analysis (e.g., Ca, Mg, Na, K, Al). Trace metal analysis (e.g., ^{238}U, Fe, Mn, Sr, Ba) was conducted using a ThermoScientific ELEMENT2 high resolution inductively-coupled plasma mass spectrometer at the Wisconsin State Laboratory of Hygiene Trace Elements Clean Laboratory.

4.3.6 Isotopic analysis

Radium (^{226}Ra), uranium ($^{234}U/^{238}U$), and strontium ($^{87}Sr/^{86}Sr$) isotopes were analyzed using a MC-ICPMS at the Wisconsin State Laboratory of Hygiene Trace Elements Laboratory.

4.3.6.1 Radium isotope analysis

For Ra analysis preparation, each sample was spiked with 100 μL of a Ra solution purified from a Th solution (initial $^{226}Ra/^{228}Ra$: 0.8197). Each sample was then run through five purification columns prior to MC-ICPMS analysis.[48,49] All reagents used in column purification were Optima grade. The first column used ~7 M HNO_3 to separate the cation matrix, through AG1-X8 (100 - 200 mesh) anion exchange resin. The second column isolated the Ra + Ba fraction from the rest of the cation matrix, using progressively stronger HCl washes through AG50W-X8

(200 – 400 mesh) cation exchange resin. Using Eichrom SrSpec, Ra was isolated from Ba with 3 M HNO_3; this column method was repeated to ensure separation. Finally, a fifth column, similar to the first column with a smaller column volume (CV), was run to separate Ra from ^{228}Th formed via decay during the column process. Further details are available in Mathews et al., 2021.[50]

Radium isotope ratios were measured using mean beam intensities on the Neptune Plus MC-ICPMS using a single SEM/RPQ detector in dynamic mode. The ^{228}Ra isotope spike was calibrated to the average literature $^{226}Ra/^{228}Ra$ for the rock standards (S1).[48] The measured $^{226}Ra/^{228}Ra$ ratio was used to calculate the ^{226}Ra for each sample, converted from fg/g solution Ra activities to mBq/L of water or mBq/g of rock, after which aquifer system physical properties were used to calculate mBq/cm^3 aquifer (Table D-3). The ion counter detector was calibrated prior to each analysis with a dilute tuning solution containing ^{238}U. A natural uranium solution was used to correct $^{226}Ra/^{228}Ra$ for mass bias by analyzing for $^{238}U/^{235}U$.

4.3.6.2 Uranium isotope ratio

The uranium activity ratio $^{234}U/^{238}U$ was analyzed by MC-ICPMS after sample purification. The U fraction was collected using 1 M HCl and 1 M hydrobromic acid (HBr) after the Ra fraction eluted off the first purification column previously discussed in sect. 4.3.6.1. Each sample was dried, then dissolved in 1 CV of ~11 M HCl + H_2O_2. For the second U purification column, AG1-X8 (100 - 200 mesh) anion exchange resin was conditioned with 8 M HCl and ~11 M HCl + 30% H_2O_2, then the sample is loaded onto the column. Two CV of ultrapure water and 3 CV of 1 M HBr are collected for the sample U fraction. Each sample was dried down, then 2 mL of 2% HNO_3 was added; the solution was covered and heated at 110 °C for ~ 30 min to dissolve. Samples were analyzed for ^{238}U, ^{235}U, and ^{234}U on the MC-ICPMS, bracketing samples between natural U standards in order to correct for the background. ^{238}U and ^{235}U were measured

on Faraday cups, while ^{234}U was measured on the SEM/RPQ. The cup configuration was set by using a natural U solution to align the H1 and H3 Faraday cups to the center SEM.

4.3.6.4 Strontium isotopes

The $^{87}Sr/^{86}Sr$ isotope ratio was analyzed by MC-ICPMS after sample purification. The Sr fraction was collected prior to the Ra fraction from the second purification column (See section 2.6.1). Samples were dried and redissolved in 0.5 mL 3 M HNO_3. After washing 1 CV of SrSpec resin with ultrapure water and 6 M HCl, the resin was conditioned with 3 mL of 3 M HNO_3. The sample was loaded, followed by 3 washes of 0.5 mL 3 M HNO_3, collecting the sample with 4 mL of ultra pure water. The Sr fraction was dried down, and redissolved in 2 mL 2% HNO_3 + 0.01% HF for analysis. Samples were bracketed between measurements of NIST standard NBS987. To internally correct for mass fractionation, measured values of $^{87}Sr/^{86}Sr$ were normalized by a value of 1.000061, calculated from the change from the literature value for NIST standard NBS987 (0.71024). Sr ratio values for the rock standards AGV-2, BCR-2, and TML varied by < 0.1% from literature averages.[49]

4.3.7 Quality assurance

Average ^{226}Ra yield after column purification was calculated from literature values of standard reference materials (SRM) AGV-2, BCR-2, and TML, resulting in a correction factor of 2.83% (D1).[47] Recovery for the digestion experiment was 89 ± 7%, determined from the quantity of ^{238}U measured for the SRMs and a correction factor of 1.12 was applied to all digestion concentrations (Table D-1). Further Quality Assurance details can be found in the Supplementary Information (D-2).

Table 4.1 Field parameters and inorganic ions for water samples from well MP16. < LOQ = Less than the limit of instrumental quantitation. DBS = depth below ground surface; R = Readstown member, TC = Tunnel City group, W = Wonewoc formation, EC = Eau Claire formation, MS = Mount Simon formation

Sample	Port	Ground-water Sampling Date	Open port interval (DBS, m)	Core depth (DBS, m)	pH	TDS (mg/L)	ORP (mV)	Alkalinity (mg $CaCO_3$/L)	Chloride (mg/L)	Sulfate (mg/L)
R-35	40	11/16/19	35 – 36	35	7.91	283	217	226	4.06	5.21
TC-59	30	11/16/19	58 – 60	59	7.95	322	172	260	7.41	3.81
TC-67	27	11/16/19	67 – 68	67	7.22	375	155	328	< LOQ	3.65
TC-75	24	11/15/19	74 – 76	75	8.00	394	143	348	0.73	2.31
W-85	19	11/15/19	85 – 87	85	7.94	383	103	349	< LOQ	1.71
EC-109	12	11/15/19	107 – 109	109	7.51	453	-16	376	< LOQ	3.82
EC-114	10	11/14/19	113 – 115	114	7.82	437	-9	392	1.75	4.00
MS-132	4	11/14/19	131 – 133	132	7.09	473	-43	388	< LOQ	5.49

4.4 Results

4.4.1 Uranium and radium activity ratios

Parent and daughter (i.e., [$^{234}U/^{238}U$]) nuclide ratios vary with stratigraphy at the study site. Activity (A) is defined as the decay of a radionuclide (Eq. 4.1), where the activity ratio is the ratio of parent and daughter nuclide activities represented by the fraction of the two isotopes, with activity designated by brackets.

$$A = N * \lambda \tag{4.1}$$

Here, N represents the number of atoms of a radionuclide, while λ is the radioactive decay constant. Aqueous [$^{234}U/^{238}U$] varies across stratigraphy, ranging from 4.707(2) to 11.107(6) (Figure 4.2a, Table 4.2). Values of aqueous [$^{234}U/^{238}U$] above 6 are observed in R-35, TC-59, and TC-75, peaking at 11.107(6) (R-35). All other samples contain aqueous [$^{234}U/^{238}U$] below 6,

averaging 4.9(2). Note that the associated uncertainty for each measurement is represented in parentheses.

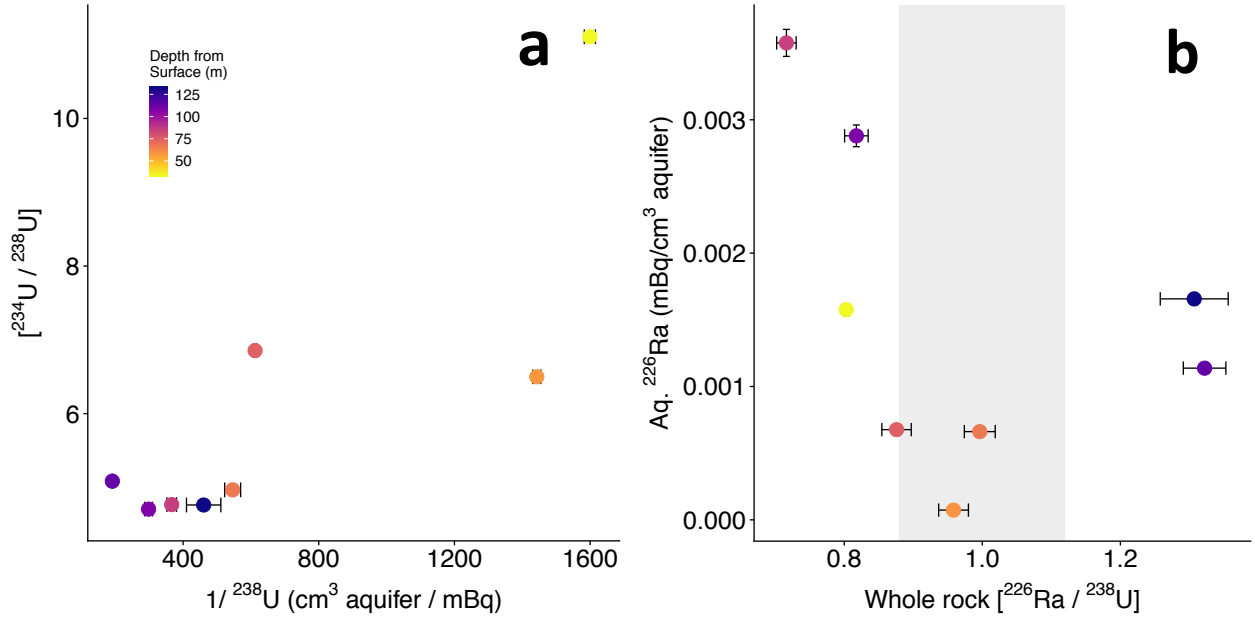

Figure 4.2 Radionuclide ratios from well MP16 water and rock samples. a) Aqueous [^{234}U/^{238}U] with the inverse of aqueous ^{238}U activity. b) Aqueous ^{226}Ra activity per volume of aquifer compared to the whole rock ratio of ^{226}Ra and ^{238}U activities. Gray-shaded area represents secular equilibrium, ranging from 0.88 to 1.12.

Parent and daughter (i.e., [^{226}Ra/^{238}U]) nuclide activity ratios vary with stratigraphy and aqueous ^{226}Ra at the study site. The whole-rock (i.e., sum of the radionuclide from each experimental fraction) [^{226}Ra/^{238}U] is compared to an equilibrium range of 0.9 to 1.1 determined from several HF-digested standard reference materials (SRM). Sample whole rock [^{226}Ra/^{238}U] range from 0.72 to 1.32 for samples at depth (Figure 4.2b), with [^{226}Ra/^{238}U] in five ports (i.e., 4, 10, 12, 19, 40) outside the equilibrium range. Whole-rock [^{226}Ra/^{238}U] for TC-75, TC-67, and TC-59 lies within the SRM equilibrium range. Overall, aqueous ^{226}Ra ranges from 0.000073(2) to 0.0036(1) mBq/cm^3 aquifer. W-85 contains the greatest aqueous ^{226}Ra activity and lowest [^{226}Ra/^{238}U]. The three samples within the [^{226}Ra/^{238}U] equilibrium range contain the lowest aqueous ^{226}Ra activities.

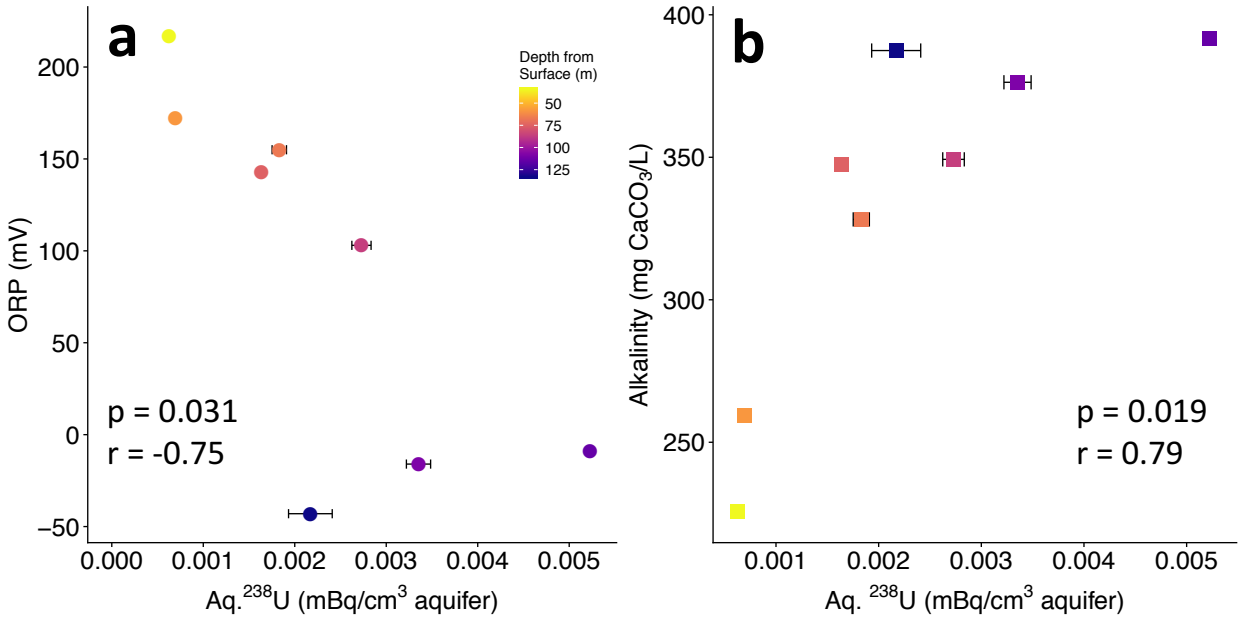

Figure 4.3 Geochemical factors associated with aqueous ^{238}U from well MP16. a) Oxidative-reduction potential (ORP) association with aqueous ^{238}U. b) Alkalinity relationship with aqueous ^{238}U. Error bars represent instrumental uncertainty. Pearson statistical analysis p-value (p) and correlation coefficient (r) distinguish strength of trend.

4.4.2 Association of geochemical factors with aqueous ^{238}U and ^{226}Ra

Aqueous ^{238}U is associated with geochemical factors (e.g., ORP, alkalinity) across sampled stratigraphy (Figure 4.3a,b). Generally, ORP values decrease with increasing aqueous ^{238}U (p-value = 0.031, pearson coefficient = -0.75). In the oxic system (R-35, TC-59, TC-67, TC-75, and W-85), as ORP decreases from 217 mV to 103 mV, aqueous ^{238}U increases (p-value = 0.028, pearson coefficient = -0.92). In the anoxic system (EC-109, EC-114, and MS-132), ORP ranges from -9 mV to -43 mV. Alkalinity increases with depth, along with aqueous ^{238}U (p-value = 0.019, pearson coefficient = 0.79). Alkalinity values range from 226 mg $CaCO_3$/L (R-35) to 392 mg $CaCO_3$/L (EC-114). EC-114 and EC-109, the two samples with greatest aqueous ^{238}U (0.00523(3) and 0.0034(1) mBq/cm^3 aquifer, respectively), both draw water from the Eau Claire, a shaley sandstone unit.

Aqueous ^{226}Ra is examined in relationship to geochemical factors (e.g., ORP, TDS) across sampled stratigraphy in Figure 4.4. Aqueous ^{226}Ra generally increases with depth from surface. A wide range of aqueous ^{226}Ra is observed in the oxic system (0.00066(2) mBq/cm3 aquifer to 0.0036(1) mBq/cm3 aquifer). A smaller range of ^{226}Ra is observed in the anoxic system (0.00114(3) mBq/cm^3 aquifer to 0.00288(8) mBq/cm^3 aquifer). TDS increases with depth from surface, ranging from 283 mg/L to 473 mg/L. In general, higher aqueous ^{226}Ra levels occur at greater TDS levels, although this is not consistent across all samples.

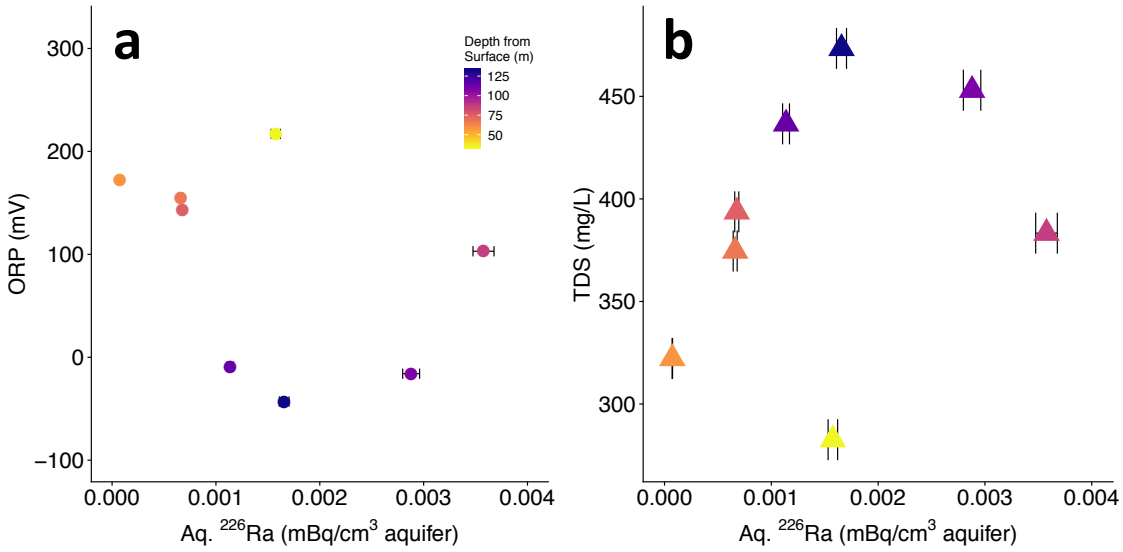

Figure 4.4 Geochemical factors associated with aqueous ^{226}Ra from well MP16. a) Oxidation-reduction potential (ORP) associated with ^{226}Ra. b) Total dissolved solids (TDS) associated with aqueous ^{226}Ra. Error bars represent instrumental uncertainty.

4.4.3 Strontium isotope ratios

Strontium isotope ratios (^{87}Sr/^{86}Sr) vary in samples across experimental fractions (Figure 4.5a). In the aqueous fraction, ^{87}Sr/^{86}Sr generally increases at depth from surface, ranging from 0.709653(8) to 0.712519(8). In the extracted fraction ^{87}Sr/^{86}Sr is similar to the aqueous fraction for R-35, TC-75, and EC-114 (respectively, 0.71028(1), 0.710512(8), and 0.712531(6)). However, extracted ^{87}Sr/^{86}Sr for TC-59, TC-67, W-85, EC-109, and MS-132 differs from aqueous

$^{87}Sr/^{86}Sr$ (ranging from 0.711770(7) to 0.723803(7)). In the HF-digested fraction, $^{87}Sr/^{86}Sr$ for R-35 and MS-132 is similar to the aqueous samples (respectively, 0.70954(1) and 0.7124(4)). HF-digested $^{87}Sr/^{86}Sr$ for all other ports vary widely from their aqueous counterparts, ranging from 0.721595(7) to 0.743646(9). Results from TC-67 were removed from analysis of the HF-digested fraction as an outlier, due to highly elevated $^{87}Sr/^{86}Sr$.

Aqueous $^{87}Sr/^{86}Sr$ is associated with aqueous ^{226}Ra, and related to the geologic period of the stratigraphy (Figure 4.5b). For all samples, aqueous ^{226}Ra and the $^{87}Sr/^{86}Sr$ ratio correlate at the sampling site (p-value = 0.046, pearson coefficient = 0.74). While all other ports source water from Cambrian stratigraphy, R-35 is open to the Readstown member, an Ordovician stratigraphic unit. When only ports open to Cambrian stratigraphy are included, the correlation between aqueous $^{87}Sr/^{86}Sr$ ratio and ^{226}Ra is stronger (p-value = 0.0028, pearson coefficient = 0.96; Figure D-3).

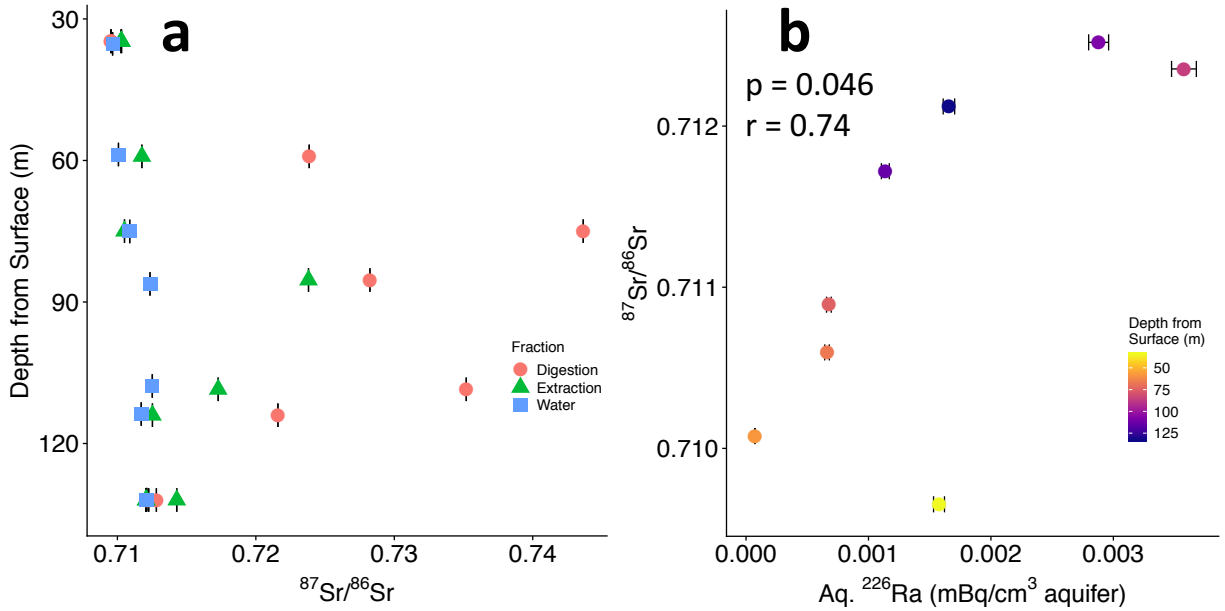

Figure 4.5 Relationship between strontium isotope ratio and aquifer parameters. a) $^{87}Sr/^{86}Sr$ ratio for each experimental fraction at depth from surface. TC-67 was exempted from this dataset as an outlier. b) Association between aqueous ^{226}Ra activity and $^{87}Sr/^{86}Sr$ from MP16. Error bars represent instrumental error. Pearson statistical test p-value (p) and correlation coefficient (r) represent fit of trend line.

Table 4.2 Isotopic data for water, extraction, and digestion samples from MP16. Uncertainty is attributed to calculated dilution uncertainty (^{226}Ra) or instrumental error (U, Sr), unless otherwise indicated. *For extraction and digestion fractions: Average of triplicate measurements, with standard deviation representing uncertainty.

	Water Fraction			Extraction Fraction			HF-Digested Fraction		
Sample	^{226}Ra (mBq/cm^3 aquifer)	$^{238}U/^{234}U$	$^{87}Sr/^{86}Sr$	^{226}Ra (mBq/cm^3 aquifer)	$^{238}U/^{234}U$	$^{87}Sr/^{86}Sr$	^{226}Ra (mBq/cm^3 aquifer)	$^{238}U/^{234}U$	$^{87}Sr/^{86}Sr$
MS-132*	0.00166 ± 0.00005	4.763 ± 0.002	0.712122 ± 0.000008	0.9 ± 0.5	1.428 ± 0.009	0.713 ± 0.001	10 ± 2	0.908 ± 0.002	0.7124 ± 0.0004
EC-114	0.00114 ± 0.00003	5.086 ± 0.001	0.711720 ± 0.000007	7.1 ± 0.2	1.1001 ± 0.0006	0.712531 ± 0.000006	58 ± 1	0.720 ± 0.001	0.721595 ± 0.000007
EC-109	0.00288 ± 0.00008	4.707 ± 0.002	0.712519 ± 0.000008	25.3 ± 0.7	1.1892 ± 0.0007	0.717279359 ± 0.000007	71 ± 2	0.6932 ± 0.0007	0.735196 ± 0.000007
W-85	0.0036 ± 0.0001	4.769 ± 0.002	0.712354 ± 0.000007	5.3 ± 0.2	0.9332 ± 0.0004	0.723803 ± 0.000007	8.0 ± 0.2	0.699 ± 0.002	0.728241 ± 0.000009
TC-75	0.00068 ± 0.00002	6.855 ± 0.002	0.710892 ± 0.000008	4.3 ± 0.1	1.440 ± 0.001	0.710512 ± 0.000008	36.7 ± 0.9	0.875 ± 0.002	0.743646 ± 0.000009
TC-67	0.00066 ± 0.00002	4.969 ± 0.002	0.710596 ± 0.000007	5.4 ± 0.2	1.0796 ± 0.0008	0.717075 ± 0.000007	30.5 ± 0.8	0.840 ± 0.001	0.97297 ± 0.00001
TC-59	0.000073 ± 0.000002	6.500 ± 0.002	0.710077 ± 0.000007	9.9 ± 0.3	2.808 ± 0.003	0.711770 ± 0.000008	40 ± 1	0.927 ± 0.001	0.723851 ± 0.000008
R-35*	0.00158 ± 0.00004	11.107 ± 0.006	0.709653 ± 0.000008	5.2 ± 0.7	1.34 ± 0.01	0.71028 ± 0.00001	53 ± 6	0.830 ± 0.007	0.709539 ± 0.00001

4.5 Discussion

4.5.1 Uranium and radium equilibrium

Comparing the activities of parent and daughter nuclides provides information about radionuclide mobilization in aquifer systems. In systems undisturbed for time periods much longer than the daughter isotope half-life, secular equilibrium (i.e., equivalent activities of parent and daughter nuclides) is expected. However, if the daughter isotope is removed from the site of parent decay, the ratio will not be in unity.[51] In the MCOAS, the $^{238}U/^{226}Ra$ ratio varies across different types of bedrock units; equilibrium dominates in many stratigraphic units, although ^{226}Ra leaching is observed in sandstone and shale units.[50] The quantity of Ra available to partition from rock to water also differs across available solid-phase associations. For example, glauconitic sandstone contains more Ra associated with reducible minerals (e.g., Fe oxides) compared to shale, in which more Ra is more associated with the acido-soluble fraction (e.g., carbonate minerals).[50]

As alpha recoil ejects ^{234}U from the decay of ^{238}U, [$^{234}U/^{238}U$] typically represents groundwater-rock interactions, with preferential flow paths etched by alpha recoil damage.[52,53] A correlation between reciprocal ^{238}U and [$^{234}U/^{238}U$] indicates a two-component mixture solution.[54] In this study, there is not a significant association between 1/[^{238}U] and aqueous [$^{234}U/^{238}U$] (p-value = 0.058) indicating that there are many U sources in the subsurface at the study site (Figure 4.2a). However, the higher levels of [$^{234}U/^{238}U$] for R-35, TC-59, and TC-75 (respectively, 11.107(6), 6.500(2), and 6.855(2)) compared to deeper samples suggests that water-rock interactions influencing U mobility vary across stratigraphy. Larger [$^{234}U/^{238}U$] values, like those found in these ports, is likely due to increased rock dissolution and weathering at these stratigraphic units.

Non-equilibrium [$^{226}Ra/^{238}U$] also indicates transport of aqueous radionuclides (Figure 4.2b). In this study, five ports (e.g., MS-132, EC-109, W-85, TC-75, and R-35) have whole rock [$^{226}Ra/^{238}U$] outside the equilibrium range, indicating ^{226}Ra and/or ^{238}U leaching. Aqueous [$^{226}Ra/^{238}U$] varies across ports, indicating that leaching extent also varies depending on available solid-phases, similar to relationships observed for [$^{234}U/^{238}U$] with aqueous ^{234}U. Three samples are below the equilibrium range, namely EC-109, W-85, and R-35. W-85 contains the largest [$^{226}Ra/^{238}U$] and the greatest amount of aqueous ^{226}Ra (0.0036(1) mBq/cm^3 aquifer). Three samples within the [$^{226}Ra/^{238}U$] equilibrium range are from the Tunnel City sandstone unit (TC-75, TC-67, TC-59). Finally, the two deepest ports contain [$^{226}Ra/^{238}U$] above the equilibrium value (MS-132, EC-114). The variation in [$^{226}Ra/^{238}U$] across differing stratigraphic units suggests that solid-phase associations are important controls for radionuclide partitioning.

Groundwater samples collected from adjacent depths in the aquifer have similar ratios of [$^{226}Ra/^{238}U$] (Figure 4.2b). For example, the two deepest samples contain similar ^{226}Ra levels and similar [$^{226}Ra/^{238}U$]; the three ports completed in the Tunnel City sandstone have similar ratios and all fall within the equilibrium range. W-85 and EC-109 contain the greatest ^{226}Ra levels and the lowest [$^{226}Ra/^{238}U$]. These similarities across stratigraphy could be due to alpha recoil and/or mineral lattice damage from ^{238}U decay within similar rock units; it could also be due to the ^{226}Ra partitioning with the solid-phase at the site of ^{238}U decay, and subsequent mobility or retardation. While groundwater quality reflects the chemistry of nearby aquifer solids, this is a difficult trend to use for predicting elevated aqueous Ra at discrete intervals in the MCOAS due to its overall geologic heterogeneity. However, the trend may provide insight into radionuclide associations in municipal wells completed in more homogeneous hydrogeologic settings. Comparison of aqueous

^{238}U and ^{226}Ra demonstrates variability in radionuclide mobilization across stratigraphy at discrete intervals.

4.5.2 Geochemical influence on aqueous radionuclide levels

Geochemical factors (e.g., redox, alkalinity) influence ^{238}U solubility in groundwater. After release of U from uranium-bearing minerals (e.g., desorption, dissolution), U forms soluble uranyl carbonate complexes ($UO_2(CO_3)_2^{2-}$, $UO_2(CO_3)_3^{4-}$), which can travel along groundwater flow paths.[52,55-58] Alkalinity correlates with aqueous ^{238}U at the study site (Figure 4.3b; pearson correlation coefficient r = 0.79), indicating potential carbonate or calcium carbonate complex formation ($Ca_2UO_2(CO_3)_3$, $CaUO_2(CO_3)_3^{2-}$).[55-57] Downward gradients caused by pumping can even pull shallow, oxic water potentially elevated in U to deeper aquifers.[59] In the anoxic part of this system, decreasing aqueous ^{238}U is observed at depth which may be explained by the overlapping redox potentials of U(IV/VI) and Fe(II/III) typically resulting in low aqueous U levels in Fe-reducing systems, likely due to the reduction of U(VI) to insoluble U(IV) (Figure 4.3a).[60,61] Trends between aqueous U and geochemical indicators (e.g., alkalinity, ORP) across the variety of stratigraphic units at the study site show that formation of U mobile complexes may have more influence on U mobility than solid-phase interactions in the MCOAS.

While geochemical factors (e.g., redox state, TDS) influence ^{226}Ra partitioning from aquifer solids in the MCOAS, their effect is difficult to observe at the discrete scale at depth in the aquifer system (Figure 4.4a,b). Aqueous ^{226}Ra is not significantly associated with TDS or ORP at the discrete intervals examined in this study. The presence of Fe oxide minerals in each examined stratigraphic unit demonstrates that despite major geologic differences between stratigraphic units, ORP will impact presence/absence of oxide minerals (Figure C-1); the lack of correlation between Ra and ORP suggests that other geochemical factors have more control on

Ra partitioning (e.g., available solid-phase associations). The correlation between TDS and ^{226}Ra is stronger when TDS ranges 3000 to 10000 mg/L, rather than the lower TDS values measured in this study.[62] However, the limited impact of TDS and ORP on aqueous Ra in the subsurface at the study site demonstrates that specific geochemical influences are effective in releasing Ra to the aqueous system only if corresponding solid-phase associations are present. Geochemical associations broadly describe factors that can mobilize Ra in groundwater, but do not fully describe the heterogeneity typically found within this region of the MCOAS.[12,24,25,36,38] For example, anoxic conditions may promote dissolution or absence of Fe oxide minerals, reducing the number of sorption sites. However, if these conditions occur in an aquifer such as the Mt Simon, where quartz sandstone generally dominates over Fe oxides, the dissolution or absence of Fe oxide minerals may not be a major control on Ra release. The heterogeneous distribution of parent nuclides U and Th, found in clay-rich formations dominated by shale, granite, and in some sandstone, also affects Ra generation.[63] If ORP affects Fe oxides in anoxic portions of the Mt Simon, but there are few clay-rich minerals and minimal U concentration, then aqueous Ra will remain low despite fewer available sorption sites.

4.5.3 Association of aqueous ^{87}Sr/^{86}Sr and ^{226}Ra

Isotopic data (aqueous ^{87}Sr/^{86}Sr) provides information about rock-water interactions. Aqueous ^{87}Sr/^{86}Sr is related to the weatherable Sr present in the subsurface; this ratio is not fractionated by chemical or mechanical subsurface interactions, but is released from specific rock phases.[64-68] Aqueous ^{87}Sr/^{86}Sr for Cambrian and Ordovician units usually range from 0.709 – 0.713.[38,68] In general, elevated ^{87}Sr/^{86}Sr is more likely to be correlated with rock of late Cambrian era, than Ordovician.[69] As ^{87}Sr is produced from the decay of ^{87}Rb ($t_{1/2}$ = 49 Ga), minerals that have greater Rb/Sr ratios will contain greater ^{87}Sr/^{86}Sr.[68]

$^{87}Sr/^{86}Sr$ varies by experimental fraction, indicating that mineral associations releasing Sr to the aqueous system vary from the overall Sr pool (Figure 4.5a). In the aqueous fraction, $^{87}Sr/^{86}Sr$ ranges from 0.709653(8) to 0.712519(8), overall increasing at depth but peaking at W-85 (85 – 87 m), indicating this interval contains the highest abundance of high Rb/Sr minerals leaching into groundwater. In the extraction fraction, $^{87}Sr/^{86}Sr$ is also greatest at W-85, increasing from the surface to 85 – 87 m, then decreasing with depth past W-85. In the HF-digested fraction, the $^{87}Sr/^{86}Sr$ follows a similar pattern to the extracted fraction, ranging from 0.709526(8) to 0.743646(9), other than an outlier sample from TC-67 (0.97297(1)) which is likely due to selective digestion of aquifer solids highly enriched in ^{87}Sr. The $^{87}Sr/^{86}Sr$ ratio range is consistent with previous observations of the MCOAS, where Cambrian sandstone usually has more ^{87}Sr than Ordovician carbonate; R-35, open to the Ordovician system, has the lowest $^{87}Sr/^{86}Sr$ of the samples (~0.709), but similar amounts of aqueous ^{226}Ra to Cambrian ports with greater $^{87}Sr/^{86}Sr$ levels (~0.712).[38] Because the range of $^{87}Sr/^{86}Sr$ is much smaller in the aqueous fraction than the ranges in the extracted and digested fractions, it is likely that associations between Sr and specific minerals (e.g., feldspar, dolomite, clays) are the main contributors of Sr to the aqueous system, while Sr entrapped within the mineral lattice is less likely to be mobilized.

Aqueous ^{226}Ra and $^{87}Sr/^{86}Sr$ correlate to stratigraphy, suggesting water-leachable solid-phase associated with elevated ^{87}Sr are more likely to leach ^{226}Ra as well (Figure 4.5b). While a trend is observed between aqueous ^{226}Ra and $^{87}Sr/^{86}Sr$ for all samples, it is stronger when only including the Cambrian samples (pearson correlation coefficient $r = 0.74$ and $r = 0.96$, respectively). The increase in aqueous $^{87}Sr/^{86}Sr$ with increasing depth from the surface could be related to more mineralized groundwater, the anoxic and TDS conditions associated with greater depths, or the solid-phase associations present within the stratigraphy. As $^{87}Sr/^{86}Sr$ is an indicator

of mineral release of metals, via desorption or dissolution, to the aqueous system, the correlation between $^{87}Sr/^{86}Sr$ and ^{226}Ra suggests that the minerals associated with radiogenic Sr (e.g., feldspar, dolomite, clays) may also be important factors in Ra partitioning.[38,70-72] Specifically, minerals associated with elevated radiogenic Sr may also be associated with elevated ^{226}Ra in this system at greater depths within this system. Additionally, there is no significant trend between the $^{87}Sr/^{86}Sr$ ratio and aqueous total Sr, demonstrating different mechanisms releasing ^{226}Ra and total Sr to groundwater (Figure C-2). This isotopic data supports the preferential leaching of Ra-solid phase associations to the aqueous system, as demonstrated by relationship to specific $^{87}Sr/^{86}Sr$ values and weaker correlation with total Sr.

4.6 Conclusions

This study demonstrates the use of isotopic signatures ($^{87}Sr/^{86}Sr$, $^{234}U/^{238}U$) to examine U and Ra partitioning between aquifer solids and groundwater at discrete intervals in the MCOAS. At some intervals, there is evidence for Ra leaching with mobilization of Ra from the site of U decay. However, most of the system is close to secular equilibrium, suggesting that the quantity of U controls the amount of Ra available to partition to the aqueous system. Once emitted by parent nuclides, local geochemical factors (e.g., ORP, TDS) within the stratigraphic unit and available solid-phase interactions control Ra mobility (e.g., sorption sites). Due to geologic and geochemical heterogeneity within the aquifer system, contact time between the groundwater and aquifer solids and the leachability of Ra-solids associations within respective stratigraphy are important factors affecting aqueous Ra levels. Overall, this study examines the effect of parent nuclide U within stratigraphic intervals on Ra water-rock partitioning, and the complexity resulting from solid-phase associations and aqueous geochemistry (ORP, TDS) at discrete intervals in the MCOAS.

This work concludes a series of investigations in the solubility of Ra at discrete intervals in the MCOAS.[25,50] Although solid-phase sources of Ra are observed in the MCOAS across a range of hydrostratigraphic intervals, geochemical factors (e.g., TDS) and absence of available sorption sites remain the primary drivers of Ra partitioning from aquifer solids to the aqueous system. However, while general trends (TDS, redox state) used to predict the state of Ra association with aquifer solids can broadly examine aqueous Ra levels, they do not transfer to predicting Ra levels at specific well locations in the MCOAS. As this work concludes, the mobilization of Ra is difficult to predict at specific well locations due to complex Ra-solid-phase interactions and a heterogeneous aquifer system. Therefore, if water utilities are dealing with borderline or elevated Ra concentrations, installation of treatment facilities, rather than detailed geochemical and hydrologic examination for targeted well construction, is the practical and more efficient method to maintain EPA compliance.

4.7 Acknowledgements

This work was supported with directed cooperative matching funds from the U.S. Geological Survey Water Availability and Use Science Program as well as the Wisconsin Department of Natural Resources. We thank many associated with the University of Guelph for support with field data collection, including Jessica Meyer, Beth Parker, Jessica Bulova, and Marina Nunes. Rock samples in this report are curated at the Wisconsin Geological and Natural History Survey's (WGNHS) core repository. We thank WGNHS for providing access to samples from core 13001214, descriptions, and lab facilities. Laboratory assistance provided by Christa Dahman, Amy Plechacek, and James Lazarcik was greatly appreciated. We also thank the Wisconsin State Laboratory of Hygiene Trace Metal Laboratory for support and access to multi-collector inductively coupled plasma mass spectrometry, and specifically Joel Overdier for trace

metal analysis. The authors gratefully acknowledge use of facilities and instrumentation supported by NSF through the University of Wisconsin Materials Research Science and Engineering Center (DMR-1720415).

4.8 References

1. van Vliet, M. T. H.; Flörke, M.; Wada, Y., Quality matters for water scarcity. *Nature Geoscience* **2017,** *10*, (11), 800-802.
2. Liu, J.; Liu, Q.; Yang, H., Assessing water scarcity by simultaneously considering environmental flow requirements, water quantity, and water quality. *Ecological Indicators* **2016,** *60*, 434-441.
3. Famiglietti, J. S., The global groundwater crisis. *Nature Climate Change* **2014,** *4*, (11), 945-948.
4. Konikow, L. F.; Kendy, E., Groundwater depletion: A global problem. *Hydrogeology Journal* **2005,** *13*, (1), 317-320.
5. Grützmacher, G.; Kumar, P. J. S.; Rustler, M.; Hannappel, S.; Sauer, U., Geogenic groundwater contamination—definition, occurrence and relevance for drinking water production. *Zbl Geol Paläont Teil I* **2013,** *1*, 69-75.
6. Burri, N.; Weatherl, R.; Moeck, C.; Schirmer, M., A review of threats to groundwater quality in the anthropocene. *Science of The Total Environment* **2019,** *684*.
7. US EPA *Radionuclides rule: a quick reference guide*; 2001.
8. US EPA, National primary drinking water regulations. *Federal Register* **2000,** *65*, (236).
9. Cohn, P.; Skinner, R.; Burger, S.; Falgiano, J.; Klotz, J., Radium in Drinking Water and the Incidence of Osteosarcoma: A Report to the New Jersey Department of Environmental Protection. **2003**.
10. Evans, R. D., Radium poisoning: a review of present knowledge. *American Journal of Public Health and the Nations Health* **1933,** *23*, (10), 1017-1023.
11. Guse, C. E.; Marbella, A. M.; George, V.; Layde, P. M., Radium in Wisconsin drinking water: an analysis of osteosarcoma risk. *Archives of Environmental Health: An International Journal* **2002,** *57*, (4), 294-303.
12. Szabo, Z.; dePaul, V. T.; Fischer, J. M.; Kraemer, T. F.; Jacobsen, E., Occurrence and geochemistry of radium in water from principal drinking-water aquifer systems of the United States. *Applied Geochemistry* **2012,** *27*, (3), 729-752.
13. Dematatis, M.; Plechacek, A.; Mathews, M.; Wright, D. B.; Udenby, F.; Gotkowitz, M. B.; Ginder-Vogel, M., Spatial and temporal variability of radium in the Wisconsin Cambrian-Ordovician aquifer system. *AWWA Water Science* **2020**.
14. DeSimone, L. A.; McMahon, P. B.; Rosen, M. R. *The quality of our Nation's waters - Water quality in Principal Aquifers of the United States, 1991-2010*; U.S. Geological Survey: 2014; p 151.
15. Swift Bird, K.; Navarre-Sitchler, A.; Singha, K., Hydrogeological controls of arsenic and uranium dissolution into groundwater of the Pine Ridge Reservation, South Dakota. *Applied Geochemistry* **2020,** *114*, 104522.
16. Schreiber, M. E.; Simo, J. A.; Freiberg, P. G., Stratigraphic and geochemical controls on naturally occurring arsenic in groundwater, eastern Wisconsin, USA. *Hydrogeology Journal* **2000,** *8*, (2), 161-176.
17. Izbicki, J. A.; Wright, M. T.; Seymour, W. A.; McCleskey, R. B.; Fram, M. S.; Belitz, K.; Esser, B. K., Cr(VI) occurrence and geochemistry in water from public-supply wells in California. *Applied Geochemistry* **2015,** *63*, 203-217.

18. Ginder-Vogel, M.; Fendorf, S., Chapter 11 Biogeochemical Uranium Redox Transformations: Potential Oxidants of Uraninite. In *Developments in Earth and Environmental Sciences*, Barnett, M. O.; Kent, D. B., Eds. Elsevier: 2007; Vol. 7, pp 293-319.
19. Fendorf, S.; Wielinga, B. W.; Hansel, C. M., Chromium Transformations in Natural Environments: The Role of Biological and Abiological Processes in Chromium(VI) Reduction. *International Geology Review* **2000,** *42*, (8), 691-701.
20. Friedly, J. C.; Davis, J. A.; Kent, D. B., Modeling hexavalent chromium reduction in groundwater in field-scale transport and laboratory batch experiments. *Water resources research* **1995,** *31*, (11), 2783-2794.
21. Berg, M.; Trang, P. T. K.; Stengel, C.; Buschmann, J.; Viet, P. H.; Van Dan, N.; Giger, W.; Stüben, D., Hydrological and sedimentary controls leading to arsenic contamination of groundwater in the Hanoi area, Vietnam: The impact of iron-arsenic ratios, peat, river bank deposits, and excessive groundwater abstraction. *Chemical Geology* **2008,** *249*, (1), 91-112.
22. Oden, J. H.; Szabo, Z. *Arsenic and radionuclide occurrence and relation to geochemistry in groundwater of the Gulf Coast Aquifer System in Houston, Texas, 2007–11*; 2016.
23. Polizzotto, M. L.; Harvey, C. F.; Li, G.; Badruzzman, B.; Ali, A.; Newville, M.; Sutton, S.; Fendorf, S., Solid-phases and desorption processes of arsenic within Bangladesh sediments. *Chemical Geology* **2006,** *228*, (1), 97-111.
24. Stackelberg, P. E.; Szabo, Z.; Jurgens, B. C., Radium mobility and the age of groundwater in public-drinking-water supplies from the Cambrian-Ordovician aquifer system, north-central USA. *Applied Geochemistry* **2018,** *89*, 34-48.
25. Mathews, M.; Gotkowitz, M.; Ginder-Vogel, M., Effect of geochemical conditions on radium mobility in discrete intervals within the Midwestern Cambrian-Ordovician aquifer system. *Applied Geochemistry* **2018,** *97*, 238-246.
26. Ames, L. L.; McGarrah, J. E.; Walker, B. A., Sorption of trace constituents from aqueous solutions onto secondary minerals. II. Radium. *Clays and clay minerals* **1983,** *31*, (5), 335-342.
27. Bassot, S.; Mallet, C.; Stammose, D., Experimental Study and Modeling of the Radium Sorption onto Goethite. *MRS Proceedings* **2000,** *663*, 1081.
28. Ames, L. L.; McGarrah, J. E.; Walker, B. A.; Salter, P. F., Uranium and radium sorption on amorphous ferric oxyhydroxide. *Chemical Geology* **1983,** *40*, (1), 135-148.
29. Chen, M. A.; Kocar, B. D., Radium Sorption to Iron (Hydr)oxides, Pyrite, and Montmorillonite: Implications for Mobility. *Environmental Science & Technology* **2018,** *52*, (7), 4023-4030.
30. Sajih, M.; Bryan, N. D.; Livens, F. R.; Vaughan, D. J.; Descostes, M.; Phrommavanh, V.; Nos, J.; Morris, K., Adsorption of radium and barium on goethite and ferrihydrite: A kinetic and surface complexation modelling study. *Geochimica et Cosmochimica Acta* **2014,** *146*, 150-163.
31. Hammond, D. E.; Zukin, J. G.; Ku, T. L., The kinetics of radioisotope exchange between brine and rock in a geothermal system. *Journal of Geophysical Research: Solid Earth* **1988,** *93*, (B11), 13175-13186.
32. Nathwani, J. S.; Phillips, C. R., Adsorption of 226Ra by soils in the presence of Ca2+ ions. Specific adsorption (II). *Chemosphere* **1979,** *8*, (5), 293-299.
33. Tamamura, S.; Takada, T.; Tomita, J.; Nagao, S.; Fukushi, K.; Yamamoto, M., Salinity dependence of 226Ra adsorption on montmorillonite and kaolinite. *Journal of Radioanalytical and Nuclear Chemistry* **2014,** *299*, (1), 569-575.
34. Zhu, C., Coprecipitation in the barite isostructural family: 1. binary mixing properties. *Geochimica et Cosmochimica Acta* **2004,** *68*, (16), 3327-3337.

35. Zhang, T.; Gregory, K.; Hammack, R. W.; Vidic, R. D., Co-precipitation of radium with barium and strontium sulfate and its impact on the fate of radium during treatment of produced water from unconventional gas extraction. *Environmental Science and Technology* **2014,** *48*, (8).
36. Grundl, T.; Cape, M., Geochemical factors controlling radium activity in a sandstone aquifer. *Ground Water* **2006,** *44*, (4), 518-527.
37. Weaver, T. R.; Bahr, J., Geochemical evolution in the Cambrian-Ordovician sandstone aquifer, eastern Wisconsin: 1. Major ion and radionuclide distribution. *Ground Water* **1991,** *29*, (3), 350-356.
38. Vinson, D. S.; Lundy, J. R.; Dwyer, G. S.; Vengosh, A., Implications of carbonate-like geochemical signatures in a sandstone aquifer: Radium and strontium isotopes in the Cambrian Jordan aquifer (Minnesota, USA). *Chemical Geology* **2012,** *334*, 280-294.
39. Parsen, M. J.; Bradbury, K. R.; Hunt, R. J.; Feinstein, D. T., *The 2016 groundwater flow model for Dane County, Wisconsin*. 2016; p 56-56.
40. Meyer, J. R.; Parker, B. L.; Arnaud, E.; Runkel, A. C., Combining high resolution vertical gradients and sequence stratigraphy to delineate hydrogeologic units for a contaminated sedimentary rock aquifer system. *Journal of hydrology* **2016,** *534*, 505-523.
41. Meyer, J. R.; Parker, B. L.; Cherry, J. A., Detailed hydraulic head profiles as essential data for defining hydrogeologic units in layered fractured sedimentary rock. *Environmental Geology* **2008,** *56*, (1), 27-44.
42. Nordstrom, D. K.; Wilde, F. D. *Chapter A6. Section 6.5. Reduction-Oxidation Potential (Electrode Method)*; 09-A6.5; Reston, VA, 2005.
43. Brezonik, P. L.; Arnold, W. A., *Water chemistry : an introduction to the chemistry of natural and engineered aquatic systems*. 2011; p 782-782.
44. Weis, D.; Kieffer, B.; Maerschalk, C.; Barling, J.; De Jong, J.; Williams, G. A.; Hanano, D.; Pretorius, W.; Mattielli, N.; Scoates, J. S., High-precision isotopic characterization of USGS reference materials by TIMS and MC-ICP-MS. *Geochemistry, Geophysics, Geosystems* **2006,** *7*, (8).
45. Park, S.-H.; Langmuir, C. H.; Sims, K. W. W.; Blichert-Toft, J.; Kim, S.-S.; Scott, S. R.; Lin, J.; Choi, H.; Yang, Y.-S.; Michael, P. J., An isotopically distinct Zealandia–Antarctic mantle domain in the Southern Ocean. *Nature Geoscience* **2019,** *12*, (3), 206-214.
46. Phillips, E. H.; Sims, K. W. W.; Blichert-Toft, J.; Aster, R. C.; Gaetani, G. A.; Kyle, P. R.; Wallace, P. J.; Rasmussen, D. J., The nature and evolution of mantle upwelling at Ross Island, Antarctica, with implications for the source of HIMU lavas. *Earth and Planetary Science Letters* **2018,** *498*, 38-53.
47. Scott, S. R.; Sims, K. W. W.; Reagan, M. K.; Ball, L.; Schwieters, J. B.; Bouman, C.; Lloyd, N. S.; Waters, C. L.; Standish, J. J.; Tollstrup, D. L., The application of abundance sensitivity filters to the precise and accurate measurement of uranium series nuclides by plasma mass spectrometry. *International Journal of Mass Spectrometry* **2019,** *435*, 321-332.
48. Faure, G.; Mensing, T. M., *Isotopes: principles and applications*. 2005.
49. Raczek, I.; Jochum, K. P.; Hofmann, A. W., Neodymium and Strontium Isotope Data for USGS Reference Materials BCR-1, BCR-2, BHVO-1, BHVO-2, AGV-1, AGV-2, GSP-1, GSP-2 and Eight MPI-DING Reference Glasses. *Geostandards Newsletter* **2003,** *27*, (2), 173-179.
50. Mathews, M.; Scott, S. R.; Gotkowitz, M. B.; Ginder-Vogel, M., Association of Radionuclide Isotopes with Aquifer Solids in the Midwestern Cambrian–Ordovician Aquifer System. *ACS Earth and Space Chemistry* **2021**.

51. IUPAC, *Compendium of Chemical Terminology*. Blackwell Scientific Publications: Oxford, 1997.
52. Andrews, J. N.; Kay, R. L. F., The U contents and 234U/238U activity ratios of dissolved uranium in groundwaters from some Triassic sandstones in England. *Chemical Geology* **1983,** *41*, 101-117.
53. Moreira-Nordemann, L. M., Use of 234U/238U disequilibrium in measuring chemical weathering rate of rocks. *Geochimica et Cosmochimica Acta* **1980,** *44*, (1), 103-108.
54. Faure, G.; Mensing, T. M., Isotopes: principles and applications. John Willey and Sons. *Inc., Hoboken, NJ* **2005**, 464.
55. Burow, K. R.; Belitz, K.; Dubrovsky, N. M.; Jurgens, B. C., Large decadal-scale changes in uranium and bicarbonate in groundwater of the irrigated western U.S. *Science of The Total Environment* **2017,** *586*, 87-95.
56. Elless, M. P.; Lee, S. Y., Uranium Solubility of Carbonate-Rich Uranium-Contaminated Soils. *Water, Air, and Soil Pollution* **1998,** *107*, (1/4), 147-162.
57. Blake, C. A.; Coleman, C. F.; Brown, K. B.; Hill, D. G.; Lowrie, R. S.; Schmitt, J. M., Studies in the carbonate-uranium system. *Journal of the American Chemical Society* **1956,** *78*, (23), 5978-5983.
58. Fröhlich, K.; Gellermann, R., On the potential use of uranium isotopes for groundwater dating. *Chemical Geology: Isotope Geoscience section* **1987,** *65*, (1), 67-77.
59. Jurgens, B. C.; Fram, M. S.; Belitz, K.; Burow, K. R.; Landon, M. K., Effects of Groundwater Development on Uranium: Central Valley, California, USA. *Groundwater* **2010,** *48*, (6), 913-928.
60. Riedel, T.; Kübeck, C., Uranium in groundwater – A synopsis based on a large hydrogeochemical data set. *Water Research* **2018,** *129*, 29-38.
61. Ginder-Vogel, M.; Criddle, C. S.; Fendorf, S., Thermodynamic Constraints on the Oxidation of Biogenic UO2 by Fe(III) (Hydr)oxides. *Environmental Science & Technology* **2006,** *40*, (11), 3544-3550.
62. Vinson, D. S.; Tagma, T.; Bouchaou, L.; Dwyer, G. S.; Warner, N. R.; Vengosh, A., Occurrence and mobilization of radium in fresh to saline coastal groundwater inferred from geochemical and isotopic tracers (Sr, S, O, H, Ra, Rn). *Applied Geochemistry* **2013,** *38*, 161-175.
63. Okoro, E. E.; Okolie, A. G.; Sanni, S. E.; Joel, E. S.; Agboola, O.; Omeje, M., Assessment of naturally occurring radiation in lithofacies of oil field in Niger Delta region and its possible health implications. *Journal of Environmental Management* **2020,** *264*, 110498.
64. Bain, D. C.; Bacon, J. R., Strontium isotopes as indicators of mineral weathering in catchments. *Catena* **1994,** *22*, (3), 201-214.
65. Voerkelius, S.; Lorenz, G. D.; Rummel, S.; Quétel, C. R.; Heiss, G.; Baxter, M.; Brach-Papa, C.; Deters-Itzelsberger, P.; Hoelzl, S.; Hoogewerff, J., Strontium isotopic signatures of natural mineral waters, the reference to a simple geological map and its potential for authentication of food. *Food chemistry* **2010,** *118*, (4), 933-940.
66. Shand, P.; Darbyshire, D. P. F.; Love, A. J.; Edmunds, W. M., Sr isotopes in natural waters: Applications to source characterisation and water–rock interaction in contrasting landscapes. *Applied Geochemistry* **2009,** *24*, (4), 574-586.
67. Åberg, G.; Jacks, G.; Hamilton, P. J., Weathering rates and 87Sr/86Sr ratios: an isotopic approach. *Journal of Hydrology* **1989,** *109*, (1-2), 65-78.

68. Hunt, R. J.; Bullen, T. D.; Krabbenhoft, D. P.; Kendall, C., Using stable isotopes of water and strontium to investigate the hydrology of a natural and a constructed wetland. *Groundwater* **1998,** *36*, (3), 434-443.
69. Denison, R. E.; Koepnick, R. B.; Burke, W. H.; Hetherington, E. A., Construction of the Cambrian and Ordovician seawater 87Sr/86Sr curve. *Chemical Geology* **1998,** *152*, (3), 325-340.
70. Armstrong, S. C.; Sturchio, N. C.; Hendry, M. J., Strontium isotopic evidence on the chemical evolution of pore waters in the Milk River Aquifer, Alberta, Canada. *Applied Geochemistry* **1998,** *13*, (4), 463-475.
71. Bullen, T. D.; Krabbenhoft, D. P.; Kendall, C., Kinetic and mineralogic controls on the evolution of groundwater chemistry and 87Sr/86Sr in a sandy silicate aquifer, northern Wisconsin, USA. *Geochimica et Cosmochimica Acta* **1996,** *60*, (10), 1807-1821.
72. Salifu, M.; Aiglsperger, T.; Hällström, L.; Martinsson, O.; Billström, K.; Ingri, J.; Dold, B.; Alakangas, L., Strontium (87Sr/86Sr) isotopes: A tracer for geochemical processes in mineralogically-complex mine wastes. *Applied Geochemistry* **2018,** *99*, 42-54.

Chapter 5

Impact of a short-term pumping test on radium levels in the Midwestern Cambrian-Ordovician aquifer system

5.1 Abstract

Radium (Ra) is a geogenic contaminant which frequently occurs at high levels in the Midwestern Cambrian-Ordovician aquifer system (MCOAS), requiring water utilities to resort to expensive treatment methods or alternative water sources in order to maintain quality drinking water. Geochemical conditions, such as anoxic conditions or elevated dissolved solids, impact Ra partitioning from solids to the aqueous system. While these trends have been examined at broad geographic scales and within specific geologic units or minerals, it is unclear how water withdrawal conditions in municipal wells open to long depths of the aquifer impact Ra mobility. Here we show that Ra concentrations with a single municipal well in Wisconsin are consistent despite varied pumping conditions. However, analytical methods used to measure Ra vary in precision, with uncertainty values varying by an order of magnitude, at the relevant ultra trace concentrations. Specifically, mass spectrometry measured more precise Ra concentrations than decay counting methods at the levels observed in this study (< 185 mBq/L). Our results demonstrate that continued development of better tools, like precise analytical methods and isotopic indicators of Ra occurrence, can provide information that will help predict Ra occurrence in aquifer systems like the MCOAS. It may be beneficial for water utilities concerned with determining precise temporal Ra trends in their wells to compare Ra analysis between decay counting and mass spectrometry methods, in order to increase confidence that water treatment decisions are based on precise and accurate data.

5.2 Introduction

Radium (Ra), a geogenic contaminant formed via the radioactive decay of its parent nuclides uranium (U) and thorium (Th), can occur at elevated levels in groundwater. Ingestion of Ra, typically through drinking water sourced from aquifer systems, is associated with osteosarcoma and other bone diseases.[1-4] Because of this, the United States Environmental Protection Agency (EPA) has set a maximum contaminant level (MCL) of 185 mBq/L (5 pCi/L) for the combined activity of two major isotopes, ^{226}Ra and ^{228}Ra.[5,6] In the US, groundwater in the Midwestern Cambrian-Ordovician aquifer system (MCOAS) has the most frequent occurrence of elevated Ra.[7,8] This makes it necessary for many water utilities sourcing water from the MCOAS to find treatment methods or alternative sources of drinking water to remain in compliance.

Elevated Ra in wells pumping water from the MCOAS frequently occurs in the Midwestern United States. In Wisconsin, 116 wells exceeded the Ra MCL at least once from 2019-2020. At a broad geographic scale, combined Ra ([^{226}Ra + ^{226}Ra]) levels in the MCOAS in Wisconsin appear to be increasing in recent years, although local variation may also play a role.[9] Some municipalities, like the City of Waukesha, Wisconsin, have been forced to seek new sources of drinking water. For Waukesha, though new sources are expensive and difficult to obtain, they are necessary due to elevated levels of Ra and other impacts of heightened drawdown in the local aquifer system.[10-12]

Local geochemistry near geologic units elevated in U and Th in the MCOAS impacts Ra partitioning to aquifer solids, and can mobilize Ra to the groundwater system.[8,13] Elevated Ra concentrations are associated with low dissolved oxygen (DO) or high total dissolved solids (TDS) due to increased ion competition and/or loss of sorption sites; these conditions are frequently found in confined aquifer systems which contain older, more mineralized water.[7,8,14-

[22] Increased aqueous Ra (> 185 mBq/L) is correlated with anoxic conditions, in particular due to the dissolution of iron and manganese (hydro)oxide minerals and therefore presence of fewer Ra sorption sites.[23,24] Elevated TDS indicates greater ion content in groundwater, which can take up sorption sites, increasing the likelihood of aqueous Ra.[25,26]As geochemical influences can impact Ra partitioning within aquifer systems, the mixing of chemically distinct groundwater across stratigraphy can promote Ra desorption and overall mobility, which can be caused by well water withdrawal.[8,21] Wells open to multiple stratigraphic units may foster solution mixing across well boreholes, potentially causing uptake of groundwater elevated in Ra.

This study examines trends in Ra levels at a single municipal well in in the MCOAS in Wisconsin, investigating the influence of pumping conditions on aqueous geochemistry. While geochemical trends associated with elevated Ra in the MCOAS have been examined from a broad geographic scale to discrete stratigraphy, interactions within boreholes have yet to be studied as potential contributors to elevated Ra uptake by wells in the MCOAS.[8,13,20,27-29] Additionally, we compare two methods of Ra analysis to compare precision at the relevant ultra trace concentrations of Ra. Overall, this study provides new insight on examining Ra trends in municipal wells due to the effects of water withdrawal on geochemical interactions within the well borehole.

5.3 Methods

5.3.1 Short-term pumping test

Madison Well 19 was drilled in 1970, and is open to the MCOAS in Dane County, Wisconsin. Overall, the MCOAS is mainly composed of marine sandstones and carbonate rock, cemented with calcite and dolomite; local or regional shale confining layers are present at intervals across the aquifer system.[30,31] At Madison Well 19, glacial drift (~5 m) overlies the

Tunnel City unit (30 m), which is composed of sandstone with calcite-dolomite cement and trace glauconite. Below the Tunnel City is 34 m of the Wonewoc unit, a sandstone with some dolomite or calcite-dolomite cement and more abundant silica cement, overlying the shale and sandstone of the Eau Claire unit (11 m). Below the Eau Claire lies the Mt Simon unit (139 m), a sandstone with dolomitic cement and occasional interbedded green shale. Madison Well 19 is screened open to the Mt Simon sandstone (137 m). The base of the well borehole strikes the Precambrian crystalline bedrock (~2 m).

Madison Well 19 was selected as the site for the short-term pumping test due to elevated combined Ra levels recently observed under normal operating conditions. A construction project aimed at treating dissolved iron, manganese, and Ra levels is planned to begin in 2023.[32,33] Madison Well 19 pumped 318 million gallons/year in 2019 to the surrounding area, with a five-year average of 363 million gallons/year.[34] On average from 2011 to 2019, the well withdrew $5x10^8 \pm 2x10^8$ gallons/year of water. For this study, the well was left stagnant (i.e., not pumped) from 12am on Nov. 27, 2019 until 9am on Dec. 7, 2019. At this point, the well was pumped continuously at ~2300 gal/min for 48 hours; water samples were taken throughout pumping with samples taken every five minutes during the initial half hour as pumping resumed, after which samples were collected at ~12-24 hour intervals (Table 5.1). Based on borehole volume and pumping speed, the initial 2-3 minutes of pumping withdraw water contained within the cased region of the well, which has not been in contact with the aquifer while the well was left stagnant. Over the next thirty minutes, the well withdrew a mix of water from the open borehole and the aquifer, until enough borehole volumes have been removed to be confident that the pumped water is withdrawn from the aquifer system, and is assumed to be representative of current aquifer conditions.

5.3.2 Groundwater characterization

For the pumping test, we examined variation in geochemical parameters over time. At each time point, field parameters such as pH, conductivity, dissolved oxygen (DO), and temperature were obtained (Table 5.1). DO was measured in a flow-through cell. Field samples consisting of 4 L for Ra isotope analysis via decay counting and 1 L for geochemical characterization were taken at each time point. Samples for Ra analysis via decay counting were not filtered, but were preserved with acid (pH < 2). Due to sampling error, sample PT 8 measured by decay counting was not initially acidified but was preserved ten days after sampling; as it was acidified prior to analysis, we assume that Ra dissolved into the solution and analysis was accurate within analytical uncertainty. Samples for general geochemical analysis were filtered (0.45 μm), and kept at 4 °C; from these, subsamples were further preserved with acid (pH < 2) for dissolved metal analysis and Ra analysis by multi-collector inductively coupled plasma mass spectrometry (MC-ICPMS). Additionally, two grab samples, collected before and after the pumping test during normal pumping conditions, are included in this dataset; these samples were preserved with acid, but were not filtered.

5.3.3 Radium isotope analysis

Decay counting analysis for Ra isotopes ([^{226}Ra] and [^{228}Ra], where radioactive activity is designated by brackets) was conducted by Eurofins Eaton Analytical, Inc. in a manner consistent with EPA methods “7500-Ra B”, which uses co-precipitation and alpha counting to measure radioactive decay of ^{226}Ra, and “7500-Ra D”, which uses precipitation and beta counting to measure radioactive decay of ^{228}Ra and daughter isotopes.[35] In this study, we will refer to this type of analysis as ‘decay counting’. All 10 pumping test samples well samples were analyzed via decay counting.

Mass spectrometry analysis for Ra isotopes ([^{226}Ra] and [^{228}Ra]) was conducted at the Wisconsin State Laboratory of Hygiene Trace Elements Clean Laboratory, using isotope dilution and column purification to analyze samples for ^{226}Ra and ^{228}Ra using a Neptune Plus MC-ICPMS using a single SEM/RPQ detector in dynamic mode.[36,37] Each sample was spiked with 100 μL of a ^{228}Ra standard solution prior to purification; further information about the purification technique and spike calibration can be found in Mathews et al., 2021.[37] Two samples of each time period were analyzed on the MC-ICPMS, using the initial measured ^{226}Ra/^{228}Ra to calculated concentrations for both ^{226}Ra and ^{228}Ra. Prior to each analysis, the MC-ICPMS ion counter detector was calibrated with a dilute tuning solution, and a natural uranium solution was used to correct ^{226}Ra/^{228}Ra for mass bias. The MC-ICPMS method was used for 5 pumping test samples.

Table 5.1 Field parameters for each sampling time point during the short-term pumping test. PT = Pumping Test, GS = Grab Sample. Well discharge is defined as a mixture of water sitting in the open borehole and aquifer water.

Sample	Date	Time	Well Status	pH	Temperature (°C)	Conductivity (μS/cm)	Dissolved oxygen (mg/L)
PT1	12/07/19	9:03am	Water sitting in the cased region of the well for 10 days	7.4	11.1	570	0.18
PT2	12/07/19	9:06am	Well discharge	7.4	10.9	560	0.14
PT3	12/07/19	9:12am	Well discharge	7.4	10.8	560	0.21
PT4	12/07/19	9:17am	Well discharge	7.4	10.9	560	0.06
PT5	12/07/19	9:23am	Well discharge	7.3	10.8	550	0.00
PT6	12/07/19	9:28am	Well discharge	7.3	10.9	550	0.09
PT7	12/07/19	10:00am	Representative of the aquifer system	7.3	10.9	560	0.05

PT8	12/07/19	9:00pm	Representative of the aquifer system	7.4	11.2	550	0.08
PT9	12/08/19	9:00am	Representative of the aquifer system	7.3	11.2	550	0.08
PT10	12/09/19	9:00am	Representative of the aquifer system	7.4	11.1	550	0.03
GS1	1/25/19	---	Grab Sample	---	---	---	---
GS2	3/02/20	---	Grab Sample	---	---	---	---

5.4 Results

5.4.1 Aqueous geochemistry during pumping test

Radium is a contaminant of concern at Madison Well 19 (Figure D-1). Recent samples from this well are elevated, with compliance samples from Mar. 2019 to Feb. 2020 averaging 150 ± 30 mBq/L (4.1 ± 0.8 pCi/L) combined Ra (Figure E-1). It is difficult to distinguish trends from this long-term dataset, due to the increased frequency of samples in recent years. However, compliance samples measured range from 72 mBq/L to 220 mBq/L combined Ra, averaging 130 ± 30 mBq/L from 2010 to 2020. During this time period, ^{226}Ra averaged 60 ± 20 mBq/L, while ^{228}Ra averaged 60 ± 30 mBq/L. Municipal Ra compliance data is typically measured by the EPA methods 7500-Ra B and 7500-Ra D, discussed in section 2.3, or other similar counting methods EPA-approved.

Initial disturbance is observed in geochemical measurements over time during the pumping test before geochemical stability (Table 5.1). During the first hour of pumping, DO is initially at 0.18 mg/L then drops to 0.00 mg/L on the fifth sampling point. After an hour of pumping, the field measurements for dissolved oxygen ranges from 0.03 to 0.08 mg/L for the rest of the pumping period. Initially, field-measured conductivity is 570 μS/cm, then slowly drops to

550 µS/cm as water representative of the aquifer system is drawn based on borehole v. Conductivity remains at 550 µS/cm through the end of the pumping test.

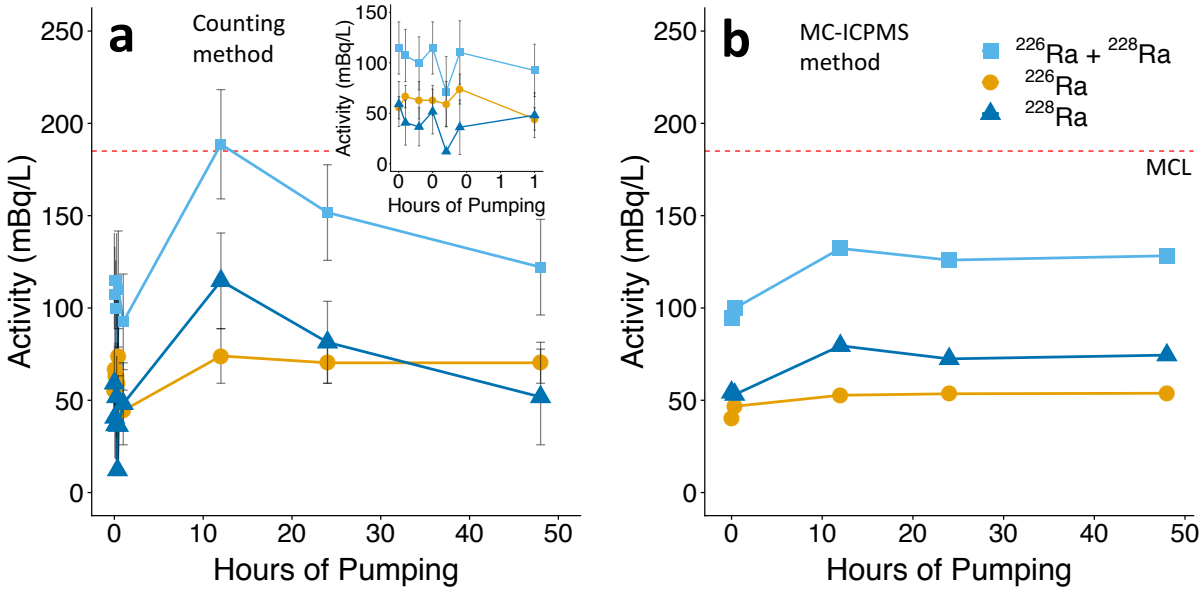

Figure 5.1 Radium activities over time during a short-term pumping test conducted at Madison Well 19. Light blue squares represent combined Ra activities ([^{226}Ra + ^{228}Ra]), gold circles represent ^{226}Ra activities, and dark blue triangles represent ^{228}Ra activities. Maximum contaminant level (MCL) is designated by the dashed red line. a) Ra activities for all samples measured via decay counting and associated analytical uncertainty.[38] Inset shows sample variability for each isotope during the first hour of pumping. b) Ra activities conducted on samples 1, 5, 8-10 by the MC-ICPMS method and associated analytical uncertainty. Error bars representing analytical uncertainty are on the order of the point size.

5.4.2 Combined radium during pumping test

As with other dissolved constituents, there is a period of initial variability followed by stabilization in Ra level. Radium activities over time during the pumping test conducted at Well 19 vary in concentration and instrumental uncertainty when comparing measurements by the counting or MC-ICPMS method (Table 5.2). Decay counting measures an average of 100 ± 20 mBq/L combined Ra for samples from the first half hour of pumping (Figure 5.1a). Over the next 47 hours, the samples average 140 ± 40 mBq/L combined Ra. Five samples from the pumping test were measured via the MC-ICPMS method (time 0 min, 30 min, 12 hours, 24 hours, and 48

hour), which range from 94 ± 3 mBq/L combined Ra at the first time point to an average of 135 ± 3 mBq/L combined Ra over the samples taken during 12 – 48 hours (Figure 5.1b). Radium activities and uncertainties associated with the measurement vary depending on the method of analysis.

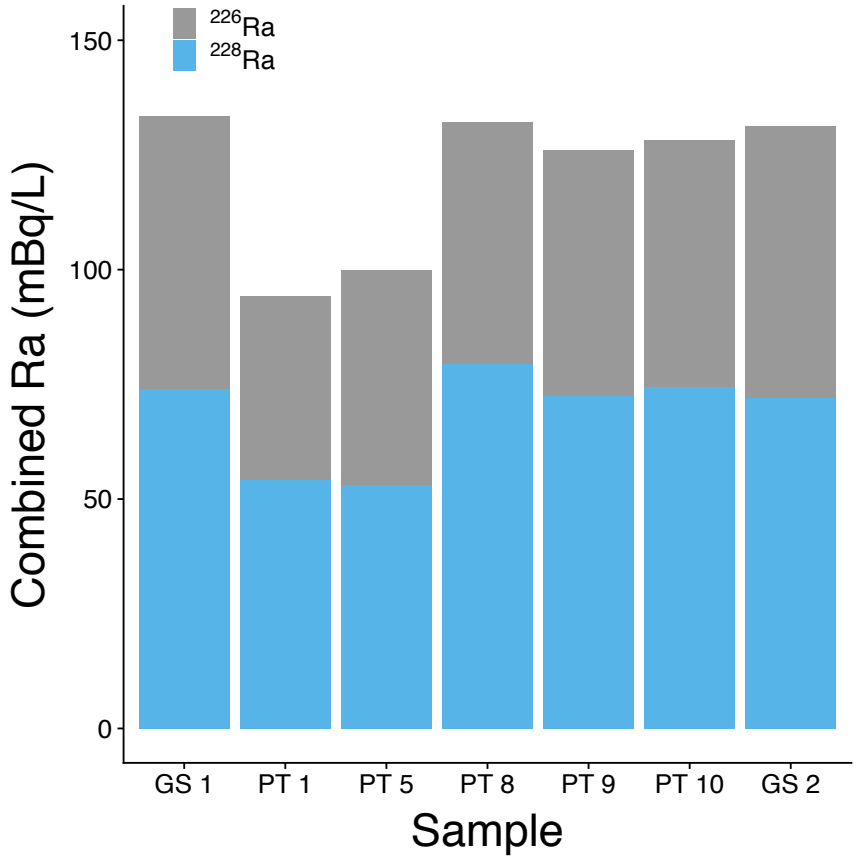

Figure 5.2 Combined Ra ([^{226}Ra + ^{228}Ra]) comparison from the pumping test, and two grab samples collected ~1 year apart. Samples were measured by the MC-ICPMS method. PT = Pumping Test, GS = Grab Sample

Comparing measurements of combined Ra by the MC-ICPMS method over time from both the pumping test and grab samples demonstrates consistency in aquifer conditions over time (Figure 5.2). The initial two samples (PT1, PT5) measured via MC-ICPMS are lower (94 ± 3 and 100 ± 3 mBq/L). Samples collected later in the pumping test (PT8-10), and grab samples collected during typical pumping conditions (GS1, GS2) average 130 ± 3 mBq/L, all analyzed via the MC-

ICPMS method (Table 5.2). This is similar to the average of long-term data (2010 – 2020) reported for compliance, 130 ± 30 mBq/L.

Table 5.2 Sampling time points and radium activities (all in mBq/L), distinguished by method of analysis, where PT refers to the pumping test and GS refers to the grab samples. Uncertainty is determined by instrumental error. Counting = Georgia Tech method[38], MC-ICPMS = Multi-collector inductively coupled plasma mass spectrometry analysis. PT = Pumping Test, GS = Grab Sample.

Sample	[^{226}Ra] (Counting)	[^{228}Ra] (Counting)	[^{226}Ra + ^{228}Ra] (Counting)	[^{226}Ra] (MC-ICPMS)	[^{228}Ra] (MC-ICPMS)	[^{226}Ra + ^{228}Ra] (MC-ICPMS)
PT1	60 ± 10	60 ± 20	110 ± 30	40 ± 1	54 ± 2	94 ± 3
PT2	70 ± 10	40 ± 20	110 ± 30	---	---	---
PT3	60 ± 20	40 ± 20	100 ± 30	---	---	---
PT4	60 ± 10	50 ± 20	110 ± 30	---	---	---
PT5	60 ± 20	10 ± 30	70 ± 30	47 ± 1	53 ± 2	100 ± 3
PT6	70 ± 10	40 ± 30	110 ± 30	---	---	---
PT7	40 ± 10	50 ± 20	90 ± 30	---	---	---
PT8	70 ± 10	110 ± 30	190 ± 30	53 ± 1	80 ± 2	132 ± 4
PT9	40 ± 10	80 ± 20	150 ± 30	54 ± 2	72 ± 2	126 ± 4
PT10	70 ± 10	50 ± 30	120 ± 30	54 ± 1	74 ± 2	128 ± 4
GS1	---	---	---	59.4 ± 0.7	74.0 ± 0.9	133 ± 2
GS2	---	---	---	59.1 ± 0.7	72.01 ± 0.9	131 ± 2

5.5. Discussion

5.5.1 Radium trends during pumping test

During the short-term pumping test, there is an initial period of variability as the system discharges after which conditions return to water quality representative of the aquifer. As the well turns over water that remained stagnant in the borehole for ten days, aqueous chemistry is quite variable. Once the well draws water representative of aquifer conditions, the concentrations stabilize after 30 minutes of pumping. This trend of initial variability before stabilization is observed for conductivity, DO, and combined Ra (Table 5.1, Figure 5.1).

Time required to reach stable geochemical conditions vary for Ra levels when comparing results from the counting and the MC-ICPMS methods. For samples PT8-10, decay counting

measures 150 ± 30 mBq/L while the MC-ICPMS method measures 129 ± 3 mBq/L combined Ra. Analytical uncertainty associated with decay counting is greater, as the method counts radioactive decays rather than atoms; additionally, minimum reporting limit for decay counting is 37 mBq/L (1 pCi/L). It is difficult to measure Ra precisely at these ultra trace levels, where only a few (e.g., 10 – 20) radioactive decays may be measured in the sample during the time of analytical measurement. However, the ultra trace levels of Ra present in groundwater that are necessary for water utilities to examine in order to maintain MCL compliance lie close to the reporting limits of decay counting. In contrast, the MC-ICPMS method has both lower detection limits and higher precision for Ra.[39] Notably, combined Ra values for all samples measured via the MC-ICPMS method fall within overall uncertainty from values measured via decay counting, indicating that both methods are measuring similar accuracy, although precision varies. Water utilities must make decisions for Ra treatment for their drinking water systems based upon their reported compliance data, which depends on the precision and accuracy of the analytical method used to measure Ra.

5.5.2 Differences in radium analyses

MC-ICPMS analysis shows consistent combined Ra the initial period of well flushing, which are consistent with samples taken during standard pumping periods. Grab samples taken in January 2019 and March 2020 contain 133 ± 2 mBq/L and 131 ± 2 mBq/L combined Ra, respectively (Figure 5.2). These values are within analytical uncertainty of combined Ra activities in samples PT8 – 10 and GS1-2, which average 129 ± 3 mBq/L by MC-ICPMS measurement. The consistency among samples collected suggests that combined Ra levels in groundwater sourced by Madison Well 19 were steady over the course of 2019. Additionally, this trend is more easily observed in the precise measurements of the MC-ICPMS method than decay counting.

To identify increasing trends in combined Ra in municipal wells, comparison of precise measurements with EPA-approved methods may provide a more accurate picture. Water utilities must use EPA-approved analysis (e.g., decay counting) for reporting combined Ra levels for compliance. While decay counting likely provides information on overall general Ra levels, it is much less precise than the MC-ICPMS method at the ultra trace levels relevant to groundwater. As water utilities examine Ra trends in groundwater over time, awareness of analytical method limitations and instrumental uncertainty must be included in analysis and subsequent actions. Reporting of analytical uncertainty to compliance data collected by state agencies (e.g., Wisconsin Department of Natural Resources) will further aid utilities in examining long-term trends. Additionally, if financially feasible, secondary analysis of well samples by laboratories equipped to examine Ra via the MC-ICPMS method, would be beneficial to verify decay counting findings. Comparison of results between the counting and MC-ICPMS methods to verify that drinking water treatment is necessary will guide management decisions.

The results of this study suggest that there is geochemical variability during initial well pumping after a period of stagnation, before the well withdraws water representative of the aquifer system and geochemical conditions stabilize. Additionally, comparison between two analytical methods for measuring Ra suggests that decay counting used to report ^{226}Ra and ^{228}Ra levels in drinking water for municipal compliance is not sensitive to measuring small changes in the trace Ra concentrations close to the regulatory value (e.g., 0 – 185 mBq/L). The sensitivity of mass spectrometry methods measures more precise values of Ra in water samples but is not approved for EPA compliance. It is important to understand the accuracy and precision of the methods currently used to report water quality conditions in drinking water, particularly to verify consistent temporal trends like that observed in Madison Well 19. Analytical methods used to examine Ra

occurrence and which help determine water availability based on quality must be able to fully describe the system.

5.6 Conclusions

Wells used for municipal drinking water are typically open to long intervals of an aquifer system, making complex geochemical interactions between aquifer solids and geogenic contaminants difficult to predict. Specifically, while geochemical trends can be used to predict Ra levels at both broad geographic scales and specific mineral interactions, they are difficult to translate to geochemical interactions within well boreholes that may impact aqueous Ra. In this study, we show that trends in combined Ra levels in a well remain stable over the period of ~1 year, during short-term pumping after a period of stagnation and during pumping for typical municipal use. Additionally, analytical methods used to measure Ra must address the precision required for the ultra trace Ra quantities relevant for drinking water systems in order to best inform decision-making on water treatment installation. Additional analysis of well samples from municipal systems located in other parts of Wisconsin or other states open to the MCOAS would be beneficial for contributing to understanding to how isotopic indicators can help predict Ra occurrence. Nonetheless, this study demonstrates that consistency in Ra levels is observed over varied pumping patterns, and that estimating accurate trends of Ra concentrations may be highly dependent on the chosen analytical method. Water utilities reporting combined Ra for compliance may send additional samples to labs equipped for more precise analysis, to verify compliance results prior to implementing treatment.

5.7 Acknowledgements

This work was supported with directed cooperative matching funds from the U.S. Geological Survey Water Availability and Use Science Program as well as the Wisconsin

Department of Natural Resources. Thank you to the Madison Water Utility for their support of sampling measures across many municipal wells; thanks also to the Sussex Water Utility, Fond du Lac Water Utility, the Villa Louis Historic Site, Cambria Water Utility, and Winneconne Water Utility. We thank Amy Plechacek, Gabrielle Campagnola, Marie Dematatis, Anna Frehner, Madeline Gotkowitz, and Pete Chase for support with field data collection. Laboratory assistance provided by Amy Plechacek, and James Lazarcik was greatly appreciated. We thank the Wisconsin State Laboratory of Hygiene Trace Metal Laboratory for support and access to multi-collector inductively coupled plasma mass spectrometry, and specifically Joel Overdier for trace metal analysis. Thanks to Lily Schacht for providing excellent insight into the writing of the manuscript.

5.8 References

1. Evans, R. D., Radium poisoning: a review of present knowledge. *American Journal of Public Health and the Nations Health* **1933,** *23*, (10), 1017-1023.
2. Cohn, P.; Skinner, R.; Burger, S.; Falgiano, J.; Klotz, J., Radium in Drinking Water and the Incidence of Osteosarcoma: A Report to the New Jersey Department of Environmental Protection. **2003**.
3. Mays, C. W.; Rowland, R. E.; Stehney, A. F., Cancer risk from the lifetime intake of Ra and U isotopes. *Health physics* **1985,** *48*, (5), 635-47.
4. Guse, C. E.; Marbella, A. M.; George, V.; Layde, P. M., Radium in Wisconsin drinking water: an analysis of osteosarcoma risk. *Archives of Environmental Health: An International Journal* **2002,** *57*, (4), 294-303.
5. US EPA, National primary drinking water regulations. *Federal Register* **2000,** *65*, (236).
6. US EPA *Radionuclides rule: a quick reference guide*; 2001.
7. Szabo, Z.; dePaul, V. T.; Fischer, J. M.; Kraemer, T. F.; Jacobsen, E., Occurrence and geochemistry of radium in water from principal drinking-water aquifer systems of the United States. *Applied Geochemistry* **2012,** *27*, (3), 729-752.
8. Stackelberg, P. E.; Szabo, Z.; Jurgens, B. C., Radium mobility and the age of groundwater in public-drinking-water supplies from the Cambrian-Ordovician aquifer system, north-central USA. *Applied Geochemistry* **2018,** *89*, 34-48.
9. Dematatis, M.; Plechacek, A.; Mathews, M.; Wright, D. B.; Udenby, F.; Gotkowitz, M. B.; Ginder-Vogel, M., Spatial and temporal variability of radium in the Wisconsin Cambrian-Ordovician aquifer system. *AWWA Water Science* **2020**.
10. Great Lakes-St. Lawrence River Basin Water Resources Council, Final Decision. In 2016.
11. Luczaj, J.; Masarik, K., Groundwater Quantity and Quality Issues in a Water-Rich Region: Examples from Wisconsin, USA. *Resources* **2015,** *4*, (2), 323-357.
12. Grundl, T.; Bradbury, K.; Feinstein, D.; Friers, S.; Hart, D., A Combined Hydrologic/Geochemical Investigation of Groundwater Conditions in the Waukesha County Area, WI.
13. Mathews, M.; Gotkowitz, M.; Ginder-Vogel, M., Effect of geochemical conditions on radium mobility in discrete intervals within the Midwestern Cambrian-Ordovician aquifer system. *Applied Geochemistry* **2018,** *97*, 238-246.
14. Vinson, D. S.; Vengosh, A.; Hirschfeld, D.; Dwyer, G. S., Relationships between radium and radon occurrence and hydrochemistry in fresh groundwater from fractured crystalline rocks, North Carolina (USA). *Chemical Geology* **2009,** *260*, (3-4), 159-171.
15. Gilkeson, R. H. *Isotopic studies of the natural sources of radium in groundwater in Illinois*; 1984; pp 50-50.
16. Szabo, Z.; Fischer, J. M.; Hancock, T. C. *USGS Fact Sheet 2010-3113: Principal aquifers can contribute radium to sources of drinking water under certain geochemical conditions*; 2012; pp 6-6.
17. Tomita, J.; Satake, H.; Fukuyama, T.; Sasaki, K.; Sakaguchi, A.; Yamamoto, M., Radium geochemistry in Na–Cl type groundwater in Niigata Prefecture, Japan. *Journal of Environmental Radioactivity* **2010,** *101*, (3), 201-210.

18. Krishnaswami, S.; Bhushan, R.; Baskaran, M., Radium isotopes and 222Rn in shallow brines, Kharaghoda (India). *Chemical Geology: Isotope Geoscience section* **1991,** *87*, (2), 125-136.
19. Vinson, D. S.; Tagma, T.; Bouchaou, L.; Dwyer, G. S.; Warner, N. R.; Vengosh, A., Occurrence and mobilization of radium in fresh to saline coastal groundwater inferred from geochemical and isotopic tracers (Sr, S, O, H, Ra, Rn). *Applied Geochemistry* **2013,** *38*, 161-175.
20. Grundl, T.; Cape, M., Geochemical factors controlling radium activity in a sandstone aquifer. *Ground Water* **2006,** *44*, (4), 518-527.
21. Ayotte, J. D.; Szabo, Z.; Focazio, M. J.; Eberts, S. M., Effects of human-induced alteration of groundwater flow on concentrations of naturally-occurring trace elements at water-supply wells. *Applied Geochemistry* **2011,** *26*, (5), 747-762.
22. Wilson, J. T., Water-quality assessment of the Cambrian-Ordovician aquifer system in the Northern Midwest, United States. *U.S. Geological Survey Scientific Investigations Report 2011-5229* **2012**, 154.
23. Reynolds, B. C.; Wasserburg, G. J.; Baskaran, M., The transport of U- and Th-series nuclides in sandy confined aquifers. *Geochimica et Cosmochimica Acta* **2003,** *67*, (11), 1955-1972.
24. Tricca, A.; Wasserburg, G. J.; Porcelli, D.; Baskaran, M., The transport of U-and Th-series nuclides in a sandy unconfined aquifer. *Geochimica et Cosmochimica Acta* **2001,** *65*, (8), 1187-1210.
25. Tamamura, S.; Takada, T.; Tomita, J.; Nagao, S.; Fukushi, K.; Yamamoto, M., Salinity dependence of 226Ra adsorption on montmorillonite and kaolinite. *Journal of Radioanalytical and Nuclear Chemistry* **2014,** *299*, (1), 569-575.
26. Nathwani, J. S.; Phillips, C. R., Adsorption of 226Ra by soils in the presence of Ca2+ ions. Specific adsorption (II). *Chemosphere* **1979,** *8*, (5), 293-299.
27. Sturchio, N. C.; Banner, J. L.; Binz, C. M.; Heraty, L. B.; Musgrove, M., Radium geochemistry of ground waters in Paleozoic carbonate aquifers, midcontinent, USA. *Applied Geochemistry* **2001,** *16*, (1), 109-122.
28. Weaver, T. R.; Bahr, J. M., Geochemical evolution in the Cambrian-Ordovician sandstone aquifer, eastern Wisconsin: 2. Correlation between flow paths and ground-water chemistry. *Ground Water* **1991,** *29*, (4), 510-515.
29. Weaver, T. R.; Bahr, J., Geochemical evolution in the Cambrian-Ordovician sandstone aquifer, eastern Wisconsin: 1. Major ion and radionuclide distribution. *Ground Water* **1991,** *29*, (3), 350-356.
30. Young, H. L.; Siegel, D. I., Hydrogeology of the Cambrian-Ordovician Aquifer System in the Northern Midwest, United States. *U.S. Geological Survey Professional Paper 1405-B 99.* **1992**.
31. Young, H. L., *Summary of ground-water hydrology of the Cambrian-Ordovician aquifer system in the northern Midwest, United States*. US Department of the Interior, US Geological Survey: 1992; Vol. 1405.
32. Hubbuch, C., Radium found in Near West Side well; follow-up test results pending. *Wisconsin State Journal* Nov. 27, 2019, 2019.
33. Madison Water Utility Well 19 - Iron, Manganese & Radium Treatment. https://www.cityofmadison.com/water/projects/well-19-iron-manganese-radium-treatment
34. Madison Water Utility *Well 19 Quality Report*; 2019.

35. Office of Environmental Policy and Assistance - Air, W. a. R. D. E.-. *Compendium of EPA-approved analytical methods for measuring radionuclides in drinking water*; US Department of Energy: 1998.
36. Sims, K. W. W.; Hart, S. R.; Reagan, M. K.; Blusztajn, J.; Staudigel, H.; Sohn, R. A.; Layne, G. D.; Ball, L. A.; Andrews, J., 238U-230Th-226Ra-210Pb-210Po, 232Th-228Ra, and 235U-231Pa constraints on the ages and petrogenesis of Vailulu'u and Malumalu Lavas, Samoa. *Geochemistry, Geophysics, Geosystems* **2008,** *9*, (4).
37. Mathews, M.; Scott, S. R.; Gotkowitz, M. B.; Ginder-Vogel, M., Association of Radionuclide Isotopes with Aquifer Solids in the Midwestern Cambrian–Ordovician Aquifer System. *ACS Earth and Space Chemistry* **2021**.
38. Georgia Institute of, T., The determination of radium-226 and radium-228 in drinking water by gamma-ray spectrometry using HPGE or Ge(Li) detectors, revision 1.2. **2004**.
39. Scott, S. R.; Sims, K. W. W.; Reagan, M. K.; Ball, L.; Schwieters, J. B.; Bouman, C.; Lloyd, N. S.; Waters, C. L.; Standish, J. J.; Tollstrup, D. L., The application of abundance sensitivity filters to the precise and accurate measurement of uranium series nuclides by plasma mass spectrometry. *International Journal of Mass Spectrometry* **2019,** *435*, 321-332.

Chapter 6

Conclusions

6.1 Summary

The primary purpose of this research is to examine radium (Ra) interactions with aquifer solids at discrete stratigraphy within the Midwestern Cambrian-Ordovician aquifer system (MCOAS), in order to better understand how local-scale geochemical exchanges influence Ra partitioning to groundwater, under aquifer system conditions. A novel aspect of these investigations is the coupling of aqueous and solid-phase analysis, through studying Ra content and aqueous geochemistry in groundwater samples collected at discrete intervals. Additionally, we examine Ra-solid-phase associations via sequential extractions on aquifer solids, using sensitive analytical techniques like multi-collector inductively coupled plasma mass spectrometry (MC-ICPMS) to measure Ra at expected ultra-trace levels. We also compare Ra levels in groundwater samples from discrete intervals within the MCOAS with levels from solid-phase experiments, using isotopic tools to study the contribution of specific stratigraphy to Ra levels observed in long-stemmed wells. Finally, we examine the impact of short-term water withdrawal on Ra levels in a municipal well, comparing methods of analysis to determine Ra temporal trends with precision.

In Chapter 2, we examine the association of geochemical conditions (e.g., redox state, total dissolved solids) with aqueous Ra at discrete intervals within the MCOAS. We collected groundwater samples from short-screened monitoring wells to investigate aqueous Ra distribution at specific stratigraphic units in the MCOAS. Parent nuclides U and Th were observed at low concentrations in groundwater and aquifer solid samples. While most samples contained low

levels of Ra (0 – 89 mBq/L, or 0 – 2.4 pCi/L), certain geochemical conditions were associated with more elevated levels (> 150 mBq/L, or > 4 pCi/L). Specifically, in the anoxic portion of the aquifer system, greater levels of aqueous Ra were observed (170 ± 30 mBq/L or 4.6 ± 0.7 pCi/L); in the unconfined aquifer, elevated total dissolved solids (TDS) is associated with greater levels of Ra (190 ± 30 mBq/L or 5.2 ± 0.8 pCi/L). Geochemical conditions likely impact mineral presence and/or dissolution (e.g., iron (hydr)oxides), or the availability of sorption sites due to ion competition, therefore influencing Ra partitioning from aquifer solids. Overall, this work builds on knowledge of geochemical conditions associated with elevated Ra in the MCOAS by examining it at discrete levels.

In Chapter 3, we conducted sequential extraction experiments on aquifer solids to investigate solid-phase interactions between Ra and specific stratigraphy. Secular equilibrium between U and Ra is observed across stratigraphy, although leaching potential appears greater in the Maquoketa shale and St Peter sandstone units. Geochemical associations (water-soluble, acido-soluble, reducible minerals) between Ra and aquifer solid-phases vary across stratigraphy; namely, acido-soluble associations dominate in the Maquoketa shale unit while reducible mineral interactions are bigger controls in the Tunnel City, a glauconitic sandstone. The range in both total quantity of Ra and solid-phase Ra associations within the aquifer solids demonstrates the importance of local-scale geochemical conditions and mineral associations on the partitioning of Ra from aquifer solids to the aqueous system.

In Chapter 4, we utilize isotopic tools to more closely examine water-rock interactions influencing Ra partitioning from aquifer solids at discrete intervals in the MCOAS. Specifically, we collected groundwater samples at discrete intervals associated with elevated levels of U relative to the specific stratigraphy, and examined geochemical conditions at each examined

interval. Additionally, we ran solid-phase experiments on associated aquifer solids to examine Ra-solid-phase interactions. Evidence for Ra leaching is clear from disequilibrium between whole-rock U and Ra, where five samples contain [$^{226}Ra/^{238}U$] outside of equilibrium values, while three samples from the Tunnel City sandstone are observed at equilibrium. However, local geochemical factors (ORP, TDS) have minimal impact on Ra partitioning at discrete intervals at the study site, while redox state and alkalinity content influence aqueous ^{238}U. Correlation between $^{87}Sr/^{86}Sr$ and aqueous ^{226}Ra suggests that minerals releasing radiogenic ^{87}Sr to groundwater are also releasing ^{226}Ra. In sum, the study examines at the local scale how parent nuclide U aquifer associations inform Ra water-rock interactions, influenced by available mineral associations and aqueous geochemistry (ORP, TDS) in the MCOAS.

In Chapter 5, we explore the integration of geochemical and isotopic tools in examining geochemical interactions influencing Ra partitioning in a long-stemmed municipal well during a short-term pumping test. Trends in combined Ra ($^{226}Ra + ^{228}Ra$) remain stable over the period of a year, throughout normal and atypical pumping conditions. However, analytical methods used to report compliance data to state records must be precise enough to accurately reflect Ra concentrations that municipal wells are sourcing at the relevant ultra-trace levels. Additionally, preliminary data suggests that isotopic indicators ($^{87}Sr/^{86}Sr$, [$^{234}U/^{238}U$]) can also be used to examine hydrologic and geologic context for mixing in municipal wells (Appendix E). In particular, association between [$^{234}U/^{238}U$] and combined Ra could be a new tool to help estimate Ra levels in municipal wells across Wisconsin (Appendix E). Overall, precise mass spectrometry analysis for isotopic indicators can be developed to further inform well construction aimed at reducing uptake of water elevated in Ra in the MCOAS.

Together, this research identifies the impact of aqueous geochemistry and mineral associations on Ra partitioning at discrete intervals in the MCOAS. Geochemical indicators (ORP, TDS) are used as general predictors at the large geographic scale but struggle to predict Ra levels at the discrete interval scale. The results indicate that quantity and presence of parent nuclides, as well as availability of mineral associations are also important considerations for Ra levels. While this study focuses on short- and long-screened wells open to the MCOAS only in Wisconsin, this approach provides new insight into how specific water-rock interactions contribute Ra to the aqueous system within an aquifer, and how these interactions can be used to estimate Ra at the municipal well scale.

6.2 Suggestions for future research

Based on these conclusions, there are several topics within the scope of this research that have not yet been addressed. Specifically, the question of how local water-rock interactions influence Ra across multiple stratigraphic units must be examined. The impact of changing aqueous geochemistry and differing mineral associations between two stratigraphic units (e.g., a shaley confining layer over a sandstone aquifer) may influence Ra partitioning, particularly across well boreholes open to multiple stratigraphic units. Alongside this potential investigation lies the question of how long-term water withdrawal may impact Ra partitioning as well. In order to understand the contribution of Ra from MCOAS stratigraphy to the aqueous system, better understanding of the impact of aquifer drawdown on U and Ra associations is important. Additionally, the question of how the mixing of water with different chemical composition across a long-screened municipal well might mobilize Ra must also be examined. A geochemical model calculating interactions between Ra and aquifer solids at discrete intervals designed here begins to examine how the presence of different minerals impacts aqueous Ra levels (Appendix F).

Further geochemical and hydrologic modeling using this model may start to address the above questions.

Furthermore, to better understand the implications of long-term Ra trends in municipal wells in the MCOAS, future studies should address the analytical precision and associated uncertainty of Ra measurements in municipal compliance datasets. Increased precision in Ra measurements could better inform water utilities as to how to provide clean drinking water to constituents, with less uncertainty about the need for treatment. In order to address this, research must examine the ability of current EPA-approved analytical methods to predict Ra levels at ultra-trace concentrations relevant to drinking water. Additionally, more accurate long-term temporal trends in municipal compliance data could be determined if the reporting of analytical methods and their associated uncertainty was included in analysis.

Additionally, the research clearly illustrates that water-rock interactions influence Ra trends from municipal wells pulling water across long sections of the aquifer, but it also raises the question of how to best determine and predict the occurrence of elevated Ra in aquifer systems. There is a potential use for isotopic tools ($^{87}Sr/^{86}Sr$, [$^{234}U/^{238}U$]) in estimating Ra levels in municipal wells, but further research is required. Examination of Ra trends with isotopic tools across broad geographic and geologic regions within the MCOAS is necessary to further determine the use and applicability of isotopes in assessing Ra levels.

Appendix A

Supplementary Information for Chapter 2

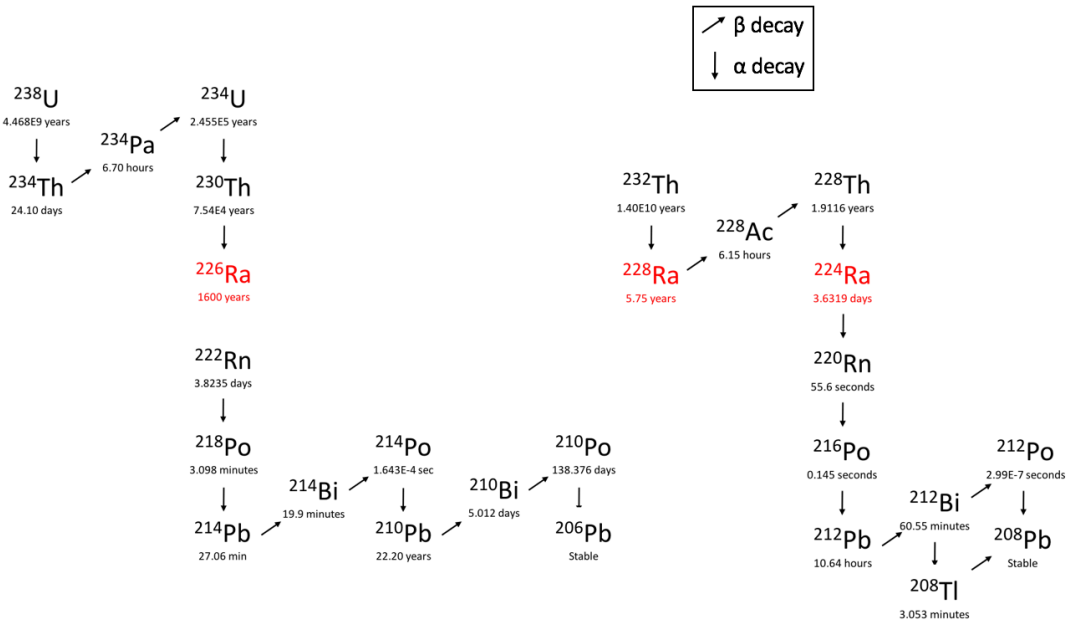

Figure A-1 Decay chain for radioactive decay of major radium isotope parent nuclides: ^{238}U and ^{232}Th.

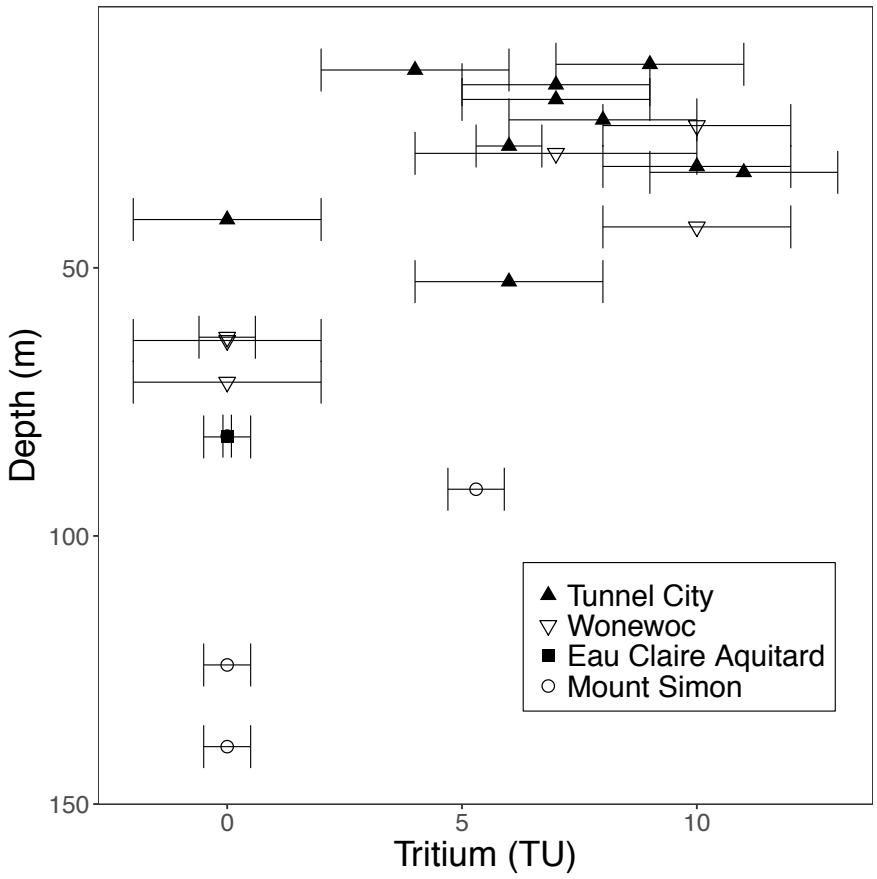

Figure A-2 Tritium concentration at depth from surface, differentiated by hydrostratigraphic unit.[1]

Table A-1 Concentrations of major ions and trace metal parent nuclides from sampled monitoring wells. All values in mg/L unless otherwise noted. Samples below detectable concentration are designated as non-detectable (n.d.).

Sampling Date	Well	NO_2^- + NO_3^-	SO_4^{2-}	Cl^-	^{232}Th (µg/L)	^{238}U (µg/L)	Ba	Ca	Mg	Mn	Na
10/27/16	MW-PL1	0.0311	0.0273	0.108	**	**	n.d.	n.d.	n.d.	n.d.	3.47 ± 0.08
5/31/17	MW-PL2	0.003	0.014	0.295	0	0.000399 ± 0.000008	n.d.	n.d.	n.d.	n.d.	n.d.
10/24/16	MW-7S	1.44	79.0	662	**	**	0.0507 ± 0.0006	216 ± 2	96.1 ± 0.6	n.d.	182.8 ± 0.7
5/30/17	MW-7S	5.49	49.5	435	0.005 ± 0.002	0.50 ± 0.03	0.035 ± 0.002	222.6 ± 0.2	105.5 ± 0.1	n.d.	130.6 ± 0.1
10/21/16	MW-11S	3.96	27.5	447	**	**	0.0395 ± 0.0009	127 ± 2	57.6 ± 0.5	n.d.	234 ± 1
5/25/17	MW-11S	4.34	31.7	444	0.0032 ± 0.0003	0.36 ± 0.02	0.045 ± 0.003	168.0 ± 0.8	85.2 ± 0.2	n.d.	225.2 ± 0.2
10/14/16	MW-19S	3.15	25.4	238	**	**	0.0153 ± 0.0002	107 ± 2	49.5 ± 0. 9	n.d.	115 ± 1
10/14/16	MW-30S	7.62	28.8	42.5	**	**	0.0077 ± 0.0001	107 ± 2	49 ± 1	n.d.	25.8 ± 0.3
10/24/16	MW-13S	4.38	29.5	309	**	**	0.0201 ± 0.0002	112 ± 3	54 ± 2	n.d.	145 ± 3
10/17/16	SW - port 1	7.00	35.6	276	**	**	0.0083 ± 0.0005	118 ± 1	56.3 ± 0.9	n.d.	120.6 ± 0.7
10/14/16	FB-11S	13.5	24.4	34.5	**	**	0.0084 ± 0.0003	100. ± 0.8	46 ± 2	n.d.	18.3 ± 0.4
5/22/17	FB-11S	12.6	26.6	33.3	0.0015 ± 0.0003	0.3095 ± 0.0009	n.d.	120.4 ± 0.7	61.8 ± 0.1	n.d.	15.0 ± 0.2
10/24/16	MW-13D	5.58	22.7	49.7	**	**	n.d.	97 ± 2	50. ± 2	n.d.	17.4 ± 0.23

Sampling Date	Well	NO_2^- + NO_3^-	SO_4^{2-}	Cl^-	^{232}Th (µg/L)	^{238}U (µg/L)	Ba	Ca	Mg	Mn	Na
10/14/16	MW-30D	6.56	15.5	33.2	**	**	n.d.	99 ± 1	50.8 ± 0.5	n.d.	11.4 ± 0.2
5/25/17	MW-30D	7.42	20.9	37.3	0.0039 ± 0.0004	0.52 ± 0.02	n.d.	120. ± 0.4	70.65 ± 0.05	n.d.	9.18 ± 0.05
10/14/16	FB-11D	0.222	3.31	0.400	**	**	n.d.	72.7 ± 0.6	35.5 ± 0.1	n.d.	7.98 ± 0.08
10/21/16	MW-11D	3.88	32.4	165	**	**	0.0072 ± 0.0002	115 ± 2	56.9 ± 0.9	n.d.	61.1 ± 0.6
5/22/17	MW-11D	3.55	39.5	149	0.0013 ± 0.0004	0.45 ± 0.02	n.d.	150.4 ± 0.8	80.92 ± 0.07	n.d.	45.60 ± 0.08
10/24/16	MW-7D	5.36	51.2	548	**	**	0.0231 ± 0.0005	165 ± 3	78 ± 2	n.d.	226 ± 4
5/30/17	MW-7D	4.98	55.6	594	0.0010 ± 0.0002	0.247 ± 0.006	0.012 ± 0.002	213.7 ± 0.6	116.4 ± 0.1	n.d.	236.6 ± 0.1
10/14/16	MW-19D	7.39	59.2	513	**	**	0.0550 ± 0.0004	167 ± 2	80. ± 2	n.d.	145 ± 2
5/22/17	MW-19D	3.60	58.4	410.	0.0013 ± 0.0003	0.273 ± 0.005	0.065 ± 0.003	204.0 ± 0.2	105.10 ± 0.09	n.d.	131.60 ± 0.07
10/17/16	SW - port 2	0.543	3.18	1.54	**	**	n.d.	72.5 ± 0.9	39.1 ± 0.6	n.d.	9.1 ± 0.2
10/24/16	MW-7VD	3.23	42.1	11.7	**	**	0.0183 ± 0.0004	104 ± 3	50. ± 2	0.0094 ± 0.0002	10.2 ± 0.2
5/30/17	MW-7VD	3.47	45.0	10.6	0.0010 ± 0.0003	0.57 ± 0.02	n.d.	124.9 ± 0.3	65.08 ± 0.05	n.d.	6.0 ± 0.1
10/21/16	LE-D	1.44	14.3	5.13	**	**	n.d.	76 ± 2	38 ± 1	0.0033 ± 0.0003	8.80 ± 0.06
5/30/17	LE-D	1.65	20.6	5.24	0.0010 ± 0.0002	0.34 ± 0.02	n.d.	90.3 ± 0.2	49.91 ± 0.05	n.d.	5.4 ± 0.2

Sampling Date	Well	NO_2^- + NO_3^-	SO_4^{2-}	Cl^-	^{232}Th (µg/L)	^{238}U (µg/L)	Ba	Ca	Mg	Mn	Na
5/12/16	SW - port 3	0.0364	4.93	0.432	**	**	n.d.	71 ± 1	44.5 ± 0.7	n.d.	7.1 ± 0.1
10/17/16	SW - MS-132	3.79	19.8	11.9	**	**	n.d.	77 ± 1	39 ± 1	n.d.	8.7 ± 0.1
5/25/17	SW - MS-132	4.04	22.7	10.3	0.00046 ± 0.00005	0.6936 ± 0.0008	n.d.	83 ± 0.3	50.30 ± 0.07	n.d.	5.1 ± 0.09
10/21/16	LE-VD	0.266	22.9	7.71	**	**	0.0051 ± 0.0002	80 ± 2	49.2 ± 0.4	0.159 ± 0.002	8.6 ± 0.2
5/30/17	LE-VD	0.177	23.8	8.036	0.0032 ± 0.0006	5.3 ± 0.1	n.d.	93.7 ± 0.3	63.79 ± 0.03	n.d.	4.8 ± 0.1
10/17/16	SW - port 5	0.0155	3.35	0.563	**	**	0.014 ± 0.001	85 ± 1	36.0 ± 0.3	0.1542 ± 0.0005	6.06 ± 0.07
5/25/17	SW - port 5	0.223	4.49	0.545	0.0008 ± 0.0002	0.163 ± 0.004	n.d.	93.6 ± 0.2	44.15 ± 0.06	n.d.	2.34 ± 0.04
10/21/16	SW - port 6	0	18.7	2.26	**	**	0.0120 ± 0.0005	76 ± 1	41.2 ± 0.5	0.0328 ± 0.0008	7.32 ± 0.06
5/25/17	SW - port 6	0.176	19.5	2.07	0.0004 ± 0.0002	1.04 ± 0.01	n.d.	82.8 ± 0.2	52.73 ± 0.05	n.d.	3.63 ± 0.04

**Samples were not evaluated for analysis.

Table A-2 Tritium values for monitoring wells. [a]Data from Gokowitz et al., 2015[1]

Well	Sampling Date	Tritium (TU)
[a]FB-11D	06/20/12	6 ± 2
[a]FB-11S	06/20/12	10 ± 2
[a]LE-D	06/25/12	< 0.8 ± 2
[a]LE-VD	06/25/12	< 0.8 ± 0.09
[a]MW-11D	06/27/12	10 ± 2
[a]MW-11S	06/27/12	4 ± 2
[a]MW-13D	06/21/12	11 ± 2
[a]MW-13S	06/21/12	8 ± 2
[a]MW-19D	06/18/12	10 ± 2
[a]MW-19S	06/18/12	7 ± 2
[a]MW-30D	06/19/12	< 0.8 ± 2
[a]MW-30S	06/19/12	7 ± 2
[a]MW-7D	06/26/12	7 ± 3
[a]MW-7S	06/26/12	9 ± 2
[a]MW-VD	06/26/12	< 0.8 ± 2
SW – port 1	4/28/14	6 ± 0.7
SW – port 2	4/28/14	< 0.8 ± 0.6
SW – port 3	4/28/14	< 0.8 ± 0.5
SW – MS-132	4/28/14	5.3 ± 0.6
SW – port 5	4/28/14	< 0.8 ± 0.5
SW – port 6	4/28/14	< 0.8 ± 0.5

Calculation A-1: Estimated barite activity calculations[2,3]

Barite activities for each groundwater sample are calculated from measured specific conductance values according to:

$$A_i = \gamma_{\pm 2} C_i \qquad \mathbf{A-1}$$

where A_i is the activity of the *i*th ion, $\gamma_{\pm 2}$ is the activity coefficient for divalent cations or anions, and C_i is the measured concentration of the *i*th ion. The activity coefficient is calculated via the extended form of the Debye-Hückel equation:

$$\log \gamma_{\pm 2} = -A z_i^2 \left(\frac{\sqrt{I}}{1 + B a_i \sqrt{I}} \right) \qquad \mathbf{A-2}$$

where A and B are tabulated Debye-Hückel constants (A = 0.511, B = 0.329x10^8 for water at 25°C), z_i^2 represents the charge value of the *i*th ion, and a_i is the ion size parameter (a_{barium} = 5x10^{-8} cm, $a_{sulfate}$ = 4x10^{-8} cm).[4] Ionic strength is estimated from the following relationship to measured specific conductance:

$$\mathrm{I} \cong (1.6\mathrm{x}10^{-5})(\text{Specific Conductance}) \qquad \mathbf{A-3}$$

where I is the ionic strength of the sample.

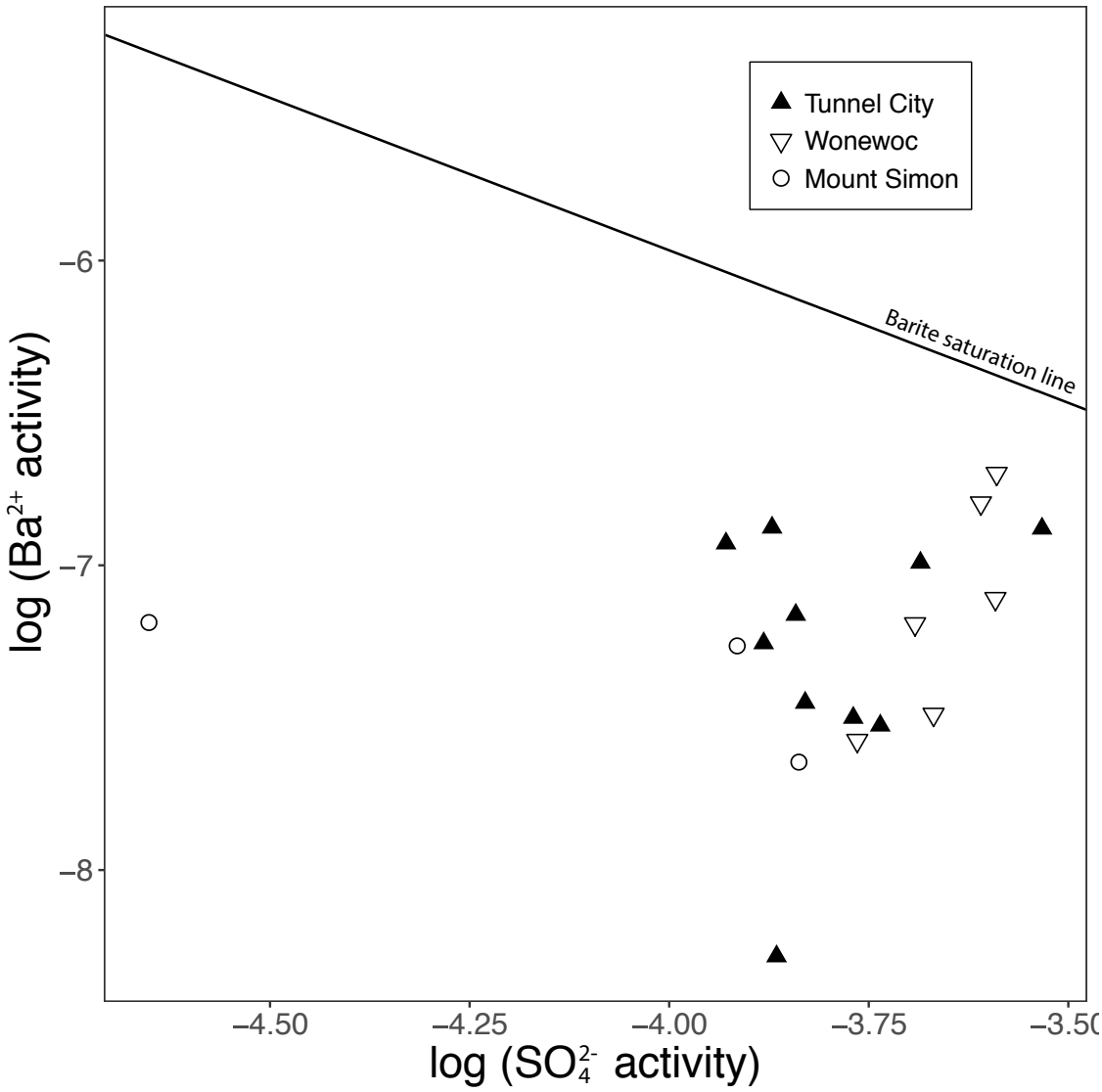

Figure A-3 Barium activity as a function of sulfate activity from samples above the detection level in both sampling sessions.

Appendix A: References

1. Gotkowitz, M. B. Evaluating remedies for pathogen contamination of urban groundwater. 2015.
2. Brezonik, P. L.; Arnold, W. A., *Water chemistry : an introduction to the chemistry of natural and engineered aquatic systems*. 2011; p 782-782.
3. Ponnamperuma, F. N.; Tianco, E. M.; Loy, T. A., Ionic strength of the solutions of flooded soils and other natural aqueous solutions from specific conductance. *Soil Science* **1966,** *102*, (6), 408-413.
4. Cohn, P.; Skinner, R.; Burger, S.; Falgiano, J.; Klotz, J., Radium in Drinking Water and the Incidence of Osteosarcoma: A Report to the New Jersey Department of Environmental Protection. **2003**.

Appendix B

Supplementary Information for Chapter 3

Table B-1 Select geophysical parameters for examined rock core. Note that porosity and dry bulk density were measured for the specific core; caution would need to be applied when extrapolating these values to the entire unit due to variability of cementation and grain size distribution within geologic units.[1]

Formation	Depth for geophysical properties (m)	Porosity	Dry bulk density (g/cm^3)
Maquoketa Shale	230	0.08	2.58
Galena Dolostone	326	0.05	2.69
St Peter Sandstone	395	0.12	2.33
Tunnel City Sandstone	423	0.17	2.20

Calculation B-1: Aquifer volume calculations

Formation: Maquoketa Shale
Total ^{226}Ra (pCi/g rock): 0.8 ± 0.2

$$^{226}Ra \text{ per aquifer volume (water} - \text{soluble fraction)} = \frac{mBq\ ^{226}Ra}{g\ rock} * porosity \qquad \mathbf{B-1}$$

^{226}Ra per aquifer volume (acido-soluble, reducible, HF digested fractions) =

$$\frac{mBq\ ^{226}Ra}{g} * (1 - porosity) * Dry\ bulk\ density\left(\frac{g}{cm^3}\right) \qquad \boldsymbol{B-2}$$

Table B-2 Distribution of ^{226}Ra across the non-HF digested fractions.

Sample	Fraction	Non-HF digested ^{226}Ra (mBq/cm^3)	Non-HF digested ^{226}Ra (%)	Non-HF digested ^{238}U (mBq/cm^3)	Non-HF digested ^{238}U (%)
Maquoketa Shale	Water-soluble	0.004 ± 0.001	0.2	0.010 ± 0.002	0.1
	Acido-soluble	1.00 ± 0.08	63	5 ± 1	77
	Reducible	0.6 ± 0.1	37	1.5 ± 0.2	23
Galena Dolostone	Water-soluble	0.0027 ± 0.0009	0.6	0.0039 ± 0.0003	0.07
	Acido-soluble	0.10 ± 0.02	22	3.4 ± 0.4	58
	Reducible	0.36 ± 0.06	77	2.41 ± 0.02	42
St Peter Sandstone	Water-soluble	0.0027 ± 0.0007	0.6	0.0027 ± 0.0003	1
	Acido-soluble	0.17 ± 0.07	35	0.13 ± 0.01	63
	Reducible	0.32 ± 0.07	64	0.07 ± 0.01	36
Tunnel City Sandstone	Water-soluble	0.0047 ± 0.0005	0.4	0.017 ± 0.003	0.6
	Acido-soluble	0.06 ± 0.03	6	1.8 ± 0.4	66
	Reducible	1.1 ± 0.3	94	0.89 ± 0.04	33

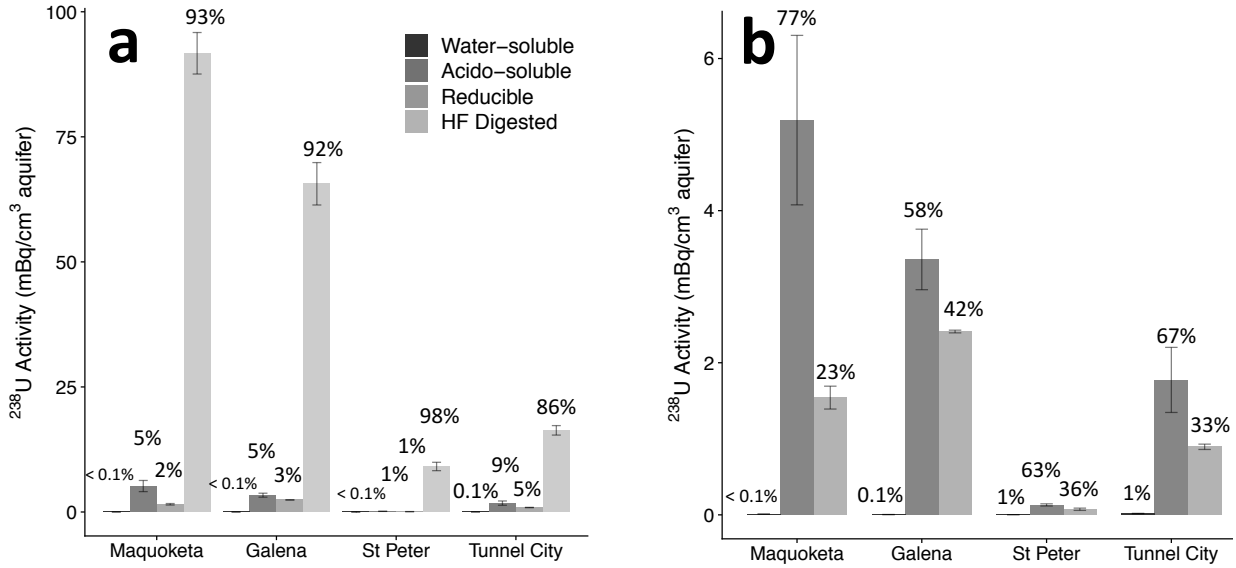

Figure B-1 Average ^{238}U per aquifer volume, separated into sequential extraction and digestion fractions for each stratigraphic unit. (a) shows distribution across all fractions including the digestion. Percentage values indicate the proportion of the specified fraction in comparison to the total ^{238}U for the stratigraphic unit. (b) shows the distribution within each stratigraphic unit for the non-HF digested fractions. Percentage values indicate the proportion of the specified fraction in comparison to the total non-HF digested ^{238}U for the stratigraphic unit. In both, error bars represent sample variability. Note different y-axis ranges.

Table B-3 Analyte concentrations from water-soluble leachate, for each stratigraphic unit. Uncertainty is attributed to instrumental error.

Stratigraphic Unit	Mg^{2+} (μg/cm^3)	Fe(II) (μg/cm^3)	Mn(II) (μg/cm^3)	K^+ (μg/cm^3)
Maquoketa shale	22 ± 2	0.02 ± 0.02	0.043 ± 0.004	13 ± 1
Galena dolostone	9.5 ± 0.7	0.007 ± 0.004	0.0048 ± 0.0002	2.9 ± 0.2
St Peter sandstone	0.4 ± 0.1	0.027 ± 0.004	0.0031 ± 0.0003	0.5 ± 0.1
Tunnel City	4 ± 1	0.02 ± 0.01	0.24 ± 0.06	2.5 ± 0.5

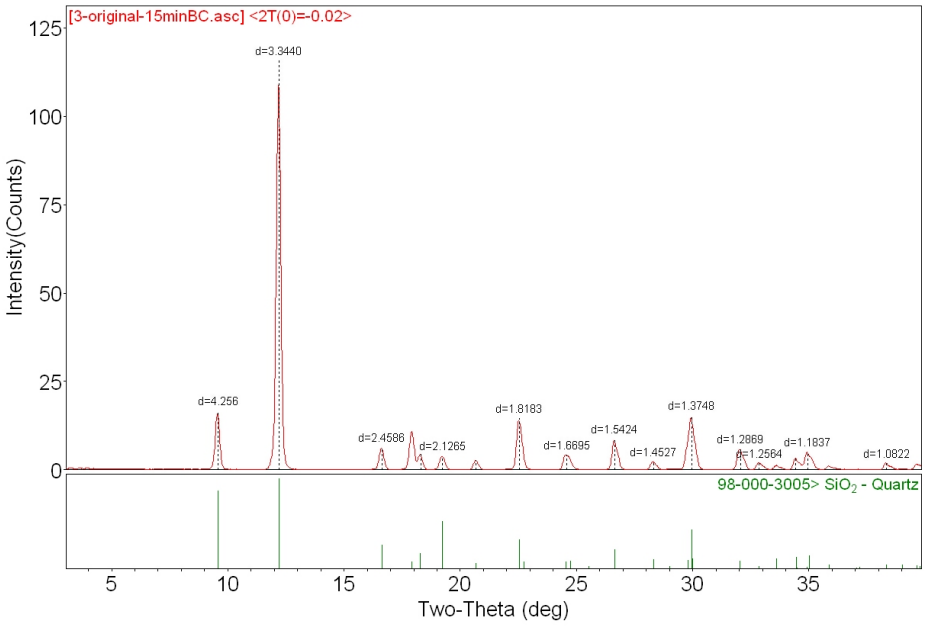

Figure B-2 X-ray diffraction (XRD) data for a selected sample from the Tunnel City rock samples, prior to the sequential extraction.

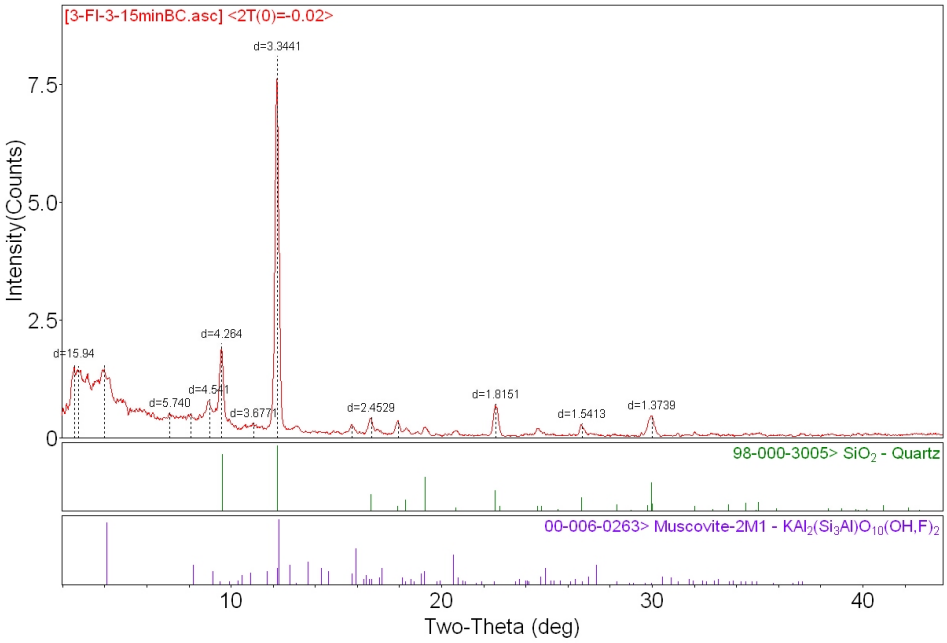

Figure B-3 X-ray diffraction (XRD) data for a selected sample from the Tunnel City rock samples, after the sequential extraction.

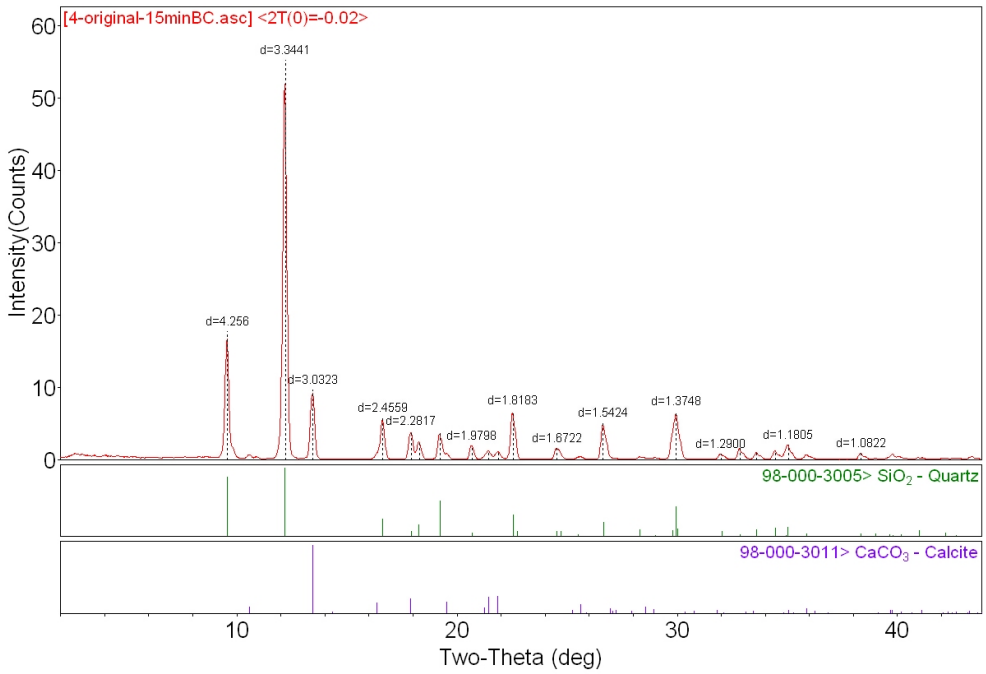

Figure B-4 X-ray diffraction (XRD) data for a selected sample from the St Peter rock samples, prior to the sequential extraction.

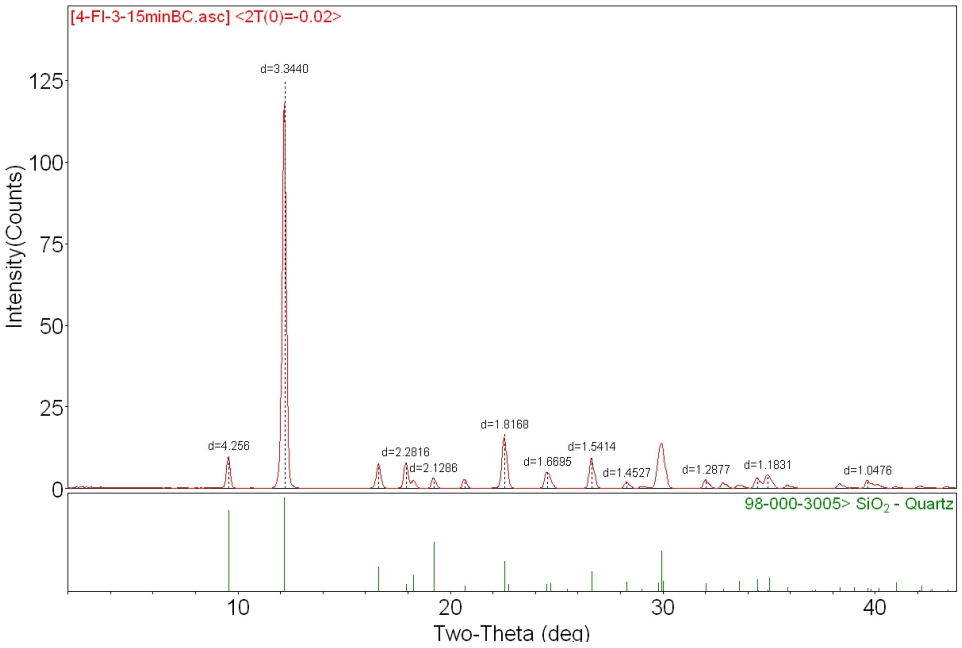

Figure B-5 X-ray diffraction (XRD) data for a selected sample from the St Peter rock samples, after the sequential extraction.

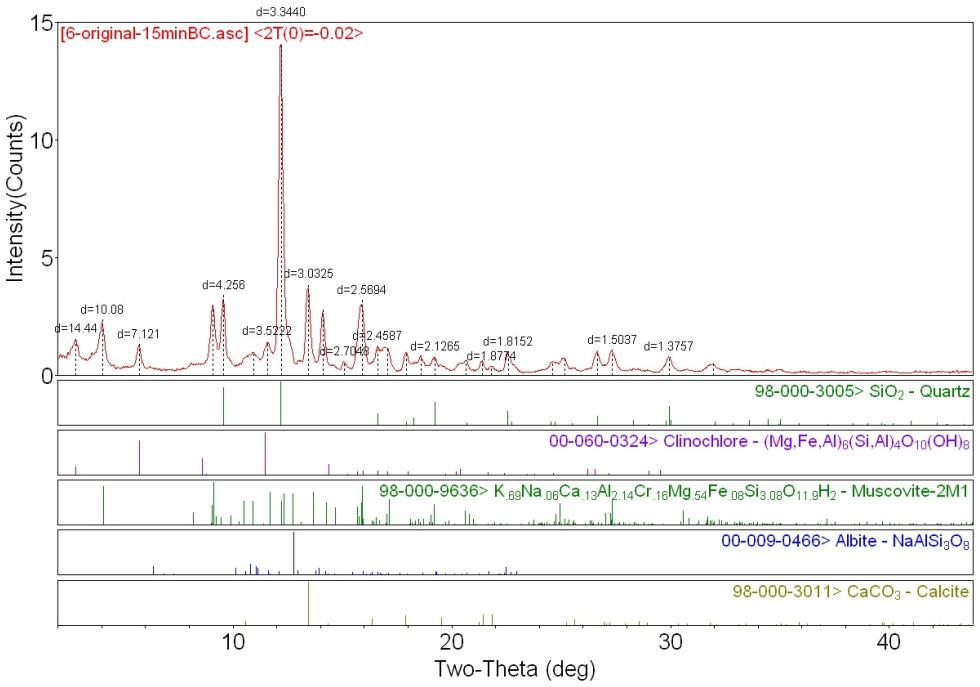

Figure B-6 X-ray diffraction (XRD) data for a selected sample from the Maquoketa rock samples, prior to the sequential extraction.

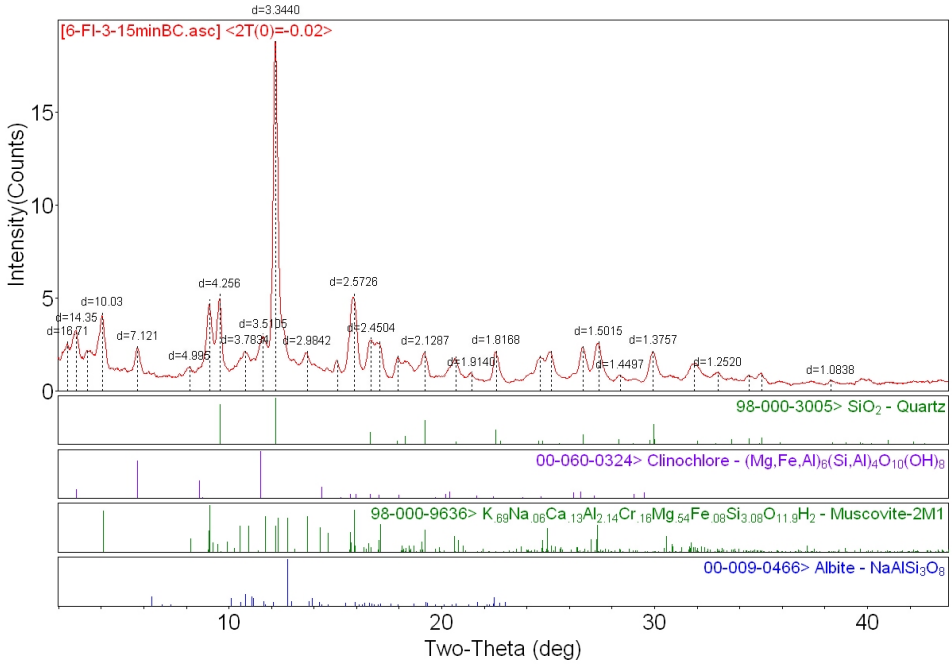

Figure B-7 X-ray diffraction (XRD) data for a selected sample from the Maquoketa rock samples, after the sequential extraction.

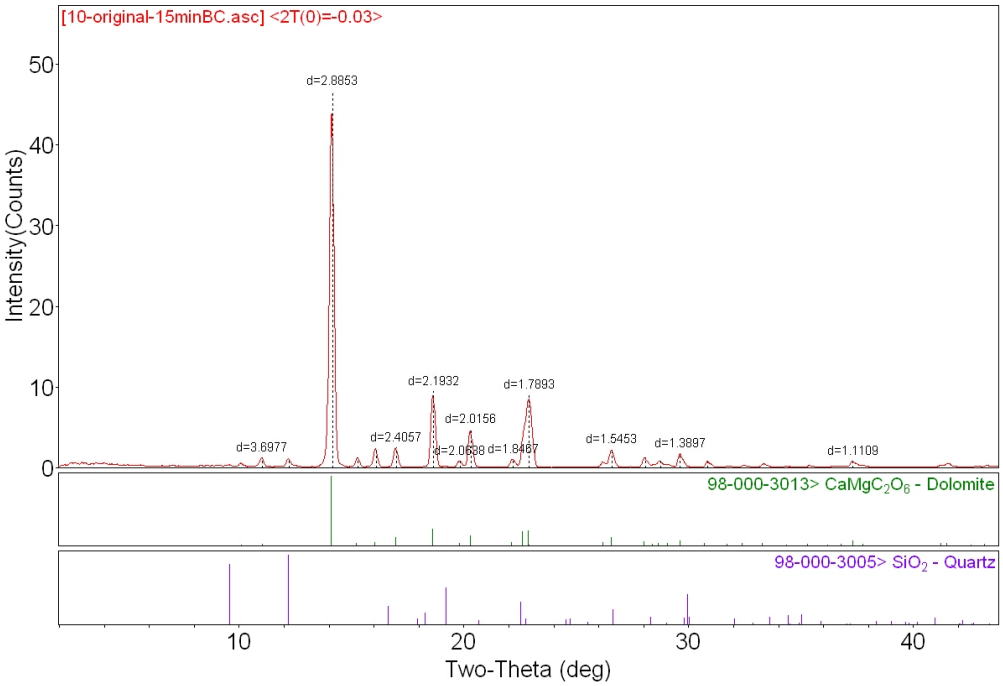

Figure B-8 X-ray diffraction (XRD) data for a selected sample from the Galena rock samples, prior to the sequential extraction.

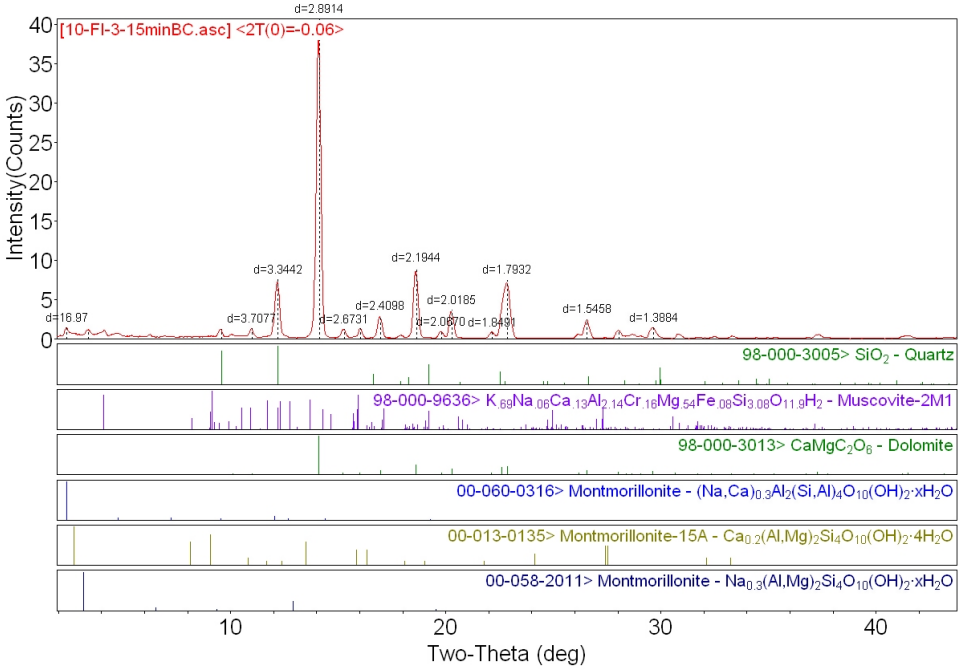

Figure B-9 X-ray diffraction (XRD) data for a selected sample from the Galena rock samples, after the sequential extraction

Appendix B: References

1. Porosities and densities of Wisconsin's aquifers and aquitards. https://wgnhs.wisc.edu/maps-data/data/rock-properties/porosity-density-measurements-data/

Appendix C

Supplementary Information for Chapter 4

Calculation C-1: ^{228}Ra spike calibration

The ^{228}Ra isotope spike was calibrated to the average literature ^{226}Ra/^{228}Ra for the rock standards using the following calculations (equation C-1).

$$R_m = \frac{Ab_N^A N + Ab_S^A S}{Ab_N^B N + Ab_S^B S} \qquad (C-1)$$

where R_m is the ratio of the abundances of isotopes A (^{226}Ra) and B (^{228}Ra) for an element, Ab_N^A represents the abundance of isotope A in the sample, Ab_S^A is the abundance of isotope A in the spike, Ab_N^B is the abundance of isotope B in the sample, and Ab_S^B is the abundance of isotope B in the spike. Here, N and S are the number of atoms of the sample or spike, respectively.

The concentration of analyte in a sample can be quantified by substituting equation C-2 into C-1, and rearranging the calculation to solve for the isotope of interest (equation C-3).

$$N_W = \frac{N * W_N}{A} \qquad (C-2)$$

where N_W is the weight of the isotope of interest, N is the number of atoms, W_N is the molecular weight of the analyte in the sample, and A is 6.022 x 10^{23} atoms/mole (Avogadro's number).

$$N_W = S_W \left(\frac{W_N}{W_S}\right)\left(\frac{Ab_S^A - R_m * Ab_S^B}{R_m * Ab_N^B - Ab_N^A}\right) \qquad (C-3)$$

where N_W and S_W are the weights of the sample and the spiked sample in units of mass. The decay of ^{228}Ra and ^{226}Ra over time was also included in the analysis via an age-correction.

Table C-1 Literature and measured values of ^{226}Ra used to calibrate the ^{228}Ra isotope spike.[1]

Standard Reference Material	^{226}Ra literature value (fg/g)	Literature uncertainty	Measured ^{226}Ra (fg/g)	Percent Digested (%)
AGV-2	631	3.4%	515	82
BCR-2	566	2.2%	542	96
TML	3614	2.9%	3272	91

To calibrate the spike, the following literature values of ^{226}Ra were used to calculate the concentration of Ra in the spike solution in mg/L, averaging an uncertainty value of 2.83% (Table S1). Note that the error is sourced from the rock standards that the spike is calibrated against; it is the lowest possible error for these samples, although other sources of error may contribute as well. This calibration was then used to estimate the percent of digestion completion for the experiment. An average of 89 ± 7% digestion was determined for the three SRM. Each digested sample was then divided by 0.89 to estimate the impact of digestion completion.

Note C-1: Further Quality Assurance Details

Notably, digestion reagent blank B2070_33 had measurable ^{226}Ra (15.1 ± 0.4 mBq/L). While there may have been addition of Ra to the sample during the purification process, this was determined to not impact overall study results. The sample contained expected blank levels of ^{238}U (0.00006 ± 0.00002 μg/L). Additionally, a second reagent blank measured in the same analysis run contained expected blank levels of ^{226}Ra (1.74 ± 0.05 mBq/L) and outliers were not observed for 2 samples run in triplicate in the same analysis run (MS-132 and 40) as well.

Table C-2 Literature values for $^{87}Sr/^{86}Sr$.[2-4]

Standard Reference Material	$^{87}Sr/^{86}Sr$ normalized literature value (mean)	Study
AGV-2	0.70398 ± 9 [a]	Weis et al., 2006
BCR-2	0.70501 ± 10 [a]	Weis et al., 2006
TML	0.705584 ± 9 [b]	Phillips et al., 2018
	0.705589 ± 0.000008 [c]	Park et al., 2019

[a] Uncertainty represents 2SD, the standard deviation on the mean of the rock standard analyses.

[b] Uncertainty represents internal precision (2σ) for the last two decimal places.

[c] Uncertainty represents the internal precision for the individual measurement (2σ/√n).

Table C-3 Physical properties of the aquifer system, estimated at each port depth from geophysical measurements of nearby wells.

Sample	Porosity	Bulk Density (g/cm^3 rock)
MS-132	0.1455	2.36
EC-114	0.090	2.52
EC-109	0.237	2.01
W-85	0.1535	2.24
TC-75	0.216	2.079
TC-67	0.193	2.22
TC-59	0.099	2.447
R-35	0.198	2.13

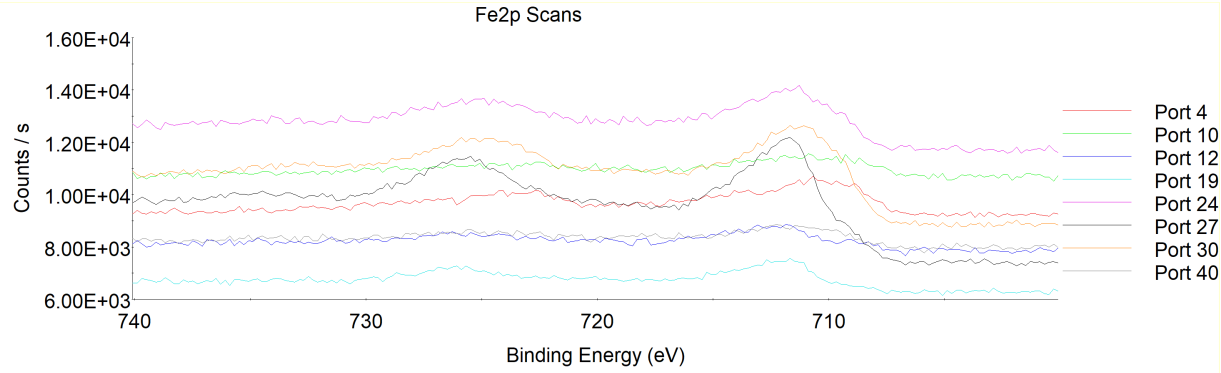

Figure C-1 Scans of iron binding energies from X-ray photoelectron spectra for samples of each MP16 port.

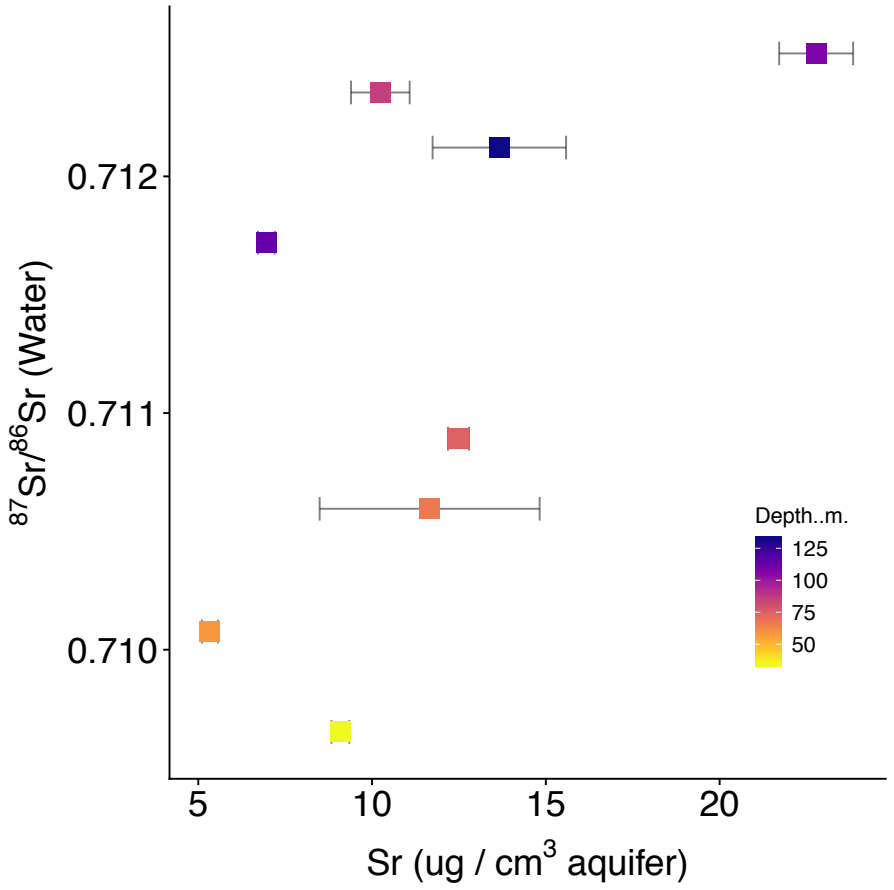

Figure C-2 Association between $^{87}Sr/^{86}Sr$ ratio and aqueous Sr for MP16 water samples at depth.

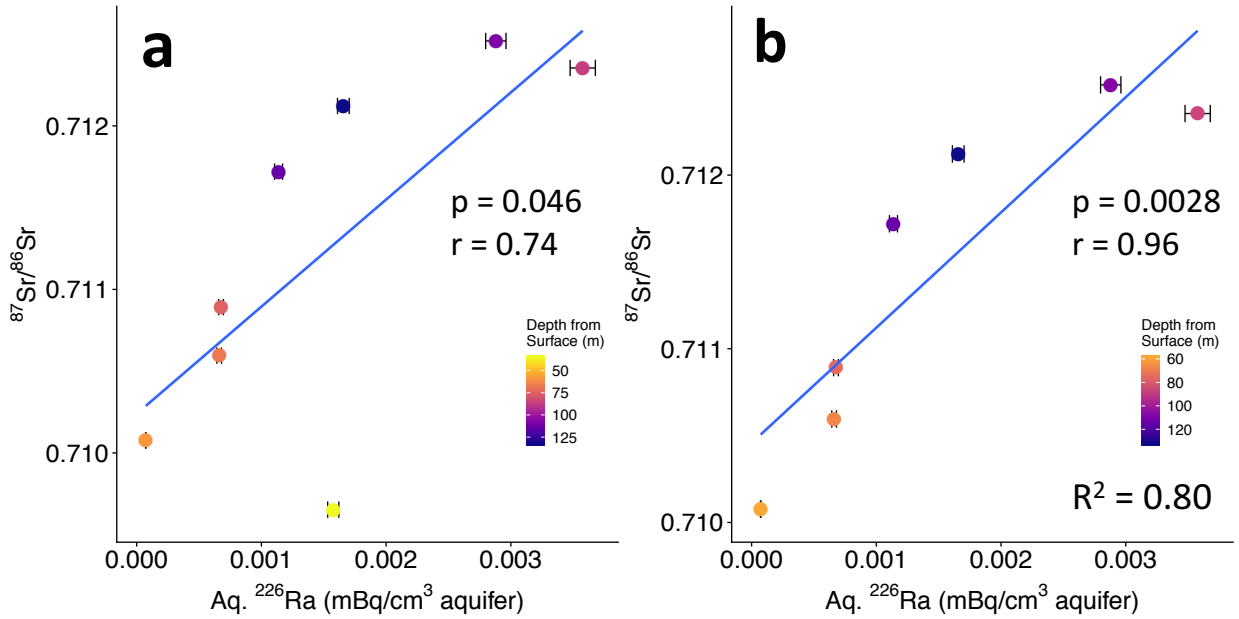

Figure C-3 Correlation between aqueous $^{87}Sr/^{86}Sr$ ratio and ^{226}Ra for ports open to Cambrian and Ordovician stratigraphy (a), and for ports open to only Cambrian stratigraphy (b).

Appendix C: References

1. Scott, S. R.; Sims, K. W. W.; Reagan, M. K.; Ball, L.; Schwieters, J. B.; Bouman, C.; Lloyd, N. S.; Waters, C. L.; Standish, J. J.; Tollstrup, D. L., The application of abundance sensitivity filters to the precise and accurate measurement of uranium series nuclides by plasma mass spectrometry. *International Journal of Mass Spectrometry* **2019,** *435*, 321-332.
2. Weis, D.; Kieffer, B.; Maerschalk, C.; Barling, J.; De Jong, J.; Williams, G. A.; Hanano, D.; Pretorius, W.; Mattielli, N.; Scoates, J. S., High-precision isotopic characterization of USGS reference materials by TIMS and MC-ICP-MS. *Geochemistry, Geophysics, Geosystems* **2006,** *7*, (8).
3. Phillips, E. H.; Sims, K. W. W.; Blichert-Toft, J.; Aster, R. C.; Gaetani, G. A.; Kyle, P. R.; Wallace, P. J.; Rasmussen, D. J., The nature and evolution of mantle upwelling at Ross Island, Antarctica, with implications for the source of HIMU lavas. *Earth and Planetary Science Letters* **2018,** *498*, 38-53.
4. Park, S.-H.; Langmuir, C. H.; Sims, K. W. W.; Blichert-Toft, J.; Kim, S.-S.; Scott, S. R.; Lin, J.; Choi, H.; Yang, Y.-S.; Michael, P. J., An isotopically distinct Zealandia–Antarctic mantle domain in the Southern Ocean. *Nature Geoscience* **2019,** *12*, (3), 206-214.

Appendix D

Supplementary Information for Chapter 5

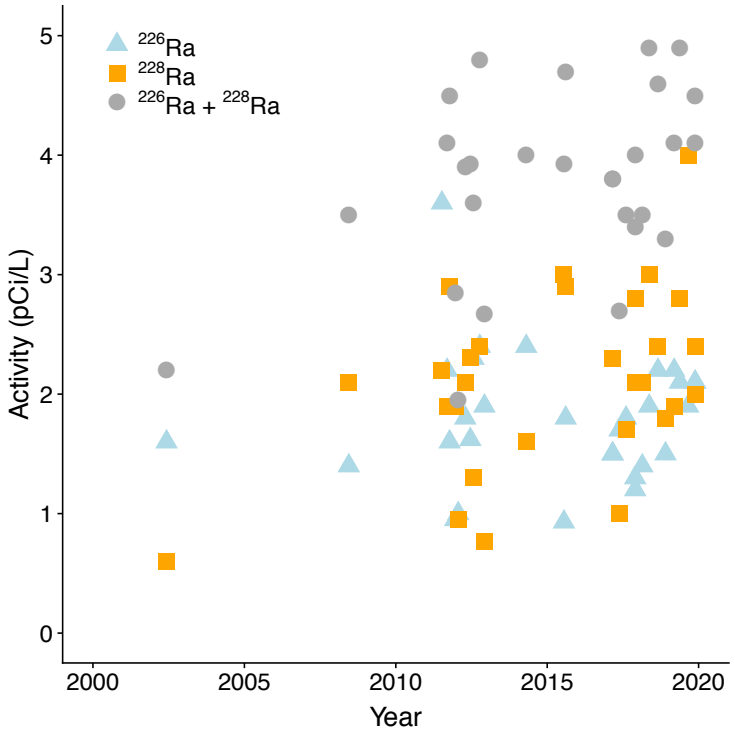

Figure D-1 Radium activities in Madison Well 19 over time, from reported WI DNR data. Blue triangles indicate ^{226}Ra activities, orange squares represent ^{228}Ra activities, and grey circles the combined activities of ^{226}Ra + ^{228}Ra.

Appendix E

Supplementary Information for Chapter 5

E-1 Background

In addition to the pumping test, municipal well samples from across Wisconsin were collected to examine state-wide implications of municipal water withdrawal on Ra levels (Figure E-1). Madison well samples were not filtered prior to acidification and were measured via mass spectrometry for Ra. All other groundwater samples were filtered prior to acidification for Sr and U isotope analysis (0.45 μm); for Ra analysis they were not filtered, but acidified and measured via the Georgia Tech counting method. 56 samples were analyzed for $^{87}Sr/^{86}Sr$ and $^{234}U/^{238}U$; of these, 46 groundwater samples were also analyzed for Ra. Reported Ra data for 8 municipal well samples were averages of long-term reported compliance data from the Wisconsin Department of Natural Resources database (Table E-1); for these, standard deviation over the examined time period represents uncertainty.[1] For hydrologic isotopic context, surface water samples were also collected; these were taken in the field, filtered in lab (0.45 μm), then evaporated in beakers in preparation for mass spectrometry analysis. A seawater standard reference material (CASS-4) was also analyzed via mass spectrometry for $^{87}Sr/^{86}Sr$ and $^{234}U/^{238}U$.

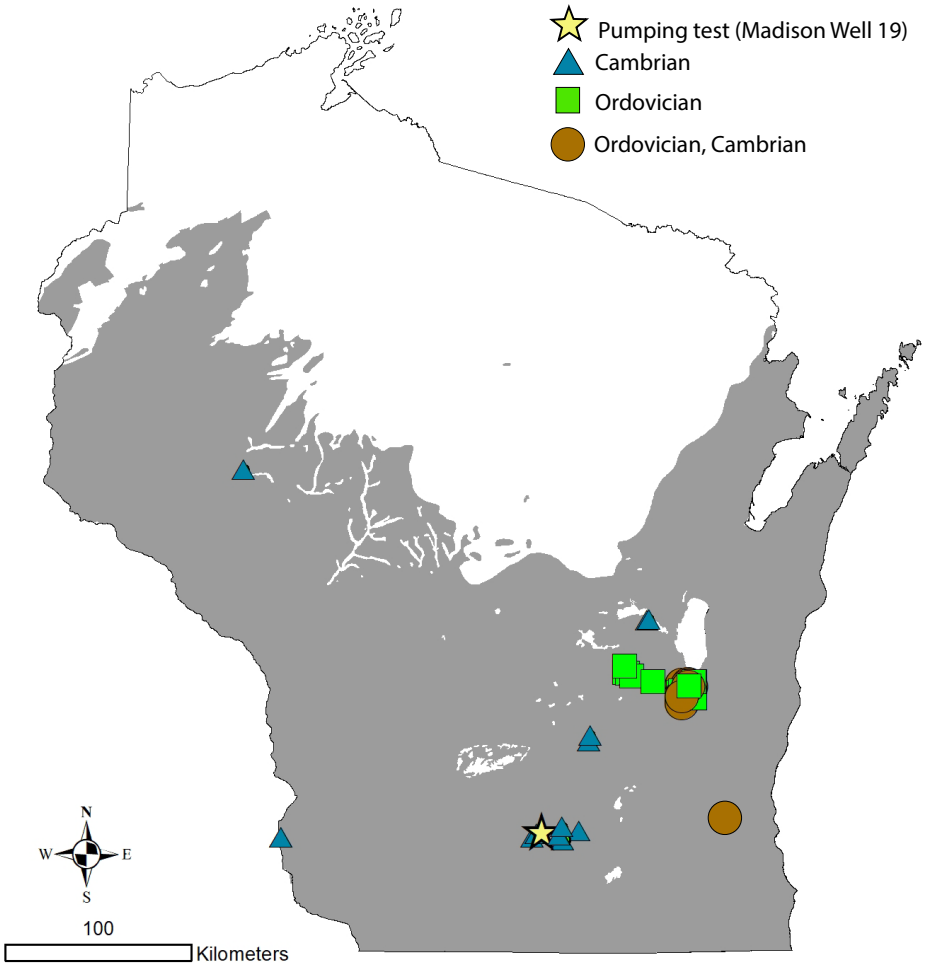

Figure E-1 Geographic distribution and broad geologic description of sampling sites at municipal wells across the extent of the Midwestern Cambrian-Ordovician aquifer system in Wisconsin. Star represents location of Madison Well 19, site of the pumping test from Chapter 5.

E-2 Methods

E-2.1 Radium isotope analysis

Scintillation counting analysis for Ra isotopes ([^{226}Ra] and [^{228}Ra], where radioactive activity is designated by brackets) was conducted by Eurofins Eaton Analytical, Inc. in a manner consistent with the 'Georgia Tech' method, which uses co-precipitation of radium with barite ($BaSO_4$) and gamma counting analysis to measure radioactive decay of ^{226}Ra and ^{228}Ra daughter isotopes.[2,3] In this study, we will refer to this method as 'scintillation counting. 38 municipal well samples were analyzed via scintillation counting.

Mass spectrometry analysis for Ra isotopes ([^{226}Ra] and [^{228}Ra]) was conducted at the Wisconsin State Laboratory of Hygiene Trace Elements Clean Laboratory, using isotope dilution and column purification to analyze samples for ^{226}Ra and ^{228}Ra using a Neptune Plus MC-ICPMS using a single SEM/RPQ detector in dynamic mode.[4,5] Each sample was spiked with 100 μL of a ^{228}Ra standard solution prior to purification; further information about the purification technique and spike calibration can be found in Mathews et al., 2021.[5] Two samples of each time period were analyzed on the MC-ICPMS, using the initial measured ^{226}Ra/^{228}Ra to calculated concentrations for both ^{226}Ra and ^{228}Ra. Prior to each analysis, the MC-ICPMS ion counter detector was calibrated with a dilute tuning solution, and a natural uranium solution was used to correct ^{226}Ra/^{228}Ra for mass bias. 7 municipal well samples.

E-2.2 Uranium isotope ratio

For [^{234}U/^{238}U] analysis, isotopes ^{238}U, ^{235}U, and ^{234}U were measured on the MC-ICPMS for select samples, with ^{238}U and ^{235}U measured on Faraday cups and ^{234}U measured on the SEM/RPQ. Further information about sample preparation can be found in Mathews et al., 2021.[5] During analysis, each sample was run on 30 cycles with 16 second integration, with natural uranium standards analyzed before and after each unknown sample.

E-2.3 Strontium isotopes

For ^{87}Sr/^{86}Sr analysis, ^{87}Sr and ^{86}Sr were measured on the MC-ICPMS for select samples. Further information about sample preparation can be found in Mathews et al., 2021.[5] During analysis, each sample was run on 60 cycles with 8 second integration, with NIST standard NBS987 ran before and after each sample. Internal mass fractionation was corrected using ^{86}Sr/^{88}Sr = 0.1194, then externally normalized to ^{87}Sr/^{86}Sr = 0.71024 using the 1.000061 factor.

Table E-1 Isotopic analysis of MCOAS groundwater and surface water samples in Wisconsin. O = Ordovician, C = Cambrian OC = Ordovician and Cambrian, SW = Surface water; MC = Multi-collector inductively coupled plasma mass spectrometry, GT = Georgia Tech method. [a]Cited data is taken from Plechacek et al., *in preparation.*[6] [b]Data from Wisconsin DNR database

Well	Sampling Date	Open Well Interval	$^{87}Sr/^{86}Sr$	$[^{234}U/^{238}U]$	$^{226}Ra + ^{228}Ra$ (mBq/L)	Ra analysis
Cambria Well 3	7/16/19	C	0.712438 ± 0.000007	4.854 ± 0.006	80 ± 30	GT
Cambria Well 4	7/16/18	C	0.709327 ± 0.000006	4.532 ± 0.003	120 ± 30	GT
Madison Well 14	1/25/19	C	0.710271 ± 0.000008	2.511 ± 0.001	19.6 ± 0.6	MC
Madison Well 16	1/25/19	C	0.709715 ± 0.000008	3.921 ± 0.001	18.0 ± 0.5	MC
Madison Well 19	1/25/19	C	0.711703 ± 0.000006	3.919 ± 0.001	133 ± 4	MC
Madison Well 19	3/2/20	C	0.711700 ± 0.000007	3.957 ± 0.001	131 ± 4	MC
Madison Well 29	1/25/19	C	0.711539 ± 0.000007	6.128 ± 0.002	68 ± 2	MC
Madison Well 31	1/25/19	C	0.710663 ± 0.000007	8.401 ± 0.003	68 ± 1	MC
Madison Well 9	1/25/19	C	0.709201 ± 0.000007	4.545 ± 0.002	48 ± 1	MC
[6]Ripon 5	7/25/19	C	0.710139 ± 0.000007	6.680 ± 0.005	40 ± 20	GT
Villa Diann	7/13/18	C	0.708862 ± 0.000008	1.73 ± 0.01	310 ± 40	GT
Villa Louis 1	4/21/18	C	0.709389 ± 0.000007	11.76 ± 0.01	250 ± 40	GT
Villa Louis 2	4/21/18	C	0.709429 ± 0.000009	15.11 ± 0.01	240 ± 50	GT
Winneconne Well 1	7/20/18	C	0.710158 ± 0.000008	8.411 ± 0.003	280 ± 40	GT
Winneconne Well 2	7/20/18	C	0.710066 ± 0.000005	8.157 ± 0.002	160 ± 30	GT
BP039[6]	8/21/19	O	0.710653 ± 0.000009	3.9 ± 0.03	30 ± 20	GT
MU025[6]	8/19/19	O	0.710952 ± 0.000007	2.314 ± 0.004	---	GT
NY261[6]	8/21/19	O	0.710201 ± 0.000009	9.339 ± 0.007	130 ± 20	GT
[a]Ripon 6	7/25/19	O	0.710278 ± 0.000009	2.760 ± 0.002	40 ± 10[b]	GT
[a]Ripon 9	7/25/19	O	0.710491 ± 0.000008	5.525 ± 0.002	30[b]	GT
[a]SP471	8/21/19	O	0.709248 ± 0.000009	1.945 ± 0.001	110 ± 20	GT
[a]UR218	8/21/19	O	0.709266 ± 0.000008	1.915 ± 0.002	50 ± 20	GT
[a]XL281	8/19/19	O	0.71088 ± 0.00001	3.27 ± 0.05	---	GT
[a]XO078	8/12/19	O	0.710681 ± 0.000009	3.39 ± 0.01	30	GT

[a]XU220	8/12/19	O	0.710528 ± 0.000008	5.81 ± 0.02	---	GT
[a]XV125	8/19/19	O	0.710392 ± 0.000006	2.25 ± 0.05	50 ± 30	GT
[a]XW677	8/12/19	O	0.710497 ± 0.000008	6.32 ± 0.02	---	GT
[a]YB930	8/12/19	O	0.710800 ± 0.000007	3.86 ± 0.01	70 ± 40	GT
[a]BC066	8/12/19	OC	0.710756 ± 0.000008	8.94 ± 0.005	160 ± 40	GT
[a]Fond du Lac 10 (BF796)	7/15/19	OC	0.71043 ± 0.00001	7.13 ± 0.01	310 ± 30	GT
[a]Fond du Lac 11 (BF797)	7/15/19	OC	0.710733 ± 0.000007	5.6 ± 0.09	200 ± 40[b]	GT
[a]Fond du Lac 12 (BF798)	7/15/19	OC	0.710453 ± 0.000008	3.102 ± 0.003	140 ± 60[b]	GT
[a]Fond du Lac 13 (BF799)	7/15/19	OC	0.710500 ± 0.000006	12.560 ± 0.004	380 ± 40	GT
[a]Fond du Lac 14 (BF800)	7/15/19	OC	0.710459 ± 0.00007	18.0 ± 0.01	170 ± 30	GT
[a]Fond du Lac 15 (BF801)	7/15/19	OC	0.710485 ± 0.000009	5.124 ± 0.005	240 ± 70[b]	GT
[a]Fond du Lac 16 (BF802)	7/17/19	OC	0.711155 ± 0.000006	11.061 ± 0.005	230 ± 40	GT
[a]Fond du Lac 17 (BF803)	7/17/19	OC	0.710990 ± 0.000008	17.365 ± 0.004	130 ± 40	GT
[a]Fond du Lac 18 (BF804)	7/17/19	OC	0.710699 ± 0.000007	16.01 ± 0.01	210 ± 50	GT
[a]Fond du Lac 19 (BF805)	7/17/19	OC	0.710759 ± 0.000006	10.088 ± 0.003	280 ± 30	GT
[a]Fond du Lac 20 (BF806)	7/17/19	OC	0.710922 ± 0.000007	9.246 ± 0.004	300 ± 30[b]	GT
[a]Fond du Lac 21 (YP877)	7/17/19	OC	0.710769 ± 0.000007	11.315 ± 0.005	290 ± 30	GT
[a]Fond du Lac 23 (AY377)	7/17/19	OC	0.710925 ± 0.000007	10.841 ± 0.006	200 ± 30	GT
[a]Fond du Lac 24 (AY378)	7/31/19	OC	0.711100 ± 0.000007	16.299 ± 0.005	210 ± 30	GT
[a]Fond du Lac 25 (AY379)	7/17/19	OC	0.710950 ± 0.000009	16.890 ± 0.009	130 ± 40	GT
[a]Fond du Lac 26 (YJ236)	7/15/19	OC	0.710470 ± 0.000008	17.240 ± 0.006	370 ± 40[b]	GT
Sussex well #1 (BH424)	11/27/18	OC	0.710142 ± 0.000007	23.52 ± 0.01	200 ± 40[b]	
19SWA-10 "Field 19"	1/14/19	SW	0.709209 ± 0.000007	1.707 ± 0.02	---	---
Badfish Creek	10/27/18	SW	0.709914 ± 0.000009	2.127 ± 0.001	---	---
Bell-1, Bell-2	9/6/18	SW	0.709560 ± 0.000008	1.318 ± 0.008	---	---
Devil's Lake (East)	10/13/18	SW	0.709161 ± 0.000009	1.20 ± 0.01	---	---
Frost Woods Beach	10/14/18	SW	0.70988 ± 0.00001	1.888 ± 0.001	---	---
Monona Boat Launch	11/19/18	SW	0.709843 ± 0.000007	1.886 ± 0.001	---	---

Sugar River	2/23/19	SW	0.709496 ± 0.000008	2.009 ± 0.001	---	---
West Branch Sugar River	2/23/19	SW	0.709516 ± 0.000008	2.174 ± 0.001	---	---
WSLH Surface Runoff	3/14/19	SW	0.708852 ± 0.000007	1.008 ± 0.003	---	---
Yahara River Pier-1, 2	9/30/18	SW	0.709835 ± 0.000008	2.160 ± 0.001	---	---

E-3 Results

E-3.1 Isotopic analysis of Wisconsin groundwater

Comparison of $^{87}Sr/^{86}Sr$ and $[^{234}U/^{238}U]$ in MCOAS groundwater sourced from municipal wells across Wisconsin varies across broad geologic characteristics (Figure 4a). The widest range of $^{87}Sr/^{86}Sr$ is observed in wells open to Cambrian stratigraphy, ranging from 0.708862 ± 0.000008 to 0.712519 ± 0.000008. In wells open to Ordovician stratigraphy and wells open to both Ordovician and Cambrian bedrock, $^{87}Sr/^{86}Sr$ falls in a smaller range (respectively, 0.709248 ± 0.000009 to 0.710952 ± 0.000007 and 0.71043 ± 0.00001 to 0.711155 ± 0.000006). However, wells open to Ordovician and Cambrian stratigraphy have the widest range of $[^{234}U/^{238}U]$, varying from 3.102 ± 0.003 to 18.00 ± 0.01. Wells sourcing water from Cambrian stratigraphy or Ordovician stratigraphy had a smaller range of $[^{234}U/^{238}U]$, namely 1.73 ± 0.01 to 15.34 ± 0.01 and 1.915 ± 0.002 to 11.107 ± 0.006, respectively. Surface water samples generally had lower $^{87}Sr/^{86}Sr$ and $[^{234}U/^{238}U]$ values, ranging from 0.708852 ± 0.000007 to 0.709914 ± 0.000009 and 1.008 ± 0.003 to 2.174 ± 0.001, respectively.

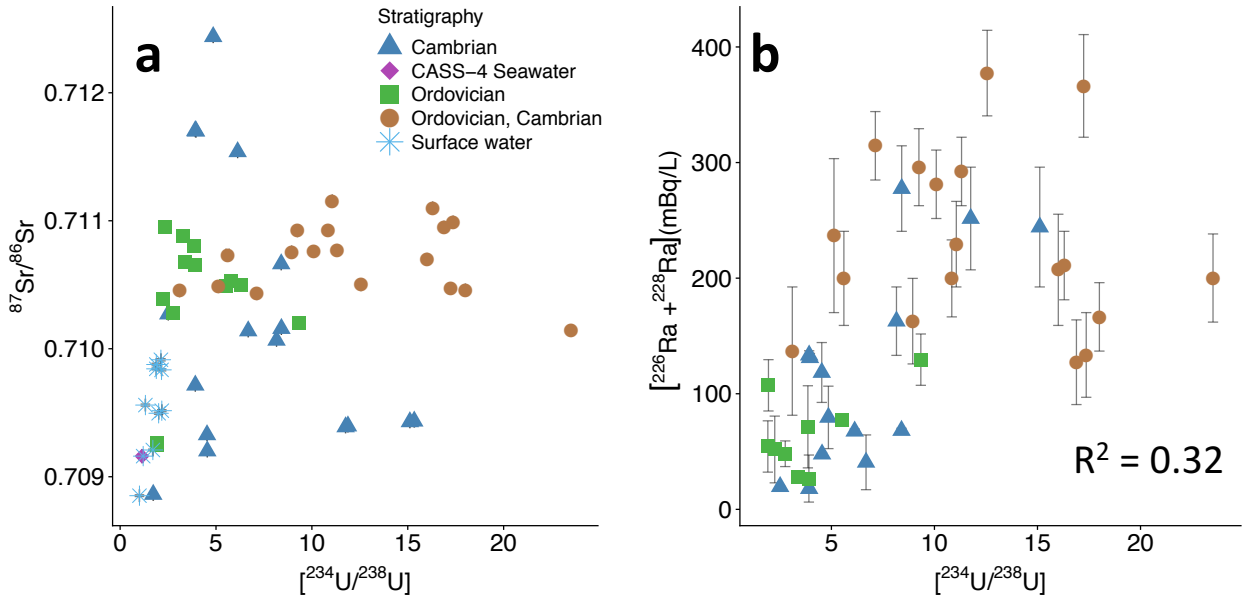

Figure E-2 Isotopic analysis of groundwater sourced from the MCOAS across Wisconsin, distinguished by broad geologic characteristics. a) $^{87}Sr/^{86}Sr$ compared to $[^{234}U/^{238}U]$ for samples from surface water and groundwater samples. b) Combined Ra ($[^{226}Ra + ^{228}Ra]$) levels for available samples with $[^{234}U/^{238}U]$. Error bars represent analytical uncertainty, which is dependent on method, or standard deviation of long-term trends in compliance datasets. Note that sample Villa Diann was not included in 4b, due to acidic groundwater conditions (pH = 5.8) impacting Ra levels.

Combined Ra and $[^{234}U/^{238}U]$ measured in groundwater sourced from the MCOAS in Wisconsin are associated across the state (Figure E-2). For sampled wells open to Cambrian bedrock, combined Ra ranges from 17.9 ± 0.5 to 310 ± 40 mBq/L, averaging 130 ± 100 mBq/L (Table). Ordovician stratigraphy ranges from 30 ± 20 to 130 ± 20 mBq/L, averaging 70 ± 30 mBq/L combined Ra. Wells open to both Cambrian and Ordovician stratigraphy average 230 ± 80, ranging from 130 ± 40 to 380 ± 40 mBq/L combined Ra. Aqueous Ra and $[^{234}U/^{238}U]$ are weakly correlated in this dataset (R^2 = 0.32). In general, wells open to both Ordovician and Cambrian stratigraphy had the highest values of aqueous ^{226}Ra (18 wells), while wells open to

only Ordovician or Cambrian stratigraphy tended to have lower Ra levels (14 wells and 24 wells, respectively).

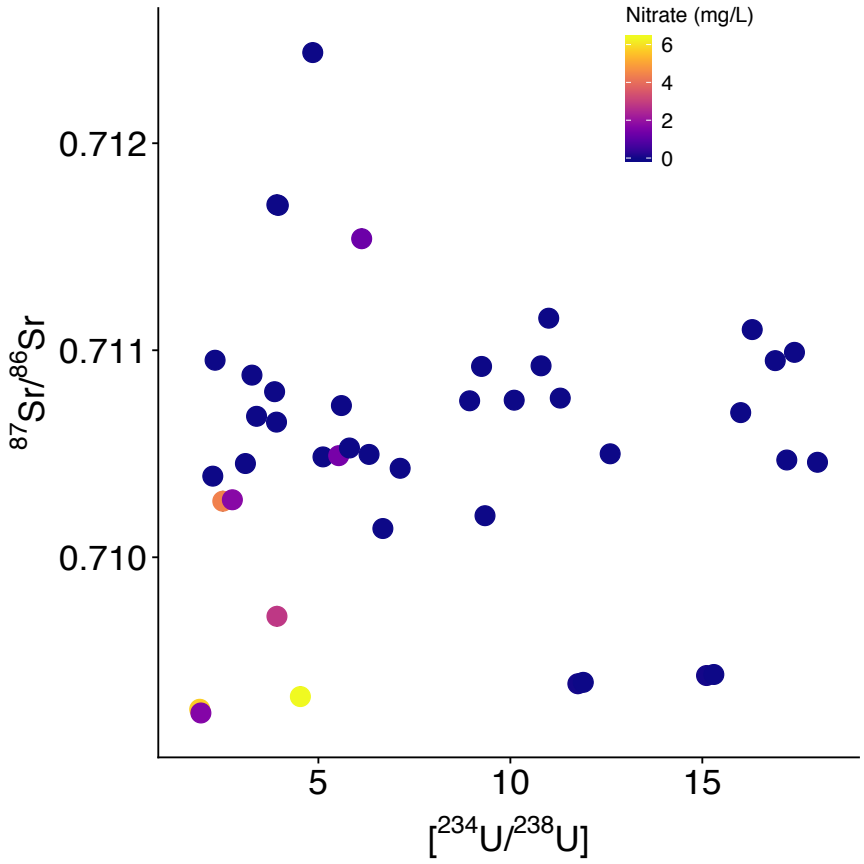

Figure E-3 Isotopic analysis of groundwater sourced from the MCOAS across Wisconsin, distinguished by measured nitrate concentration, comparing $^{87}Sr/^{86}Sr$ and $[^{234}U/^{238}U]$.

E-4 Discussion

E-4.1 Isotopic indicators of groundwater interactions with aquifer solids

To better support how water utilities provide clean drinking water to the public, development of better tools measuring degraded water quality, such as Ra analysis methods or other isotopic indicators, is necessary. Factors playing a role in Ra release from mineral associations include rock-water interaction, mineral dissolution, and Ra desorption.[5,7-10] Isotopic

tools can provide information about water-rock interaction, and elaborate on the potential for elevated aqueous levels of geogenic contaminants. Strontium isotopes are reflective of geologic time, as aqueous $^{87}Sr/^{86}Sr$ is released from specific rock phases to the aqueous system and is not otherwise fractionated by subsurface exchanges; typically, Cambrian and Ordovician $^{87}Sr/^{86}Sr$ ranges from 0.709 and 0.713.[8,11-15] Uranium isotopes ($[^{234}U/^{238}U]$) demonstrate water-rock interaction, due to the preferential leaching of ^{234}U due to mineral lattice damage from the alpha decay of ^{238}U.[16]

Comparison of $^{87}Sr/^{86}Sr$ and $[^{234}U/^{238}U]$ in groundwater samples provides information on groundwater interactions with specific stratigraphy (Figure 4a). Lower levels of $^{87}Sr/^{86}Sr$ (e.g., ~ 0.709) suggests water interactions closer to seawater or surface water, particularly when samples also contain low levels of $[^{234}U/^{238}U]$ (e.g., 1 – 3). Likely, groundwater with lower levels of $^{87}Sr/^{86}Sr$ and $[^{234}U/^{238}U]$ are more heavily influenced by surface water, resulting in isotopic ratios more similar to surface water or seawater. Nitrate presence in groundwater samples that also contain low levels of $^{87}Sr/^{86}Sr$ and $[^{234}U/^{238}U]$ closer to equilibrium supports the influence of surface water intrusion on these samples (Figure E-3).

While samples with minimal $^{87}Sr/^{86}Sr$ and $[^{234}U/^{238}U]$ demonstrates surface water influence, elevated values indicate groundwater interactions with specific stratigraphy (Figure E-2a). Samples at elevated $^{87}Sr/^{86}Sr$ (> 0.711) may be influenced by the leaching of elevated levels of ^{87}Sr from Precambrian crystalline bedrock.[17] Cambrian samples sourcing water from geologic units further from the Precambrian (e.g., Tunnel City) typically have lower ^{87}Sr, closer to values representative of seawater from the Cambrian geologic era (e.g., ~ 0.7090).[18] While Ordovician marine records suggest similar low $^{87}Sr/^{86}Sr$ (~0.708 – 0.709), the greater range of $^{87}Sr/^{86}Sr$ (~0.710 – 0.711) in the samples from this study may be due to enriched ^{87}Sr in dolomitized

carbonates from hydrothermal brine from the Michigan Basin transported during the Paleozoic era.[6,19,20] The influence of carbonate and/or dolomite dissolution on $^{87}Sr/^{86}Sr$ may also impact Sr release in samples taken from wells open to both Ordovician and Cambrian stratigraphy. However, samples open to both Cambrian and Ordovician stratigraphy contain a wider range of [$^{234}U/^{238}U$] than samples only open to Ordovician stratigraphy. Samples with elevated [$^{234}U/^{238}U$] are mostly found in the regionally confined portion of the aquifer system. Glacial recharge elevated in ^{234}U to the Cambrian and Ordovician aquifer system during the Wisconsinan glaciation, as well as increased water-rock interaction time, may contribute to the greater [$^{234}U/^{238}U$] values.[21]

Groundwater elevated in ^{234}U, whether due to glacial recharge or water-rock interaction, may play a large role in sourcing elevated Ra to groundwater. [$^{234}U/^{238}U$] and combined Ra weakly correlate ($R^2 = 0.32$) across samples taken from a wide geographic and geologic range. This suggests that [$^{234}U/^{238}U$] may be a useful tool to estimate elevated aqueous combined Ra levels within long-stemmed municipal wells. Elevated Ra is also associated with greater groundwater age, another indicator of potential glacial recharge or more mineralized water.[22] Unlike other isotopic groundwater age indicators (e.g., tritium), [$^{234}U/^{238}U$] indicates rock interactions, rather than water residence time, due to the increased leachability of ^{234}U after alpha recoil damage to the mineral lattice from ^{238}U decay. Within these complex aquifer systems, the concept of residence time must be considered as a dual transport model. Specifically, water can move through the aquifer in multiple ways at different rates, such as fracture flow in comparison to pore water. This indicates that different groundwater flow paths will experience different times periods for leaching radionuclides from aquifer solids. To further complicate hydrologic influences on contaminant mobility, water-rock interactions mix across these long-stemmed

municipal wells, which may influence how contaminants are mobilized to drinking water systems. Thus, isotopic indicators such as $^{87}Sr/^{86}Sr$ and $[^{234}U/^{238}U]$ provide hydrologic and geologic context for well groundwater uptake; comparison of $[^{234}U/^{238}U]$ and combined Ra can also be used to help predict Ra occurrence in groundwater systems.

E-5 References

1. Wisconsin Department of Natural Resources Public Drinking Water System Data. https://dnr.wi.gov/dwsviewer
2. United States Environmental Protection Agency *Method 903.0: Alpha-Emitting Radium Isotopes in Drinking Water*; 1980.
3. Georgia Institute of, T., The determination of radium-226 and radium-228 in drinking water by gamma-ray spectrometry using HPGE or Ge(Li) detectors, revision 1.2. **2004**.
4. Sims, K. W. W.; Hart, S. R.; Reagan, M. K.; Blusztajn, J.; Staudigel, H.; Sohn, R. A.; Layne, G. D.; Ball, L. A.; Andrews, J., 238U-230Th-226Ra-210Pb-210Po, 232Th-228Ra, and 235U-231Pa constraints on the ages and petrogenesis of Vailulu'u and Malumalu Lavas, Samoa. *Geochemistry, Geophysics, Geosystems* **2008,** *9*, (4).
5. Mathews, M.; Scott, S. R.; Gotkowitz, M. B.; Ginder-Vogel, M., Association of Radionuclide Isotopes with Aquifer Solids in the Midwestern Cambrian–Ordovician Aquifer System. *ACS Earth and Space Chemistry* **2021**.
6. Amy Plechacek, S. R. S., Madeline B. Gotkowitz, and Matthew Ginder-Vogel, Effects of recharge history on radium and strontium occurrence in the Midwestern Cambrian-Ordovician aquifer system. In.
7. Tricca, A.; Porcelli, D.; Wasserburg, G. J., Factors controlling the groundwater transport of U, Th, Ra, and Rn. *Journal of Earth System Science* **2000,** *109*, (1), 95-108.
8. Vinson, D. S.; Lundy, J. R.; Dwyer, G. S.; Vengosh, A., Implications of carbonate-like geochemical signatures in a sandstone aquifer: Radium and strontium isotopes in the Cambrian Jordan aquifer (Minnesota, USA). *Chemical Geology* **2012,** *334*, 280-294.
9. Gilkeson, R. H.; Specht, S. A.; Cartwright, K.; Griffin, R. A.; Larson, T. E., Geologic studies to identify the source for high levels of radium and barium in Illinois ground-water supplies: a preliminary report. **1978**.
10. International Atomic Energy Agency, The environmental behaviour of radium: revised edition. *Technical Reports Series No. 476* **2014**, (476), 44-51.
11. Bain, D. C.; Bacon, J. R., Strontium isotopes as indicators of mineral weathering in catchments. *Catena* **1994,** *22*, (3), 201-214.
12. Voerkelius, S.; Lorenz, G. D.; Rummel, S.; Quétel, C. R.; Heiss, G.; Baxter, M.; Brach-Papa, C.; Deters-Itzelsberger, P.; Hoelzl, S.; Hoogewerff, J., Strontium isotopic signatures of natural mineral waters, the reference to a simple geological map and its potential for authentication of food. *Food chemistry* **2010,** *118*, (4), 933-940.
13. Shand, P.; Darbyshire, D. P. F.; Love, A. J.; Edmunds, W. M., Sr isotopes in natural waters: Applications to source characterisation and water–rock interaction in contrasting landscapes. *Applied Geochemistry* **2009,** *24*, (4), 574-586.
14. Åberg, G.; Jacks, G.; Hamilton, P. J., Weathering rates and 87Sr/86Sr ratios: an isotopic approach. *Journal of Hydrology* **1989,** *109*, (1-2), 65-78.
15. Hunt, R. J.; Bullen, T. D.; Krabbenhoft, D. P.; Kendall, C., Using stable isotopes of water and strontium to investigate the hydrology of a natural and a constructed wetland. *Groundwater* **1998,** *36*, (3), 434-443.
16. Moreira-Nordemann, L. M., Use of 234U/238U disequilibrium in measuring chemical weathering rate of rocks. *Geochimica et Cosmochimica Acta* **1980,** *44*, (1), 103-108.

17. Hoppe, W.; Montgomery, C.; Van Schmus, W., Age and significance of Precambrian basement samples from northern Illinois and adjacent states. *Journal of Geophysical Research: Solid Earth* **1983,** *88*, (B9), 7276-7286.
18. McArthur, J. M.; Howarth, R.; Bailey, T., Strontium isotope stratigraphy: LOWESS version 3: best fit to the marine Sr-isotope curve for 0–509 Ma and accompanying look-up table for deriving numerical age. *The Journal of Geology* **2001,** *109*, (2), 155-170.
19. Luczaj, J. A., Evidence against the Dorag (mixing-zone) model for dolomitization along the Wisconsin arch: A case for hydrothermal diagenesis. *AAPG Bulletin* **2006,** *90*, (11), 1719-1738.
20. Davies, G. R., *Hydrothermal Dolomite Reservoir Facies: Global and Western Canadian Perspectives.* Second ed.; Graham Davies Geological Consultants LTD: Calgary, Alberta, 2000; p 214.
21. Gilkeson, R. H. *Isotopic studies of the natural sources of radium in groundwater in Illinois*; 1984; pp 50-50.
22. Stackelberg, P. E.; Szabo, Z.; Jurgens, B. C., Radium mobility and the age of groundwater in public-drinking-water supplies from the Cambrian-Ordovician aquifer system, north-central USA. *Applied Geochemistry* **2018,** *89*, 34-48.

Appendix F

Supplementary Geochemical Model for Chapter 4

Section F-1: Model background

A geochemical model was constructed to examine radium (Ra) interactions with aquifer solids, as determined by aqueous and solid-associated Ra concentrations measured in groundwater and rock samples from ports sampled at well MP16. A mineralogy report, based on X-ray diffraction analysis of well cuttings from a municipal well in Pewaukee, Wisconsin (PW-10), was used to differentiate many of the prominent minerals in the stratigraphy. It is important to note that, while PW-10 and MP16 have many general stratigraphic intervals in common, stratigraphy is heterogeneous and varies in mineral content geographically across the Midwestern Cambrian-Ordovician aquifer system (MCOAS). However, the mineralogy report provided a starting basis for estimating mineral content. The U.S. Geological Survey (USGS) geochemical modeling software PHREEQC was used to estimate Ra speciation and mineral associations (Table F-1).[1] Additionally, the USGS calibration software PEST was used to calibrate and verify the model.[2] Several sources were helpful in developing the geochemical model, namely conversation with David Parhurst (PHREEQC author), the USGS PHREEQC manual 'Techniques and Methods 6-A43',[3] and review of questions and answers on the PhreeeqcUser Forum.[4] Results from the geochemical model agree closely with observed values for aqueous ^{226}Ra, varying from |0.001| to |0.31| by percent difference across the eight ports examined (Table F-2).

Table F-1 Input file for examining Ra sorption in MP16 MS-132.

```
DATABASE C:\Users\Maddie\Desktop\pest-run\MS-132\llnl.dat
TITLE   Testing Ra sorption in a sandstone aquifer
# Well MP16 MS-132, depth from surface 131-133m. Likely the Mt Simon unit; sandstone
# Trace minerals are calculated as 0.001 - 0.1% of # a rock's composition
# Mineral composition: Quartz (99+%), Illite/Mica (trc), Illite/smectite (trc)
# This mineral composition is estimated from the Pewaukee 10 mineralogy report (PW-10-1170)
# Assume 99.8% Quartz and 0.2% Illite

SOLUTION_MASTER_SPECIES
# Below are the specified master species in solution, as different from the database (llnl.dat)
# Isotopic mass is distinguished in the far right column
# Isotope names are distinguished by mass value prior to the element, in the name
Ra                  Ra+2                        0                   Ra                  226.02541033
Rn Rn 0 Rn 222.01758
[238U] [238U]+4 0 U                             238.050788423
[238U](4)           [238U]+4            0       238.050788423
[238U](5)           [238U]O2+           0       238.050788423
[238U](6)           [238U]O2+2          0       238.050788423
[234U] [234U]+4 0           U           234.0409523
[234U](4)           [234U]+4            0       234.0409523
[234U](5)           [234U]O2+           0       234.0409523
[234U](6)           [234U]O2+2          0       234.0409523
Th Th+4 0 Th 230.033134313


SOLUTION_SPECIES
# Here, the speciation of master species already defined is distinguished.
# This example includes very minimal solution interactions for species
# If further solution chemistry is desired, it may need to be added here
Ra+2 = Ra+2
            log_k     0.0
Rn = Rn
            log_k     0.0
H2O = H2O
 log_k     0.0
[238U]+4 = [238U]+4
            log_k               0.0
[238U]+4 + 4H2O = [238U](OH)4 + 4H+
            log_k               -8.538
            delta_h   24.760 kcal
[238U]+4 + 5H2O = [238U](OH)5- + 5H+
            log_k               -13.147
            delta_h   27.580
#secondary master species for U(5)
[238U]+4 + 2 H2O = [238U]O2+ + 4H+ + e-
            log_k               -6.432
            delta_h   31.130 kcal
#secondary master species for U(6)
[238U]+4 + 2H2O = [238U]O2+2 + 4H+ + 2e-
            log_k               -9.213
            delta_h   34.430 kcal
[238U]O2+2 + H2O = [238U]O2OH+ + H+
```

```
        log_k           -5.782
        delta_h  11.015 kcal
2[238U]O2+2 + 2H2O = ([238U]O2)2(OH)2+2 + 2H+
        log_k           -5.626
        delta_h  -36.04 kcal
3[238U]O2+2 + 5H2O = ([238U]O2)3(OH)5+ + 5H+
        log_k           -15.641
        delta_h  -44.27 kcal
[238U]O2+2 + CO3-2 = [238U]O2CO3
        log_k           10.064
        delta_h  0.84 kcal
[238U]O2+2 + 2CO3-2 = [238U]O2(CO3)2-2
        log_k           16.977
        delta_h  3.48 kcal
[238U]O2+2 + 3CO3-2 = [238U]O2(CO3)3-4
        log_k           21.397
        delta_h  -8.78 kcal

Th+4 = Th+4
        log_k 0.0
[234U]+4 = [234U]+4
        log_k           0.0
[234U]+4 + 4H2O = [234U](OH)4 + 4H+
        log_k           -8.538
        delta_h  24.760 kcal
[234U]+4 + 5H2O = [234U](OH)5- + 5H+
        log_k           -13.147
        delta_h  27.580
#secondary master species for U(5)
[234U]+4 + 2 H2O = [234U]O2+ + 4H+ + e-
        log_k           -6.432
        delta_h  31.130 kcal
#secondary master species for U(6)
[234U]+4 + 2H2O = [234U]O2+2 + 4H+ + 2e-
        log_k           -9.213
        delta_h  34.430 kcal
[234U]O2+2 + H2O =[234U]O2OH+ + H+
        log_k           -5.782
        delta_h  11.015 kcal
2[234U]O2+2 + 2H2O = ([234U]O2)2(OH)2+2 + 2H+
        log_k           -5.626
        delta_h  -36.04 kcal
3[234U]O2+2 + 5H2O = ([234U]O2)3(OH)5+ + 5H+
        log_k           -15.641
        delta_h  -44.27 kcal
[234U]O2+2 + CO3-2 = [234U]O2CO3
        log_k           10.064
        delta_h  0.84 kcal
[234U]O2+2 + 2CO3-2 = [234U]O2(CO3)2-2
        log_k           16.977
        delta_h  3.48 kcal
[234U]O2+2 + 3CO3-2 = [234U]O2(CO3)3-4
        log_k           21.397
        delta_h  -8.78 kcal

SURFACE_MASTER_SPECIES
```

```
        Quartz    Quartz
        Illite    Illite

SURFACE_SPECIES
# K is the constant describing the adsorption/desorption equilibrium for each reactant in contact with a surface
# See calculations for log k from "mp16data" excel file, tab "Kd calcs"
Quartz = Quartz
 log_k 0
Ra+2 + Quartz = QuartzRa+2
 log_k -9.78E+01
Illite = Illite
 log_k 0
Ra+2 + Illite= IlliteRa+2
 log_k -9.75E+01

END

SOLUTION 1
# This solution is only water; this can be used for 'pulse' contaminant column models
END

SOLUTION 2
#         This data is from well MP16 MS-132 (Mt Simon); sampled 11/14/2019
 temp 8.9
 pH 7.09
 pe 2.64
 redox pe
 units mg/l
 density 1
 # The 238U is calculated from the amount of U needed to produce estimated total 226Ra
# See calculations from "mp16data" excel file, tab "phreeqc decay calcs" and "phreeqc outputs"
 [238U] 8.99528E-7 mol/L
 Al 6.8 ug/l
 Alkalinity 387.5
 Ba 3.16 ug/l
 Ca 63.01
 Fe 486 ug/l
 K 1.42
 Mg 59.71
 Mn 18.9 ug/l
 Na 1.29
 S(6) 5.5
 Sr 93.9 ug/l
 -water 1 # kg

PHASES
# These are the thermodynamic values for RaSO4 and barite, for calculating co-precipitation in
# SOLID_SOLUTIONS
RaSO4
 RaSO4 = Ra+2 + SO4-2
 log_k 11.506000000
 delta_h 5.4392000000 kJ
Barite
 BaSO4 = Ba+2 + SO4-2
 log_k -9.9800000000
 delta_h 2.6568500E+01 kJ
```

```
SOLID_SOLUTIONS 1
# This calculates co-precipitation for Ba(Ra)SO4
 Ra (x) Ba (1-x) SO4
 -comp RaSO4 0
 -comp Barite 0
        -Gugg_nondim .360000000 # Zhu 2004 estimate a Margules parameter (wsubH) of about 210 cal/mol
# based on partition coefficient for RaII/barite interaction in 0.005 mol/L HCl determined by
# Doerner and Hoskins 1925.[5] A value of wsubH ~ 210 cal/mol corresponds to a Guggenheim
# interaction parameter of alpha ~ 0.36.

SURFACE 1
# This examines the interactions between the previously defined solids and Solution 2
 -equilibrate with solution 2
 Illite 1e+100 100.0000 0.2
 Quartz 1e+100 .0400000 99.8

RATES
# These are the rate calculation for radionuclide decay
 Ra_decay
-start
10 k = parm(1)
# parm(1) draws the decay constant value defined in KINETICS 1
20 Ra = SYS('Ra')
# SYS(Ra) looks at all the Ra in the system (not just in solution) – so it will all be included in decay calculations
30 rate = k * Ra
# Decay calculation: dN/dt = - λ*N (neg. value is assumed due to formula assigned in
# KINETICS)
40 SAVE rate * TIME
-end
 234U_decay
-start
10 k = parm(1)
20 Ur = TOT('[234U]')
30 rate = k * Ur
40 SAVE rate * TIME
-end
 238U_decay
-start
10 k = parm(1)
20 U = TOT('[238U]')
30 rate = k * U
40 SAVE rate * TIME
-end
Th_decay
-start
10 k = parm(1)
20 Th = TOT('Th')
30 rate = k * Th
40 SAVE rate * TIME
-end

KINETICS 1
```

```
Ra_decay
 -formula Ra -1 Rn 1
# Here we tell the software that 1 mole of Ra is removed, and 1 mole of Rn formed
 -m 1
 -m0 1
 -parms 1.37372205685555e-11
# this is the decay constant
 -tol 1e-08
234U_decay
 -formula Th 1 [234U] -1
 -m 1
 -m0 1
 -parms 8.94860064721471e-14
 -tol 1e-08
238U_decay
 -formula [234U] 1 [238U] -1
 -m 1
 -m0 1
 -parms 4.91819e-18
 -tol 1e-08
Th_decay
 -formula Ra 1 Th -1
 -m 1
 -m0 1
 -parms 2.90796371053249e-13
 -tol 1e-08
-steps 6e13 in 100 steps # 3.15e13 = 1 My
# number of steps would align with length of time, if that's what you're looking at.
-step_divide 1
-runge_kutta 3
-bad_step_max 500
-cvode true
-cvode_steps 100
-cvode_order 5
END

INCREMENTAL_REACTIONS true

USE solution 2
USE surface 1
USE solid_solution 1
USE kinetics 1

SELECTED_OUTPUT
        -file mp16_4.sel
        -reset false

EQUILIBRIUM_PHASES
O2(g) -50 10
# This keeps Fe and U in solution. If you are looking at mineral solubility, then you will need to
# change this value. Otherwise, it helps the software handle adding/removing Th and Ra in
# KINETICS. If Fe and U mineral solubility is important, the redox effects of the KINETICS
# reactions should be investigated to make sure that Fe and U mineral saturation indices are not affected.

USER_PRINT
# This prints the values you care about to the output of the code.
```

```
10 k_Ra = 1.37372205685555e-11
20 k_U = 8.94860064721471e-14
30 k_Th = 2.90796371053249e-13
40 PRINT "Secular Th/U ratio: ", K_U / K_Th
50 PRINT "Secular Ra/U ratio: ", K_U / K_Ra
60 PRINT "Secular Ra/Th ratio: ", K_Th / K_Ra
70 PRINT "Aq Ra/Th: ", TOT("Ra")/TOT("Th")
80 PRINT "Sys Ra/Th: ", SYS("Ra")/TOT("Th")
70 PRINT "Tot(Ra): ", TOT("Ra")
80 PRINT "SYS(Ra): ", SYS("Ra")
90 PRINT "Tot(Al): ", TOT("Al")
100 PRINT "Tot(Ba): ", Tot("Ba")
110 PRINT "Tot(Ca): ", Tot("Ca")
115 PRINT "Tot(Fe): ", Tot("Fe")
120 PRINT "Tot(K): ", Tot("K")
130 PRINT "Tot(Mg): ", Tot("Mg")
140 PRINT "Tot(Mn): ", Tot("Mn")
150 PRINT "Tot(Na): ", Tot("Na")
160 PRINT "Tot(S): ", Tot("S")
170 PRINT "Tot(Sr): ", Tot("Sr")
180 PRINT "Tot(Th): ", Tot("Th")
190 PRINT "Tot(234U): ", Tot("[234U]")
200 PRINT "Tot(238U): ", Tot("[238U]")

END
```

Table F-2 Results from PHREEQC geochemical model calculating ^{226}Ra interactions with aquifer solids in comparison to observed ^{226}Ra values. DPS = Depth from surface

Port	DPS (m)	Stratigraphic unit	Geologic description	Minerals (%)	Observed ^{226}Ra (mol/L)	Calculated ^{226}Ra (mol/L)	Percent Difference (%)
4	131 - 133	Mt Simon	Sandstone	Quartz (99.8), Illite (0.2)	1.37672×10^{-15}	1.37670×10^{-15}	0.001
10	113 – 115	Eau Claire	Fine-grained & silty sandstone	Quartz (35), Feldspar (9), Dolomite (2), Fe oxide (3), Illite (51)	1.5314×10^{-15}	1.5317×10^{-15}	0.01
12	107 - 109	Eau Claire	Fine-grained & silty sandstone	Quartz (35), Feldspar (9), Dolomite (2), Fe oxide (3), Illite (51)	1.4717×10^{-15}	1.4714×10^{-15}	0.02
19	85 – 87	Wonewoc	Sandstone	Quartz (99.5), Illite (0.2), Fe oxide (0.2), Dolomite (0.1)	2.8167×10^{-15}	2.8165×10^{-15}	0.007
24	74 – 76	Tunnel City	Glauconitic sandstone	Quartz (42.9), Glauconite (42), Feldspar (15), Illite (0.1)	3.7781×10^{-16}	3.7795×10^{-16}	-0.04
27	67 – 68	Tunnel City	Glauconitic sandstone	Quartz (43), Glauconite (42), Feldspar (15)	4.1434×10^{-16}	4.1423×10^{-16}	0.03
30	58 – 60	Tunnel City	Glauconitic sandstone	Quartz (43), Glauconite (42), Feldspar (15)	8.9168×10^{-17}	8.93×10^{-17}	-0.13
40	35 - 36	Readstown (St Peter)	Interbedded sandstone, clay, and dolostone	Quartz (99.4), Feldspar (0.1), Calcite (0.1), Dolomite (0.1), Fe oxide (0.1), Illite (0.2)	9.6225×10^{-16}	9.6520×10^{-16}	-0.31

F-2 References

1. Parkhurst, D. L.; Charlton, S. R. *PHREEQC (Version 3)—A Computer Program for Speciation, Batch-Reaction, One-Dimensional Transport, and Inverse Geochemical Calculations*, USGS: 1998.
2. White, J. T.; Hunt, R. J.; Fienen, M. N.; Doherty, J. E. *Approaches to highly parameterized inversion: PEST++ Version 5, a software suite for parameter estimation, uncertainty analysis, management optimization and sensitivity analysis*; 2328-7055; US Geological Survey: 2020.
3. Charlton, S. R.; Parkhurst, D. L. *Description of input and examples for PHREEQC version 3—A computer program for speciation, batch-reaction, one-dimensional transport, and inverse geochemical calculations*; 2013.
4. The PhreeqcUsers Forum. https://phreeqcusers.org/index.php
5. Doerner, H. A.; Hoskins, W. M., Co-Precipitation of Radium and Barium Sulfates1. *Journal of the American Chemical Society* **1925,** *47*, (3), 662-675.